ARSENITE REMOVAL FROM SYNTHETIC CONTAMINATED WATER BY USING CALCINED OYSTER SHELLS AND OS-TRHA ADSORBENT PELLET

PICHNIPA KHOWNPURK

A THESIS SUBMITTED IN FULFILLMENT
OF THE REQUIREMENT FOR THE DEGREE OF
DOCTOR OF ENGINEERING IN CHEMICAL ENGINEERING
FACULTY OF ENGINEERING
KING MONGKUT'S INSTITUTE OF TECHNOLOGY LADKRABANG
2019

KMITL-2019-EN-D-228-041

การกำจัดสารอาร์เซไนท์ในน้ำปนเปื้อนสังเคราะห์ด้วยเปลือกหอยนางรมเผาและเม็ดสารดูดซับ OS-TRHA

ARSENITE REMOVAL FROM SYNTHETIC CONTAMINATED WATER BY USING CALCINED OYSTER SHELLS AND OS-TRHA ADSORBENT PELLET

พิชญ์นิภา ขวัญเผือก

PICHNIPA KHOWNPURK

วิทยานิพนธ์นี้สำหรับการศึกษาตามหลักสูตรปริญญาวิศวกรรมศาสตรดุษฎีบัณฑิต

สาขาวิชาวิศวกรรมเคมี

คณะวิศวกรรมศาสตร์

สถาบันเทคโนโลยีพระจอมเกล้าเจ้าคุณทหารลาดกระบัง

พ.ศ. 2562

KMITL-2019-EN-D-228-041

ARSENITE REMOVAL FROM SYNTHETIC CONTAMINATED WATER BY USING CALCINED OYSTER SHELLS AND OS-TRHA ADSORBENT PELLET

PICHNIPA KHOWNPURK

A THESIS SUBMITTED IN FULFILLMENT
OF THE REQUIREMENT FOR THE DEGREE OF
DOCTOR OF ENGINEERING IN CHEMICAL ENGINEERING
FACULTY OF ENGINEERING
KING MONGKUT'S INSTITUTE OF TECHNOLOGY LADKRABANG
2019

KMITL-2019-EN-D-228-041

หัวข้อวิทยานิพนธ์	การกำจัดสารอาร์เซไนท์ในน้ำปนเปื้อนสังเคราะห์ด้วยเปลือกหอยนางรมเผาและเม็ดสารดูดซับ OS-TRHA
นักศึกษา	นางสาวพิชญ์นิภา ขวัญเผือก
รหัสประจำตัว	56601054
ปริญญา	วิศวกรรมศาสตรดุษฎีบัณฑิต
สาขาวิชา	วิศวกรรมเคมี
พ.ศ.	2562
อาจารย์ที่ปรึกษาวิทยานิพนธ์	ผศ.ดร. วลัยรัตน์ จันทรอัมพร

บทคัดย่อ

งานวิจัยนี้ศึกษาการกำจัดสารอาร์เซไนท์ (As(III)) ในน้ำปนเปื้อนสังเคราะห์ด้วยเปลือกหอยนางรมเผา (COS) และเม็ดสารดูดซับ OS-TRHA โดยในงานวิจัยนี้ ได้แบ่งการทดลองออกเป็นสองส่วน ในส่วนแรก (part A) สาร COS ถูกใช้เป็นตัวดูดซับสำหรับการกำจัดสาร As(III) ออกจากน้ำปนเปื้อนสังเคราะห์ โดยสาร COS เตรียมได้จากการเผาเปลือกหอยนางรมบด (OS) ขนาด 150 - 250 ไมโครเมตร ที่อุณหภูมิ 700°C เป็นระยะเวลา 8 ชั่วโมง จากนั้น สาร COS ถูกนำไปวิเคราะห์ด้วย BET XRD XRF และ วิธีโพเทนชิเมตริแมสไทเทรชัน (potentiometric mass method) ซึ่งผลการวิเคราะห์ด้วย XRD และ XRF พบว่า สาร OS ประกอบด้วยสารแคลเซียมคาร์บอเนต ($CaCO_3$) เป็นส่วนใหญ่ ในขณะที่ 97 เปอร์เซ็นต์โดยน้ำหนักของสาร COS เป็นสารแคลเซียมออกไซด์ (CaO) ค่า pH_{zpc} ของสาร COS มีค่าประมาณ 12.1 ในส่วนของหัวข้อนี้ ได้ทำการศึกษาผลกระทบของแอนไอออน (NO_3^- SO_4^{2-} และ HPO_4^{2-}) ต่อประสิทธิภาพการดูดซับสาร As(III) ในน้ำเสีย นอกจากนี้ค่าคงที่อัตราการดูดซับของสาร As(III) และแอนไอออนบนสาร COS สามารถคำนวณหาค่าทำนายเริ่มต้นได้จากวิธี extended geometric method และจำนวนไซต์ (sorption sites) ที่สาร As(III) และแอนไอออนถูกดูดซับ สามารถคำนวณได้จากวิธี Runge-Kutta โดยจากผลการทดลอง พบว่า ในระบบไอออนคู่ (bi-solutes) สาร HPO_4^{2-} มีผลกระทบต่อประสิทธิภาพการดูดซับสาร As(III) มากที่สุด ในขณะที่สาร NO_3^- และ SO_4^{2-} มีผลกระทบต่อประสิทธิภาพการดูดซับสาร As(III) อย่างไม่มีนัยสำคัญ ในระบบไอออนสาม (tri-solutes) และระบบไอออนสี่ (tetra-solutes) พบว่าประสิทธิภาพการดูดซับสาร As(III) มีค่าลดลงแตกต่างกันขึ้นอยู่กับ (1) แรงดึงดูดระหว่างตัวดูดซับกับตัวถูกดูดซับ (binding affinity) (2) ค่าคงที่อัตราการดูดซับของตัวถูกดูดซับ (observed adsorption rate constant) (3) ปฏิกิริยาระหว่างตัวถูกดูดซับ (interaction between adsorbates) (4) ผลกระทบของแรงดึงดูด หรือแรงผลักระหว่างประจุของตัวดูดซับและตัวถูกดูดซับ (electrostatic

attraction/repulsion between the adsorbent surface charge and adsorbates charge) นอกจากนี้ลักษณะพื้นผิว (morphology) ของสาร OS สาร COS ก่อนและหลังดูดซับสาร As(III) และแอนไอออน ได้ถูกนำไปวิเคราะห์ด้วยเทคนิค SEM จากภาพที่ได้จากการวิเคราะห์ SEM พบว่าลักษณะพื้นผิวของสาร COS เปลี่ยนจากลักษณะพื้นผิวที่มีรูพรุนเป็นลักษณะพื้นผิวที่แตกต่างกันขึ้นอยู่กับชนิดของตัวถูกดูดซับ (adsorbates) และจำนวนของตัวถูกดูดซับที่อยู่ในสารละลาย

สำหรับหัวข้อที่สอง (part B) ตัวดูดซับได้ถูกพัฒนาให้อยู่ในรูปของเม็ด เพื่อให้ง่ายต่อการแยกตัวดูดซับจากน้ำที่ผ่านกระบวนการบำบัดน้ำเสียแล้ว โดยนำเปลือกหอยนางรมและเถ้าแกลบ (RHA) มาเป็นวัตถุดิบในการเตรียมเม็ดสารดูดซับ OS-TRHA โดยในขั้นแรกได้นำ RHA มาทำการทรีตด้วยการเผาที่อุณหภูมิ 600°C เป็นระยะเวลา 13 ชั่วโมง เพื่อกำจัดสารปนเปื้อนที่อยู่ในเถ้าแกลบก่อนที่จะนำมาเตรียมเม็ดสารดูดซับ OS-TRHA ซึ่ง RHA ที่ผ่านการทรีตด้วยความร้อนเรียกว่า treated rice husk ash (TRHA) จากนั้น ชั่งสาร OS (ขนาด <106 ไมโครเมตร 106-150 ไมโครเมตร และ 150-250 ไมโครเมตร) และสาร TRHA แล้วนำมาผสมกับน้ำปริมาณเล็กน้อย ซึ่งส่วนผสมดังกล่าวจะถูกนำไปอัดเป็นเม็ดด้วยแม่พิมพ์โลหะ (metal mold) จากนั้นนำเม็ดที่ได้ไปเผาที่อุณหภูมิ 700°C เป็นระยะเวลา 8 ชั่วโมง และเรียกว่า เม็ดสารดูดซับ OS-TRHA โดยเม็ดสารดูดซับดังกล่าวจะถูกนำไปวิเคราะห์ด้วยเทคนิค XRD และ ทดสอบการละลาย (solubility test) จากผลการวิเคราะห์ พบว่า เม็ดสารดูดซับ OS-TRHA ประกอบด้วย สาร CaO สารแคลเซียมซิลิเกต ($CaSiO_3$) สารประกอบแคลเซียมซิลิเกตไฮเดรต (C-S-H compounds) ผลการทดสอบการละลาย พบว่าปริมาณสาร CaO ที่ละลายในสารละลายของเม็ดสารดูดซับ OS-TRHA ที่เตรียมจาก OS ในทุกช่วงขนาดอนุภาคที่ศึกษา มีปริมาณน้อยกว่าปริมาณ CaO ที่ละลายในสารละลายของสาร COS ที่เตรียมจากสาร OS ในช่วงขนาดอนุภาคเดียวกัน ในส่วนนี้ยังได้ศึกษาผลกระทบของขนาด OS และอัตราส่วนระหว่าง OS ต่อ TRHA ต่อความคงรูป (stability) ของเม็ดสารดูดซับ OS-TRHA และประสิทธิภาพในการกำจัดสาร As(III) ที่ปนเปื้อนในน้ำเสียสังเคราะห์ จากผลการทดลอง พบว่าเม็ดสารดูดซับ OS-TRHA ที่เตรียมจาก OS ขนาดเล็กกว่า 106 ไมโครเมตร ในอัตราส่วน OS ต่อ TRHA เท่ากับ 0.7 ต่อ 0.3 เหมาะสมที่สุดในการเตรียมเม็ดสารดูดซับ OS-TRHA โดยที่เม็ดสารดูดซับดังกล่าวมีความสามารถในการดูดซับสาร As(III) สูงสุด (maximum adsorption capacity) ประมาณ 26.10 มิลลิกรัมต่อกรัม ลักษณะพื้นผิวของเม็ดสารดูดซับ OS-TRHA ก่อน และหลังการทดลอง การดูดซับสาร As(III) ได้ถูกวิเคราะห์ด้วยเทคนิค SEM โดยผลการวิเคราะห์ด้วย XRD SEM และผลการทดลองการดูดซับสาร As(III) พบว่า เม็ดสารดูดซับ OS-TRHA สามารถแบ่งออกเป็น 2

ส่วนคือ (1) ส่วนที่เป็นสาร CaO ซึ่งสามารถทำการดูดซับสาร As(III) ในรูปของ Ca-As-O และ (2) ส่วนที่เป็นสาร $CaSiO_3$ และสารประกอบ C-S-H ซึ่งทำหน้าที่เป็นตัวประสาน (binder) อนุภาคสารที่อยู่ในเม็ดสารดูดซับ OS-TRHA เพื่อไม่ให้เกิดการแตกหักของเม็ดดังกล่าว สำหรับการศึกษาจลนพลศาสตร์การดูดซับ แบบจำลอง Pseudo-first order และแบบจำลอง Pseudo-second order ได้ถูกนำมาทำนายกับข้อมูลผลการทดลองการดูดซับ โดยผลการวิเคราะห์ พบว่า ข้อมูลผลการทดลองการดูดซับสาร As(III) สอดคล้องกับแบบจำลอง Pseudo-second order โดยที่ค่าคงที่อัตราการดูดซับโดยเฉลี่ยมีค่าเท่ากับ 0.0034 กรัมต่อ มิลลิกรัม นาที นอกจากนี้ Langmuir และ Frundlich ไอโซเทอร์ม ได้ถูกนำมาทำนายกับข้อมูลการดูดซับในช่วงที่กระบวนการดูดซับเข้าสู่สภาวะสมดุลเพื่อศึกษาลักษณะการดูดซับของสาร As(III) บนเม็ดสารดูดซับ OS-TRHA ผลการวิเคราะห์ พบว่า ข้อมูลการทดลองสอดคล้องกับไอโซเทอมการดูดซับแบบ Langmuir มากกว่า ไอโซเทอมการดูดซับแบบ Frundlich นอกจากนี้จากการทดลองการนำเม็ดสารดูดซับ OS-TRHA ไปทำการดูดซับน้ำเสียสังเคราะห์ที่มีความเข้มข้นของสาร As(III) เท่ากับแหล่งน้ำปนเปื้อนในไทย ผลการทดลอง พบว่า เม็ดสารดูดซับ OS-TRHA สามารถกำจัดสาร As(III) ได้สูงถึง 98.95%

Thesis	Arsenite Removal from Synthetic Contaminated Water by using Calcined Oyster Shells and OS-TRHA Adsorbent Pellet
Student	Ms. Pichnipa Khownpurk
Student ID.	56601054
Degree	Doctor of Engineering
Program	Chemical Engineering
Year	2019
Thesis Advisor	Asst. Prof. Dr. Walairat Chandra-ambhorn

ABSTRACT

This research studies arsenite (As(III)) removal from synthetic contaminated water by using calcined oyster shells (COS) and OS-TRHA adsorbent pellet. In this research, the experiments were divided into two parts. In part A, COS was used as an adsorbent for removing As(III) from contaminated water. The COS was prepared by calcining oyster shells powder (OS) with particle size range of 150 - 250 micrometer at 700 °C for 8 h. The OS and COS were characterized BET, XRD, XRF and potentiometric mass titration method. The XRD and XRF results indicated that OS mainly composed of $CaCO_3$ while 97wt% of COS was CaO. The pH_{zpc} of COS is about 12.1. In this part, the effect of anions (NO_3^-, SO_4^{2-} and HPO_4^{2-}) on As(III) adsorption performances was studied. In addition, the observed adsorption rate constants of As(III) and anions adsorption on COS initially estimated by using the extended geometric method and the values of As(III) and anions occupied sites were solved by Runge-Kutta method. The result showed that, in bi-solutes, HPO_4^{2-} was strongly effect on As(III) adsorption performance. Meanwhile, NO_3^- and SO_4^{2-} insignificantly affected As(III) adsorption performances. In the cases of tri- and tetra-solutes, the As(III) adsorption performances decreased in the different values depending on (1) binding affinity between the adsorbent and adsorbates, (2) the observed adsorption rate constants of adsorbates, (3) the interaction between the adsorbates and (4) the

electrostatic attraction/repulsion between the adsorbent surface charge and adsorbates charge. Moreover, the morphologies of OS, COS before and after adsorbing As(III) and anions were observed by SEM. SEM images showed that morphology of COS changed from porous structure into the different morphologies depended on type of adsorbates and number of adsorbates containing in the solution.

For part B, the adsorbent was developed into pellets in order to be easily separated the adsorbent from treated water. The oyster shells and rice husk ash (RHA) were used as the raw materials for OS-TRHA adsorbent pellet preparation. Firstly, the RHA was treated by calcining at 600°C for 13 h in order to remove impurity which contained in RHA before OS-TRHA preparation. After heat treatment, RHA was called treated rice husk ash (TRHA). Then, the OS (particle size ranges of <106 μm, 106-150 μm and 150-250 μm) and TRHA were weighed and mixed with a few drops of water. The mixture was pelletized by a metal mould. The pellets were calcined at 700 °C for 8 h and named as OS-TRHA adsorbent pellets. The OS-TRHA adsorbent pellets were characterized by XRD and solubility test. The XRD result indicated that the OS-TRHA adsorbent pellets composed of CaO, $CaSiO_3$ and C-S-H compounds. Meanwhile, the solubility test indicated that the dissolving of CaO in OS-TRHA adsorbent pellets prepared from every observed OS particle size range was less than that in COS prepared from the same OS particle size rages. In this part, the effects of OS particle size rages and the ratios between OS:TRHA on the stability of OS-TRHA adsorbent pellets and As(III) removal performance were also studied. The results showed that the OS-TRHA adsorbent pellet prepared from OS particle size range of < 106 μm with OS:TRHA ratio of 0.7:0.3 is the best condition for OS-TRHA adsorbent pellet preparation. It could provide the As(III) maximum adsorption capacity about 26.10 mg/g. The morphologies of the OS-TRHA adsorbent pellets before and after As(III) adsorption tests were also observed by SEM. The XRD, SEM and As(III) adsorption results indicated that the OS-TRHA adsorbent pellet could be

classified into two parts. (1) CaO could adsorb As(III) in the form of Ca-As-O. (2) $CaSiO_3$ and C-S-H compounds could bind the precursors powder in the OS-TRHA adsorbent pellet to be stable without cracking. For the adsorption kinetics, pseudo-first order and pseudo-second order models were applied to the adsorption data. The result showed that the As(III) adsorption data were fitted with pseudo-second order model. The average observed adsorption rate constant was approximately 0.0034 g/mg min. Furthermore, Langmuir and Frundlich isotherms were applied to the equilibrium data to study the adsorption behavior of As(III) adsorption on the OS-TRHA adsorbent pellet. The result showed that the equilibrium data were fitted with Langmuir isotherm than Frundlich isotherm. In addition, the OS-TRHA adsorbent pellets were also used as the adsorbent to remove As(III) in synthetic contaminated water which has concentration equivalent to the contaminated water resources in Thailand. The result showed that the OS-TRHA adsorbent pellets could remove As(III) as high as 98.95%.

Acknowledgements

This thesis becomes to reality with the kind support and help of many individuals. I would like to extend my sincere thanks to all of them.

Firstly, I would like to express my sincere gratitude to my advisor Asst. Prof. Dr. Walairat Chandra-ambhorn for her patience, motivation, immense knowledge and the continuous support of my Ph.D study and related research. I really appreciate for her kindness, her patience and guidance. I cannot have imagined having a better advisor and mentor for my Ph.D study.

Besides my advisor, I would like to thank the staff of teachers and support staff at the Department of Chemical Engineering, Faculty of Engineering, King Mongkut's Institute of Technology Ladkrabang and the staff at the Center of Advance Instrument for Research in Engineering of King Mongkut's Institute of Technology Ladkrabang for their advice, instruction, knowledge and instruments that were very helpful and useful to this thesis.

I also would like to thank King Mongkut's Institute of Technology Ladkrabang for research funding and place to run the experiments.

Last but not least, I would like to thank my parents and my sister for supporting me spiritually throughout the research process and writing this thesis and also my life in general.

Pichnipa Khownpurk

Contents

Contents (Con't)

Contents (Con't)

Contents (Con't)

Contents (Con't)

Contents (Con't)

List of Tables

List of Tables (Con't)

Tables Page

List of Figures

List of Figures (Con't)

Figures Page

List of Figures (Con't)

List of Figures (Con't)

List of Figures (Con't)

Chapter 1

Introduction

1.1 Research background

Arsenic (As) is a metalloid that exists in various oxidation states such as -3, 0, +3 and +5. Arsenic contaminated in soil, mineral resources, air and water caused the human health and environmental problems. The long term toxicity of arsenic has been reported in terms of many types of cancers, i.e. skin, liver, bladder and kidney cancers, nerve tissue injuries, pigmentation change, neurological disorders, muscular weakness [1-4], Blackfoot disease [5],etc. It also has been reported that there are many areas around the world such as Argentina [6], Chile [7], Bangladesh [8], India [9], China [10], Vietnam [11] and Thailand [12, 13] affected by the toxicity of arsenic. In Thailand, it was reported that many areas of 25 provinces particularly in Suphanburi Province, Ubon Ratchathani and Nakorn Si Thammarat [14-18] were affected by the toxicity of arsenic.

When arsenic contaminates in water, it exists in the forms of arsenite (As(III)) and arsenate (As(V)). The toxicity, the mobility and the difficulty to remove from contaminated water of As(III) are much more than those of As(V) [12, 19-23]. Moreover, As_2O_3 is used in many industries e.g., agricultural pesticides, the glass industry and copper refining industry [24]. Thus, As(III) should be expected as the main form of arsenic contaminated in waste water and it needs to be removed from the contaminated water.

Several processes were applied in order to remove arsenic from contaminated water such as oxidation or/and reduction, precipitation, solid/liquid separation, reverse osmosis, biological removal process, adsorption, etc. [4].

Adsorption is the ubiquitous method used to eliminate arsenic from contaminated water because of its simplicity and low operating cost. There are many kinds of materials used as the adsorbent to remove arsenic from contaminated water such as char-carbon [25], iron oxide coated cement (IOCC) [26], activated red mud (ARM) [27], goethite [28, 29], copper (II) oxide nanoparticles [30], amorphous iron hydroxide (HFO) [29], activated carbon [25], etc.

Oysters are one favorite seafood in many countries causing about 4 million tons of waste oyster shells around the world [31]. In Thailand, oysters have been being cultivated in many areas in the eastern and southern of Thailand in order to trade in domestic and export. The consumption of oysters caused a lot of waste oyster shells. It was reported that the oyster shells could be used as landfill, soil fertilizer, poultry farming, additives in animal husbandry, cement-based brick, etc. [31-34]. However, it has been limited to use and remained as the environmental problem. In previous work, the oyster shells were ground, sieved and calcined at 700°C for 8 h. The calcined oyster shells (COS) was used as an adsorbent to remove As(III) from synthetic contaminated water. The adsorption results showed that COS could remove As(III) with maximum adsorption capacity of 195.5 mg/g (pH 11) [35]. However, in water resources, there are many species of ions contained in water. Those soluble ions containing in water such as sulphate (SO_4^{2-}), bicarbonate (HCO_3^-), carbonate (CO_3^{2-}), chloride (Cl^-), nitrate (NO_3^-), phosphate (HPO_4^{2-}, PO_4^{3-}), etc. may affect As(III) removal performance [19, 36-38]. Therefore, it is necessary to understand the effect of other ions containing in the contaminated water on As(III) adsorption performance.

Furthermore, after As(III) adsorption, the fine powder of COS was difficult to separate from treated water. Thus, COS adsorbent should be developed into the

form that could be easily separated from treated water. There are many methods used to solve this problem e.g. increasing the particle size of the adsorbent or transformation of the adsorbent powder into granules [39]. Pelletization is an alternative method that can also be used to solve this problem by combining the material which could remove As(III) (COS) with other compounds and shaping the mixture into the pellet. In this method, the shape and size of the adsorbent pellet can be controlled to be easier to separate from treated water.

Thailand is a rice industrial crops area and most of Thai people consume rice as the main dish thus there are plenty of rice husk waste. Almost rice husk is used as a fuel in many industrials causing a lot of rice husk ash (RHA) waste. It was reported that the potential global RHA production was approximately 70-78 million tons per year [40, 41]. It was also reported that RHA mainly composed of SiO_2 which was used in many processes such as concrete production, ceramic production, bio-fertilizer production, etc. [42]. However, RHA is still the environmental problem. In Thailand, there are also a lot of waste RHA causing the environmental problem and it also needs to be gotten rid of. Moreover, it was reported that amorphous SiO_2 could react with $Ca(OH)_2$, called pozzolanic reaction and form calcium silicate hydrate compound (C-S-H) which could improve the strength of concrete, mortar, compacted soil block, etc. [41-47]. Thus, in this work, RHA was used as a precursor for adsorbent pellet preparation.

1.2 The objectives of this study

The main objectives of this research are

(1) To remove As(III) from contaminated water by using the waste materials i.e. oyster shell powder (OS) and RHA as raw materials to prepare an adsorbent.

(2) To understand the effect of anions containing in contaminated water on As(III) removal performance.

(3) To develop COS adsorbent into the form that is easy to separate from treated water after water treatment process.

In order to achieve these main objectives, some sub-objectives can be determined:

(1.) To study the effect of anions i.e. NO_3^-, SO_4^{2-} and HPO_4^{2-} on As(III) removal by COS in bi-, tri- and tetra-solutes.

(2.) To study the adsorption kinetics of As(III) and anion(s) on COS in single-solute, bi-, tri- and tetra-solutes

(3.) To study the interfacial phenomena of As(III) and anion(s) adsorption on COS surface.

(4.) To determine the adsorbates interaction and adsorption kinetics of As(III) and anions on their adsorption performances in bi-, tri- and tetra-solutes.

(5.) To develop the As(III) adsorbent into the pellet in order to be easily separated from treated water after used by using OS and RHA as raw materials.

(6.) To determine the most appropriate particle size range of OS for preparation of OS-TRHA adsorbent pellet to remove As(III) from contaminated water.

(7.) To determine the most appropriate ratio of OS and treated rice husk ash (TRHA) for preparation of OS-TRHA adsorbent pellet to remove As(III) from contaminated water.

(8.) To study the adsorption kinetics and adsorption behavior of As(III) on OS-TRHA adsorbent pellet.

(9.) To study the mechanism of As(III) adsorption on OS-TRHA adsorbent pellet.

1.3 The scope of this study

This research studied about As(III) removal from contaminated water by using COS and OS-TRHA adsorbent pellet. The experiments were performed by batch tests. In this work, the experiments of As(III) removal from contaminated water were

classified into two parts. The first part studied the effect of anions i.e. NO_3^-, SO_4^{2-} and HPO_4^{2-} on As(III) removal performance in bi-, tri- and tetra-solutes by using COS as the adsorbent. In this part, the properties of COS such as solubility, pH_{zpc}, chemical composition and surface morphologies were determined. The precipitation between Ca^{2+} and As(III) or anions, the adsorption kinetics and the mechanism of As(III) and anions adsorption on COS were also investigated. In adsorption kinetics of As(III) and anions adsorption on COS, the observed adsorption rate constants of As(III) and anion(s) in single-solute, bi-, tri- and tetra-solutes were determined by extended geometric method proposed by Azizian et al. [48, 49] to evaluate the appropriate initial guess values for solving the rate equations by forth order Runge-Kutta method [50, 51]. Furthermore, the interfacial phenomena of As(III) and anions adsorption on COS surface, the adsorbates interaction and the effect of observed adsorption rate constants of As(III) and anions on their adsorption performances were also studied and discussed.

The second part focused on the process to fabricate COS which is the fine powder into the pellet in order to be easier to separate from the treated water. In this part, OS and RHA were used as the raw materials for preparation oyster shell powder-treated rice husk ash (OS-TRHA) adsorbent pellet. The best condition for OS-TRHA adsorbent pellet preparation was determined. The OS-TRHA adsorbent pellets were characterized by XRD. The solubility, stability and As(III) adsorption capacity of OS-TRHA adsorbent pellets were performed by batch tests. The morphologies of OS-TRHA adsorbent pellets before and after As(III) adsorption tests were also observed by SEM. Furthermore, the mechanism of As(III) adsorption on OS-TRHA adsorbent pellet was proposed. The adsorption kinetics and adsorption isotherms were also investigated. In addition, the amount of $CaSiO_3$ and C-S-H compounds contained in OS-TRHA adsorbent pellet was determined. Moreover, OS-TRHA adsorbent pellets were used to eliminate As(III) from the synthetic contaminated water which contained As(III) concentration as in water resources in Thailand.

Chapter 2

Literature reviews

2.1 Arsenic

2.1.1 Arsenic contamination

Arsenic (As) is a metalloid that widespread in nature. Arsenic releases in the environment through weather, volcanism and geological process. Then, it can contaminate in atmosphere, ores, rock, soil sediment and water [52-55]. Some arsenic compounds that were found in the environment are presented in Table 2-1.

Table 2-1 Some arsenic compounds in the environment [12].

Name	Formula or structure
Methylarsine	CH_3AsH_2
Dimethylarsine	$(CH_3)_2AsH$
Trimethylarsine	$(CH_3)_3As$
Monomethylarsonic acid	$CH_3AsO(OH)_2$
Monomethylarsenous acid	$CH_3As(OH)_2$
Dimethylarsinic acid	$(CH_3)_2AsO(OH)$
Dimethylarsenous acid	$(CH_3)_2AsOH$
Trimethylarsinic oxide	$(CH_3)_3AsO$
Tetramethylarsonium ion	$(CH_3)_4As^+$
Arsenobetaine	$(CH_3)_3As^+CH_2COO^-$
Arsenocholine	$(CH_3)As^+CH_2\ CH_2OH$

It was reported that arsenic was used in many processes e.g. mining and smelting, fertilization, tannin and wood preservation, pesticide and herbicide, coal combustion, ceramic process and animal feed additive [54, 56, 57] as shows in Table 2-2. These processes caused the arsenic contaminated in environment.

Table 2-2 The applications of arsenic and its compounds [58].

Composition	Chemical formula	Application
Lead arsenate	$PbHAsO_4$	pesticide
Cupric arsenite	$Cu(AsO_2)_2$	Dye
Cupric acetoarsenate	$Cu(C_2H_3O_2)_2 \cdot 3\ Cu(AsO_2)_2$	pesticide
3-nitro-4hydroxy phenylarsonic acid	$C_6H_6AsNO_6$	Animal feed additive and veterinary medicines
Arsenilic acid	$C_6H_8AsNO_3$	animal feed additive
Arsenic oxides	As_2O_3 and As_2O_5	glass-making
Metallic arsenic	As	metallurgical
Arsenamide	$C_{11}H_{12}AsNO_5S_2$	Veterinary medicines
Potassium arsenite	$KAsO_2$	glass-making

Due to its high toxicity and carcinogenicity [12], arsenic is a serious worldwide problem. The long term toxicity of arsenic has been reported in terms of many type of cancers such as skin, liver, bladder and kidney cancers, nerve tissue injuries, pigmentation change, neurological disorders, muscular weakness [1-4], Blackfoot disease [5], etc. It was also reported that more than 100 million people around the world were affected by toxicity of arsenic [1, 3-5, 7]. The World Health Organization (WHO), the US Environmental Protection Agency (USEPA) and the European Commission have set the guideline of the maximum drinking standard as 10 µg/L. However, many reserchers reported that the amount of arsenic contaminated in water of many countries around the world (Table2-3) was greater than the standard limit [2, 11, 59-62]. In Thailand, many areas of 25 provinces were also affected by the toxicity of arsenic e.g. Suphanburi Province, Ubon Ratchathani and Nakorn Si Thammarat [14-18].

Table 2-3 The reported areas affected by the toxicity of arsenic contaminated in water (only in Asia) [12].

Location	Water resources	Concentration (µg/L)
Bangladesh	Well water	<10-> 100
Calcutta, India	Near pesticide production plant	<50-23,080
West Bengal, India	Arsenic-rich sediment	3-3700
Nepal	Drinking water	8-2660
Hanoi, Vietnam	Arsenic-rich sediment	1-3050
Xinjiang, PR China	Well water	0.05-850
Shanxi, PR China	Well water	0.03-1.41
Inner Mongolia, China	Drinking water bore	1-2400
Ronpibool, Thailand	Water contaminated by tin mining waste	1-500
Nakhon Si Thammarat Province, Thailand	shallow (Alluvial) groundwater, mining	1.25-5114
Fukuoka, Japan	Natural origin	0.001-0.293
Mekong River floodplain, Cambodia	Deep ground water	1-1340

2.1.2 Classification of arsenic

Arsenic can be classified into three groups depending on its physical properties, chemical properties and toxicity as shows in Figure 2-1 [63].

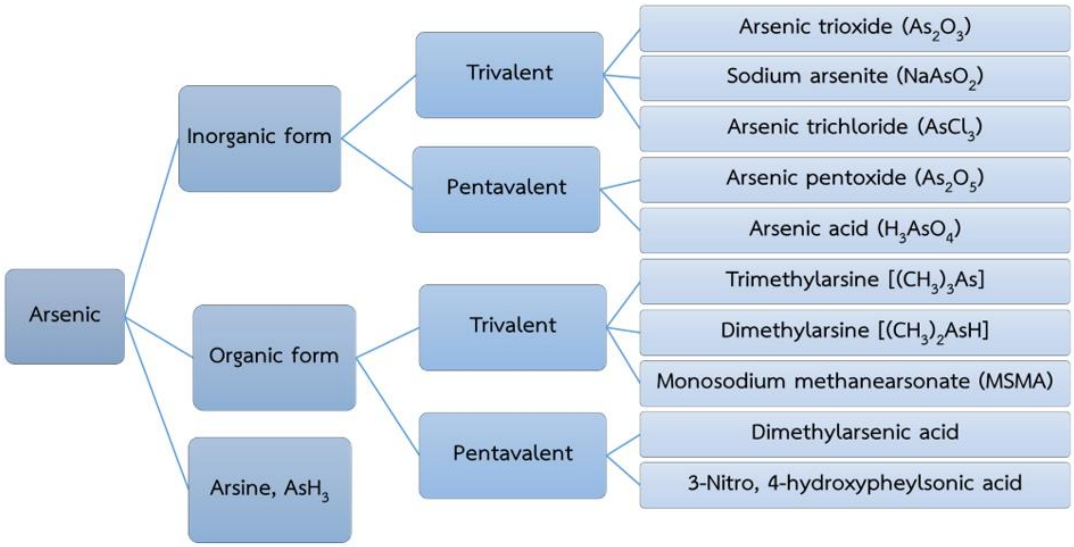

Figure 2-1 The classification of arsenic compounds.

As seen in Figure 2-1, arsenic can be divided into three main groups depending on its physical and chemical properties; inorganic compounds, organic compounds and arsine gas. The inorganic and organic compounds can be further classified into trivalent and pentavalent compounds. The trivalent compounds which has oxidation state equivalent to +3 is called arsenite (As(III)) such as As_2O_3, trimethylarsine, sodium arsenite, etc. The pentavalent compounds that has oxidation state equivalent to +5 is named as arsenate (As(V)) e.g. arsenic pentoxide, arsenic acid, dimethylarsenic acid, disodium methylarsenate, arsanilic acid, sodium arsanilate, etc. The toxicity of arsenic depends on its species. The toxicity of inorganic species is greater than that of organic species [12]. As(III) compounds are more toxic than As(V) compounds [12, 21]. The greater toxicity of As(III) is related to its high affinity to born with sulfhydryl groups of biomolecules such as glutathione (GSH), lipoic acid and the cysteinyl residues of many enzyme [64]. The formation of As(III)-sulfur bonds results in various harmful effects i.e. inhibiting the activities of enzymes such as glutathione reductase, glutathione peroxidases and thioredoxin peroxidase [65-67]. In addition, the mobility and the difficulty to remove of As(III) are also greater than that of As(V) [21, 62].

2.1.3. Effect of pH on arsenic species

pH is a logarithmic scale that is used to measure concentration of H^+ or H_3O^+ containing in the solution in order to specify the acidity or basicity of the aqueous solution. pH values of solution can be calculated as in Equation (2-1).

$$pH = -\log [H^+] \tag{2-1}$$

In aqueous solution, the acid substances can ionize or dissociate as Reaction (2-2). The ability or tendency to lose H^+ of the ion during the dissociation process is called acid strength.

$$AH_{(aq)} \longleftrightarrow A^-_{(aq)} + H^+_{(aq)} \tag{2-2}$$

where AH is acid substance that can dissociate into conjugate base of acid (A^-) and hydrogen ion (H^+) that can further combine with water molecule in the form of hydronium ion (H_3O^+).

If the dissociation process reaches equilibrium, acid dissociation constant (K_a) can be also calculated as in Equation (2-3).

$$K_a = \frac{[H^+][A^-]}{[AH]} \tag{2-3}$$

K_a value is written in the form of logarithmic constant as in Equation (2-4)

$$pK_a = -\log [K_a] \tag{2-4}$$

Considering Equations (2-1), (2-3) and (2-4), the relation of pH and pK_a values can be written as in Equation (2-5).

$$pH = pK_a + \log\left(\frac{[A^-]}{[AH]}\right) \tag{2-5}$$

when $[A^-] = [AH]$, pH should be approximately equivalent to pK_a.

When As(III) and As(V) dissolved in solution, it dissociated into various forms depending on pH of the solution as shown in Reactions (2-6) – (2-11) [12].

$$As(OH)_3 \longleftrightarrow As(OH)_2O^- + H^+ \quad pK_a = 9.2 \quad (2\text{-}6)$$

$$As(OH)_2O^- \longleftrightarrow As(OH)O_2^{2-} + H^+ \quad pK_a = 12.1 \quad (2\text{-}7)$$

$$As(OH)O_2^{2-} \longleftrightarrow AsO_3^{3-} + H^+ \quad pK_a = 12.7 \quad (2\text{-}8)$$

$$AsO(OH)_3 \longleftrightarrow AsO_2(OH)_2^- + H^+ \quad pK_a = 2.3 \quad (2\text{-}9)$$

$$AsO_2(OH)_2^- \longleftrightarrow AsO_3(OH)^{2-} + H^+ \quad pK_a = 6.8 \quad (2\text{-}10)$$

$$AsO_3(OH)^{2-} \longleftrightarrow AsO_4^{3-} + H^+ \quad pK_a = 11.6 \quad (2\text{-}11)$$

2.2 Adsorption process

In order to eliminate the contaminated substances from contaminated water, several methods were applied in water treatment process such as oxidation or/and reduction, precipitation, ion-exchange, coagulation, electrocoagulation, co-precipitation, solid/liquid separation, reverse osmosis, biological removal process, adsorption, etc. [1, 4].

Adsorption is the widespread method used in the water treatment because it is simplicity to handle, has low operating cost and high efficiency. In this process, the atoms, ions or molecules of liquid solutes (adsorbates or adsorptive) deposit or accumulate on the sorption sites and form molecular or ionic or atomic film on the surface of the adsorbent [68].

2.2.1. Classification of adsorption process

Adsorption process can be classified into two types depending on strength of binding forces between adsorbent and adsorbates.

1) Physisorption or physical adsorption.

The adsorbate bonds with adsorbent via weak van der Waal's forces, hydrogen bonding [69]. In physisorption, the adsorbates are not specific to be adsorbed on the sorption sites of the adsorbent. It means that the adsorbates can be adsorbed on the surface of adsorbent, although the adsorbent surface does not consist of the functional group. Then, those adsorbates can be adsorbed on the adsorbent surface with multilayer (Figure 2-2 (a)). The bonding energy between adsorbates and adsorbent is in the range of 10-70 kJ/mol [70]. Due to the low bonding energy, the physisorption process should be reversible reaction and easy to be desorbed.

2) Chemisorption or chemical adsorption

The adsorbates are adsorbed on the specific sorption sites on the adsorbent surface. It means that the adsorbates can be adsorbed only on the sorption sites which contained functional group that can form the bonding with those adsorbates. Thus, the adsorbates are adsorbed on the adsorbent surface with monolayer (Figure 2-2 (b)). The bonding between adsorbates and adsorbent is electrostatic bonding, covalent bonding and co-ordinate displacements [69]. Therefore, the bonding energy between those adsorbates and sorption sites in chemisorption (200 – 500 kJ/mol) is much greater than that of the physisorption [70]. Due to the high energy bonding, the chemisorption process should be irreversible reaction or less be desorbed.

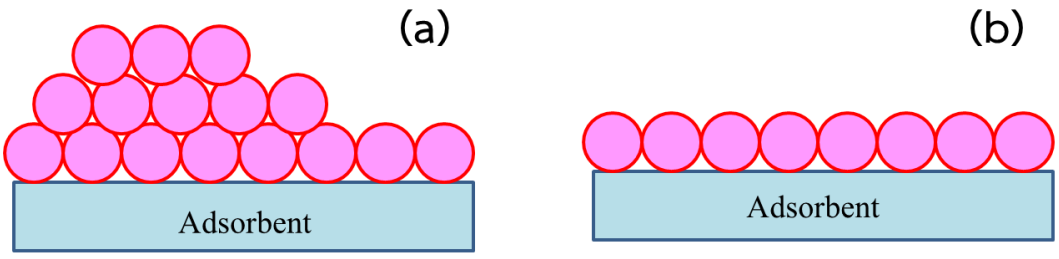

Figure 2-2 Types of adsorption process; (a) physisorption and (b) chemisorption.

2.2.2. Factors influencing adsorption

The adsorption process is affected by several factors i.e. nature of adsorbent, surface area of adsorbent, pH of solution, nature of adsorbate, mixed solutes, agitation speed and temperature.

1) Nature of adsorbent

As mentioned before, the adsorption process is an interfacial phenomenon of adsorbent surface. Then, chemical and physical properties of the adsorbent such as selectivity, chemical composition, sorption sites, chemical structure, morphology, crystallinity, surface area, porous structure, pore size of the adsorbent, etc. can affect adsorption performance. Lenoble et al. [71] who studied about arsenic removal by synthesized iron (III) phosphate in the forms of crystalline and amorphous structures reported that As(III) adsorption capacity of amorphous iron (III) phosphate (21 mg/g) was greater than that of crystalline form (16 mg/g). This should be because the specific surface area of amorphous iron (III) phosphate (53.6 ± 0.8 m^2/g) was greater than that of the other one (35.9 ± 0.5 m^2/g). In addition, As(III) could be adsorbed on the iron (III) phosphate both in crystalline and amorphous forms greater than As(V). It means that the sorption sites of iron (III) phosphate tend to adsorb As(III) than As(V). Furthermore, Bang et al.[72] and Bang et al.[73] works showed that silicate and PO_4^{3-} strongly interfered with arsenic removal by iron hydroxide but those ions were insignificantly interfered with arsenic removal by TiO_2 at neutral pH. This should be because the chemical and physical properties of those adsorbents are different causing the different adsorption capacities of silicate, PO_4^{3-} and arsenic on those adsorbents. In the case of iron hydroxide, the capabilities to adsorb silicate and PO_4^{3-} were greater than that of arsenic causing the strong interference of those ions on arsenic removal. In contrast, the TiO_2 sorption sites were preferably to adsorb arsenic than those of silicate and PO_4^{3-}. Then, the arsenic adsorption performances by using TiO_2 as an adsorbent were insignificantly interfered by those ions.

2) Nature of adsorbate

In adsorption process, the solute (adsorbate) contained in solution should dissociate from the solute-solvent bonding before being adsorbed on the sorption sites containing on the adsorbent surface. If the solubility of solute is greater, the solute-solvent bond is stronger. Then, it is more difficult to break the solute-solvent bond causing the lower adsorption performance. Furthermore, the structure of adsorbate is also the one affecting adsorption performance. If the adsorbate has bigger molecular size and greater weight, the adsorption performance will increase. In addition, the adsorption performance of the branched chain structure adsorbate is also greater than that of the straight chain structure adsorbate [74].

3) pH of solution

pH of solution affects species of adsorbate and the surface charge of adsorbent. As mentioned above, when pH of solution increased, the species of As(III) can be deprotonated by OH^- containing in the solution and change into the different forms depending on pH of solution. Thus, the mechanisms of those As(III) species are different and causing the various adsorption performances. Furthermore, pH of solution also affects the surface charge of the adsorbent surface. In some kinds of adsorbent, its surface can protonate or deprotonate with water when the adsorbent contacted with the solution causing the temporary positive or negative surface charge on the adsorbent surface. The positive surface charge of adsorbent is preferable to adsorb anions (negative charge) while the negative surface charge of adsorbent better adsorbs the cations (positive charge).

4) Temperature

Temperature is one factor that should be determined in the adsorption process. As previously mentioned, the physisorption is a reversible process. The adsorbate bonds with sorption sites via weak van der Waal's forces which has low

energy bonding. Thus, the increase in temperature can break the adsorbent-adsorbate bonding causing the lower adsorption performance. However, the chemisorption needs more energy to bond. The higher the temperature, the more energy of adsorbates to bond with the sorption sites on adsorbent surface causing the increase in adsorption performance. In addition, the increase in temperature also causes the increase in adsorption rate.

5) Mixed solutes

In water resources, there are many kinds of ions containing in water and some of them can interfere adsorption performance. Some ions cause the increase in the adsorption performance while some ions cause the decrease in the adsorption performance. Maiti et al. [75] who studied arsenic removal by raw laterite (RL) and treated laterite (TL) reported that, when the solution contained Mg^{2+}, Ca^{2+}, Fe^{2+} (prepared from $MgCl_2$, $CaCl_2$, $FeCl_2{\cdot}4H_2O$, respectively), adsorption performances of both As(III) and As(V) increased. Meanwhile, As(III) and As(V) adsorption performances decreased when the solution contained PO_4^{3-} and silicate (prepared from NaH_2PO_4, $Na_2SiO_3{\cdot}9H_2O$, respectively). The interference of ions containing in solution on the adsorption performance depending on many factors e.g. nature of adsorbent, interaction between adsorbates, the affinity between adsorbent and adsorbates, etc. Therefore, the effect of ions containing in water resources on adsorption performance should be determined.

6) Agitation speed

During the adsorption process, the adsorbates containing in solution move from bulk solution, pass through the film (film diffusion) which covers the adsorbent surface and be adsorbed on the sorption sites. Meanwhile, some of them move forward into the pore of adsorbent and penetrate to the sorption sites containing in the porous of adsorbent. Agitation influences the distribution of the solute (adsorbates) in the bulk solution. It also affects the formation of external film

boundary that covers the adsorbent surface. The increase in agitation speed can reduce the thickness of the film boundary layer surrounding the adsorbent particle causing the increase of adsorption rate.

7) Contact time

In adsorption process, several mechanisms such as external mass transfer, particle diffusion and chemical reactions would occur and take time to proceed. The different adsorbent materials and adsorbate species require the different contact time in the adsorption process. Then, the contact time of the adsorption process is also necessary to determine in order to provide the greatest adsorption performance.

2.2.3. Adsorption capacity

The As(III) adsorption capacity, q_t (mg of adsorbate/g of adsorbent) is calculated by the following equation:

$$q_t = \frac{(C_0 - C_e)V}{W} \qquad (2\text{-}12)$$

where C_0 and C_e are As(III) concentration remaining in the solution at initial time and at equilibrium time (mg/L), respectively. V is the volume of solution (L) and W is mass of adsorbent used (g).

2.2.4. Adsorption kinetics

In order to determine the adsorption kinetics of As(III) and anions on the adsorbents, pseudo-first order model, pseudo-second order model and extended geometric method were studied.

1) Pseudo-first order model

Pseudo-first order model was presented by Lagergren (1898) [76-79]. The equation of this model is presented as the following.

$$\frac{dq_t}{dt} = k_{a,1}(q_e - q_t) \quad (2\text{-}13)$$

The linear form of pseudo-first order model can be expressed as in Equation (2-14)

$$\ln(q_e - q_t) = \ln q_e - k_{a,1}\, t \quad (2\text{-}14)$$

where q_t and q_e are the amount of As(III) adsorbed at time t and equilibrium (mg/g), respectively. $k_{a,1}$ is adsorption rate constant of pseudo-first order (1/min).

2) Pseudo second order model

Pseudo-second order model was presented by Ho[80, 81]. This model is expressed as the following equation.

$$\frac{dq_t}{dt} = k_{a,2}(q_e - q_t)^2 \quad (2\text{-}15)$$

The linear form of pseudo-second order model is written as in Equation (2-16)

$$\frac{t}{q_t} = \frac{1}{k_{a,2}q_e^2} + \frac{1}{q_e}t \quad (2\text{-}16)$$

where $k_{a,2}$ is adsorption rate constant of pseudo-second order (g /mg min).

3) Extended geometric method

Extended geometric method was proposed by Azizian et al.[48, 49] This model proposed that the adsorption kinetics followed Langmuir–Freundlich equation. This model explained that if the solution containing substance A which is removed via the adsorption process. The adsorption, desorption and overall rates of substance A can be written as the following Equations.

Adsorption rate: $r_a = k_a C(1-\theta)^n$ (2-17)

Desorption rate: $r_d = k_d \theta^n$ (2-18)

Overall rate: $\frac{d\theta}{dt} = r_a - r_d = k_a C(1-\theta)^n - k_d \theta^n$ (2-19)

where r_a, r_d are adsorption rate and desorption rate, respectively, k_a and k_d are adsorption rate constant and desorption rate constant, respectively. θ is the fraction of sorption sites covered by substance A ($0 \leq \theta \leq 1$) and n is a constant which represents the heterogeneity. It is noted that, for the Langmuir isotherm, n is equivalent to 1.

Since the concentration of substance A in the bulk solution decreased by adsorption of substance A on the sorption sites of the adsorbent, therefore

$$C = C_0 - \beta\theta \tag{2-20}$$

where C_0 is the initial concentration of substance A (mg/L) and β is a constant defined as in Equation (2-21).

$$\beta = \frac{W_c q_m}{M_A V} \tag{2-21}$$

where W_c is mass of adsorbent (g), q_m is the maximum capacity of the adsorbent (mg/g), M_A is molecular weight of substance A (g/mol) and V is volume of solution (L).

Considering Equations (2-19) and (2-20), the overall rate can be written and be rearranged as in Equations (2-22) and (2-23), respectively.

$$\frac{d\theta}{dt} = k_a(C_0 - \beta\theta)(1-\theta)^n - k_d\theta^n \tag{2-22}$$

$$\frac{d\theta}{dt} = k_a C_0 (1-\theta)^n - k_d\theta^n - k_a\beta\theta (1-\theta)^n \tag{2-23}$$

When the substance A is adsorbed on the sorption sites, the adsorption result is presented as in Figure 2-3.

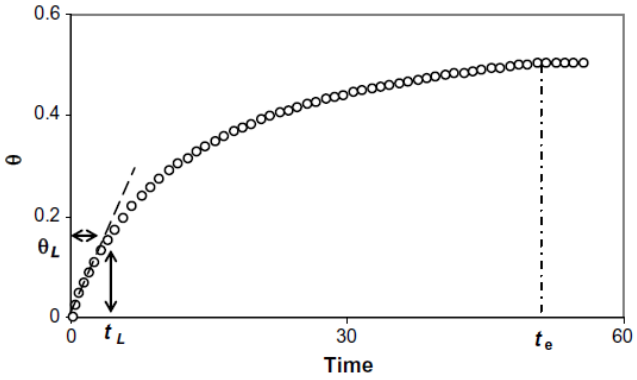

Figure 2-3 The variation of θ with time for the synthetic kinetic data [48].

As seen in Figure 2-3, at initial adsorption period, θ increases linearly with time. The slope of the linear line in Figure 2-3 is k_0. Considering the linear region, the integration of Equation (2-23) for the boundary conditions at t=0, θ =0 and at t=t_L, $\theta = \theta_L$ is

$$\int_0^{\theta_L} d\theta = \int_0^{t_L} \left(k_a C_0 (1-\theta)^n - k_d \theta^n\right) dt - \int_0^{t_L} \left(k_a \beta \theta (1-\theta)^n\right) dt \qquad (2\text{-}24)$$

Considering Equations (2-17) - (2-19), the synthetic kinetic data of adsorption rate, desorption rate and $k_a C_0(1-\theta)^n$ are illustrated in Figure 2-4.

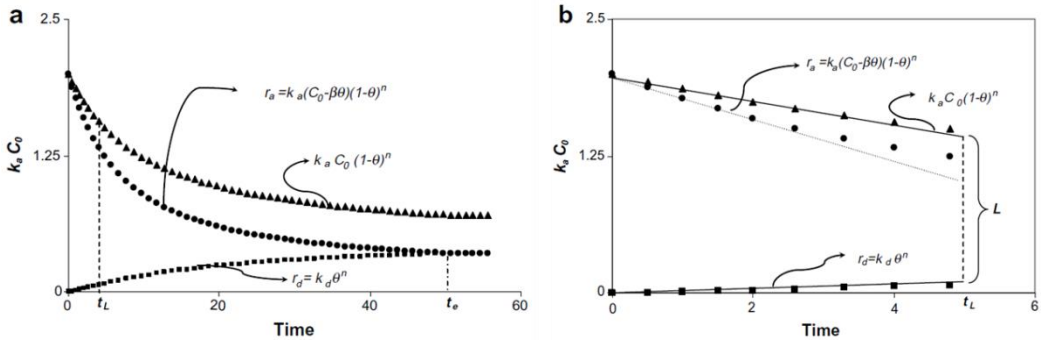

Figure 2-4 Variation of overall rate components, r_a, r_d and $k_a C_0(1-\theta)^n$ with time for the synthetic kinetic data (a) up to the equilibrium time (b) up to t_L [48].

Considering at t=0 to t=t_L in Figure 2-4(b), the first term on the right hand of Equation (2-24) is the area of trapezoid so this term can be substituted by the geometric area of trapezoid as in Equation (2-25).

$$\int_0^{t_L}\left(k_a C_0(1-\theta)^n - k_d\theta^n\right)dt \approx \frac{1}{2}t_L(k_a C_0 + L) \qquad (2\text{-}25)$$

The value of L in Equation (2-25) can be defined by using the similarity of two triangle as shown in Figure 2-5.

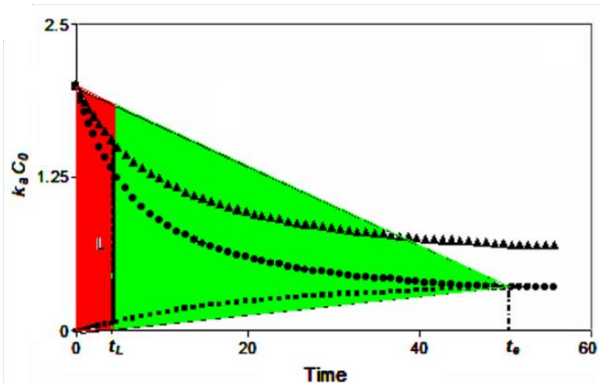

Figure 2-5 Variation of overall rate components, r_a, r_d and $k_a C_0(1-\theta)^n$ with time for the synthetic kinetic data up to the equilibrium time with representing of triangles (''green'' and ''green+red'' triangles) for L value estimation [48].

Then, Equation (2-25) can be rewritten as the following.

$$\int_0^{t_L}\left(k_a C_0(1-\theta)^n - k_d\theta^n\right)dt \cong \frac{1}{2}t_L k_a C_0\left(2-\frac{t_L}{t_0}\right) \qquad (2\text{-}26)$$

Considering the linear region in Figure 2-3, $\theta = k_0 t$ and $\theta_L = k_0 t_L$. The second term on the right hand and the left hand term can be calculated (at t=0, θ =0 and at $t=t_L$, $\theta = \theta_L$) by Equations (2-27) and (2-28), respectively.

$$\int_0^{t_L}\left(k_a\beta k_0 t(1-k_0 t)^n\right)dt \approx k_a\beta\left(\frac{1}{2}k_0 t_L^2 - \frac{n}{3}k_0^2 t_L^3 + \frac{n(n-1)}{8}k_0^3 t_L^4\right) \qquad (2\text{-}27)$$

$$\theta_L = k_0 t_L \qquad (2\text{-}28)$$

After substituting Equations (2-26) - (2-28) into Equation (2-24) and rearranging it, the adsorption rate constant and desorption rate constant can be calculated as in Equations (2-29) and (2-30), respectively.

$$k_a = \frac{k_0}{C_0\left(1 - \frac{t_L}{2t_e}\right) - \beta k_0 t_L\left(\frac{1}{2} - \frac{n}{3}k_0 t_L + \frac{n(n-1)}{8}k_0^2 t_L^2\right)} \quad (2\text{-}29)$$

$$k_d = \frac{k_a}{K} \quad (2\text{-}30)$$

2.2.5. Adsorption isotherms

The adsorption process relates with interfacial interaction between adsorbent and adsorbate. The process reaches equilibrium with different time and provides the different adsorption capacity depending on the type of adsorbent and species of adsorbate. Thus, the adsorption behavior of adsorbates on the adsorbent is necessary to study. The adsorption isotherm experiment is useful for describing the adsorption behavior and adsorption capacity of the different adsorbent used to estimate the other information such as the appropriate adsorbent, the regenerate adsorbent, etc. Then, those data can also be used to develop the water treatment process. There are two isotherms that well known and are used in this work.

1) Langmuir isotherm [82-87]

Langmuir isotherm was proposed by Irving Langmuir in 1916 [87]. In this model, the number of available adsorption sites or vacant sites on the surface of adsorbent are fixed. All these available sites are equivalent e.g. size, shape, etc. The adsorbates take place at the specific homogeneous sorption sites on the adsorbent surface. Thus, those adsorbates are monolayer adsorbed on the sorption sites. There is no significant interaction among adsorbates species adsorbed on the sorption sites. The equation of Langmuir isotherm is given in Equation (2-31).

$$q_e = \frac{q_m K_L C_e}{1 + K_L C_e} \quad (2\text{-}31)$$

The linear form is expressed as the following.

$$\frac{1}{q_e} = \frac{1}{q_m} + \frac{1}{K_L q_m C_e} \quad (2\text{-}32)$$

where C_e is equilibrium concentration (mg/L). K_L is Langmuir equilibrium adsorption constant. A plot between $1/q_e$ and $1/C_e$ gives a straight line. The values of K_L and q_m are calculated from the slope and the intercept, respectively.

2) Freundlich isotherm [82, 83, 88, 89]

Freundlich isotherm was proposed by Freundlich in 1909 [90]. This model was proposed that the adsorbates were adsorbed on the heterogeneous surface of adsorbent. The pattern of adsorption on the surface is non-specific and the energy distribution of adsorption over the surface is non-uniform. Due to the non-specific adsorption, the adsorbates can be multilayer adsorbed on the adsorbent surface. The equation of Freundlich isotherm is expressed as the following equation.

$$q = K_F C_e^{\frac{1}{n}} \quad (2\text{-}33)$$

The linear form is given in Equation (2-34).

$$\log q_e = \log K_F + \frac{1}{n} C_e \quad (2\text{-}34)$$

Freundlich adsorption constants, K_F and 1/n are related to adsorption capacity and intensity of adsorption, respectively. A plot between log q_e and log C_e gives a straight line with the slope 1/n and the intercept log K_F.

2.2.6. Runge-Kutta method [50, 51]

In this work, the Runge-Kutta method was used to investigate the observed adsorption rate constants. The theory of this method could be explained as the following.

In the case of single-solute, the form of differential equation is presented as in Equation (2-35)

$$\frac{dy}{dx} = f(x,y) \tag{2-35}$$

The value of y at $x = x_0$ is y_0. In order to calculate the value of y at some value of x (x_f) which is greater than x_0, initially, the interval between x_0 and x_n is divided in to N segments as in Equation (2-36).

$$\frac{x_f - x_0}{N} = \Delta x = h \tag{2-36}$$

The value of h is called step size. Since x is changed by $\Delta x = h$, the change of y can be denoted as Δy. The approximate value of the derivative on left-hand side of Equation (2-35) is

$$\frac{dy}{dx} \cong \frac{\Delta y}{\Delta x} = \frac{\Delta y}{h} \tag{2-37}$$

Considering Equation (2-37), the value of y when $x = x_n$ is y_n, and f is the average of f(x,y) over the interval between x_n and x_{n+1}. Thus, when $x = x_{n+1}$, the value of y_{n+1} can be calculated as in Equation (2-38).

$$y_{n+1} = y_n + \bar{f} \times h \tag{2-38}$$

In this wok, the value of $\bar{f}$ can be calculated by using the forth-order Runge-Kutta method as in Equation (2-39).

$$\bar{f} = \frac{1}{6}(f_1 + 2f_2 + 2f_3 + f_4) \tag{2-39}$$

The parameters of f_1, f_2, f_3 and f_4 can be evaluated as follows

$$f_1 = f(x_n, y_n) \tag{2-40}$$

$$f_2 = f\left(x_n + \frac{h}{2}, y_n + \frac{hf_1}{2}\right) \tag{2-41}$$

$$f_3 = f\left(x_n + \frac{h}{2}, y_n + \frac{hf_2}{2} \right) \quad (2\text{-}42)$$

$$f_4 = f\left(x_n + h, y_n + hf_3\right) \quad (2\text{-}43)$$

In the case of bi-solutes which simultaneously adsorbed on the sorption sites, the forms of differential equation are presented as in Equations (2-44) and (2-45).

$$\frac{dy}{dx} = f\left(x, y, z\right) \quad (2\text{-}44)$$

$$\frac{dz}{dx} = g\left(x, y, z\right) \quad (2\text{-}45)$$

Thus, the forth-order Runge-Kutta method can also be expressed as shown below.

$$y_{n+1} = y_n + \bar{f} \times h \quad (2\text{-}46)$$

$$z_{n+1} = z_n + \bar{g} \times h \quad (2\text{-}47)$$

$$\bar{f} = \frac{1}{6}\left(f_1 + 2f_2 + 2f_3 + f_4\right) \quad (2\text{-}48)$$

$$\bar{g} = \frac{1}{6}\left(g_1 + 2g_2 + 2g_3 + g_4\right) \quad (2\text{-}49)$$

The parameters of f_1, f_2, f_3, f_4, g_1, g_2, g_3 and g_4 can be evaluated as follows.

$$f_1 = f\left(x_n, y_n, z\right)_n \quad (2\text{-}50)$$

$$g_1 = g\left(x_n, y_n, z_n\right) \quad (2\text{-}51)$$

$$f_2 = f\left(x_n + \frac{h}{2}, y_n + \frac{hf_1}{2}, z_n + \frac{hg_1}{2} \right) \quad (2\text{-}52)$$

$$g_2 = g\left(x_n + \frac{h}{2}, y_n + \frac{hf_1}{2}, z_n + \frac{hg_1}{2} \right) \quad (2\text{-}53)$$

$$f_3 = f\left(x_n + \frac{h}{2}, y_n + \frac{hf_2}{2}, z_n + \frac{hg_2}{2} \right) \quad (2\text{-}54)$$

$$g_3 = g\left(x_n + \frac{h}{2}, y_n + \frac{hf_2}{2}, z_n + \frac{hg_2}{2} \right) \quad (2\text{-}55)$$

$$f_4 = f\left(x_n + h, y_n + hf_3, z_n + hg_3\right) \quad (2\text{-}56)$$

$$g_4 = g\left(x_n + h, y_n + hf_3, z_n + hg_3\right) \quad (2\text{-}57)$$

2.3 Raw materials for adsorbent preparation

In this work, oyster shells and rice husk ash were used as the raw materials for adsorbents preparation to remove As(III) from contaminated water.

2.3.1 Oyster shells

The expansion of shore ostreaculture in the eastern and southern of Thailand caused a lot of waste oyster shells. It was reported that the oyster shells could be used in many processes e.g. landfill, soil fertilizer, poultry farming and additives in animal husbandry, the active filler in a bio-contact oxidation tank, cement- based brick, substitute in mortar, concrete production, etc. [31-34, 91-94]. However, it has limited to use and remained as the environmental problem. More than 90% of oyster shells is $CaCO_3$ [95-97] (Table 2-4) which can be used in water treatment process. It was reported that oyster shells and adsorbents prepared from oyster shells could remove heavy metals such as boron, lead (Pb^{2+}), cadmium (Cd^{2+}), zinc (Zn^{2+}), iron (Fe), phosphate, copper (Cu^{2+}) nickel (Ni^{2+}) and chromium (Cr^{3+}) from contaminated water [31, 91, 96-101].

Table 2-4 The compositions contained in oyster shells [97].

$CaCO_3$ (%)	SiO_2 (%)	MgO (%)	Al_2O_3 (%)	SrO (%)	P_2O_5 (%)	Na_2O (%)	SO_3 (%)	Total (%)
95.99	0.70	0.65	0.42	0.33	0.20	0.98	0.73	100

In previous work, the oyster shells were ground and calcined at 700°C for 8 h. COS was used as the adsorbent to remove As(III) contaminated water. The results showed that COS could remove As(III) contaminated water with maximum adsorption capacity of 195.5 mg/g (pH 11) [35]. In order to determine the adsorption rate of As(III) adsorption on COS, pseudo-first and pseudo-second order models were investigated. The experimental data fitted with pseudo-second order adsorption rate with the

average adsorption rate constant of 0.00024 g/mg·min. Furthermore, the equilibrium data of As(III) adsorption on COS were also determined by Langmuir and Freundlich isotherms. The result showed that the adsorption behavior of As(III) on COS sorption sites was better described by Langmuir adsorption isotherm.

2.3.2 Rice husk ash (RHA)

Rice husk ash is a by-product from rice production process. It was reported that rice husk was produced more than 70 million tons around the world in each year [40, 41, 43]. In Thailand, rice is the most important agricultural product because it is a staple food for Thai people and a main export product of the country. Thus, a lot of rice husk is produced every year. Most of it is used as fuel in many industrials causing a lot of RHA waste. It was reported that RHA was used in many processes such as the raw material to produce bio-filter for waste water treatment, adsorbent, soil stabilizer, insecticide, bio-fertilizer production, silica gel production, ingredient in lithium batteries, graphene production, a composite in polypropylene production, activated carbon, raw material of zeolite production, semiconductor production, etc.[42, 102, 103]. However, it is still the environment problem that needs to be solved. It was reported that, after calcination process, RHA mainly composed of silica [42, 104] which is useful in many processes. The form of silica containing in RHA depends on calcined temperature during the calcination process [40, 43]. It was also reported that when RHA was calcined at temperature below 800°C, silica containing in RHA was in the form of amorphous structure that could be used in concrete production, cement admixture, and filler in rubbers, plastics and polymers [41-43, 104-106]. When the calcined temperature was greater than 800°C, the amorphous silica structure changed into the crystalline structure that could be used in steel, thermal insulator, refractory brick and ceramic production [42, 45, 105, 107, 108]. In addition, it was also reported that the amorphous silica could react with $Ca(OH)_2$; called pozzolanic reaction; and form calcium silica ($CaSiO_3$) and Calcium–Silicate–Hydrated (C–S–H) compounds that could increase the strength of materials [41-44, 46, 106, 109-111].

2.4 Pelletization

Pelletization is an agglomeration process that transforms the fine powder and added mixtures such as binder, filler, lubricant, separated agent, etc. into a small, spherical or semi-spherical shape [112-114]. This technique can control shape and size of samples (pellet). The pellet formation and growth can occur in several ways depending on types of equipment and production processes. The classification of palletization process is illustrated in Figure 2-6.

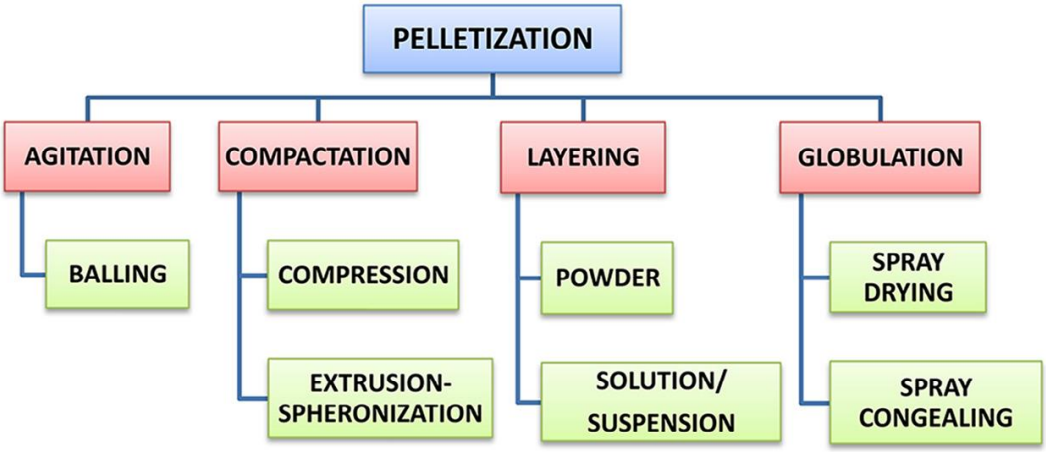

Figure 2-6 The classification of pelletization techniques [112].

In this work, OS-TRHA adsorbent pellets were prepared by using compression technique. The precursor powders were blended and put into a metal mold shown in Figure 2-7. Then, the pressure was applied to those samples by using a mechanical force to generate the well-define shape and size. At high pressure, the force against between the precursor particles undergo the elastic and plastic was deformed causing the compaction of precursor powder.

Figure 2-7 The metal mold for OS-TRHA adsorbent pellets preparation.

The cross-sectional and plan views of OS-TRHA adsorbent pellets are illustrated in Figure 2-8.

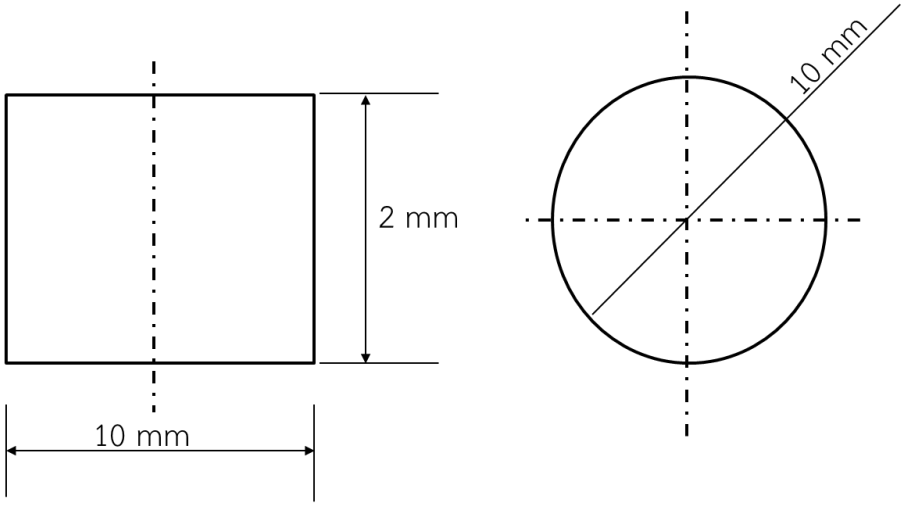

Figure 2-8 Cross-sectional and plan views of OS-TRHA adsorbent pellets.

2.5 Adsorbents characterization

In this work, the crystalline of adsorbents before and after adsorption tests was determined by using X-ray diffraction, while the morphologies of adsorbents before and after adsorption tests were also observed by a scanning electron

microscope. In addition, pH zero point of charge (pH_{zpc}) of COS adsorbent was determined by potentiometric mass titration method.

2.5.1 X-ray diffraction (XRD) [115-117]

X-ray diffraction (XRD) is a nondestructive analysis technique for crystalline materials characterization. The X-ray diffractometer is presented in Figure 2-9.

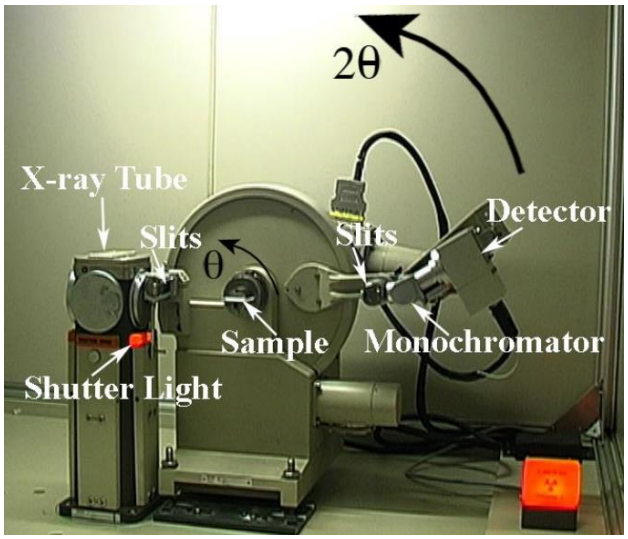

Figure 2-9 X-ray diffractometer [118].

As seen in Figure 2-9, X-rays is generated in X-ray tube. Then, those X-rays are filtered by crystal monochrometer (slits) in order to produce the monochromatic X-rays that is needed for diffraction. The monochromatic X-rays (incident rays) are collimated and directed on the sample. After those X-rays attack the sample, some of them scatter (diffract) to the detector. When the sample and the detector are rotated in the various θ and 2θ, respectively, the intensities of the reflected X-rays (diffraction ray or scattered ray) are recorded and converted into a count rate and output to a device.

As described before, when the X-rays attack on the sample, some of them scatter from the sample as shows in Figure 2-10.

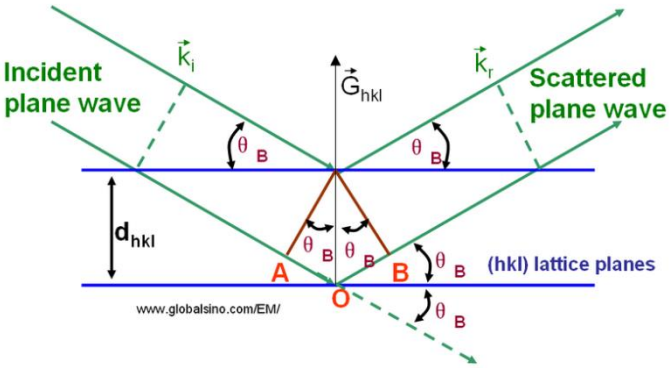

Figure 2-10 The visualization of the Bragg's law [119].

As seen in Figure 2-10, when the incident rays (incident waves) from the X-ray tube attack the sample, some of them can interact with atoms containing in the sample and scatter in the different angle depending on types of atom containing in the sample. The relation of the incident rays and the scattered rays (scattered waves) could be explained by Bragg's law as in Equation (2-58).

$$2d\sin\theta = n\lambda \tag{2-58}$$

where λ is the wavelength of X-rays, n is an integer, d is the interplanar spacing (d-spacing) and θ is the X-ray angle.

In the crystalline compounds, the atoms containing in each compound arrange in the uniform pattern. When the incident waves attack on those atoms, it will scatter in the same pattern. The scattered pattern can be used to identify what types of atom containing in the compound and how they are arranging. The different types of atoms and the unique arranging pattern of those atoms in each compound cause the different scattered pattern of X-rays.

2.5.2 Scanning electron microscope (SEM) [120, 121]

Scanning electron microscope (SEM) is one type of electron microscope. The sample surface images are produced by scanning surface of sample with a focused beam of electrons. The schematic diagram of SEM is illustrated in Figure 2-11.

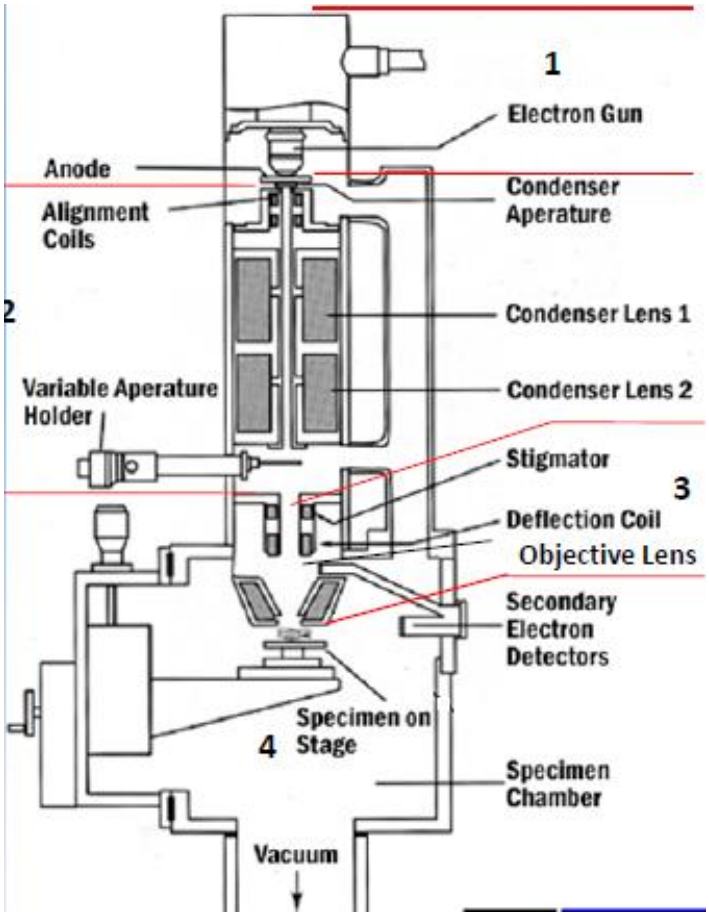

Figure 2-11 The schematic diagram of scanning electron microscope [120].

As seen in Figure 2-11, firstly, the electron gun generated a stream of electrons. Then, those electrons are accelerated toward the specimen by a positive electrical potential. After that the stream of electrons is confined and focused by metal apertures and magnetic lensed into a thin, focused and monochromatic beam. The focused electron beam attacks and scans across the surface of the sample. The interactions between electrons and sample generate secondary electrons. The secondary electrons are recorded by the detector and signal is changed into SEM images.

2.5.3 pH zero point of charge (pH_{zpc})

As mentioned before, pH of solution affects surface charge of adsorbent. Surface charge of oxide and hydroxide materials is the result of surface ionization

either protonation or deprotonation of amphoteric surface sites [122, 123]. Surface reactions could be written as follows.

$$MOH_{(surf)} + H^{+}_{(aq)} \longrightarrow MOH^{+}_{2(surf)} \quad (2\text{-}59)$$

$$MOH_{(surf)} + OH^{-}_{(aq)} \longrightarrow MO^{-}_{(surf)} + H_2O \quad (2\text{-}60)$$

where MOH and M stand for amphoteric surface sites and a metal, respectively. In this research, pH_{zpc} was determined by using potentiometric mass titration method. It was conducted by adjusting pH of 100 ml of 0.01 M NaCl solutions with 0.01 M of NaOH and/or HCl to the values between 2-13. After the adsorbent were added into each solution and the process reached equilibrium, the pHs of solution were measured. pH_{zpc} is the point where $pH_{initial}$ - pH_{final} = 0 [124-126]. If pH of solution is lower than pH_{zpc}, the net surface charge of the adsorbent will be positive charge and it can better attract anions (negative charge). Conversely, if pH of solution is greater than pH_{zpc}, net surface charge of the adsorbent will be negative charge which attracts toward cations (positive charge).

2.6 Determination of As(III) containing in solution by redox titration method [95, 127, 128]

In this work, As(III) containing in solution was analyzed by using redox titration method. In this work, $KMnO_4$ solution was used as a self-indicator titrant for As(III) concentration analysis. During the titration process, the purple color of dropped $KMnO_4$ changes into the colorless. When the titration process reaches the end point, the color of As(III) solution changes from colorless into pink solution as in Figure 2-12. The concentration of As(III) remaining in solution can be calculated by Equation (2-61).

$$5As_2O_3 + 4MnO^{-}_4 + 12H^{+} \longleftrightarrow 5As_2O_5 + 4Mn^{2+} + 6H_2O \quad (2\text{-}61)$$

Figure 2-12 The color of $KMnO_4$ solution (left) and the color of end-point As(III) solution (right).

2.7 Literature reviews

In this work, the oyster shells and rice husk ash (RHA) were used as raw materials for preparing the adsorbent to remove As(III) from contaminated water. Many researches relating with this work were reviewed.

Arsenic is a metalloid that spread in nature. Sharma and Sohn [12], Smedley and Kinniburgh [7], Nicolli et al. [6], Berg et al. [11], Williams et al. [13] Dhar et al. [8], Mandal et al. [9], and Yinlong [10] studied the arsenic contamination and its toxicity and reported that the toxicity of arsenic caused the human health and environment problems in many areas around the world such as Argentina, Chile, Bangladesh, India, China, Vietnam and Thailand. In Thailand, Pansamut and Wattayakorn [14], Siripitayakunkit et al. [15] Kohnhorst et al.[16] and Pattanapipitpaisal and Suraruk [17] reported that many areas of 25 provinces particularly in Suphanburi Province, Ubon Ratchathani and Nakorn Si Thammarat were affected by arsenic toxicity.

In 1994, Songsirikul [129] studied the effect of flood on arsenic contaminated in surface water at Amphoe Ron Phibun Nakhon Si Thammarat Province, Thailand and reported that the dissolving of arsenopyrite produced from Tin mining during the flood in 1988 caused the increase of arsenic concentration in the local water

resources. When people in that area consumed the contaminated water, the arsenic could accumulate in their body and cause the arsenic toxicity diseases. Mazumder [3], Mohan and Pittman [1], Ng et al. [2], Choong et al. [4] and Chen et al. [5] reported that the toxicity of arsenic caused the long term diseases such as Blackfoot disease, skin cancer, liver cancer, bladder cancer, pigmentation change, neurological disorders, etc.

When arsenic contaminated in water, it exists in two forms, As(III) and As(V). Phakdipin [130] who studied the ratio of As(III) : As(V) that existed in natural water by using ion chromatography to determine the concentration of As(III) and As(V) reported that, for 100 microliter of water sample, arsenic existed in the forms of As(III) and As(V) with the ratio of As(III) : As(V) approximately 1 : 20. In addition, Phakdipin [130] also reported that the toxicity of As(III) was about 25-60 times greater than that of As(V). Phakdipin [130] report agreed with Aposhian and Aposhian [64] and Sharma and Sohn [12] works which were reported that the toxicity of As(III) was greater than that of As(V) because the affinity between As(III) and sulfhydryl groups in biomolecules e.g. glutathione (GSH), lipoic acid, etc. was greater than that of As(V). In addition, Aposhian and Aposhian [64] and Sharma and Sohn [12] also reported that the formation of As(III)-sulfur bonds could inhibit the activities of enzymes such as glutathione reductase, glutathione peroxidases, thioredoxin peroxidase, etc. in human body causing the problems in the human health.

Several processes such as precipitation, oxidation-precipitation, coprecipitation, solid-liquid separation, etc. were applied in order to remove As(III) from contaminated water. In this work, adsorption process was chosen because it was easy to handle, the operating cost was low and the adsorbent could be found in the local area. Many kinds of adsorbent from synthetic materials like char-carbon [25], activated carbons [1, 38], carbon black [60], activated red mud (ARM) [27], iron oxide coated sand [131], iron oxide coated cement (IOCC) [26], or from low cost materials such as coconut husk carbon[132], soils [133], clays [1] and minerals [21, 28, 29, 62] have been applied to remove arsenic from contaminated water. In this work, oyster shells were

used as the raw material for adsorbent preparation to remove As(III) from contaminated water.

The oyster shells are a waste material that caused the environment problem and need to eliminate. Some researchers such as Tsai et al. [98], Kwon et al.[32], Xing et al. [134], and Li et al.[34] studied the properties of oyster shells and Treated oyster shells (TOS). In their works, the compositions of ground oyster shells (OS) and TOS were determined by X-ray fluorescence (XRF) technique while the crystalline compounds of those materials were characterized by X-ray diffraction (XRD). The XRD result of OS and TOS is presented in Figure 2-13.

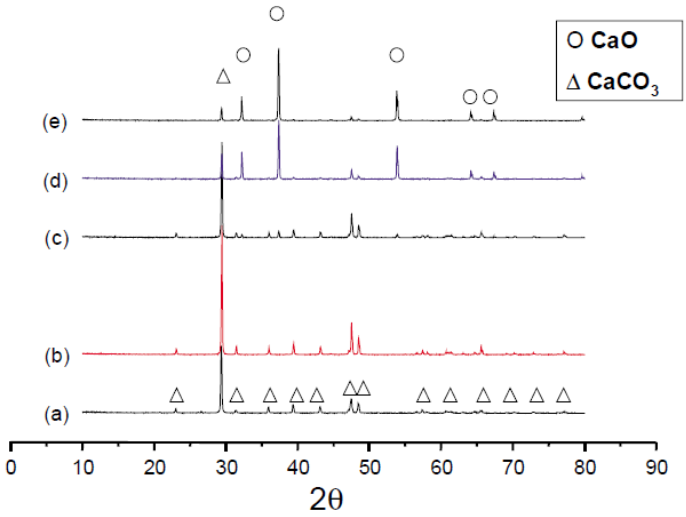

Figure 2-13 XRD patterns of (a) raw oyster shells (OS), (b) oyster shells heated under air atmosphere (TOS) at 750°C, (c), (d), and (e) the oyster shells pyrolyzed under nitrogen atmosphere at temperatures (TOS) of 650°C, 750°C, and 800°C, respectively [32].

Figure 2-13 shows that the peaks corresponding to $CaCO_3$ are detected in OS while the XRD peaks of CaO are observed in TOS which was prepared by heating or pyrolyzing OS. Based on XRF and XRD results, they reported that OS mainly composed of $CaCO_3$. When it was calcined or pyrolyzed (heating was carried out

under the presence of nitrogen) at high temperatures (650°C – 950°C), $CaCO_3$ in OS changed into CaO as in Reaction (2-62).

$$CaCO_3 \xrightarrow{\Delta} CaO + CO_2 \qquad (2\text{-}62)$$

Furthermore, Xing et al. [134] who studied the antifungal activities of scallop shells, oyster shells and their pyrolyzed products also reported that the calcination process caused the change of those shells morphologies. In their work, the scallop shells and oyster shells were calcined at 1050°C for 2 h. The morphologies of scallop shells, oyster shells and their pyrolyzed products were observed by SEM. SEM images are illustrated in Figure 2-14.

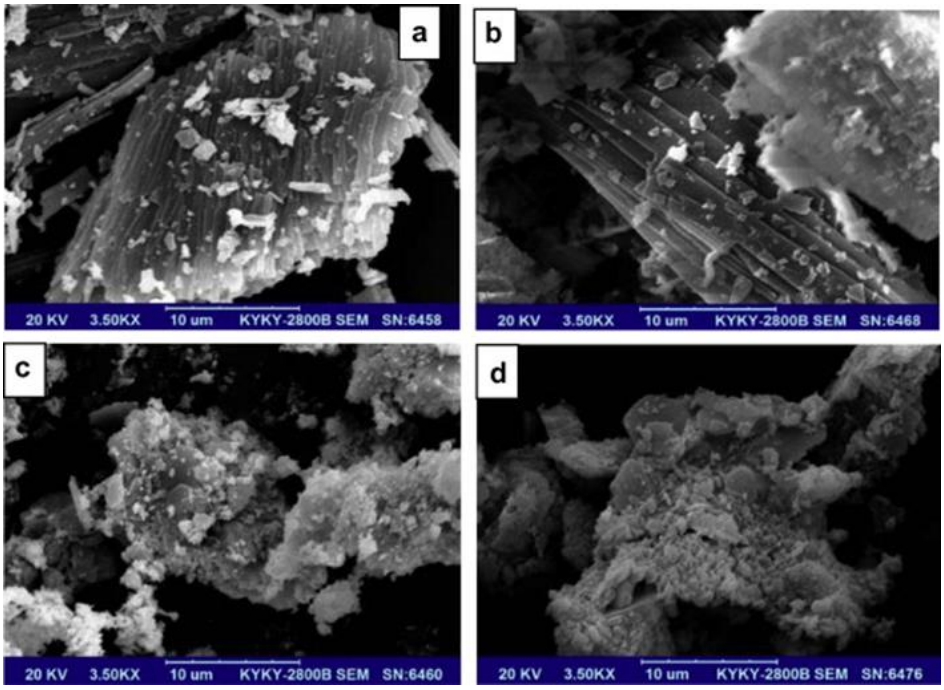

Figure 2-14 SEM images of (a) scallop shells (b) oyster shells before calcination process and (c) scallop shells and (d) oyster shells after calcination process [134].

As illustrated in Figure 2-14, before calcination process, the morphologies of scallop shells and oyster shells look like multilayer bars (Schistous) (Figure 2-14 (a) and (b)). After calcining those shells at 1050°C, the multilayer bars morphology

changed into the rough surface as in Figures 2-14 (c) and (d). Based on XRD and SEM results, they concluded that during the calcination process, $CaCO_3$ containing in scallop shells and oyster shells released CO_2 and transformed into CaO causing the morphologies change of those shells.

The calcined oyster shell (COS) was used in water treatment in order to remove the heavy metals and other hazardous substances such as lead (Pb), cadmium (Cd), iron (Fe) and copper (Cu) contaminated in water.

Wongpromrat and Suwanphapa [97] and Suthakulwirat et al. [100] studied lead (Pb), cadmium (Cd), iron (Fe) and copper (Cu) removal from contaminated water by using calcined oyster shells (COS) as an adsorbent. In their work, the COS was prepared by grinding and calcining the oyster shells at 700 °C in order to change $CaCO_3$ which was the main composition of oyster shells into CaO. In Wongpromrat and Suwanphapa [97] work, Pb, Cd, Fe and Cu removal tests were performed by batch tests. The initial concentrations of each ion in synthetic contaminated water were equivalent to 5 mg/L, 10 mg/L, 15 mg/L and 20 mg/L. They reported that COS could remove Pb, Cd, Fe and Cu from contaminated water for approximately 72.06%, 99.23 % 98.03 % and 97.01 %, respectively. Due to the high percentage of Cd removal in Wongpromrat and Suwanphapa [97] work, Suthakulwirat et al. [100] were further studied the adsorption and desorption rates of Cd removal by COS. In their work, the initial concentrations of Cd in the range of 170 mg/L - 200 mg/L were investigated. The concentrations of Cd in the samples were determined by using dithizone method. They reported that the Cd adsorption data correlated with Langmuir isotherm. The maximum Cd adsorption capacity of COS was about 1.208 g/g adsorbent. Furthermore, in their work, the adsorption and desorption rates of Cd were determined by the extended geometric method proposed by Azizian et al.[48, 49]. They found that the average adsorption and desorption rate constants of Cd were approximately 131.44 1/M-min and 828.06 1/M-min, respectively.

Moreover, Alidoust et al. [31] were also used the COS to remove Cd from aqueous solution. In their work, the results of oyster shells characterization showed that, after calcination of oyster shells at 652°C, solubility of cations (Ca^{2+}, Mg^{2+}) containing in COS increased. They reported that after OS was added into the solution, the final pH of solution was equivalent to 9.0. While, after COS calcined at 750°C was added into the solution, the final pH of solution increased from pH 9.0 to pH 12.7 because CaO in COS was greater reacted with water and formed $Ca(OH)_2$ which could further dissolve and dissociate into Ca^{2+} and OH^- than $CaCO_3$ in OS. Moreover, after calcination of OS at 750°C, 800°C and 900°C, BET results indicated that the surface area increased from 1.8 m^2/g to 64.6 m^2/g due to the formation of porous structure in COS during calcination process.

The Cd adsorption results indicated that the adsorbents used in their work could be classified by Cd adsorption performances into two groups. The first group was OS before calcination process, COS prepared by calcining OS at temperature 450°C and 650°C. Those adsorbents could adsorb Cd with the maximum adsorption capacities in the range of 25.5 mg/g - 32.36 mg/g. The other group was COS prepared by calcining OS at temperature 750°C, 850°C and 950°C that could provide the Cd adsorption capacities approximately 344.83 mg/g, 833.33 mg/g and 1,666.67 mg/g, respectively. The second group could remove Cd from aqueous solution greater than the first one because of the greater surface area and more CaO containing in their adsorbents. They found that for the calcination of OS at temperature 650°C, a few $CaCO_3$ transformed into CaO. The amount of CaO increased with the increasing in calcined temperature. When the calcined temperature reached 900°C, almost $CaCO_3$ transformed into CaO. They also found that Cd in the solution was removed by ion-exchanging with Ca^{2+}. They discussed that CaO containing in COS could dissolve and dissociate into Ca^{2+} and OH^- greater than $CaCO_3$. Thus, CaO should be easier to exchange ion with Cd than $CaCO_3$. In addition, they also reported that, when the calcined temperature of COS was greater than 750°C, the surface area of COS

significantly increased via the porous structure and sintering processes. The increase of surface area resulted in more contacted surface to react with Cd in the solution. The SEM images in Figure 2-15 show the morphologies of OS before calcination process, COS prepared by calcining OS at 650°C, 750°C and 900°C.

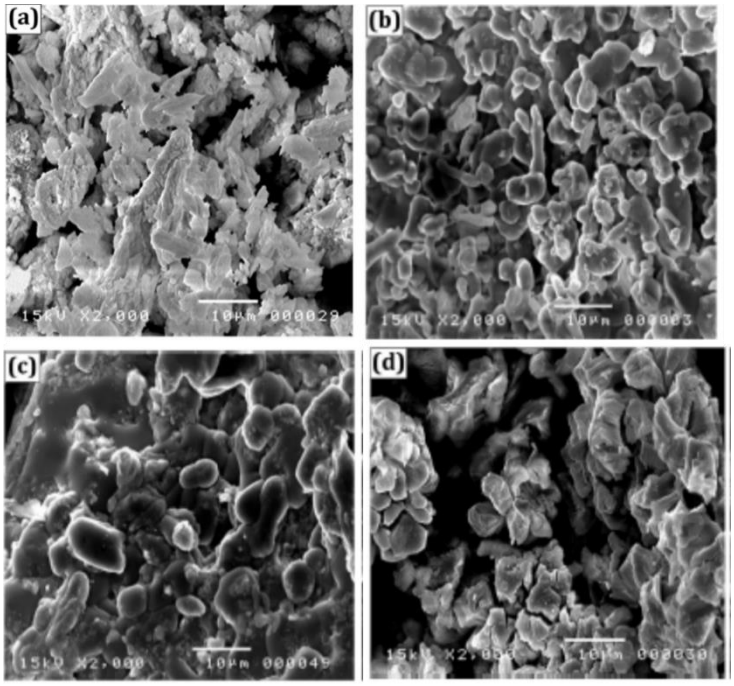

Figure 2-15 SEM images of (a) oyster shells before calcination process, COS prepared by calcining oyster shells at temperature (b) 650°C, (c) 750°C and (d) 900°C [31].

From the reports of Wongpromrat and Suwanphapa [97], Suthakulwirat et al. [100] and Alidoust et al. [31], COS was a CaO-rich material like lime which could be also used in water treatment. In Islam and Patel [135] work, ordinary and activated quick lime from dolomite mines areas (Birmitrapur, Orissa) were used to remove fluoride from aqueous solution. They reported that the activated quick lime which was treated by calcining quick lime at 450°C for 4 h could remove fluoride from aqueous solution greater than the ordinary quick lime. BET result showed that, after heat treatment, surface area of quick lime increased from 4.19 m^2/g to 11.75 m^2/g. In addition, SEM images also showed that, after heat treatment, the morphology of

ordinary quick lime in Figure 2-16 (a) changed into the morphology in Figure 2-16 (b). After fluoride adsorption test, the morphologies of activated and ordinary quick lime look like the small sphere particles covered on those surfaces as Figure 2-16 (c). They concluded that the calcination of quick lime in heat treatment process led to surface modification, structural transformation and loss of structural water molecules containing in the ordinary quick lime causing the increase of fluoride adsorption performance.

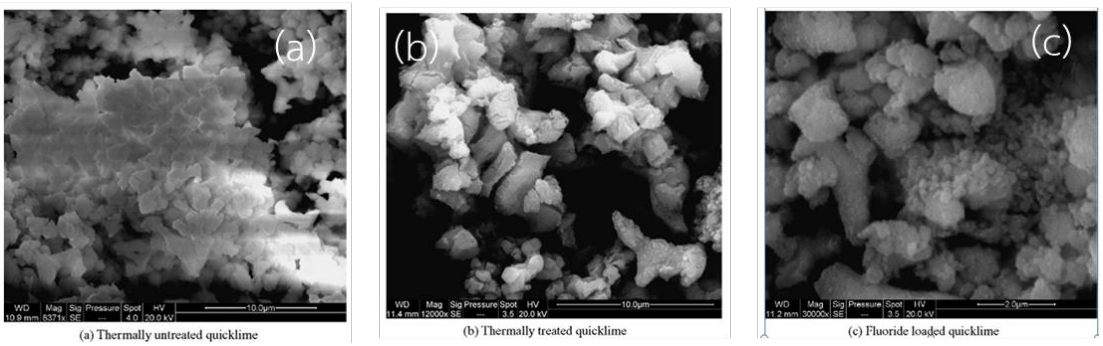

Figure 2-16 SEM images of (a) ordinary quick lime, (b) activated quick lime (c) quick lime after fluoride adsorption test [135].

Furthermore, they also reported that, after activated and ordinary quick lime were added into solution, pH of solution was always greater than 12. The result of Dubinin-Radushkevich (DR) adsorption isotherm indicated that fluoride should be adsorbed on the sorption sites by the ion exchange process. They also discussed that, after quick lime was added into the solution, CaO containing in quick lime changed into $Ca(OH)_2$. Some of it dissolved into the solution causing the increase in pH of solution while the remaining $Ca(OH)_2$ should react with fluoride ion and form CaF_2 which is an insoluble substance as in Reaction (2-63).

$$Ca(OH)_2 + 2F^- \longrightarrow CaF_2 + 2OH^- \qquad (2\text{-}63)$$

Moreover, they reported that some anions i.e. NO_3^-, SO_4^{2-} and HPO_4^{2-} affected fluoride adsorption performance. Their adsorption result showed that HPO_4^{2-} was greater affected fluoride adsorption performance than SO_4^{2-} and NO_3^-, respectively.

Furthermore, in Moon et al. [136], Dutŕe and Vandecasteele [137, 138] and Phenrat et al. [139] works, lime was used in solidification and stabilization processes in order to immobilize arsenic in the samples.

In Moon et al. [136] work, As(III) and As(V) were immobilized by lime and lime-kaolinite. In their work, aqueous lime–As suspensions (slurries) were prepared with five different Ca/As molar ratios (1:1,1.5:1, 2:1, 2.5:1 and 4:1) by using liquid to solid ratio of 10:1. The lime–As suspensions were kept for 4 days – 4 months. After that those samples were filtered and dried in air. They reported that As(III) immobilization was significantly increased with Ca/As ratio greater than 1:1 while As(V) immobilization was substantial increased with Ca/As ratio greater than or equal to 2.5:1. Moreover, they also found that As(III) and As(V) could react with lime and lime-kaolinite and further precipitated in the forms of Ca-As-O and $Ca_4(OH)_2(AsO_4)_2 \bullet 4H_2O$, respectively. Thus, Ca containing in lime should be the active sites for immobilization As(III) and As(V).

For Dutŕe and Vandecasteele [137, 138] and Phenrat et al. [139] works, lime and ordinary portland cement (OPC) were used to immobilize arsenic which contained in the fly ash and arsenic-iron sludge in solidification and stabilization process. Dutŕe and Vandecasteele [137, 138] prepared solidification and stabilization samples by casting mixture of lime, OPC, water and waste material (fly ash from metallurgical indusrty) which contained arsenic with the different recipes. Then, those samples were extracted by German standard methods for the examination of water, waste water, and sludge (DIN 38 414 S4). The leachates of those samples were filtered and analyzed for calcium, arsenic, antimony and lead by ICP–MS. They reported that, under the presence of an excess of $Ca(OH)_2$ and pH of solution was greater than

11.95, the precipitates of Ca^{2+} and As(III) and As(V) were detected in the forms of $Ca_3(AsO_4)_2$ and $CaHAsO_3$, respectively. The decrease of arsenic concentration containing in the leachate (mainly As(III)) was due to the formation of Ca-As precipitate ($CaHAsO_3$) which was an insoluble substance. The formation of insoluble $Ca_3(AsO_4)$ also caused the decrease of As(V) concentration containing in the leachate solution.

In Phenrat et al. [139] work, arsenic-iron sludge, portland cement and lime were weighed and mixed in various ratios. Then, the mixtures were casted into 5 mm diameter plastic pipe and kept for 3, 7, 14 and 28 days. The morphologies of those samples were observed by SEM while the compositions containing in those samples were analyzed by SEM-EDX. They found that arsenic immobilized in portland cement in the form of Ca-As compounds. The SEM images of calcium-arsenic (Ca-As) compounds containing in those samples are shown in Figure 2-17.

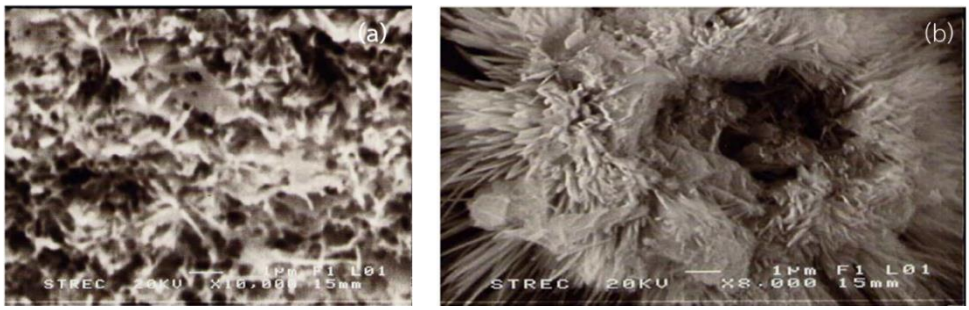

Figure 2-17 The SEM images of calcium-arsenic compounds at (a) 7 days and (b) 28 days [139].

In their work, the morphologies of Ca-As compounds were found into two forms. (1) Leafy crystal morphology (Figure 2-17 (a)) was observed on the sample at 7 days. This morphology was found in solidified/stabilized matrices of the sample. Thus, they discussed that it was supposed to form by precipitation between calcium and arsenic ions dissolving in pore fluid (the cement paste). (2) Grass-leaves like morphology or needle like shape morphology (Figure 2-17 (b)) was observed on the sample at 28 days. This morphology was detected at cement paste-sludge interface.

Due to many ions containing in water resources, those ions could affect As(III) removal tests. Many researchers studied the effect of anions on As(III) and As(V) adsorption performances such as Yu et al. [140] who studied As(III) and As(V) adsorption by Multi-amino functionalized cellulose and reported that, in bi-solutes system, under the presence of 30 mg/L of NO_3^- and SO_4^{2-} (prepared from $NaNO_3$ and Na_2SO_4), the As(III) and As(V) adsorption performances insignificantly changed. Thus, they concluded that the NO_3^- and SO_4^{2-} binding affinities for active sites were much weaker than those of As(III) and As(V). The effects of SO_4^{2-} and NO_3^- on As(V) adsorption performances in Yu et al. [140] work agreed with the result of Yang et al. [141] work.

In Yang et al. [141] work, the effects of anions i.e. Cl^-, NO_3^-, HCO_3^-, SO_4^{2-} and PO_4^{3-} (prepared from NaCl, $NaNO_3$, $NaHCO_3$, Na_2SO_4 and H_3PO_4, receptively) and cations i.e. K^+, Na^+, Ca^{2+} and Mg^{2+} (prepared from KCl, NaCl, $CaCl_2$ and $MgCl_2$, receptively) on As(V) adsorption performances were studied. In their work, the porous hematite was used as an adsorbent. They reported that, under the presence of anion in bi-solutes system, As(V) adsorption capacity strongly decreased when the solution contained PO_4^{3-}. In the case that HCO_3^- was combined in As(V) solution, the As(V) adsorption capacity slightly reduced and it insignificantly changed when As(V) combined with Cl^-, NO_3^- and SO_4^{2-}. They discussed that PO_4^{3-} was the greatest inhibition of As(V) adsorption on porous hematite because the chemical properties of As(V) and PO_4^{3-} were similar. Furthermore, when HCO_3^- contained in the solution, the solution became weak alkaline which was unfavorable for As(V) adsorption causing the slightly decrease in As(V) adsorption capacity. In the case of cation, they reported that K^+ and Na^+ insignificantly affected As(V) adsorption performance while the As(V) adsorption capacity increased when the solution contained Ca^{2+} and Mg^{2+} because Ca^{2+} and Mg^{2+} could precipitate with As(V).

Maiti et al. [75] also studied the effects of anions and cations on As(III) and As(V) adsorption performances. In their work, initially, As(III) and As(V) were removed

by raw laterite from four local areas in India; Kharagpur (West Bangal, KRL) Sonamukhi (Bankura, West Bangal, BRL) Manbazar (Purulia, West Bangal, PRL1) and Purulia city (Purulia, West Bangal, PRL2). They found that KRL could remove As(III) and As(V) greater than the others. Then, KRL was used as an adsorbent for removing As(III) and As(V) under the presence of anions and cations. pH of solution was in the range of 6.7 - 7.3. For As(III) and As(V) removal under the presence of anions, Cl^-, NO_3^-, HCO_3^-, SO_4^{2-}, PO_4^{3-}, chromate and silicate with common cation Na^+ were individually added into As(III) or As(V) solution. They reported that PO_4^{3-}, chromate and silicate strongly interfered on As(III) and As(V) adsorption. In the case of PO_4^{3-}, they discussed that the chemical behavior of arsenic species similar to that of PO_4^{3-} like Yang et al. [141] work. However, Cl^-, NO_3^-, HCO_3^-, SO_4^{2-} were slightly interfered on both As(III) and As(V) adsorption performance as the adsorption results in Yu et al. [140] and Yang et al. [141] works. In Maiti et al. [75] work, the effect of HCO_3^- on As(V) adsorption performance was stronger than that of As(III). They discussed that, when HCO_3^- contained in the solution, the pH of solution became more alkaline causing the negative adsorbent surface charge. Thus, As(V) in the form of negative charge could be less adsorbed on the adsorbent.

In the case cations, Ca^{2+}, Mg^{2+} and Fe^{2+} with common anion Cl^- were also individually added into As(III) or As(V) solution. They reported that, when the solution contained Ca^{2+} Mg^{2+} and Fe^{2+}, both As(III) and As(V) adsorption performances increased. The effects of Ca^{2+} and Mg^{2+} on As(III) and As(V) adsorption performances in Maiti et al. [75] work agreed with the adsorption results in Yang et al. [141] work. In the case of Ca^{2+}, they discussed that Ca^{2+} could adsorb As(III) and As(V) and co-precipitate on the adsorbent surface. For Fe^{2+}, it could be adsorbed on the KRL surface and cause the increasing of As(III) and As(V) adsorption performances.

In addition, in their work, under the presence of anions mixed with cations, they reported that the adsorption performances of As(III) and As(V) were lowest when the solution contained HCO_3^-, PO_4^{3-} and silicate. Conversely, when the solution

contained Ca^{2+}, HCO_3^-, SO_4^{2-}, PO_4^{3-} and silicate, the adsorption performances of As(III) and As(V) became positive effect.

As the adsorption results in Yu et al. [140], Yang et al. [141] and Maiti et al. [75] works, some anions strongly interfered with As(III) and As(V) adsorption performances. Thus, many researchers such as Rajapaksha et al.[133] and Guan et al. [142] tried to discuss and explain the interfering of those anions on As(III) and As(V) adsorption.

In Rajapaksha et al.[133] work, the effects of NO_3^-, SO_4^{2-} and PO_4^{3-} on arsenic removal by natural red earth (NRE) which consisted of Fe_2O_3 and Al_2O_3 were studied. They reported that As(III) and As(V) adsorption performances strongly decreased when the solution contained PO_4^{3-}. The effect of PO_4^{3-} on As(V) adsorption performance was greater than that of As(III) because PO_4^{3-} could be adsorbed on the sorption sites in the form of bidentate binuclear like As(V) (Figures 2-18 (a) and (b)), while As(III) formed monodentate mononuclear with the sorption sites as shown in Figure 2-18 (c).

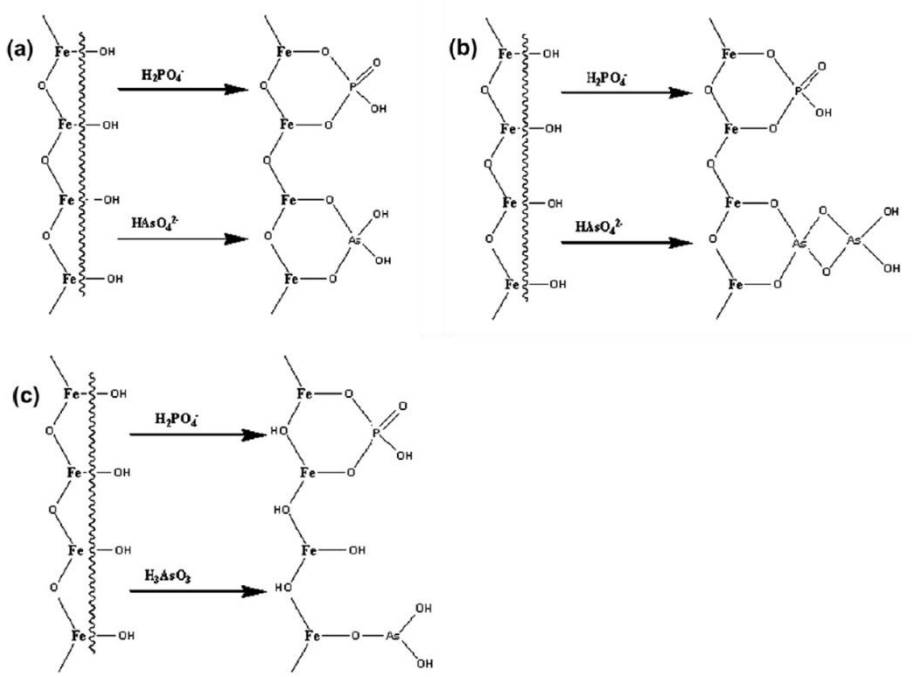

Figure 2-18 Adsorption mechanisms of (a), (b) As(V) and PO_4^{3-} and (c) As(III) and PO_4^{3-} on the sorption sites [133].

Guan et al. [142] also studied the effect of competitive ions on As(III) removal in $KMnO_4$-Fe(II) process. The As(III) containing in the solution was oxidized by $KMnO_4$ in order to change As(III) into As(V) and further removed by adsorption on Fe(II). They reported that, in the case of SO_4^{2-} with initial concentration of 50-100 mg/L, the percentages of arsenic removal negligibly changed at pH 4-5 but it decreased by 6.5% - 36% over pH 6-9. They discussed that (1) SO_4^{2-} binding affinity on ferric hydroxide or alumina containing in the adsorbent was much weaker than As(V) [143] binding affinity; (2) in the case of As(V) which had weak affinity, SO_4^{2-} could compete and occupy in those active sites. In the case of phosphate ion (its form was depending on pH as in Figure 2-19), under the presence of phosphate (1 mg/L), the percentages of arsenic removal over pH 4-6 decreased by 29.8 - 47.3%. At pH 7-9, the percentages of arsenic removal dramatically dropped from 48 - 87% to 5.6 – 9%. In addition, they also found that phosphate could precipitate with Fe(III). In this case, they discussed that (1) phosphate had similar structure and deprotonation constants as As(V). These similarities caused the competition between phosphate and As(V) to be adsorbed on the same active sites. (2) Phosphate could inhibit the forming of Fe precipitate and reduction of surface sites causing the decrease of As(III) removal in $KMnO_4$ -Fe(II) process.

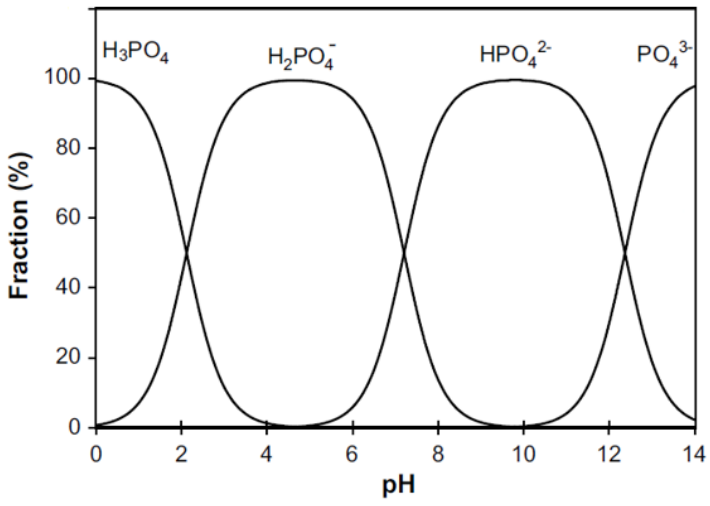

Figure 2-19 Species distribution diagram of phosphate with pH [142].

Moreover, in some researches, the electrostatic attraction and repulsion effects were used to explain the adsorption results and the effects of anions on the adsorption process.

Park et al. [144] who studied Cd(II) removal from aqueous solution by activated biochar (torrefied loblolly pine) reported that Cd(II) adsorption performance increased with increasing of pH (from pH 3 to 8) because of the electrostatic attraction effect. They discussed that, when pH of solution was lower than pH 3, the solution contained more amount of H_3O^+ that could compete Cd^{2+} to be adsorbed on the negative charge of activated biochar surface. The concentration of H_3O^+ decreased with the increase of pH. Then, the negative surface charge of activated biochar should better attract the positive charge of Cd(II) causing the increase of Cd adsorption performance. When pH of solution was greater than 8, Cd^{2+} could form the soluble hydroxyl complex with OH^- such as $CdOH^+$ causing the decrease in Cd removal performance.

Das et al. [145] were also explained the adsorption results by using the electrostatic effects. In their work, fluoride was removed by calcined Zn/Al hydrotalcite-like compound (HTlc). They reported that pH_{zpc} of HTlc was equivalent to pH 8.78. The optimum pH for fluoride removal was approximately 6.0. When the solution contained PO_4^{3-} and SO_4^{2-}, the percentages of fluoride adsorption on HTlc decreased. They discussed that, due to the super abundant positive charge on the HTlc surface, fluoride and anions should be mainly adsorbed on the adsorbent (HTlc) by electrostatic attraction. In addition, higher charge density of adsorbates tended to be adsorbed on the sorption sites greater than the lower one [145-147]. Therefore, PO_4^{3-} and SO_4^{2-} which had more negative charge than fluoride could be adsorbed on the HTlc greater than fluoride and cause the decrease in percentages of fluoride adsorption. In addition, they also discussed that PO_4^{3-} strongly affected fluoride adsorption performance more than SO_4^{2-} because the affinity toward Zn/Al oxide containing in HTlc and charge density of PO_4^{3-} were greater than that of SO_4^{2-}.

As described in the introduction, due to the fine powder of COS, used COS was difficult to separate from treated water. In this work, the palletization was chosen to develop the fine powder of COS into the pellet. In some researches such as Yu et al. [148] work, the palletization was applied to prepare adsorbent.

In Yu et al. [148] work, OS with particle sizes smaller than 200 mesh and fume silica were used as raw materials for preparing a donut adsorbent to remove phosphate in contaminated water. In their work, OS and fume silica were weighed and mixed in OS : fume silica with the ratio of 58 : 42 by mass (Ca : Si = 5 : 6 mol). Then, water was added into the mixture to provide the plasticity. The mixture paste was shaped into donut shape as in Figure 2-20 and calcined at 700°C - 900°C for 1 h. After that, those adsorbents were hydrothermally cured in an autoclave at temperatures between 130°C and 180°C for 8 or 16 h. Finally, those donut adsorbents were characterized and used as the adsorbent to remove phosphate in contaminated water.

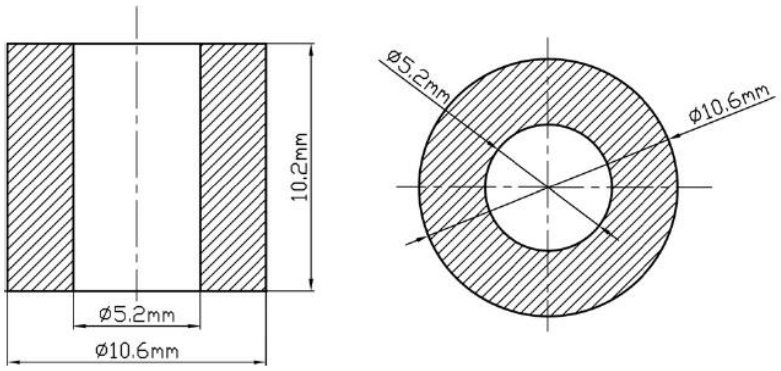

Figure 2-20 Cross-sectional and plan views of a donut adsorbent (for a dry adsorbent weight of 2.0 g) [148].

Based on their XRD results, they proposed that, during the preparation process, some of $CaCO_3$ containing in OS reacted with SiO_2 in fume silica and formed $CaSiO_3$. Then, in the calcination process, the remained $CaCO_3$ in OS released CO_2 and changed into CaO. Some of it could fuse with SiO_2 and form $CaSiO_3$. Furthermore, during hydrothermal annealing, $CaSiO_3$ transformed into calcium silicate hydrate (C-S-

H) which had complicated structure i.e. tobermorite ($Ca_5Si_6O_{16}(OH)_2 \cdot 4H_2O$ that was usually found in hydrated cement paste and metamorphosed limestone [149]. They also reported that, after phosphate removal tests, the intensity of XRD peaks corresponding to $CaSiO_3$ and $Ca_5Si_6O_{16}(OH)_2 \cdot 4H_2O$ decreased while the peaks of $Ca_5(OH)(PO_4)_3$ were observed as illustrated in Figure 2-21. Then, they discussed that the hydrated calcium silicate compounds reacted with phosphate containing in the solution and precipitated in the form of calcium phosphate (hydroxyapatite precipitate).

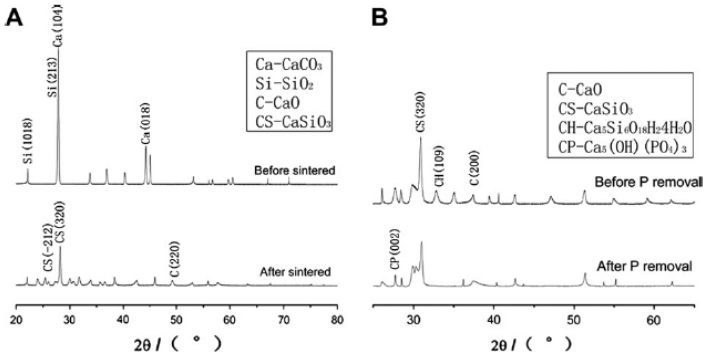

Figure 2-21 XRD results of (A) donut adsorbent before and after calcination and (B) before and after phosphate removal [148].

Moreover, the morphologies of the donut adsorbents after calcining at 800°C for 1 h, after hydrothermal annealing at 150°C for 12 h and after phosphate removal tests are illustrated in Figure 2-22.

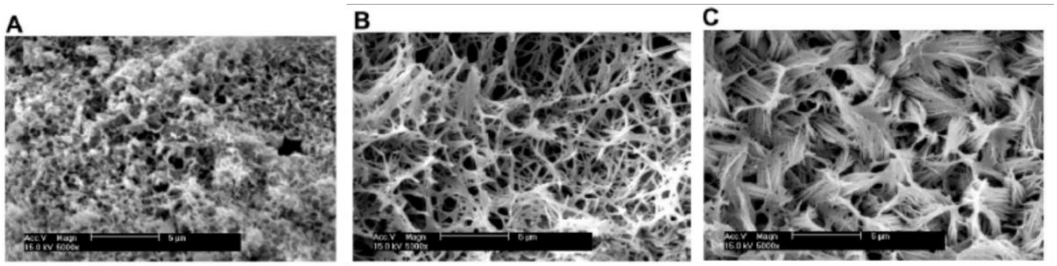

Figure 2-22 SEM images of donut adsorbent surface morphologies (a) after calcining at 800°C for 1 h, (b) after hydrothermal annealing at 150°C for 12 h and (c) after phosphate removal tests [148].

From the SEM images, they discussed that, during the calcination of donut adsorbent at 800°C for 1 h, the fine, open microstructure formed on the donut adsorbent surface as in Figure 2-22 (a). When the adsorbent was hydrothermal annealing at 150°C for 12 h, the microstructure on its surface developed to a much more open and structure texture as in Figure 2-22 (b). After phosphate removal tests, the microstructure on the adsorbent surface changed into feathering along the annealed microstructure and filled of the pore spaces as in Figure 2-22 (c). In their work, they reported that the calcination of donut adsorbent at 800°C with hydrothermal annealing at 150°C for 12 h was the optimum condition for donut adsorbent preparation. It could remove phosphate about 74% and 92% within 2 and 4 h, respectively. Furthermore, they also used the XRD, SEM and phosphate removal results to propose the mechanism of phosphate removal as the following.

(1). During calcination, $CaCO_3$ released CO_2 and changed into CaO as in Reaction (2-62).

$$CaCO_3 \xrightarrow{\Delta} CaO + CO_2 \qquad (2\text{-}62)$$

(2) CaO fused with fume silica (low temperature fusion) and formed intermediate calcium silicate as in Reaction (2-64).

$$CaO + SiO_2 \longrightarrow CaSiO_3 \qquad (2\text{-}64)$$

(3) During hydrothermal annealing process, the annealing of $CaSiO_3$ in a water-saturated atmosphere caused conversion of simple calcium silicate to a reactive hydrated calcium silicate as in Reaction (2-65).

$$5CaSiO_3 + SiO_2 + 5H_2O \longrightarrow Ca_5(Si_6O_8H_2)\cdot 4H_2O \qquad (2\text{-}65)$$

(4) During phosphate removal process, hydrated calcium silicate reacted with phosphate and precipitated in the form of calcium phosphate via Reactions (2-66) and (2-67).

$$Ca_5(Si_6O_8H_2)\cdot 4H_2O + 3H_2PO_4^- \longrightarrow Ca_5(OH)(PO_4)_3 + 6H_2SiO_3 + 2H_2O \quad (2\text{-}66)$$

$$6H_2SiO_3 \longrightarrow 6SiO_2 + 6H_2O \quad (2\text{-}67)$$

From the results and discussion in Yu et al.. [148] work, some $CaCO_3$ in OS could react with SiO_2 in fume silica and form $CaSiO_3$ which could further transform into C-S-H which was usually found in hydrated cement paste. Some researchers reported that C-S-H compound could increase the strength of materials.

Alavéz-Ramírez et al. [150] studied the improvement of durability and mechanical properties of compacted soil blocks by using sugarcane bagasse ash (SCBA) and lime as the chemical stabilizers. In their work, lime, cement and SCBA were added into the compacted soil block mixtures as shown in Table 2-5.

Table 2-5 The mixture of compacted soil blocks (by weight, kg) [150].

Mixture	Soil	Water	Lime	Cement	SCBR
NA	1863.0	175.1	-	-	-
CAL	1704.6	240.0	170.5	-	-
CEM	1766.4	235.1	-	176.6	-
CALBA	1387.5	293.0	138.75	-	138.8

They found that CaO in lime reacted with SiO_2 and Al_2O_3 containing in SCBA and formed C-S-H and calcium aluminum hydrate (C-A-H) compounds as same as the cement products which formed from the reactions between CaO and SiO_2 and Al_2O_3 that contained in portland cement. In their work, they reported that C-S-H and C-A-H compounds could increase the strength of compacted soil blocks. In addition, they also reported that unburned carbon and crystalline SiO_2 could inhibit the formation of C-S-H and C-A-H compounds in the pozzolanic reaction causing the decrease in strength of those compacted soil blocks. SEM images in Figure 2-23 present the morphologies of CAL, CALBA and CEM.

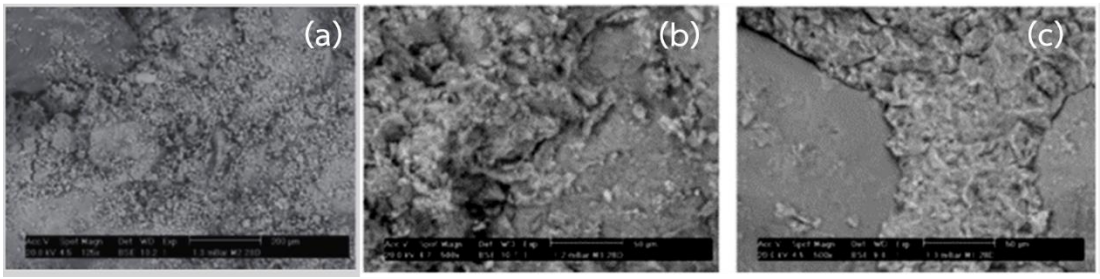

Figure 2-23 SEM images of (a) CAL, (b) CALBA and (c) CEM [150].

Yu et al. [148] and Alavéz-Ramírez et al. [150] works indicated that CaO could react with SiO_2 and form C-S-H compound that could increase the strength of materials. As mentioned above, COS was a CaO-rich material. Thus, in order to develop COS into a pellet, the SiO_2-rich material was necessary to be applied in the pellet mixture.

Prasara-A and Gheewala [42] Ugheoke and Othman [107] and Onojah et al. [105] studied the properties of RHA. They reported that SiO_2 was the main composition of RHA. It existed in two forms; amorphous structure and crystalline structure; depending on the calcined temperature. Ugheoke and Othman [107] reported that, for the calcination of rice husk at temperatures of 300°C - 450°C, pore volume of RHA increased with the increase of calcined temperature because, during the calcination process, some impurities containing in rice husk were removed and the porous structure of RHA was also formed. However, the color of RHA after calcining rice husk in this temperature range was still black due to a lot of unburned carbon and other impurities remaining in RHA. When rice husk was calcined with temperature in the range of 500°C - 600°C, the unburned carbon and impurities containing in RHA dramatically decreased causing white or grey white color of RHA depending on the duration time in calcination process. Ugheoke and Othman [107] and Prasara-A and Gheewala [42] found that the calcination rice husk at temperatures lower than 700°C could produce the amorphous SiO_2 with high surface areas. Their results agreed with the result in Habeeb and Mahmud [43] work.

Habeeb and Mahmud [43] studied RHA properties and used RHA as a cement replacement material. In their work, rice husk was calcined at temperature lower than 690°C. Figure 2-24 presents the XRD result and SEM image of RHA calcined at temperature lower than 690°C.

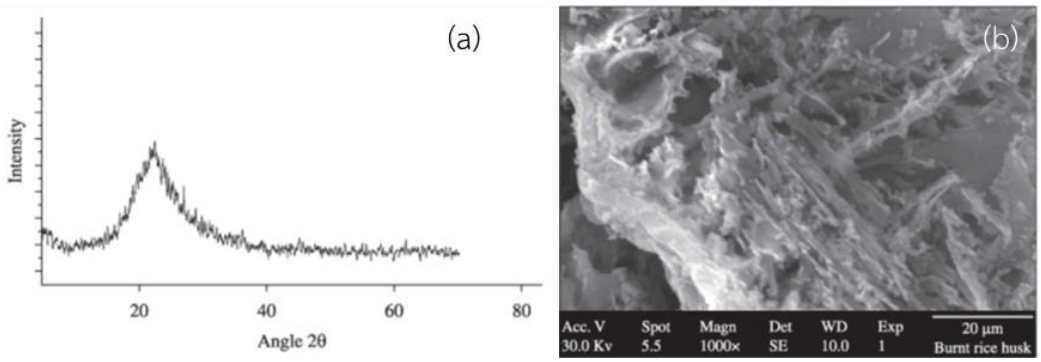

Figure 2-24 XRD result of RHA calcined at 690°C (a) and SEM image of RHA calcined at 690°C (b) [43].

Figure 2-24 (a) shows the broad smooth hump peak at a position in the range of 22° - 25° (2θ) which referred to amorphous form of SiO_2. SEM image of RHA in Figure 2-24(b) shows the multilayer and microporous surface of RHA.

For the calcination of rice husk at temperatures greater than 800°C, Prasara-A and Gheewala [42] Ugheoke and Othman [107] and Onojah et al. [105] reported that the amorphous SiO_2 transformed into the crystalline structure. Onojah et al. [105] found that, when the rice husk was calcined at temperature in the range of 1,000 - 1,200°C, the amorphous SiO_2 transformed into crystalline structure in the form of Crytobalite. Meanwhile, when the calcining temperature reached 1,250°C - 1,400°C, Crytobalite structure changed into Tridymite structure.

For the applications of RHA, Prasara-A and Gheewala [42] reported that the amorphous SiO_2 of RHA was used in concrete production, cement admixture in solidification of hazard waste, low cost of substituted material for the portland cement, aggregates and building block production and filler material in

rubbers/plastics/polymers, etc. In Habeeb and Mahmud [43] work, RHA which was calcined at temperature 690°C was added into the concreate mixture (cement replacement 5-20%). They found that the small particles of RHA reacted with $Ca(OH)_2$ in portland cement and formed calcium silicate hydrate (C-S-H) which was the pozzolanic reaction product. The C-S-H could improve the strength of concrete. In addition, the small finer RHA could distribute into the matrix and act as microfiller that could enhance the cement paste pore structure to increase the density and strength of the concrete.

Meanwhile the crystalline SiO_2 of RHA was used in steel, thermal insulator, refractory brick and ceramic production.

From literature, RHA is a SiO_2-rich material that could be applied in the pellet mixture. Due to a plenty of RHA waste in Thailand that causes the environment problem, in this work, RHA was chosen to use as the other raw material for adsorbent pellet preparation.

Chapter 3

Research methodology

3.1 Materials and equipment

3.1.1 Materials and chemicals

The materials and chemicals used in this work are presented as follows.

1. Oyster shells from restaurants in Chanthaburi province
2. Rice husk ash from a power plant in Thailand
3. Arsenic trioxide (As_2O_3), analytical grade supplied by Ajax Finechem
4. Sodium hydroxide (NaOH), analytical grade supplied by Ajax Finechem
5. Glycerol, analytical grade supplied by Ajax Finechem
6. Sodium nitrate ($NaNO_3$), analytical grade supplied by Carlo erba
7. Sodium sulphate (Na_2SO_4), analytical grade supplied by Carlo erba
8. Sodium phosphate (Na_2HPO_4), analytical grade supplied by Carlo erba
9. Antimonium molybdate, analytical grade supplied by Carlo erba
10. Antimony potassium tartrate, analytical grade supplied by Carlo erba
11. Ascorbic acid, analytical grade supplied by Carlo erba
12. Potassium permanganate ($KMnO_4$), analytical grade supplied by Carlo erba
13. Barium chloride ($BaCl_2$), analytical grade supplied by Carlo erba
14. Sulfanilic acid, analytical grade supplied by Carlo erba
15. Sodium chloride (NaCl), analytical grade supplied by Carlo erba
16. Hydrochloric acid (HCl), analytical grade supplied by Qrec
17. Sulfuric acid (H_2SO_4), analytical grade supplied by J.T.Baker
18. Brucine sulfate, analytical grade supplied by Hi-Media

3.1.2 Equipment

The equipment used in the experiments are presented as the following.

1. 200 ml, 250 ml and 1,000 ml of volumetric flasks with rubber corks
2. 500 ml and 1,000 ml of beakers
3. 100 ml, 150 ml and 250 ml of Erlenmeyer flasks
4. 25 ml of volumetric pipette or transfer pipette
5. Burette
6. Test tubes, test tube rag and test tube holder
7. Dropper
8. Glass funnel
9. Spatula
10. Stirring rod
11. Thermometers
12. Ring stand and burette clamp
13. Vernier Caliper
14. Filter paper no.1 with diameter of 110 mm supplied by Whatman
15. Metal mould
16. 0.3 mm in diameter of wire
17. Plastic mesh
18. pH meter (Hanna instrument, HI 98107)
19. Furnace (Barnstead Thermolyne, 1400 Fernace) and crucibles
20. Magnetic Stirrer (IKA, C-MAG HS 7) and magnetic bar
21. Digital Scale (METTLER TOLEDO, DRAGON 204)
22. Hydraulic press
23. Spectrophotometer

3.2 Experiments

This work studied As(III) removal by using COS and OS-TRHA adsorbent pellet. The experiments are separated into two parts. The first part (PART A) aims to study the effect of anions on As(III) adsorption performance by using COS which prepared form OS particle size range of 150-250 μm. The other part (PART B) aims to develop the COS which is the fine powder into pellet in order to be easy to separate from the treated water.

PART A : The effect of anion contamination on As(III) adsorption performance by using COS as an adsorbent

3.2.1 Preparation of COS adsorbent

COS adsorbent was prepared from oyster shells obtained from restaurants in Chanthaburi province, Thailand. Firstly, oyster shells were washed and scrubbed several times in order to remove impurities and sediment and dried in air. The washed oyster shells were ground and sieved to obtain oyster shell powder (OS) with particles sizes <106 μm, 106-150 μm and 150-250 μm. Then, OS was calcined at 700°C for 8 h. After calcination process, the OS was called COS and stored in desiccator. The elemental compositions of COS were evaluated by X-ray fluorescence spectrometer (XRF, Philips model PW2400, Philip, Japan). X-ray diffraction (XRD, XRD 6100, SHIMADZU, Japan) was also performed to determine the crystalline of OS, COS, COS after adding in water and COS after adsorption tests. The X-ray diffractometer with Cu-Kα radiation was operated at 40 kV. The X-ray spectra of these samples were measured in the ranges of 5° - 80° (in 2θ) with scan speed of 2.0°/min. Surface areas of OS and COS were also estimated by BET nitrogen gas sorption method (Belsorp max model, BEL, Japan). pH zero point of charge (pH_{zpc}) of COS was determined by potentiometric mass titration method. Furthermore, morphologies of samples i.e. OS, COS, COS after adding in water and COS after

adsorption tests were also observed by a scanning electron microscope (SEM, Carl Zeiss EVO®MA10).

3.2.2 Preparation of chemical solutions

Stock solution of As(III) was prepared by dissolving As_2O_3 in 20 ml of NaOH (50 mg/L). The As(III) solution was diluted with distilled water to obtain 1,000 mg/L of As(III) solution. NO_3^- SO_4^{2-} and HPO_4^{2-} solutions were prepared by dissolving $NaNO_3$, Na_2SO_4 and Na_2HPO_4, respectively. Then, those solutions were also diluted with distilled water to obtain 1,000 mg/L of NO_3^- , SO_4^{2-} and HPO_4^{2-}.

$KMnO_4$ solution was used as a titrant for analyzing As(III) concentration in samples. The standard solution of 1000 mg/L $KMnO_4$ was prepared by dissolving 0.2 g of $KMnO_4$ with distilled water and the final volume was made up to 200 ml. The concentration of $KMnO_4$ solution was determined by spectrophotometer (520 nm).

Brucine-sulfanilic acid reagent used for analyzing NO_3^- concentration in Brucine method was prepared by dissolving 1 g of brucine sulfate and 0.1 g of sulfanilic acid in hot distilled water. After that, 3 ml of concentrated HCl was added into the mixture and left until its temperature was equivalent to room temperature. The final volume of the mixture was made up to 100 ml by distilled water. The mixture was stored in a dark bottle at 5 °C.

Reagent A was used in Turbidimetric method for analyzing SO_4^{2-} concentration. Firstly, 75 g of NaCl was dissolved in distilled water. Then, 50 ml of glycerol, 30 ml of concentrated HCl and 100 ml of 95% ethanol were added into NaCl solution and mixed well. Then, the solution was made up to 500 ml using distilled water.

Reagent B was used to analyte HPO_4^{2-}concentration containing in the samples. Firstly, 1.375 g of antimony potassium tartrate and 20 g of crystals antimonium molybdate were individually dissolved in distilled water. Those solutions

were diluted to 500 ml by distilled water. Secondly, 1.76 g of ascorbic acid was also dissolved and diluted to 100 ml by distilled water. Then, 5 ml of antimony potassium tartrate, 15 ml of antimonium molybdate and 30 ml of ascorbic acid were added into 50 ml of 5 N H_2SO_4 and mixed well. It is noted that ascorbic acid solution should be used within 4 h after its preparation process.

3.2.3 pH zero point charge analysis

pH zero point of charge (pH_{zpc}) of COS was determined by potentiometric mass titration method. Firstly, pH of 100 ml of 0.01 M NaCl solution was adjusted to be 2, 4, 6, 8, 10, 12 and 13 by 0.01 M of NaOH and/or HCl. Secondly, 0.2 g of COS was added into each NaCl solution. Then, the solution was stirring continuously for 48 h. After that, the final pHs of solutions were measured by pH meter (Hanna instrument; HI 98107).

3.2.4 Solubility of COS at initial pH 11 and precipitation tests of As(III), NO_3^-, SO_4^{2-} and HPO_4^{2-}

In this part, solubility of COS prepared from OS particle size range of 150-250 μm was performed in Erlenmeyer flask covered with a rubber cork. Initially, 1000 mL of distilled water was adjusted pH to be 11 by 0.1 M of NaOH or/and HCl. Then, 0.3 g of COS was added into the solution and continuously stirred for 7 h. After that, the COS was separated from the solution by using Whatman filter paper no. 1. The final pHs of solution were measured by a pH meter (Hanna instrument, HI 98107).

The precipitation tests of As(III) and anions were carried out by adding As(III) stock solution into the filtrate solution with the volume ratio of 1:9 in order to obtain 1000 mL of 100 mg/L As(III). Then, the solution was continuously stirred for 7 h. After that, the solution was filtered by Whatman filter paper no. 1. The final pH of the filtrate solution and As(III) concentration were measured. The same procedure was performed with other anions; NO_3^-, SO_4^{2-} and HPO_4^{2-}.

3.2.5 Adsorption performance of individual ion (As(III), NO_3^- , SO_4^{2-} and HPO_4^{2-})

The adsorption performances of As(III), NO_3^- , SO_4^{2-} and HPO_4^{2-} were performed by batch tests. Firstly, 250 ml of As(III), NO_3^- , SO_4^{2-} and HPO_4^{2-} stock solutions were separately added into each Erlenmeyer flask. Then, pH of those solution in each flask was adjusted to be 11 by using 0.1 M of NaOH and/or HCl. After that, 1.0 g of COS was added into each solution and continuously stirred with agitation speed 750 rpm for 24 h. Finally, COS was separated from the aqueous solution by Whatman filter paper no. 1. The concentrations of As(III), NO_3^- , SO_4^{2-} and HPO_4^{2-} remaining in the solution were measured. The amounts of As(III) and anions removal by adsorption process was calculated as presented in Equation (3-1)

$$As(III)_{adsorption} = As(III)_{overall} - As(III)_{precipitaton} \quad (3\text{-}1)$$

while $As(III)_{adsorption}$ = the amount of As(III) removal by adsorption process.

$As(III)_{overall}$ = the amount of As(III) removal by adsorption and precipitation processes which was obtained from the experiments.

$As(III)_{precipitation}$ = the amount of As(III) removal by precipitation process which was obtained from the precipitation tests.

The morphologies of COS before and after As(III) and anions removal tests were observed by SEM (Carl Zeiss EVO®MA10).

3.2.6 Effect of competitive anion(s) on As(III) adsorption performance in bi-, tri- and tetra-solutes

The effect of competitive anion(s) on As(III) adsorption performance was also studied by batch test. The experiments were performed in 1,000 ml of Erlenmeyer flasks covered with rubber corks. Initially, As(III) and anions stocks solutions were mixed and diluted with distilled water to obtain the initial concentration of each ion in the mixture solutions as 100 mg/L. Secondly, pH of mixture solution was adjusted

to be 11 by 0.1 M of NaOH and/or HCl. Then, 0.3 g of COS was added into the mixture solution and continuously stirred with agitation speed of 750 rpm. During removal process, samples were taken at appropriate time intervals. After that, the samples were filtered by Whatman filter paper no. 1 to remove COS which contained in the solution. As(III) and anion concentrations remaining in those samples were analyzed. The morphologies of COS before and after As(III) and anions removal tests were also observed by SEM (Carl Zeiss EVO®MA10).

3.2.7 The desorption of As(III) and anions test

The desorption tests were performed via batch test. Initially, As(III) and anions stock solution were added into Erlenmeyer flask and diluted with distilled water to provide 100 mg/L of each anion. pH of solution was also adjusted to pH 11 by 0.1 M of NaOH and/or HCl. Then, 0.3 g of COS was added into the solution. The solution was continuously stirred with agitation speed of 750 rpm for 24 h. After that, the solution was heated from room temperature (25°C) to 40°C. The samples were taken at appropriate time. The concentrations of As(III) and anions remaining in the sample solution were determined.

3.2.8. Determination of adsorption kinetics of As(III) and anions

In this work, seven assumptions, as the following, were set in order to determine the observed adsorption rate constants of As(III) and anions.

(1) As(III) and anions were adsorbed on the sorption sites as monolayer.

(2) The sorption sites of the adsorbent were uniform.

(3) There were no interactions between adsorbates.

(4) The molecules of As(III) or anions in the bulk solution did not displace the molecules that occupied on the sorption sites.

(5) The number of active sites on COS was assumed to be equivalent to the maximum adsorption capacity of COS in As(III) combined with NO_3^-, SO_4^{2-} and HPO_4^{2-} adsorption test (838.21 mg/g).

(6) During adsorption process, desorption rates of As(III) and anions were negligible comparing with adsorption rate.

(7) The electrostatic attraction or repulsion between adsorbent and adsorbates is not significantly affect adsorption performance.

Furthermore, the adsorption rates of single-solutes, bi-, tri- and tetra-solutes were derived as the follow equations.

$$\frac{dC_i}{dt} = k_{ad,i}C_i(1-\theta_i) \quad (3\text{-}2)$$

$$\frac{dC_i}{dt} = k_{ad,i}C_i(1-\theta_A-\theta_B) \quad (3\text{-}3)$$

$$\frac{dC_i}{dt} = k_{ad,i}C_i(1-\theta_A-\theta_B-\theta_c) \quad (3\text{-}4)$$

$$\frac{dC_i}{dt} = k_{ad,i}C_i(1-\theta_A-\theta_B-\theta_C-\theta_D) \quad (3\text{-}5)$$

where $k_{ad,i}$ is observed adsorption rate constant of substance i (min^{-1}), substance i is substance A, B, C or D and θ_A, θ_B, θ_C and θ_D are the fractions of sorption sites covered by substances A, B, C and D, respectively.

Since the concentration of substance i in the bulk solution decreased by adsorption of substance i on the sorption sites of adsorbent, therefore

$$C_i = C_{0,i} - \beta_i\theta_i \quad (3\text{-}6)$$

where $C_{0,i}$ is the initial concentration of substance i (mg/L) and β_i is a constant defined as Equation (3-7).

$$\beta_i = \frac{W_c q_m}{M_i V} \quad (3\text{-}7)$$

where W_c is mass of adsorbent (g), q_m is maximum adsorption capacity of the adsorbent (mg/g), M_i is molecular weight of substance i (g/mol) and V is volume of solution (L).

The observed adsorption rate constants were initially estimated by using the extended geometric method purposed by Azizian et al. [48, 49]. After that, the values of As(III) and anions occupied sites (θ_A, θ_B, θ_C and θ_D) in Equations (3-2) – (3-5) were solved by Runge-Kutta method [50, 51] and compared with the experimental data. The observed adsorption rate constants were gradually adjusted until the values of As(III) and anion occupied sites were well fitted with the experimental data.

3.2.9 Determination of As(III) and anions concentrations

The concentrations of As(III), NO_3^-, SO_4^{2-} and HPO_4^{2-} remaining samples solution were analyzed by redox titration with $KMnO_4$, Brucine method, Turbidimetric method and Colorimetric & Ascorbic acid method, respectively.

As(III) concentration in the samples was determined by titration with $KMnO_4$. Firstly, 15 ml of each sample was added with 0.5 ml of HCl : water ratio of 1:1 and few drops of 0.001 M potassium iodide (KI). Then, the sample was titrated with 50 ppm of $KMnO_4$ until the pink color was observed and remained for 30 seconds. The concentration of $KMnO_4$ in titrant solution was measured by spectrophotometer at a wavelength of 520 nm. As(III) concentration can be calculated by using Reaction (3-8)

$$5As_2O_3 + 4MnO_4^- + 12H^+ \longleftrightarrow 5As_2O_5 + 4Mn^{2+} + 6H_2O \qquad (3\text{-}8)$$

NO_3^- concentration in the solution was estimated by Brucine method [151]. Firstly, 10 ml of sample was added into an Erlenmeyer flask and diluted to 50 ml with distilled water. Secondly, the diluted sample was pipetted into a glass tube and the volume was made up to 10 ml with distilled water. Thirdly, 10 ml of sulfuric acid 4:1 was added into the diluted sample and mixed well in cooling water bath. Then, Brucine-sulfanilic acid reagent 0.5 ml was also added into the diluted sample and

mixed well. After that, the diluted sample was heated at 95°C for 20 min in water bath and then cooled down. Finally, NO_3^- concentration remaining in the diluted sample was evaluated by spectrophotometer at a wavelength of 420 nm.

SO_4^{2-} concentration in the solution was analyzed by Turbidimetric method [152]. Initially, 15 ml of sample was diluted to 100 ml with distilled water. After that, 5 ml of reagent A was added into the diluted sample. Then, $BaCl_2$ crystals were weighed and added into the diluted sample and continuously stirred for 1 min. The turbidity of sample was measured by using spectrophotometer at wavelength 420 nm every 30 sec. for 4 min. The maximum value of absorbance was estimated and used to determine the concentration of SO_4^{2-} remaining in the solution.

HPO_4^{2-} concentration in samples solution was measured by Colorimetric & Ascorbic acid method [153, 154]. Firstly, 10 ml of sample was diluted to 50 ml with distilled water. Secondly, 1 drop of phenolphthalein was added into the diluted sample. If red color appeared, the 5 N of H_2SO_4 would be added into the diluted sample until the red color disappeared. Thirdly, 10 ml of reagent B was added into the diluted sample and kept for 10 min. Finally, the concentration of HPO_4^{2-} was determined by using spectrophotometer at a wavelength of 880 nm.

PART B : As(III) removal by using OS-TRHA adsorbent pellet

3.2.10 Preparation of treated rice husk ash (TRHA)

Rice husk ash (RHA) was collected from a power plant in Thailand. RHA was calcined at 600 °C in air for 13 h and named as treated rice husk ash (TRHA). Chemical compositions of RHA and TRHA were evaluated by XRF (Bruker model S8 Tiger). XRD (XRD 6100, SHIMADZU, Japan) was used to characterize the RHA and TRHA. RHA and TRHA morphologies were also observed by SEM (SEM, Carl Zeiss EVO®MA10).

3.2.11 Preparation of OS-TRHA adsorbent pellet

In this part, OS with particle size ranges of <106 μm, 106-150 μm and 150-250 μm and TRHA were used to prepared OS-TRHA adsorbent pellets. Firstly, OS and TRHA were weighed and mixed in various ratios. Then, few drops of distilled water were added into the mixture powder in order to provide the plasticity. The mixture paste was put into a metal mould. Then, 30 kg-f/cm^2 of pressure was applied to the mould by using the hydraulic press (Winner, model 30 tons) for 5 min. After that, the pellets were calcined at 700°C for 8 h and called as OS-TRHA adsorbent pellet. The crystalline phase of OS-TRHA adsorbent pellets before and after As(III) adsorption tests was determined by XRD (XRD 6100, SHIMADZU, Japan) using Cu-Kα radiation, at 40 kV and 2θ range from 5° to 80° with scan speed of 2.0°/min. The morphologies of OS-TRHA adsorbent pellets before and after As(III) adsorption tests were observed by SEM (Carl Zeiss EVO®MA10).

3.2.12 Solubility tests of COS and OS-TRHA adsorbent pellet

Solubilities of COS and OS-TRHA adsorbent pellets (OS:TRHA ratio of 0.7:0.3) which were prepared from OS particle size ranges of <106 μm, 106-150 μm and 150-250 μm and ground OS-TRHA adsorbent pellet prepared from OS:TRHA ratio of 0.7:0.3 with OS particle size range of <106 μm were measured via batch tests. Firstly, 100 ml of distilled water was adjusted to obtained pH at 7 by 0.1 M of NaOH and/or HCl. Then, 0.2 g of COS, OS-TRHA adsorbent pellets and the ground OS-TRHA adsorbent pellet were individually added into the solutions and kept for 24 h. The solutions were filtrated through Whatman filter paper no. 1. The final pHs of those solutions were determined by a pH meter (Hanna instrument, HI 98107). Finally, the amount of those samples dissolved in the solutions were calculated.

3.2.13 The effects of OS particle size ranges and ratios of OS:TRHA on As(III) adsorption performance of OS-TRHA adsorbent pellet

As(III) adsorption tests were performed in Erlenmeyer flasks covered with rubber corks. Firstly, As(III) stock solution was diluted with distilled water to obtain 100 mg/L of As(III). Secondly, OS-TRHA adsorbent pellets prepared from Section 3.2.11 were individually added into As(III) solution and kept for 24 h. After that, the OS-TRHA adsorbent pellet was removed from solution. The concentrations of As(III) remaining in the solution were determined by titration with $KMnO_4$.

3.2.14 Adsorption kinetics and adsorption isotherm of OS-TRHA adsorbent pellet

The adsorption kinetics and adsorption isotherm of OS-TRHA adsorbent pellet were performed by batch test. Firstly, As(III) stock solution was diluted with distilled water to obtain As(III) initial concentration between 100 mg/L- 200 mg/L. Secondly, pH of As(III) solution was adjusted to be 7 by using 0.1 M of NaOH and/or HCl. Thirdly, OS-TRHA adsorbent pellet prepared from OS:TRHA ratio of 0.7:0.3 with OS particle size range of <106 μm was individually added into those As(III) solution. The samples were taken at appropriated times and the concentrations of As(III) remaining in the samples solution were evaluated

3.2.15 The larger scale of As(III) removal by OS-TRHA adsorbent pellets

In order to observe the As(III) adsorption performance by using OS-TRHA pellets in the bigger scale, OS-TRHA adsorbent pellets (3-4 g of total weight) were put into 2 L of synthetic As(III) contaminated water. The initial As(III) concentration was equivalent to arsenic concentration that contained in water resources in Thailand i.e. 34 mg/L. The OS-TRHA adsorbent pellets were changed every 2 days for 3 times. The concentrations of As(III) remaining in the solution were measured by an

inductively coupled plasma (ICP, In-house method based on Standard Methods for Examination of Water and Wastewater 20th Edition [155]).

Chapter 4

Results and discussion

In this chapter, the experimental results and discussion were divided into 2 parts; part A and part B. For part A, COS was used as an adsorbent to remove As(III) from contaminated water. In this part, the properties of COS e.g. chemical composition, specific adsorbent surface area, pH_{zpc}, solubility, morphology, etc. were studied. The effect of anions i.e. NO_3^- and SO_4^{2-} and HPO_4^{2-} on As(III) adsorption performances in bi-, tri- and tetra-solutes systems were investigated. For part B, COS was developed into the pellet named OS-TRHA adsorbent pellet which was used as an adsorbent to remove As(III) in this part. The effects of OS particle sizes and OS : TRHA ratios on stability and As(III) adsorption performance of OS-TRHA adsorbent pellets were studied. The adsorption kinetics and adsorption isotherms of As(III) adsorption on OS:TRHA adsorbent pellet were determined.

PART A : The effect of anion contamination on As(III) adsorption performance by using COS as an adsorbent

4.1 Characterization of OS and COS

4.1.1 XRF and XRD analysis

The chemical compositions of OS and COS were evaluated by the XRF analysis. The compositions (expressed as oxides) of OS and COS are shown in Table 4-1.

Table 4-1 XRF results of OS and COS (wt%).

	% content	
Composition	OS	COS
CaO	95.99	97.00
MgO	0.65	0.90
Na_2O	0.98	0.50
SO_3	0.73	0.50
SiO_2	0.70	0.40
P_2O_5	0.20	0.20
Cl		0.10
Fe_2O_3		0.10
Al_2O_3	0.42	0.10
SrO	0.33	0.10
K_2O		0.10

It can be seen in Table 4-1 that calcium is the main composition of OS (95.55 wt%) and COS (97 wt%) followed by sodium (Na_2O), sulfur (SO_3), silicon (SiO_2) and magnesium (MgO). The slightly increase in percentage of calcium in COS should be because, during the calcination of OS at 700°C for 8 h, the moisture and some volatile compounds in OS were removed.

The crystalline phase of OS and COS was observed by the XRD. The XRD peaks of OS and COS are illustrated in Figure 4-1.

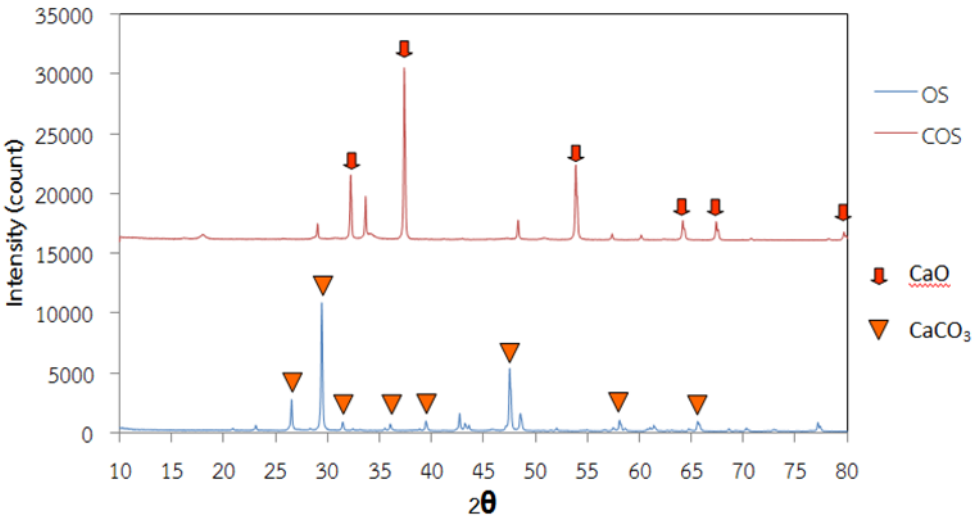

Figure 4-1 XRD patterns of OS and COS.

The XRD peaks of OS in Figure 4-1 correspond to the crystalline structure of $CaCO_3$ while the peaks of COS correspond to the crystalline structure of CaO. The XRD and XRF (Table 4-1) results indicate that OS mainly composes of $CaCO_3$ while COS consists of 97 wt% of CaO. Based on XRD and XRF results, during calcining OS at 700°C for 8 h, $CaCO_3$ in OS transformed into CaO in COS as in Reaction (2-62).

$$CaCO_3 \xrightarrow{\Delta} CaO + CO_2 \qquad (2\text{-}62)$$

4.1.2 Physical properties of COS

The physical properties of OS, COS and commercial grade CaO such as specific volume, specific surface area, total pore volume and mean pore diameter were characterized by BET (BELSORP MAX) technique. The results are shown in Table 4-2.

Table 4-2 Physical properties of OS and COS in comparison with similar materials from other sources.

Material	Property			
	Specific volume (cm^3(STP)/g)	Specific surface area (m^2/g)	Total pore volume (cm^3/g)	Mean pore diameter (nm)
OS	0.47	2.05	0.003	5.63
COS (prepared from OS particle size range of 150 - 250 μm)	3.63	15.80	0.018	4.67
Commercial grade calcium oxide	3.73	16.22	0.021	5.16
Charred dolomite [62]	-	7.31	-	-
Thermally treated quicklime [135]	-	11.75	-	-

It can be seen in Table 4-2 that the specific surface area of COS (15.80 m^2/g) is greater than that of OS (2.05 m^2/g). The increase in specific surface area of COS should be due to the absence of CO_2 during the calcination process of OS as in Reaction (2-62). The specific surface area of COS is also compared with the specific surface areas of CaO-rich materials reported by Salameh et al. [62] and Islam and Patel [135]. As also seen in Table 4-2, the specific surface area of COS is around 2 times greater than that of the dolomite charred at the same condition and also larger than that of the quicklime thermally treated at 450°C for 4 h for almost 75%.

In order to determine the surface structure of OS and COS, the surface morphologies of those samples were observed by SEM (SEM, Carl Zeiss EVO®MA10). SEM images of OS and COS are illustrated in Figure 4-2.

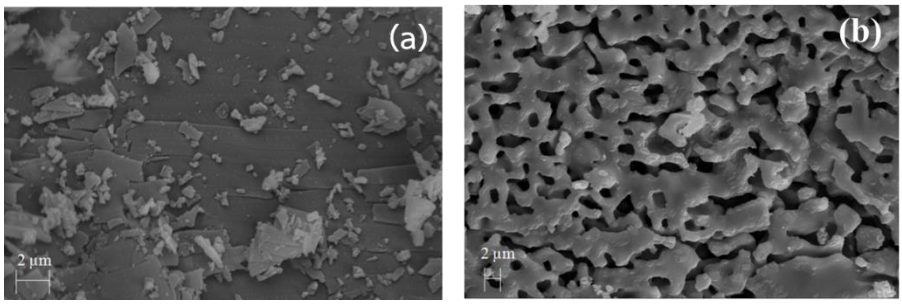

Figure 4-2 SEM images of (a) OS and (b) COS surfaces.

As seen in Figure 4-2, before calcining OS, the morphology of OS looks like smooth layer surface as in Figure 4-2(a). After calcining OS at 700°C for 8 h, the smooth layer surface of OS in Figure 4-2(a) changed into the porous structure as in Figure 4-2(b). The XRD, BET and SEM results indicate that, during the calcination process of OS, $CaCO_3$ in OS changed into CaO in COS and released CO_2 causing the formation of porous structure in COS. The formation of porous structure also caused the increase in specific surface area of COS (Table 4-2).

4.1.3 pH zero point of charge of COS (pH_{zpc})

In adsorption process, the surface of adsorbent which can behave as anionic or cationic compound depending on whether it is in an acidic or basic solution is called amphoteric surface sites. The surface charge of oxide and hydroxide materials is the result of amphoteric surface site ionization either protonation or deprotonation [122, 123]. pH_{zpc} is the point where $pH_{initial} - pH_{final} = 0$ [124-126]. It means that, at pH_{zpc}, the surface of material can protonate as well as deprotonate and cause the net surface charge of that material to be equal to zero. In this work, pH_{zpc} of COS was determined. As mentioned before, 97%wt of COS was CaO. Islam and Patel [135] reported that, during CaO contacting with water, CaO could change into $Ca(OH)_2$. Thus, XRD was used to determine the crystalline phase of COS after contacting with water. The XRD result is presented in Figure 4-3.

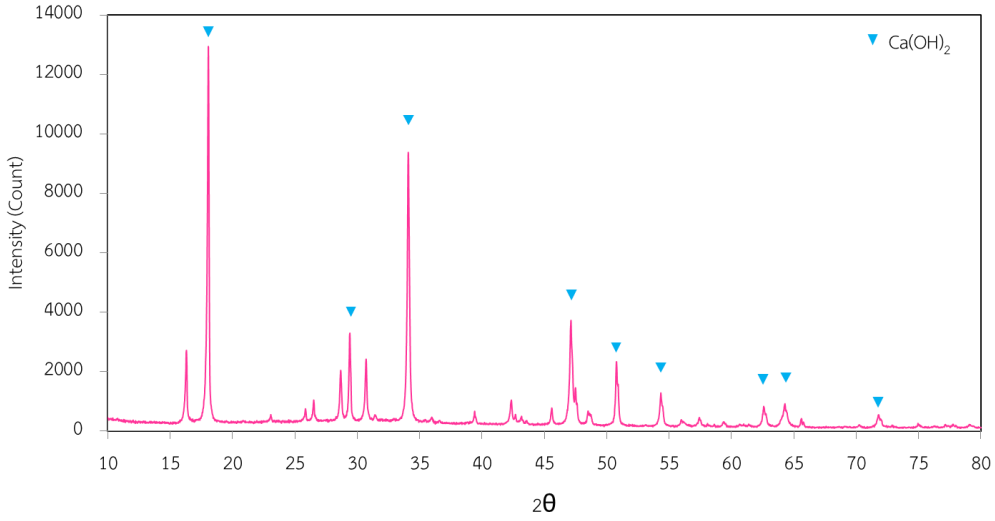

Figure 4-3 XRD peaks of COS after added into water.

Figure 4-3 shows that, XRD peaks of COS after contacting with water match with $Ca(OH)_2$ peak positions. This implies that, after adding COS into water, CaO in COS reacted with water and changed into $Ca(OH)_2$ as in Reaction (4-1). Therefore, the measured pH_{zpc} was the pH_{zpc} of COS contacting with water which should be in the form of $Ca(OH)_2$.

$$CaO + 2H_2O \longrightarrow Ca(OH)_2 \qquad (4\text{-}1)$$

The pH_{zpc} of COS contacting with water was determined by the potentiometric mass titration method. The result is illustrated in Figure 4-4.

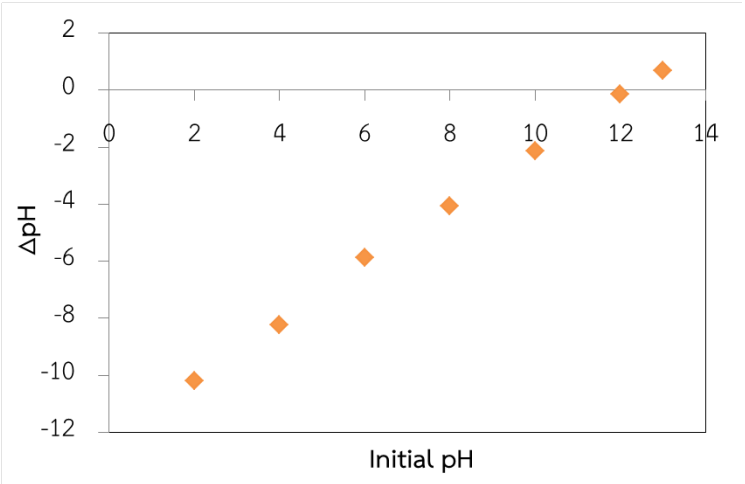

Figure 4-4 The potentiometric mass titration result of COS.

As seen in Figure 4-4, pH_{zpc} of COS contacting with water is approximately 12.1. This value is in good agreement with Ref. [23] of Atesok et al. work [156] who reported that the pH_{zpc} of $Ca(OH)_2$ was above 12. This means that, at pH 12.1, the net surface charge of COS is equal to zero because the COS surface can protonate as well as deprotonate. If pH of solution is lower than pH_{zpc} (12.1), the COS surface can protonate better than deprotonate. Then, the net surface charge of COS will be positive and better attract anions (negative charge). Conversely, if pH of solution is greater than pH_{zpc} (12.1), the COS surface can deprotonate better than protonate. Then, the net surface charge of the COS will be negative. The negatively charged surface can better attract toward cations (positive charge). However, this phenomenon is a temporary situation depending on pH of solution.

4.2 As(III) and individual anion adsorption on COS

4.2.1 The solubility test of COS and precipitation tests of As(III) and anions in COS solution

In this section, the solubility test of COS prepared from OS particle size range of 150 - 250 μm was performed by a batch test. The initial pH of solution was set at pH 11 while the final pHs were measured after adding COS into solution and being kept for 7 h. The result showed that pH of the solution changed from 11.0 to 11.6. As mentioned above, when CaO in COS was added into water, it changed into $Ca(OH)_2$ as in Reaction (4-1). Some of $Ca(OH)_2$ could dissolve in water and dissociate into Ca^{2+} and OH^- as in Reaction (4-2). The dissociated OH^- caused the increase in pH of solution. The amount of dissolved $Ca(OH)_2$ was also evaluated based on the change of pH of the solution after COS contacting with water for 7 h. The calculation indicated that about 0.0835 g or 27.8% of COS became the dissolved $Ca(OH)_2$.

$$Ca(OH)_2 \longleftrightarrow Ca^{2+} + 2OH^- \qquad (4\text{-}2)$$

Furthermore, the precipitation tests of As(III) and anions were also individually performed in Erlenmeyer flasks with rubber corks in order to observe the precipitation of As(III) and anions with the dissolved $Ca(OH)_2$. The results showed that there was no precipitate observed in As(III), NO_3^- and SO_4^{2-} solution. The concentrations of these anions and pH of solution did not significantly change. This implies that precipitation of dissolved $Ca(OH)_2$ and As(III), NO_3^- and SO_4^{2-} should not occur. Therefore, these anions should be removed by COS via adsorption process. In addition, the precipitation of As(III) was further observed for longer time. The result showed that the precipitate of As(III) and dissolved $Ca(OH)_2$ was not observed within 48 h and there was no significant change in As(III) concentration. This indicates that the precipitate of As(III) and Ca^{2+} which contained in COS solution should not occur within 48 h. The As(III) precipitation result in this work agrees with Dutŕe and Vandecasteele works [137, 138] which reported the immobilization of arsenic-containing waste by using cement and lime. They reported that Ca^{2+} in solution precipitated with $HAsO_3^{2-}$ in the form of $CaHAsO_3$ only at pH above 11.91. On the other hand, in the case of HPO_4^{2-}, the result showed that, after adding HPO_4^{2-} solution into the filtrate (COS solution), the white precipitate was clearly observed and the concentration of HPO_4^{2-} decreased by 46.6%. This means that HPO_4^{2-} could be removed by COS via both precipitation and adsorption.

4.2.2 The adsorption performances of As(III) and anions on COS

As(III) and anions adsorption performances were performed via batch tests. The initial pH 11 was chosen to be the condition of the experiments as it provided the highest removal percentage of As(III). At this pH, As(III) containing in the solution should exist in the form of $H_2AsO_3^-$ [1, 35, 157]. The As(III), NO_3^-, SO_4^{2-} and HPO_4^{2-} maximum adsorption capacities of COS are illustrated in Figure 4-5. It is noted that the precipitation effect of HPO_4^{2-} was eliminated.

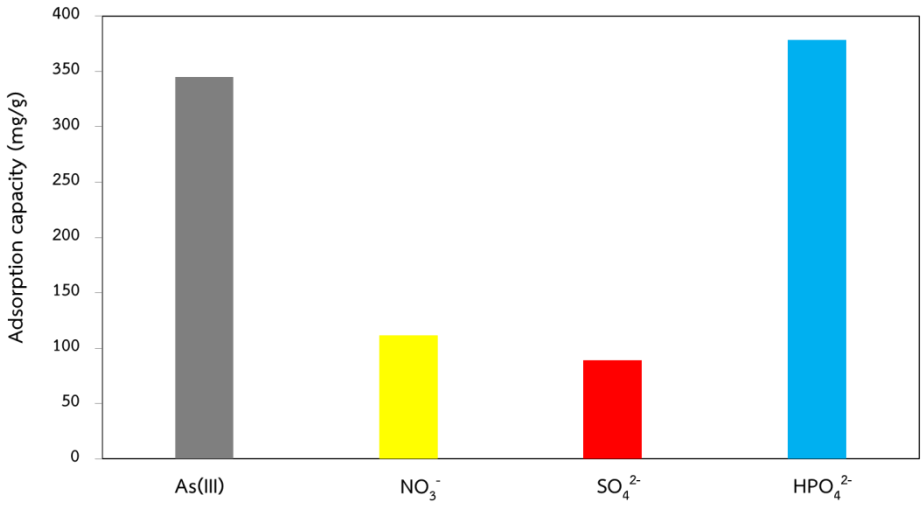

Figure 4-5 Adsorption capacities of COS corresponding to individual ions.

Figure 4-5 shows that the non-dissolved COS has capability to adsorb HPO_4^{2-} (378.40 mg of HPO_4^{2-}/g of non-dissolved COS) slightly greater than As(III) (345.09 mg of As(III)/g of non-dissolved COS) while NO_3^- (111.71 mg of NO_3^-/g of non-dissolved COS) and SO_4^{2-} (89.24 mg of SO_4^{2-}/g of non-dissolved COS) can be adsorbed by COS for less than 3 times of the amount of $H_2AsO_3^-$ and HPO_4^{2-} adsorbed. This indicates that the COS sorption sites are better adsorbed HPO_4^{2-} and $H_2AsO_3^-$ than NO_3^- and SO_4^{2-}.

4.2.3. The morphologies of COS before and after As(III) and anions removal tests

The morphologies of OS, COS, COS after contacting with water, COS after As(III) and anions removal tests were observed by SEM (Carl Zeiss EVO®MA10). The SEM images are illustrated in Figure 4-6.

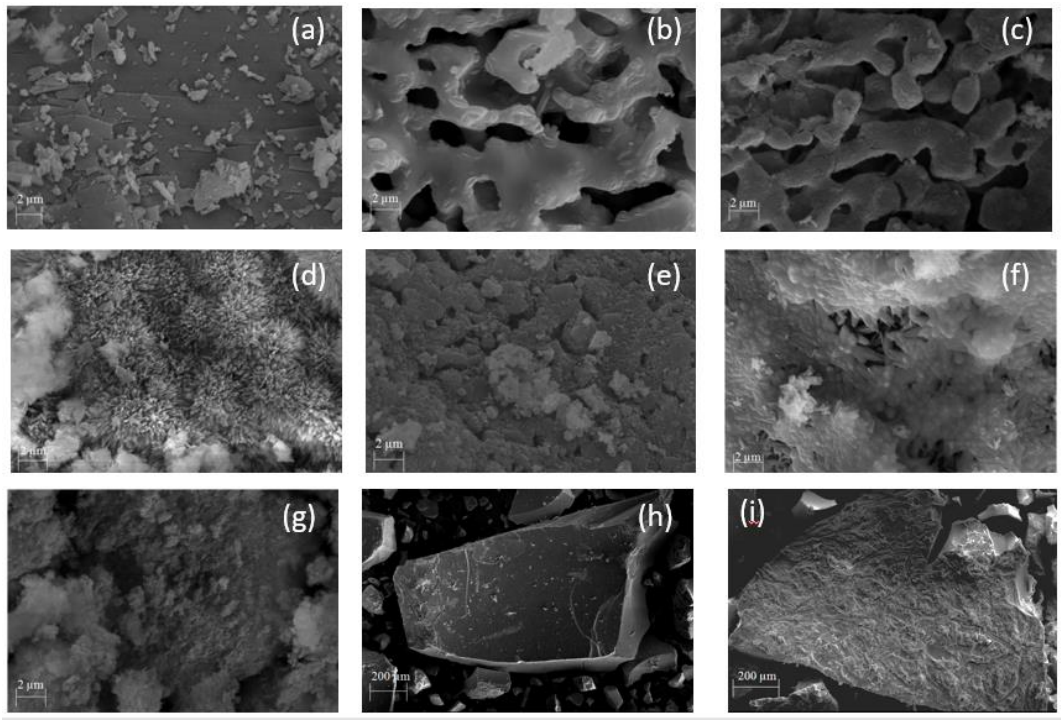

Figure 4-6 SEM images of (a) OS, (b) COS, (c) COS after contacting with water, COS after being used to remove (d) As(III), (e) NO_3^-, (f) SO_4^{2-} and (g) HPO_4^{2-} and (h)-(i) precipitate of HPO_4^{2-}.

As described before, during the calcination of OS, a smooth layer of OS (Figure 4-6 (a)) changed into the porous structure (Figure 4-6 (b)) due to the absence of CO_2. The COS surface before (Figure 4-6 (b)) and after contacting with water (Figure 4-6 (c)) are similar but the surface of COS after contacting with water looks slightly rougher. This should be because, when CaO in COS contacted with water, it transformed into $Ca(OH)_2$. It can also be seen in Figures 4-6 (d) - (g) that after As(III) and anions adsorption tests, the porous structure of COS surface in Figure 4-6 (b) changed into the different forms depending on the type of adsorbates. As illustrated in Figure 4-6 (d), the COS surface looks like it was covered by grass leaves - like matter when $H_2AsO_3^-$ was adsorbed. This morphology looked similar to the morphology of arsenic immobilized on lime in the work of Phenrat et al.[158] who studied the iron-arsenic sludge immobilized by using cement and lime. As also seen in Figure 4-6 (f), after COS adsorbing SO_4^{2-} it seems that the COS surface was covered

by small grains. Meanwhile, the COS surfaces look flaky after COS was used to remove NO_3^- and HPO_4^{2-} as shown in Figures 4-6 (e) and (g), respectively. In addition, the morphologies of phosphate precipitate were also observed by SEM. The SEM images show that it could be divided into two types; the smooths surface and the rough surface as in Figures 4-6 (h) and 4-6 (i), respectively.

4.2.4. The mechanisms of As(III) and anions adsorption on COS

The crystalline phase of COS after As(III) and individual anion removal tests was determined by XRD. The XRD results of COS after As(III), NO_3^-, SO_4^{2-} and HPO_4^{2-} removal tests are presented in Figures 4-7 - 4-10. It is noted that, in HPO_4^{2-} removal, the precipitates that occurred during the HPO_4^{2-} removal process and the COS after adsorption tests could not be separated. Thus, the XRD result of HPO_4^{2-} is the result of crystalline phase determination of both COS after HPO_4^{2-} adsorption and the precipitates of HPO_4^{2-}.

The XRD result of COS after adsorbing As(III) is displayed in Figure 4-7.

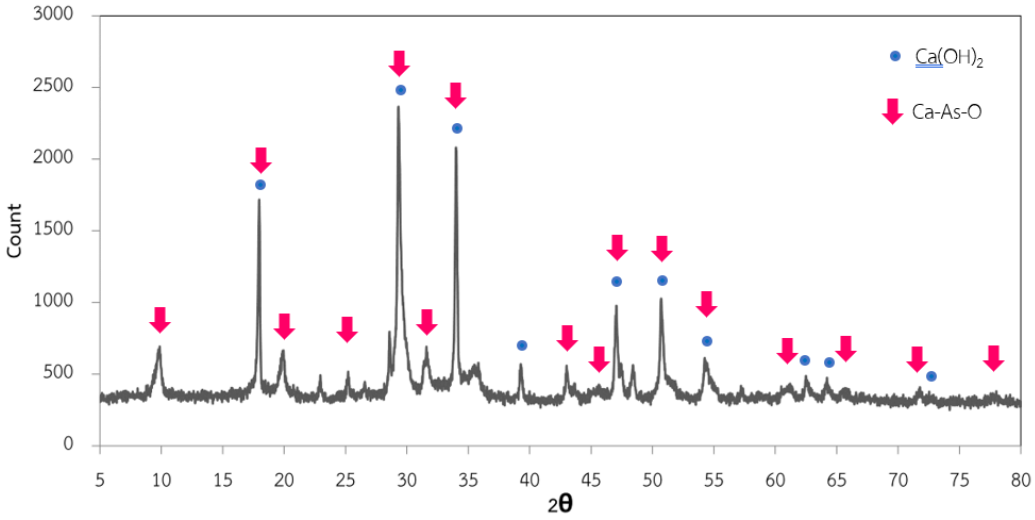

Figure 4-7 The XRD peaks of COS after As(III) adsorption test.

As described before, $CaCO_3$ which contained in OS transformed into CaO causing the appearance of CaO peaks in COS as in Figure 4-1. Considering Figure 4-7,

the peaks of $Ca(OH)_2$ and Ca-As-O were observed while the CaO peaks were not found. This implies that after COS was added into As(III) solution, CaO changed into $Ca(OH)_2$ and further adsorbed As(III) in the form of Ca-As-O.

The XRD peaks of COS after NO_3^- adsorption test are shown in Figure 4-8.

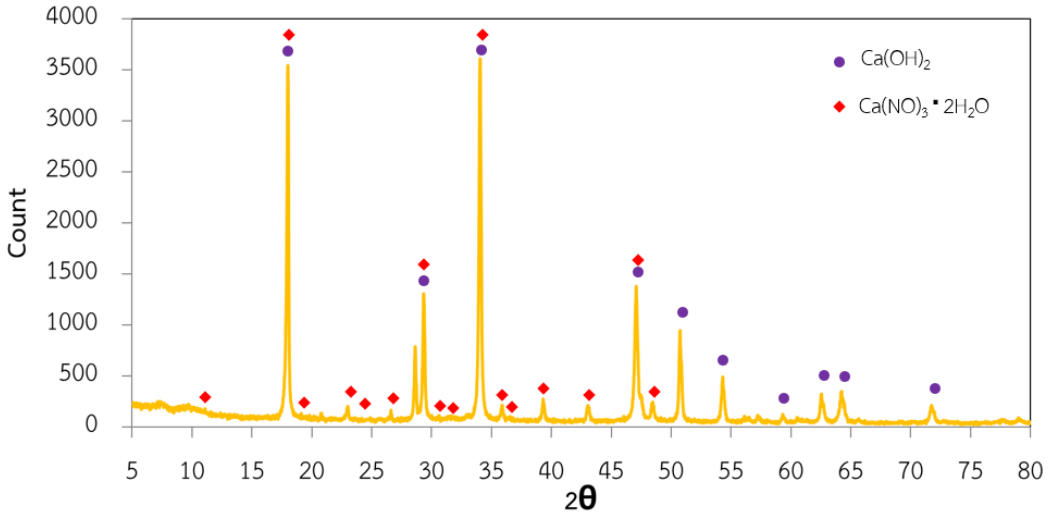

Figure 4-8 The XRD peaks of COS after NO_3^- adsorption test.

It can be seen in Figure 4-8 that after NO_3^- adsorption test, the CaO peaks of COS that appeared in Figure 4-1 could not be observed in Figure 4-8 while the XRD peaks corresponding to $Ca(OH)_2$ and $Ca(NO_3)_2 \cdot 2H_2O$ could be detected. This result implies that, after the COS was put into NO_3^- solution, CaO containing in COS transformed into $Ca(OH)_2$. Then, $Ca(OH)_2$ adsorbed NO_3^- and formed $Ca(NO_3)_2 \cdot 2H_2O$ on the COS surface.

For SO_4^{2-}, the XRD result of COS after used is illustrated in Figure 4-9.

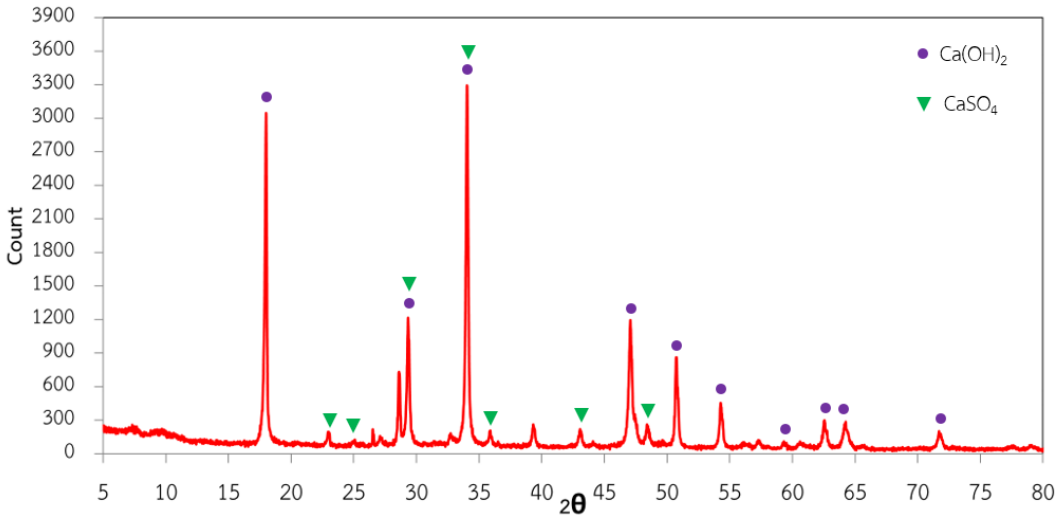

Figure 4-9 The XRD peaks of COS after SO_4^{2-} adsorption test.

After the SO_4^{2-} adsorption test, the XRD peaks of COS shows the peak patterns of $Ca(OH)_2$ and $CaSO_4$ as in Figure 4-9. Meanwhile, the CaO peaks that were observed in the XRD result of COS before SO_4^{2-} adsorption test (Figure 4-1) cannot be detected in this figure. This indicates that CaO in COS should change into $Ca(OH)_2$ and further adsorbed SO_4^{2-} in the form of $CaSO_4$.

The XRD peaks of COS after HPO_4^{2-} removal is presented in Figure 4-10.

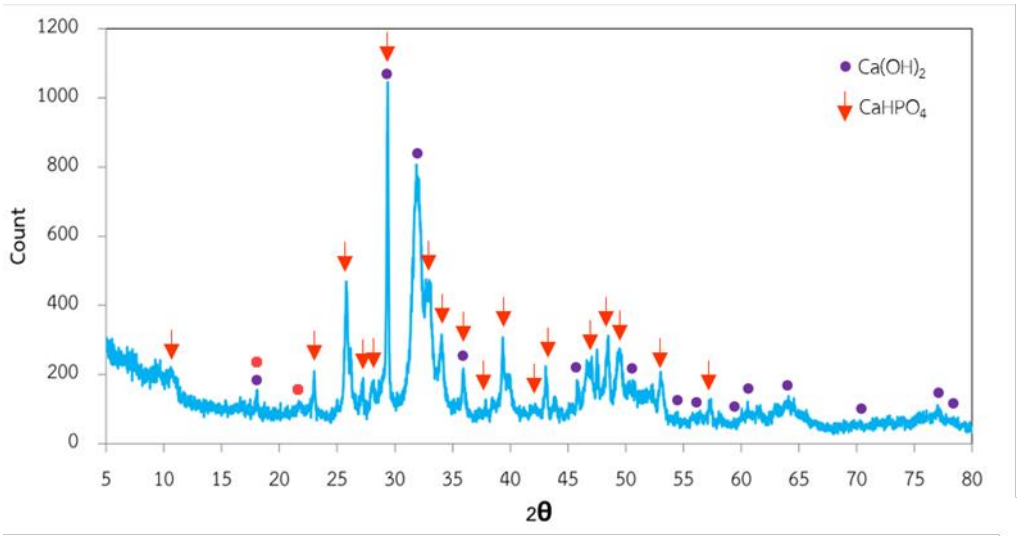

Figure 4-10 The XRD patterns of COS after HPO_4^{2-} removal test.

Considering Figures 4-1 and 4-10, after HPO_4^{2-} removal test, the peak pattern of CaO in Figure 4-1 was not observed in Figure 4-10 while the peak patterns of $Ca(OH)_2$ and $CaHPO_4$ can be observed. Based on XRD result, solubility and precipitation results indicate that some CaO in COS should dissolve and dissociate into OH^- and Ca^{2+}. Then, some Ca^{2+} precipitated with HPO_4^{2-} in the form of $CaHPO_4$. While the CaO which contained in the un-dissolved COS should change into $Ca(OH)_2$ and further adsorb HPO_4^{2-} in the form of $CaHPO_4$.

Based on XRD, solubility, precipitation and removal results, the mechanism of As(III) and anions adsorption on COS can be explained as the following reactions.

$$Ca(OH)_2 + H_2AsO_3^- \longrightarrow HCaAsO_3 + H_2O + OH^- \quad (4\text{-}3)$$

$$H_2AsO_3^- + OH^- \longrightarrow HAsO_3^{2-} + H_2O \quad (4\text{-}4)$$

$$Ca(OH)_2 + HAsO_3^{2-} \longrightarrow HCaAsO_3 + 2OH^- \quad (4\text{-}5)$$

$$Ca(OH)_2 + 2NO_3^- \longrightarrow Ca(NO_3)_2 + 2OH^- \quad (4\text{-}6)$$

$$Ca(OH)_2 + SO_4^{2-} \longrightarrow CaSO_4 + 2OH^- \quad (4\text{-}7)$$

$$Ca(OH)_2 + HPO_4^{2-} \longrightarrow CaHPO_4 + 2OH^- \quad (4\text{-}8)$$

$$Ca^{2+} + HPO_4^{2-} \longrightarrow CaHPO_4 \quad (4\text{-}9)$$

After COS was added into the solution, CaO in COS changed into $Ca(OH)_2$ as in Reaction (4-1). Some CaO could dissolve and dissociate into Ca^{2+} and OH^- causing the increase in pH of solution as in Reaction (4-2), while some of it still contained in the un-dissolved COS. Initially, pH of solution was approximately 11, thus As(III) and the other anions should be in the forms of $H_2AsO_3^-$, NO_3^-, SO_4^{2-} and HPO_4^{2-}. These anions should be adsorbed on the un-dissolved COS by ligand exchange as in Reactions (4-3), (4-6) - (4-8). It can be seen in Reactions (4-3) and (4-6) - (4-8) that, after ligand exchange, the OH^- was produced and released into the solution causing the increase in pH of the solution. Due to more amount of OH^- containing in the solution, the pH of solution increased, $H_2AsO_3^-$ was further deprotonated by OH^- into $HAsO_3^{2-}$ and adsorbed on the un-dissolving COS as in Reactions (4-4) and (4-5), respectively. As in

Reactions (4-3), (4-5), (4-7) and (4-8), it can be seen that $H_2AsO_3^-$, $HAsO_3^{2-}$, SO_4^{2-} and HPO_4^{2-} formed mononuclear bidentate complexes with Ca-OH which contained in un-dissolved COS while NO_3^- formed mononuclear monodentate complex with Ca-OH as in Reaction (4-6). Furthermore, HPO_4^{2-} could precipitate with Ca^{2+} which dissociated from $Ca(OH)_2$ (Reaction (4-2)) in the form of $CaHPO_4$ as in Reaction (4-9).

Moreover, NO_3^-, SO_4^{2-} and HPO_4^{2-} solutions which used in this work were prepared from $NaNO_3$, Na_2SO_4 and Na_2HPO_4, respectively. Thus, the solution should contain plenty of Na^+. Those Na^+ could form ionic bond with OH^- that was produced and released into solution (Reactions (4-2) - (4-3), (4-5) - (4-8)) in the form of NaOH. However, NaOH is a soluble compound that can dissolve in water as high as 1,110 g/L (20 °C) [159, 160]. In addition, as seen in XRD results (Figures 4-7 - 4-10), crystalline phase of NaOH was not detected on the COS after As(III) and anions removal tests. Thus, the formed NaOH should re-dissolve into the solution. Therefore, the effect of Na^+ on As(III) and anions removal performances should be insignificant.

4.3 Effect of anion(s) on As(III) adsorption in bi-, tri- and tetra-solutes

4.3.1. The effect of anion(s) on As(III) adsorption performance

The adsorption results in the previous section showed that the removal of As(III) and anions (NO_3^-, SO_4^{2-} and HPO_4^{2-}) by COS could occur in different ways causing the different maximum adsorption capacities (Figure 4-5) and morphologies (Figure 4-6). In water resources, there are many ions containing in water. Some ions might affect As(III) adsorption performance. Thus, in this section, the effects of anions such as NO_3^-, SO_4^{2-} and HPO_4^{2-} on the As(III) adsorption performance in bi- tri- and tetra-solutes were investigated. The experiments were performed via batch tests. The initial concentration of each anion was approximately 100 mg/L. The percentages of As(III) and anions remaining in the solution after removal tests are presented in Table

4-3. It is noted that the precipitation effect was eliminated from the adsorption percentages of HPO_4^{2-} presented in this table.

Table 4-3 Effect of competitive anion(s) on As(III) adsorption performance.

Anion(s) in the system	Adsorption percentage of each anion			
	As(III)	NO_3^-	SO_4^{2-}	HPO_4^{2-}
As(III)	74.90	-	-	-
As(III) + NO_3^-	68.46	37.62	-	-
As(III) + SO_4^{2-}	63.02	-	25.60	-
As(III) + HPO_4^{2-}	40.73	-	-	42.00
As(III) + NO_3^- + SO_4^{2-}	53.06	43.73	23.15	-
As(III) + NO_3^- + HPO_4^{2-}	20.83	67.30	-	53.95
As(III) + SO_4^{2-} + HPO_4^{2-}	40.00	-	21.19	43.44
As(III) + NO_3^- + SO_4^{2-} + HPO_4^{2-}	42.53	65.73	27.97	37.57

As seen in Table 4-3, the As(III) adsorption percentage decreased from 74.90% to the different values depending on the number and type of anions containing in the solution. In bi-solutes, the percentage of As(III) adsorption strongly decreased by 45.62% when As(III) paired with HPO_4^{2-}. Meanwhile, the percentages of As(III) adsorption insignificantly changed when As(III) mixed with NO_3^- and SO_4^{2-}. These results correlated with the maximum adsorption capacities of As(III) and anions in the individual adsorption tests (Figure 4-5).

In the case that As(III) paired with HPO_4^{2-}, the As(III) adsorption performance strongly decreased. There are five reasons that can be explained why HPO_4^{2-} strongly interfere As(III) adsorption performance.

(1) The chemical properties of phosphate (P) and Arsenic (As) such as electronegativity (EN), electron affinity (EA), ionization energy (1°, 2° and 3° ionization), etc. are similar [75, 133, 141, 161, 162]. Thus, HPO_4^{2-} should be more competitive to be adsorbed on the sorption sites which could adsorb As(III) than the other anions.

(2) The anionic radius of As(III) and HPO_4^{2-} are comparable in size. Roobottom et al.[163] studied the thermochemical radii of complex ions and reported that anionic radius of HPO_4^{2-} was approximately 0.213 nm while $H_2AsO_4^-$ had anionic radius size of 0.227 nm. The chemical structure of As(III) and As(V) are illustrated in Figure 4-11.

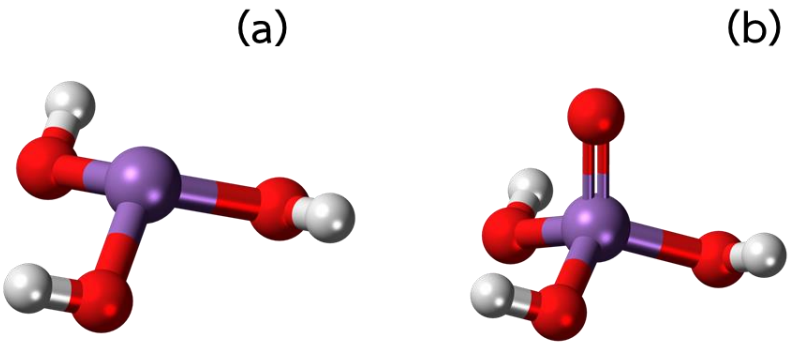

Figure 4-11 The chemical structures of (a) As(III) [164] and (b) As(V) [165].

As seen in Figure 4-11, the chemical structures of As(III) and As(V) are similar except As(V) has double bond with oxygen while As(III) has one lone paired electron. Therefore, the anionic radius of As(III) should be slightly smaller than that of As(V). Then, the anionic radii of As(III) and HPO_4^{2-} should still be comparable. In the adsorption process, the adsorbates should be adsorbed on the sorption sites where the interaction between adsorbates is insignificantly affected and radii of those adsorbates do not overlap. It means that if there are two anions (A and B) in the system, after anion A was adsorbed on the sorption sites, in order to decrease the repulsion between the negative charge of anions A and B and decrease the overlapping of those radii, the anion B should be able to be adsorbed on the sorption site that is far from the anion A occupied site. In this case, the radii of As(III) and HPO_4^{2-} were comparable in size. When HPO_4^{2-} was adsorbed on the sorption sites, it should block As(III) to be adsorbed on the neighboring sorption sites causing in lowering the available sorption sites where As(III) could be adsorbed.

(3) The nature of COS sorption sites was capable to adsorb HPO_4^{2-} better than As(III) (Figure 4-5).

(4) Charge density of HPO_4^{2-} is greater than that of As(III) ($H_2AsO_3^-$). As described before, the initial pH of As(III) and anions adsorption tests was approximately 11 which was lower than pH_{zpc} of COS. Then, the net COS surface charge should be positive and better attract anions (negative charge ion). This temporary phenomenon is called electrostatic attraction. In addition, it was reported that the multicharge anion could be better adsorbed on the positive adsorbent surface charge than the monovalent anion [145-147]. Therefore, HPO_4^{2-} which has two negative charges should be preferably adsorbed on the sorption sites than As(III) in the form of $H_2AsO_3^-$ which has one negative charge.

(5) Two negative charges of HPO_4^{2-} cause the rapid increase in electrostatic repulsion. In the adsorption process, when anions were adsorbed on the sorption sites, the negative charge of those anions would balance the positive adsorbent surface charge causing the increase of the negative charge on the adsorbent surface. Since the negative adsorbent surface charge was dominant, it repulsed the negative charge of anions called electrostatic repulsion and caused the decrease in anions adsorption performance. Due to two negative charges of HPO_4^{2-}, the positive adsorbent surface charge should be rapidly balanced by those negative charges. Then, the electrostatic repulsion between the negative charge of anions (As(III) and HPO_4^{2-}) and negative adsorbent surface charge rapidly increased causing the decrease of As(III) adsorption performance. This competitive As(III) and phosphate adsorption result is in good agreement with the results of Huang [166], Jian et al. [167] and Meng et al.[161] who studied the competitive adsorption between As(III) and phosphate on goethite, ZIF-8 nanoparticles and iron hydroxide, respectively. All of them found that the amount of As(III) adsorbed on their materials decreased when phosphate was present.

In the case of As(III) paired with NO_3^-, the percentage of As(III) adsorption decreased only 8.6% but the percentage of NO_3^- adsorption on the COS was as high as almost 38%. Four possible explanations can be given.

(1) The nature of COS sorption sites was capable to adsorb As(III) much better than NO_3^- as shown in Figure 4-5. Then, the As(III) adsorption performance was insignificantly affected by NO_3^-.

(2) The anionic radius of NO_3^- (0.2 nm [163]) is smaller than that of As(III). The atomic radii of N and As are presented in Figure 4-12.

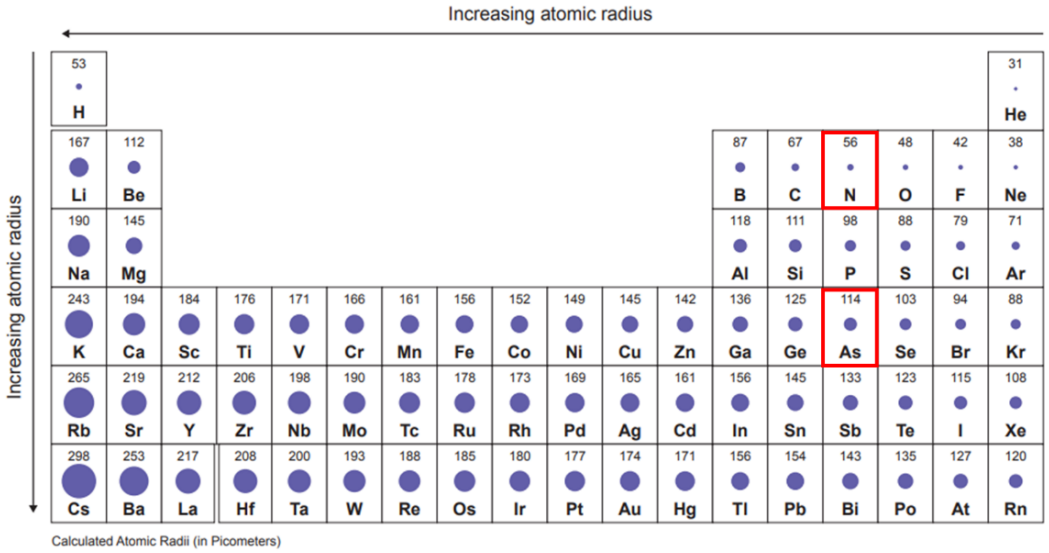

Figure 4-12 The atomic radii [168].

Figure 4-12 shows that the atomic radius of As was almost 2 times greater than that of N. Furthermore, the structure of As(III) in the form of $H_2AsO_3^-$ contained three oxygen atoms as same as the structure of NO_3^-. Then, the increase of those anionic radii should be comparable. Therefore, the anionic radius of NO_3^- should be smaller than that of As(III). As described above, in order to decrease the effects of adsorbates interaction and ionic radii overlapping, new adsorbates should be adsorbed on the sorption sites that are far from the occupied sorption site. Considering the charge of NO_3^- and As(III) ($H_2AsO_3^-$), those anions have one negative charge. Then, the negative charge repulsion between NO_3^- and $H_2AsO_3^-$ should be less than the other two cases (As(III) paired with HPO_4^{2-} and As(III) paired with SO_4^{2-}). Due to the smaller anionic radius of NO_3^- and lower adsorbates repulsion effect, NO_3^- could be adsorbed on the sorption sites where neighboring sorption sites were

occupied by As(III) without the overlapping between the radii of NO_3^- and As(III) and low adsorbates interaction. In addition, due to the smaller radius of NO_3^-, it should be better reach the sorption sites inside the pores of COS causing in high adsorption capacity of NO_3^-.

(3) As described before, NO_3^- was adsorbed on the adsorbent in the form of monomolecular monodentate complex with Ca-OH. It means that two ions of NO_3^- could be adsorbed on one sorption site. On the other hand, As(III) forms monomolecular bidentate complex with Ca-OH. Only one ion of As(III) could be adsorbed on one sorption site.

(4) Due to one negative charge of As(III) and NO_3^-, the positive charge on the adsorbent surface is slowly balanced causing in more amount of anions that could be adsorbed on the sorption sites. As described before, pH of solution in this case was lower than pH_{zpc} of COS, the positive adsorbent surface charge tended to attract anions. During the adsorption process, the negative charge of anions should balance the positive adsorbent surface causing the increase of electrostatic repulsion effect. In this case, both As(III) ($H_2AsO_3^-$) and NO_3^- have only one negative charge. Then, its negative charge should slowly balance the positive adsorbent surface charge causing in more amount of As(III) and NO_3^- adsorption on the COS sorption sites.

Table 4-3 also shows that the percentage of As(III) decreased by 15.86% when As(III) mixed with SO_4^{2-}. As seen in Figure 4-5, the COS sorption sites were capable to adsorb As(III) much better than SO_4^{2-} causing the lower decrease of As(III) adsorption percentage than the case of As(III) paired with HPO_4^{2-}. However, the As(III) adsorption percentage in this case (As(III) paired with SO_4^{2-}) is slightly lower than that of As(III) mixed with NO_3^-. Two reasons can be explained why the interference of SO_4^{2-} with As(III) adsorption performance was greater than that of NO_3^-.

(1) The radius of SO_4^{2-} (0.221 nm [163]) is larger than that of NO_3^-. Due to the larger radius of SO_4^{2-}, As(III) could not be adsorbed on the sorption sites where the near sorption sites were occupied by SO_4^{2-}.

(2) The charge density of SO_4^{2-} is also more than NO_3^-. Thus, two negative charges of SO_4^{2-} should balance the positive charge of adsorbent surface faster than one negative charge of NO_3^- causing the rapid increase in electrostatic repulsion effect. Then, the decrease of As(III) adsorption performance in the case of As(III) paired with SO_4^{2-} was greater than that of As(III) paired with NO_3^-.

The result of As(III), NO_3^-, SO_4^{2-} and HPO_4^{2-} adsorption performances in bi-solutes (Table 4-3) indicates that the binding affinity of HPO_4^{2-} on the COS sorption sites should be greater than those of As(III), SO_4^{2-} and NO_3^- respectively.

For tri- and tetra-solutes systems,, the adsorption percentages of As(III), NO_3^-, SO_4^{2-} and HPO_4^{2-} in Table 4-3 are different depending on the number and type of anions containing in the solution. Considering the adsorption results in Table 4-3, the percentages of As(III) removal in tri- and tetra-solutes systems are lower than those in bi-solutes system. For example, in bi-solutes, the As(III) adsorption percentage decreased from 74.90% to 68.46% when As(III) mixed with NO_3^- and 40.73% when the As(III) mixed with HPO_4^{2-} while the adsorption percentage of As(III) dramatically decreased to 20.83% when the As(III) solution contained both NO_3^- and HPO_4^{2-}. Conversely, the adsorption percentages of NO_3^- and HPO_4^{2-} in tri-solutes were greater than those of anions in bi-solutes system (As(III) mixed with NO_3^- and As(III) mixed with HPO_4^{2-}). This should be because the adsorbates interaction occurred during the adsorption process and affected the As(III) and those anions adsorption performances. In addition, the adsorption percentages of SO_4^{2-} presented in Table 4-3 are in the range of 21% - 29%. In order to clarify the results of As(III) and anions adsorption performances in bi-, tri- and tetra-solutes systems, the adsorption kinetics of As(III) and anions will be investigated in the next section.

4.3.2. Desorption test of As(III) and anions

As(III) and anions desorption tests were performed via batch tests. Initially, COS was added into the solution which contained As(III) and anions and kept for 24 h. The concentration of each anion was equivalent to 100 mg/L. After 24 h, the solution was heated from room temperature to 40°C. As(III) and anions concentrations were measured. The result is shown in Table 4-4. It is noted that the effect of precipitation was eliminated.

Table 4-4 Adsorption and desorption capacities of As(III) and anions.

	Adsorption or desorption capacities of each anion (mg/L)			
	As(III)	NO_3^-	SO_4^{2-}	HPO_4^{2-}
Adsorption (24 h)	38.75	69.41	14.55	40.04
Desorption	0.77	0.00	0.00	1.28

Table 4-4 shows that after COS was added into the solution and kept for 24 h, As(III), NO_3^-, SO_4^{2-} and HPO_4^{2-} were adsorbed on COS approximately 38.75 mg/L, 69.41 mg/L, 14.55 mg/L and 40.04 mg/L, respectively. After the solution was heated to 40°C, the amount of As(III) and anions desorbed from COS were lower than 1.30 mg/L. This indicates that As(III) and anions should be adsorbed on COS sorption sites via chemisorption.

4.3.3. The adsorption kinetics of As(III) and anions

In this section, the adsorption kinetics of As(III) and anions in single-solute, bi-, tri- and tetra-solutes were investigated. Seven assumptions were set. The flow chart of adsorption kinetics of As(III) and anions determination is presented in Figure 4-13.

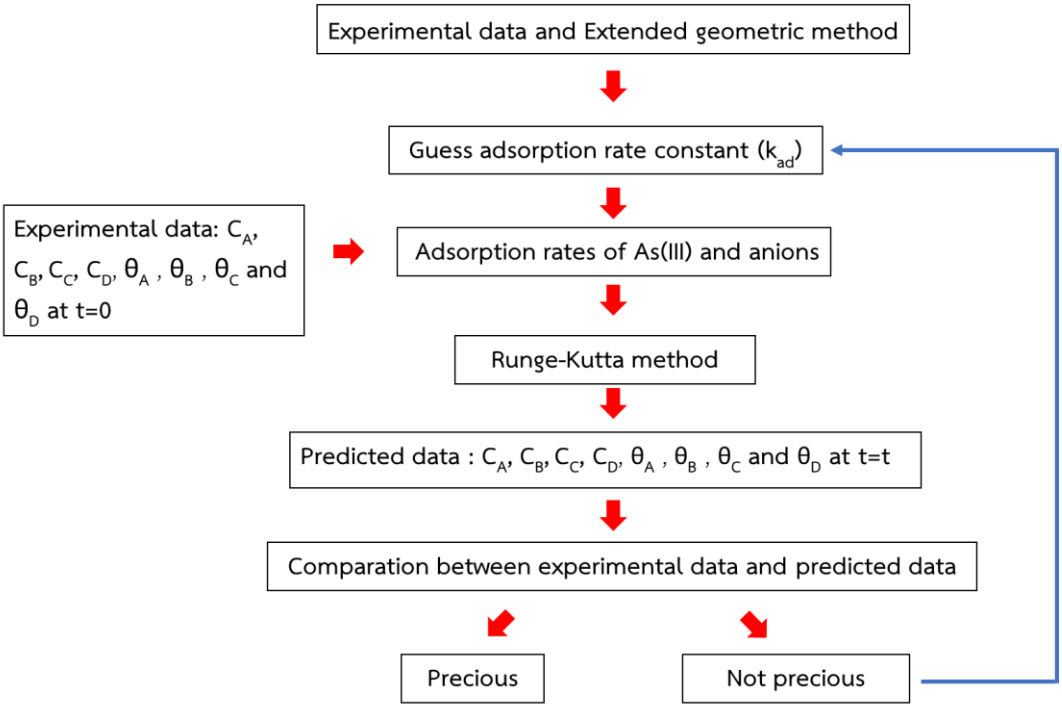

Figure 4-13 Flow charge of As(III) and anions adsorption kinetics determination.

As seen in Figure 4-13, the observed adsorption rate constants were initially estimated by using the extended geometric method purposed by Azizian et al. [48, 49]. After that the values of As(III) and anion occupied sites (θ_A, θ_B, θ_C and θ_D) in adsorption rate equations (Equations (3-2) – (3-5)) were solved by Runge-Kutta method [50, 51] and compared with the experimental results. The observed adsorption rate constants were gradually adjusted until the values of As(III) and anion occupied sites were well fitted with the experimental data. The data fitting of the fractions of sorption sites covered by As(III) and anions versus time corresponding to the case of As(III) mixed with NO_3^-, SO_4^{2-} and HPO_4^{2-} is illustrated in Figure 4-14.

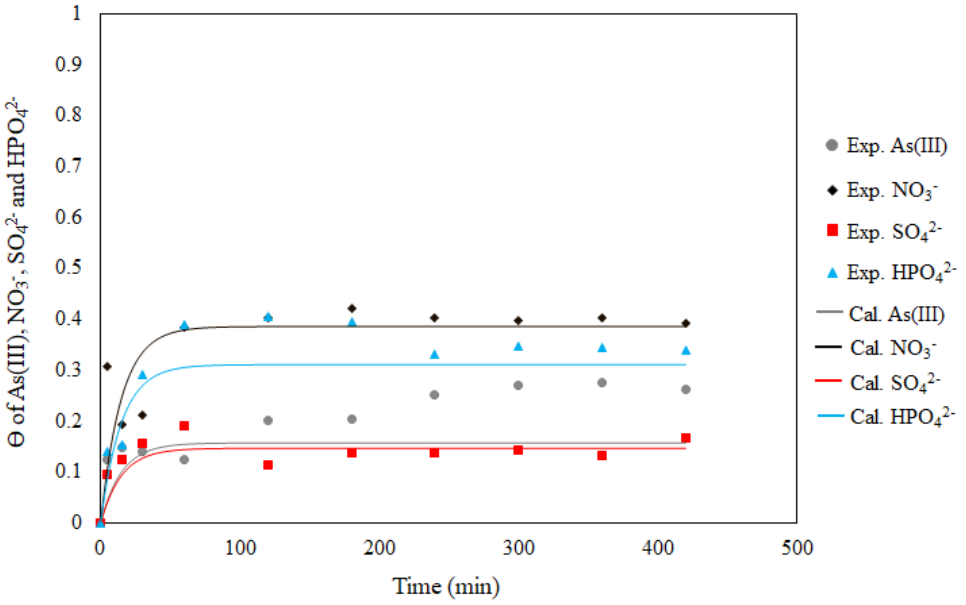

Figure 4-14 The variation of fractions of sorption sites covered (θ) by As(III), NO_3^-, SO_4^{2-} and HPO_4^{2-} with time.

Figure 4-14 shows that the fraction of sorption sites covered by As(III), NO_3^-, SO_4^{2-} and HPO_4^{2-} dramatically increased with time within 30 min because the available sorption sites of COS and solutes concentration gradient are still high. After that, the fraction of covered surface slowly increased due to the decrease in number of available sorption sites and concentration gradient. The system reaches equilibrium at approximately 300 min. It can be also seen in Figure 4-14 that the calculated results of NO_3^- and SO_4^{2-} occupied sites are well-fit with the experimental data while the calculated results of As(III) and HPO_4^{2-} considerably deviate from the experimental ones. Three possible reasons can be given to explain the deviation of calculated data.

(1). The interaction between adsorbates should affect the adsorption performance. In the assumption, it was assumed that there were no interaction between the adsorbates. However, in fact, there should be the interaction between each anion either more or less depending on charge repulsion and radius overlapping. As mentioned previously, the radii of As(III) and HPO_4^{2-} were comparable

and charge of As(III) was negative (ranging from -1 to -2 depending on pH of the solution during adsorption process) which should cause negative charge repulsion with HPO_4^{2-}. Therefore, the interaction between As(III) and HPO_4^{2-} should be significant.

(2) Some molecules of As(III) or anions in the bulk solution could displace the molecules that occupied on the sorption sites. From the assumption, after the molecules of As(III) and anions were adsorbed the sorption sites, the other molecules in the bulk solution could not hit and displace those adsorbed molecules. However, in fact, during the adsorption process, some molecules that were adsorbed on the sorption sites could be displaced by the other molecules which had greater affinity to the sorption sites than the occupied one.

(3) The electrostatic attraction or repulsion between adsorbent and adsorbates should significantly affect As(III) and anions adsorption performances. In the assumption, the electrostatic attraction or repulsion between adsorbent and adsorbates less affected As(III) and anions adsorption performance. In fact, the electrostatic attraction or repulsion between adsorbent and adsorbates should affect the adsorption performances of As(III) and anions. Considering Figure 4-14, it can be seen that, at time 120 min - 240 min, the fraction of As(III) covered surface is slightly increased while the fraction of HPO_4^{2-} covered surface slightly decreased. As described before, during the adsorption process, the negative charge of anions would balance the positive charge of adsorbent surface charge causing the increase of electrostatic repulsion. Due to the greater charge density of HPO_4^{2-}, HPO_4^{2-} adsorption performance should be more affected by the repulsion between the negative charges of adsorbent surface and negative charge of HPO_4^{2-} (electrostatic repulsion). Thus, when the net surface charge became negative, some HPO_4^{2-} could be desorbed. As explained before, the chemical properties of As(III) and HPO_4^{2-} were similar. In addition, Figure 4-5 also showed that HPO_4^{2-} could be adsorbed on the

COS sorption sites slightly better than As(III). Then, the vacant sites of HPO_4^{2-} desorption should be replaced by As(III) ($H_2AsO_3^-$).

The observed adsorption rate constants of As(III) and anions are shown in Table 4-5.

Table 4-5 The observed adsorption rate constants of As(III) and anions.

Anions in the system	Observed adsorption rate constant ($k_{ad} \times 10^5$, min^{-1})			
	As(III)	NO_3^-	SO_4^{2-}	HPO_4^{2-}
As(III)	2.3			
As(III) + NO_3^-	3.5	2.0		
As(III) + SO_4^{2-}	1.8		0.6	
As(III) + HPO_4^{2-}	2.0			4.0
As(III) + NO_3^- + SO_4^{2-}	1.6	1.5	0.6	
As(III) + NO_3^- + HPO_4^{2-}	1.2	3.4		4.0
As(III) + SO_4^{2-} + HPO_4^{2-}	1.3		0.8	2.6
As(III) + NO_3^- + SO_4^{2-} + HPO_4^{2-}	8.9	19.5	7.8	20.0

Table 4-5 shows that, in bi-solutes, the observed adsorption rate constant of As(III) is lower than that of HPO_4^{2-}. In contrast, the observed adsorption rate constants of As(III) are greater than those of NO_3^- and SO_4^{2-}. This implies that HPO_4^{2-} should be adsorbed on the COS sorption sites faster than the other anions. In tri- and tetra-solutes, Table 4-5 also shows that the adsorption rate constants of HPO_4^{2-} are still greater than those of As(III), NO_3^- and SO_4^{2-}. Then, in tri- and tetra-solutes systems, HPO_4^{2-} should be also faster adsorbed on the sorption sites than the other anions. It is interesting that, when the solution contained HPO_4^{2-}, the observed adsorption rate constants of NO_3^- are greater than those of As(III) in every case. This should be because of some interaction between HPO_4^{2-} and NO_3^- during the adsorption process. This point will be discussed in the next section. Moreover, the observed adsorption

rate constants of SO_4^{2-} in Table 4-5 are the lowest in every conditions of interest thus it should be the slowest adsorption on the sorption sites.

4.3.4. Percentages of As(III) and anions occupied on the COS sorption sites

In this section, the interaction between As(III) adsorption and anion(s) that presented in the solution during the adsorption process was investigated. The percentages of As(III) and anions occupied on the COS sorption sites were calculated by using the information from the previous sections. The flow charge of calculation percentages of As(III) and anions occupied on the COS sorption sites is illustrated in Figure 4-15.

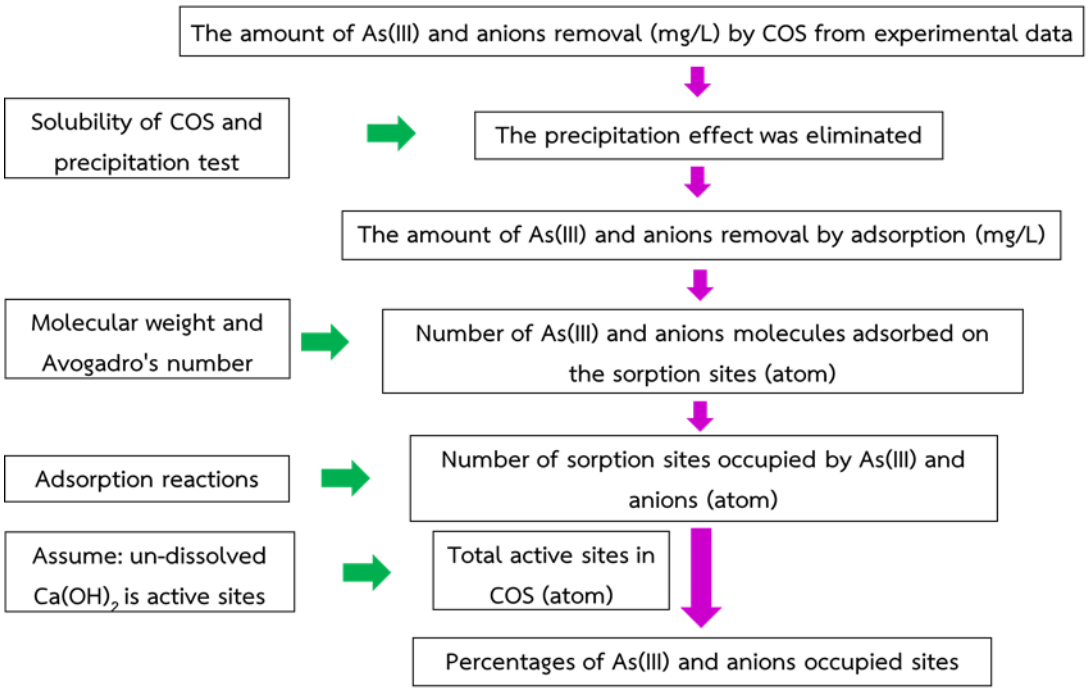

Figure 4-15 Flow charge of calculation percentages of As(III) and anions occupied on the COS sorption sites.

As seen in Figure 4-15 that, firstly, the initial and final concentrations of As(III) and anions from the experimental data were used to calculate the amount of As(III) and anions removals by COS. Then, the precipitation effect was eliminated in order

to estimate the amount of As(III) and anions removed by the adsorption process. After that, the concentrations of As(III) and anions (mg/L) were changed into the number of atom by using the molecular weight (mg/mol) and Avogadro's number (6.02×10^{23} atom/mol). Based on the adsorption and desorption experiments, As(III) and anions were assumed to be monolayer adsorption on the COS sorption sites. In addition, according to the adsorption mechanisms mentioned above, it could be assumed that As(III), SO_4^{2-} and HPO_4^{2-} form mononuclear bidentate complexes with Ca-OH while NO_3^- forms mononuclear monodentate complex with Ca-OH. Thus, the number of sorption sites of As(III) and anions occupied could be calculated. In order to estimate the percentages of As(III) and anions occupied sites, the theoretical amount of the adsorption sites of COS was estimated by assuming that one molecule of undissolved CaO represented one adsorption active site. Then, the numbers of sorption sites of As(III) and anions occupied were divided by the theoretical amount of the adsorption sites of COS in order to get the percentages of As(III) and anions occupied on the COS sorption sites.

The percentages of each anion adsorbed on the sorption sites in single-solute and bi-solutes systems were calculated. The percentages of As(III) and anions occupied sites in single-solute and bi-solutes systems are presented in Table 4-6.

Table 4-6 The percentages of As(III) and anions occupied sites in single-solute and bi-solutes systems.

	The percentage of occupied sites				
Anions in the system	As(III)	NO_3^-	SO_4^{2-}	HPO_4^{2-}	Total
As(III)	17.13	-	-	-	17.13
As(III) + NO_3^-	15.96	9.72	-	-	25.67
As(III) + SO_4^{2-}	14.97	-	8.28	-	23.25
As(III) + HPO_4^{2-}	10.05	-	-	10.82	20.87

Table 4-6 shows that, when the As(III) solution contained anion(s), the percentages of As(III) occupied sites decreased from 17.17% (without anions) to different values depending on the type of anions containing in solutions.

As seen in Table 4-6, the percentages of As(III) are slightly decreased when As(III) mixed with NO_3^- or SO_4^{2-}. There are three possible reasons that can be explained this result.

(1) The COS sorption site had capability to adsorb As(III) better than NO_3^- and SO_4^{2-} (Figure 4-5).

(2) The observed adsorption rate constants of As(III) were greater than those of NO_3^- and SO_4^{2-} (Table 4-5). Thus, As(III) should be adsorbed on the sorption sites quicker than those two anions.

(3) In the case of As(III) mixed with NO_3^-, the increase of pH in the solution during the adsorption process caused the transformation of As(III) from $H_2AsO_3^-$ into $HAsO_3^{2-}$ which was better to be adsorbed on the positive surface charge of adsorbent than NO_3^-. As explained before, during the adsorption process, some CaO in COS could dissolve and dissociate into Ca^{2+} and OH^- as in Reaction (4-2) causing the increase in pH of solution. Then, As(III) in the form of $H_2AsO_3^-$ could be deprotonated by OH^- in the solution and change into $HAsO_3^{2-}$ as in Reaction (4-4). Then, the charge density of $HAsO_3^{2-}$ was greater than that of NO_3^-. Thus, As(III) should be adsorbed on the sorption sites better than NO_3^-.

The comparison of percentages of As(III) and anions occupied sites in single-solute and bi-solutes systems is illustrated in Figure 4-16.

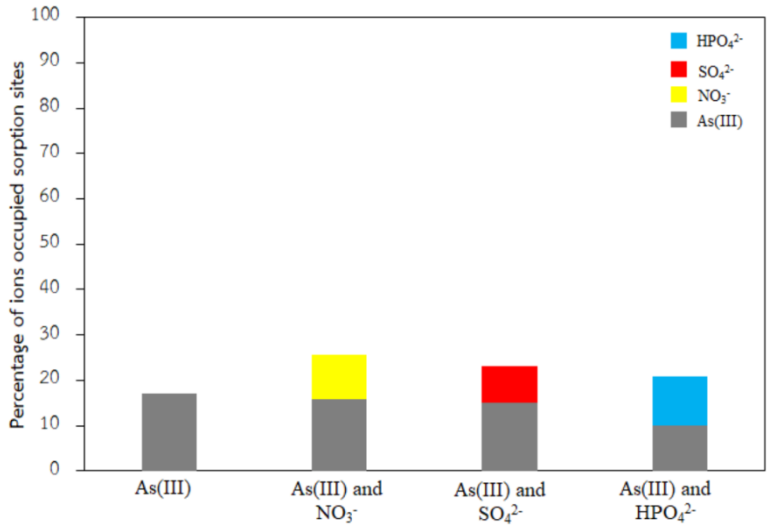

Figure 4-16 The percentages of As(III) and anions occupied sites in single-solute and bi-solutes systems.

As seen in Figure 4-16, in bi-solutes system, the total percentage of As(III) and NO_3^- occupied sites is greater than the other two cases. Two possible explanations can be given.

(1) The anionic radius of NO_3^- is smaller than the other anions and the negative charge of NO_3^- is also less than the other two anions. Thus, it should be adsorbed on the sorption sites that the neighboring sorption sites were occupied by As(III) without the radii overlapping and with low adsorbates interaction. In addition, NO_3^- should better reach the sorption sites inside the pores of COS because of its smaller size.

(2) The one negative charge of NO_3^- caused the slowly increase in electrostatic repulsion between adsorbent surface charge and adsorbate charges. Thus, the amount of As(III) and NO_3^- that could be adsorbed on the available sorption site should increase.

Figure 4-16 shows that the percentage of As(III) occupied sites dramatically decreased when As(III) mixed with HPO_4^{2-}. Five possible reasons can be explained the strong interference of HPO_4^{2-} with As(III) adsorption performance.

(1) By nature, COS sorption sites had capability to adsorb HPO_4^{2-} better than As(III) (Figure 4-5).

(2) The similar chemical properties and comparable in size of anionic radii of As(III) and HPO_4^{2-} caused the greater interference of HPO_4^{2-} with As(III) adsorption performance. Due to the similar chemical properties and comparable anionic radii of As(III) and HPO_4^{2-}, when HPO_4^{2-} was adsorbed on the sorption sites, it could block As(III) to be adsorbed on the neighboring sorption sites causing the limit available active sites that As(III) could be adsorbed.

(3) The observed adsorption rate constant of HPO_4^{2-} (Table 4-5) was about 2 times greater than that of As(III). Thus, HPO_4^{2-} should be adsorbed on the sorption sites faster than As(III). As described before, after HPO_4^{2-} occupied on the sorption sites, it could block As(III) to be adsorbed on the neighboring sorption sites causing the strong decrease in the percentage of As(III) occupied sites.

(4) The charge density of HPO_4^{2-} is greater than that of As(III). As described earlier, at initial period of adsorption process, HPO_4^{2-} which had two negative charges should be adsorbed on the positive adsorbent surface charge better than $H_2AsO_3^-$ which had only one negative charge.

(5) The two negative charges of HPO_4^{2-} could rapid increase the electrostatic repulsion effect. As explained before, HPO_4^{2-} could be adsorbed on the available sorption sites quicker than As(III) (Table 4-5). Due to two negative charges of HPO_4^{2-}, the electrostatic repulsion should rapid increase causing the decrease of As(III) ($H_2AsO_3^-$ into $HAsO_3^{2-}$) adsorption performance.

The adsorption results in bi-solutes system indicate that the binding affinity of COS sorption sites on HPO_4^{2-} is greater than that of As(III), while the binding affinity of COS sorption sites on As(III) is greater than those of SO_4^{2-} and NO_3^-, respectively.

The percentages of each anion occupied sites in tri- and tetra-solutes systems were also calculated. The calculated results are presented in Table 4-7.

Table 4-7 The percentages of As(III) and anions occupied sites in tri- and tetra-solutes systems.

Anions in the system	The percentage of occupied sites				
	As(III)	NO_3^-	SO_4^{2-}	HPO_4^{2-}	Total
As(III) + NO_3^- + SO_4^{2-}	11.66	9.98	6.47	-	28.12
As(III) + NO_3^- + HPO_4^{2-}	4.38	15.80	-	16.63	36.82
As(III) + SO_4^{2-} + HPO_4^{2-}	9.23	-	6.47	12.08	27.79
As(III) + NO_3^- + SO_4^{2-} + HPO_4^{2-}	9.84	14.82	8.18	10.34	43.18

Considering the percentages of As(III) and anions occupied sites in Tables 4-6 and 4-7, the percentages of As(III) occupied sites in tri- and tetra-solutes are lower than those in bi-solutes because the amounts of adsorbates in tri- and tetra-solutes systems were greater than those in bi-solutes. Then, those adsorbates in tri- and tetra-solutes systems should be more competitive to be adsorbed on the sorption sites than those adsorbates in bi-solutes system. The As(III) and anions adsorption performances in tri- and tetra-solutes depended on its chemical properties, its adsorption behavior, the interaction between the adsorbates and adsorbent and the interaction between adsorbates. In this work, the As(III) and anions adsorption performances were determined on a case by case basis.

As seen in Table 4-7, when As(III) solution mixed with NO_3^- and SO_4^{2-}, the percentage of As(III) occupied sites is greater than those of NO_3^- and SO_4^{2-}. Three possible reasons can be given.

(1) The COS sorption sites had capability to adsorb As(III) much better than NO_3^- and SO_4^{2-} as shown in Figure 4-5.

(2) The observed adsorption rate constant of As(III) is greater than those of the other two anions (Table 4-5). Thus, the As(III) should be adsorbed on the sorption sites faster than the other two anions.

(3) As previously mentioned, the binding affinity of COS sorption sites on As(III) was greater than those of NO_3^- and SO_4^{2-} causing the less interfering of NO_3^- and SO_4^{2-} with As(III) adsorption performance.

However, the percentage of As(III) occupied sites under the presence both of NO_3^- and SO_4^{2-} is slightly lower than those in As(III) mixed with NO_3^- and As(III) mixed with SO_4^{2-} solutions as shown in Figure 4-17.

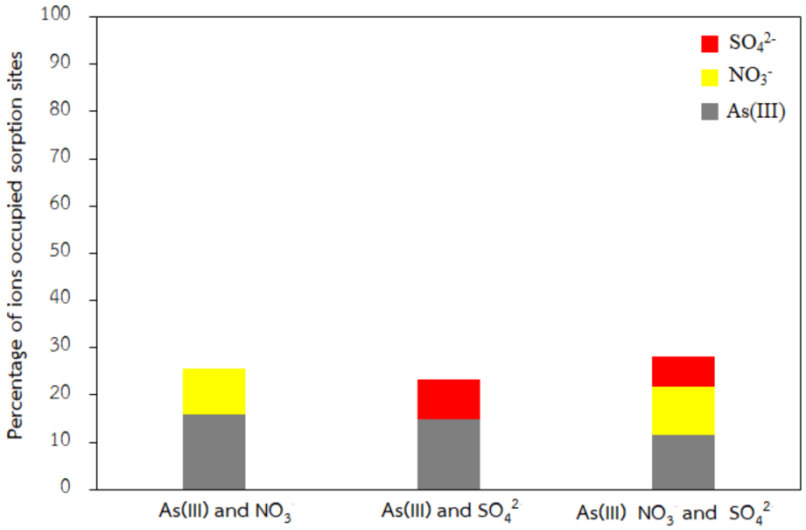

Figure 4-17 The percentages of As(III), NO_3^- and SO_4^{2-} occupied sites when As(III) mixed with NO_3^-, As(III) mixed with SO_4^{2-} and As(III) combined with NO_3^- and SO_4^{2-}.

The possible reasons of the greater decrease in percentage of As(III) occupied sites when As(III) combined with NO_3^- and SO_4^{2-} can be explained as the following.

(1) The greater number of anions containing in the tri-solutes system leads to the greater competition of those anions to be adsorbed on the sorption sites.

(2) As(III) and anions should be adsorbed on the sorption sites in comparable time. From Table 4-5, the observed adsorption rate constant of As(III) was slightly greater than NO_3^-. Thus, at initial period, As(III) and NO_3^- should be adsorbed on the sorption sites in the comparable time causing the decrease in available sorption sites for adsorbing As(III). When the time passed, SO_4^{2-} was also be adsorbed on the sorption sites. As mentioned before, the large anions radius of SO_4^{2-} could obstruct As(III) to occupy on the neighboring sorption sites. Thus, the available sorption sites which As(III) could occupy was limited.

(3) The negative charges of NO_3^- and SO_4^{2-} containing in tri-solutes should be faster balanced the positive charge of adsorbent surface than those of them in bi-solutes systems. Then, the increase in the effect of electrostatic repulsion in tri-solutes system should be quicker than those in bi-solutes systems causing in the lower As(III) adsorption performance.

It can also be seen in Figure 4-17 that the percentage of NO_3^- occupied sites in tri-solutes system is comparable with that in bi-solutes system. As discussed above, NO_3^- had smaller anionic radius and negative charge thus it could be adsorbed on the vacant sorption sites where the near sorption sites were occupied by other anions without anionic radii overlapping and less repulsion effect between NO_3^- and anions occupied on the near sorption sites. Furthermore, NO_3^- has only one negative charge thus its adsorption performance should be less affected by electrostatic repulsion causing the insignificant change in the percentages of NO_3^- occupied sites in bi- and tri-solutes systems.

Considering Figure 4-17, the percentages of SO_4^{2-} occupied sites in bi- and tri-solutes systems are lower than those of As(III) and NO_3^-. The reasons of the lowest percentages of SO_4^{2-} occupied sites in both systems can be explained as the following.

(1) The observed adsorption rate constants of SO_4^{2-} in bi- and tri-solutes systems were lower than those of the other two anions (Table 4-5) causing the slowest being adsorbed on the sorption sites.

(2) The sorption site of COS preferred to adsorb As(III) than SO_4^{2-} as shown in Figure 4-5. Thus, most sorption sites should be occupied by As(III).

(3) As stated above, the binding affinity of COS on SO_4^{2-} was lower than that of As(III) causing the less SO_4^{2-} adsorbed on the available sorption sites.

(4) SO_4^{2-} had greater negative charge and larger anionic radius than NO_3^-. Then, it could not be adsorbed on the sorption sites that the neighboring sorption sites were occupied by other anions like NO_3^- could. Thus, the available sorption sites that SO_4^{2-} could occupied were limited

(5) Due to two negative charges of SO_4^{2-}, the effect of electrostatic repulsion on SO_4^{2-} adsorption performance should be greater than those on As(III) ($H_2AsO_3^-$) and NO_3^- which have only one negative charge.

For the case of As(III) mixed with NO_3^- and HPO_4^{2-}, the percentages of As(III), NO_3^- and HPO_4^{2-} in bi- and tri-solutes were compared as presented in Figure 4-18.

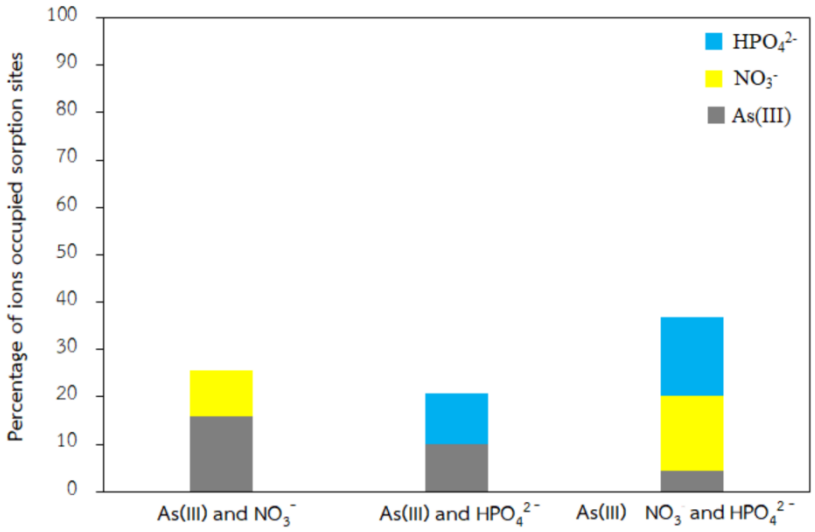

Figure 4-18 The percentages of As(III), NO_3^- and HPO_4^{2-} occupied sites when As(III) mixed with NO_3^-, As(III) mixed with HPO_4^{2-} and As(III) combined with NO_3^- and HPO_4^{2-}.

As seen in Figure 4-18, when As(III) solution contained both NO_3^- and HPO_4^{2-}, the percentage of As(III) occupied sites is extremely lower than those of As(III) in the other two cases (As(III) mixed with NO_3^- and As(III) mixed with HPO_4^{2-}). There are four reasons that can be explained the extremely low percentage of As(III) occupied sites when the solution contained both of HPO_4^{2-} and NO_3^-.

(1) In tri-solutes, the observed adsorption rate constant of As(III) was much lower than HPO_4^{2-} and NO_3^- (Table 4-5). This implies that, at initial period, HPO_4^{2-} and NO_3^- should be adsorbed on the sorption sites before As(III) causing the decrease of available sorption sites for adsorbing As(III).

(2) Most of available sorption sites were occupied by HPO_4^{2-}. As discussed in the previous section, the charge density, observed adsorption rate constant and binding affinity of HPO_4^{2-} were greater than those of As(III). In addition, the sorption sites preferred to adsorb HPO_4^{2-} than As(III) (Figure 4-5). Thus, most of sorption sites should be occupied by HPO_4^{2-} causing the less available sites for As(III) occupying.

(3) As(III) was blocked to be adsorbed on the vacant sorption sites that the neighboring sorption sites were occupied by HPO_4^{2-} because the anionic radii of As(III) and HPO_4^{2-} are comparable in size. As already stated, HPO_4^{2-} should be adsorbed before As(III) thus the available sorption sites that As(III) could occupy were limited.

(4) Due to the greater negative charges of anions in tri-solutes system, the quicker electrostatic repulsion affected the As(III) adsorption performance causing the decrease in percentage of As(III) occupied sites. As previously described, the negative charge of As(III) and anions which were adsorbed on the sorption sites caused the increase in the effect of electrostatic repulsion on As(III) and anions adsorption performances. When the effect of electrostatic repulsion is dominant, the repulsion between the negative charges of adsorbent surface and anions become stronger causing the more hindrance of As(III) to be adsorbed on the sorption sites. In addition, OH^- produced from adsorption reaction as in Reactions (4-3), (4-6) and (4-8) caused the change of As(III) ($H_2AsO_3^-$) into $HAsO_3^{2-}$. Due to two negative charges of $HAsO_3^{2-}$, the effect of electrostatic repulsion on $HAsO_3^{2-}$ should be greater than that of NO_3^- which has only one negative charge causing in the lower percentage of As(III) occupied sites.

On the other hand, Figure 4-18 shows that, in bi- and tri-solutes systems, the percentages of HPO_4^{2-} occupied sites are greater than those of As(III) and NO_3^- because of the greater observed adsorption rate constants, charge density and binding affinity. Moreover, the sorption sites of COS preferred to adsorb HPO_4^{2-} than the other anions.

It can also be seen in Figure 4-18 that, in tri-solutes system, the percentage of NO_3^- occupied sites is greater than that of As(III). Three possible reasons can be given.

(1) Due to the small anionic radius of NO_3^-, it could be adsorbed on the vacant sorption sites that neighboring sorption sites were occupied by HPO_4^{2-} or As(III). Thus, the percentage of NO_3^- occupied sites is greater than that of As(III).

(2) The observed adsorption rate constant of NO_3^- (Table 4-5) was almost 2.8 times greater than that of As(III). At initial period, NO_3^- should be adsorbed on the vacant sorption sites before As(III). Therefore, it could be more adsorbed on the available sorption sites than As(III).

(3) Due to the one negative charge of NO_3^-, the effect of electrostatic repulsion on NO_3^- adsorption performance should be less than those of As(III) ($HAsO_3^{2-}$) and HPO_4^{2-}. Thus, when the effect of electrostatic repulsion became dominant, NO_3^- should be greater occupied on sorption sites than $HAsO_3^{2-}$.

Considering Figure 4-18, the percentages of NO_3^- occupied sites in tri-solutes system is greater than that of NO_3^- in bi-solutes system. Two possible reasons can be given.

(1) In bi-solutes, the observed adsorption rate constant of NO_3^- was lower than that of As(III). NO_3^- should be adsorbed on the vacant sorption sites after As(III) causing the lowering available sorption sites for NO_3^- adsorbing. Conversely, in tri-solutes, NO_3^- could be adsorbed on the available sorption sites before As(III). Thus, in tri-solutes system, NO_3^- should be more occupied on the sorption sites greater than that of it in bi-solutes system.

(2) In tri-solutes system, the electrostatic repulsion became dominant effect quicker than the bi-solutes system. $HAsO_3^{2-}$ and HPO_4^{2-} should be less adsorbed on the sorption sites causing the more available sorption sites remaining on the un-dissolved COS. Due to the lower negative charge of NO_3^-, when the electrostatic repulsion became dominant effect, it should be better adsorbed on the sorption sites than the others anions which have more negative charges. Thus, in tri-solutes, NO_3^- should be greater occupied on those sorption site than that in bi-solutes.

In the case of As(III) mixed with SO_4^{2-} and HPO_4^{2-}, The percentage of HPO_4^{2-} occupied sites is greater than those of the other two anions because of the greater

observed adsorption rate constant of HPO_4^{2-}, the stronger binding affinity of the sorption sites on HPO_4^{2-} and more preference of un-dissolved COS sorption sites to adsorb HPO_4^{2-}.

Conversely, the percentage of SO_4^{2-} occupied sites is lower than those of As(III) and HPO_4^{2-}. This should be because (1) the observed adsorption rate constant of SO_4^{2-} (Table 4-5) was much less than those of HPO_4^{2-} and As(III), (2) the capability of COS sorption site to adsorb SO_4^{2-} was lower than those two anions and (3) the binding affinity of sorption sites on SO_4^{2-} was also weaker than the other two anions.

The calculated percentages of As(III) and anions occupied sites in tri- and tetra-solutes systems were compared as illustrated in Figure 4-19.

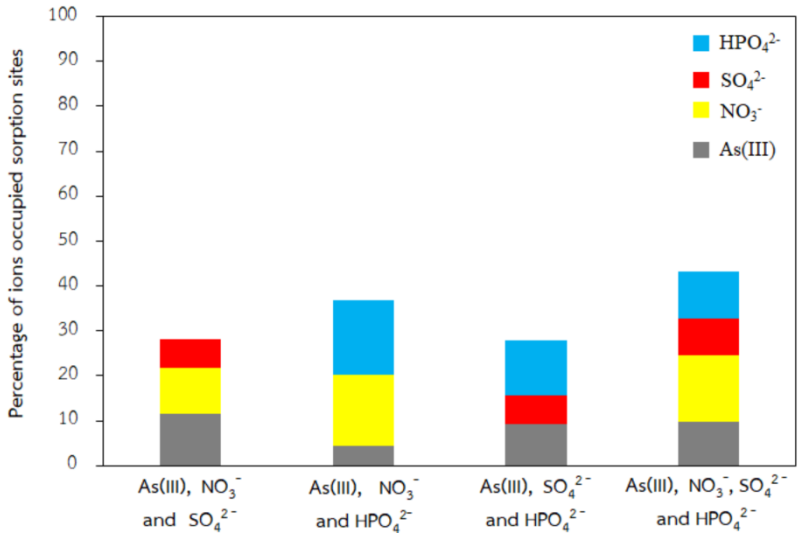

Figure 4-19 The percentages of As(III), NO_3^-, SO_4^{2-} and HPO_4^{2-} occupied sites when As(III) combined with NO_3^- and SO_4^{2-}, As(III) combined with NO_3^- and HPO_4^{2-}, As(III) combined with SO_4^{2-} and HPO_4^{2-} and As(III) combined with NO_3^-, SO_4^{2-} and HPO_4^{2-}.

Figure 4-19 shows that, in tri-solutes system, the percentage of As(III) occupied sites when As(III) combined with NO_3^- and SO_4^{2-} is greater than those of the other two cases that contained HPO_4^{2-} which could be better and faster adsorbed on the sorption sites than As(III). Due to the comparable in size of anionic radii of HPO_4^{2-} and

As(III), HPO_4^{2-} could block As(III) to be adsorbed on sorption sites that the neighboring sorption sites were occupied by HPO_4^{2-}.

Considering Figure 4-19, when SO_4^{2-} was mixed into the solution instead NO_3^- in As(III) combined with NO_3^- and HPO_4^{2-} solution, the percentage of As(III) occupied sites significantly increased while the percentage of HPO_4^{2-} occupied sites slightly decreased. In addition the total occupied sorption sites of As(III) combined with NO_3^- and HPO_4^{2-} also greater than that of As(III) combined with SO_4^{2-} and HPO_4^{2-}. Two possible reasons can be given.

(1) The anionic radii of As(III), SO_4^{2-} and HPO_4^{2-} are comparable in size. Those three anions could not be adsorbed on the sorption sites that the neighboring sorption sites were occupied by the other molecules like NO_3^- could. Then, the available sorption sites that those anions could be adsorbed should be limited. Thus, the total percentage of As(III) and anions occupied sites in As(III) combined with SO_4^{2-} and HPO_4^{2-} is lower than that in As(III) combined with NO_3^- and HPO_4^{2-}.

(2) Due two negative charges of SO_4^{2-} and HPO_4^{2-}, the effect of electrostatic repulsion should quickly become dominant causing in lowering As(III), SO_4^{2-} and HPO_4^{2-} adsorption performances. HPO_4^{2-} has negative charges greater than As(III) in the form of $H_2AsO_3^-$. The effect of electrostatic repulsion on HPO_4^{2-} adsorption performance should be stronger than that of $H_2AsO_3^-$ causing the less HPO_4^{2-} adsorbed on the sorption sites. However, in Table 4-5 and Figure 4-5, at initial period, HPO_4^{2-} could be adsorbed on the sorption sites faster and better than the other anions. Therefore, the percentage of HPO_4^{2-} occupied sites in As(III) combined with SO_4^{2-} and HPO_4^{2-} solution was slightly less than that in As(III) combined with NO_3^- and HPO_4^{2-}.

For As(III), when the electrostatic repulsion becomes dominant effect, less anions could be adsorbed on the sorption sites causing more available sorption sites remaining on the un-dissolved COS. Due to the lower negative charge of $H_2AsO_3^-$, the

effect of electrostatic repulsion on its adsorption performance should be lower than SO_4^{2-} and HPO_4^{2-} cases causing in more As(III) occupied sites in As(III) combined with SO_4^{2-} and HPO_4^{2-} solution.

For tetra-solutes system, the percentage of HPO_4^{2-} occupied sites is significantly lower than that in As(III) combined with NO_3^- and HPO_4^{2-} as illustrated in Figure 4-19. This should be because the large anionic radius of SO_4^{2-} would obstruct or block HPO_4^{2-} and As(III) from reaching the sorption sites where the neighboring sorption sites were occupied by SO_4^{2-}. However, SO_4^{2-} and HPO_4^{2-} had two negative charges while As(III) was mostly in the form of $H_2AsO_3^-$, the repulsion between two negative charge – anions should be stronger, hence SO_4^{2-} should affect the adsorption of HPO_4^{2-} more than As(III). Furthermore, the two negative charges of SO_4^{2-} caused the rapid increase of electrostatic repulsion effect. Due to the two negative charge of HPO_4^{2-}, the effect of electrostatic repulsion on its adsorption performance should be strong causing the lowering of the percentage of HPO_4^{2-} occupied sites.

It can also be seen in Figure 4-19, the percentage of As(III) occupied sites in tetra-solutes system is greater than that in As(III) combined with NO_3^- and HPO_4^{2-}. This should be because, in tetra-solutes, the electrostatic repulsion became dominant effect quicker than the tri-solutes causing the more available sorption sites remaining. As(III) in the form of $H_2AsO_3^-$ was less affected by the electrostatic repulsion. Therefore, $H_2AsO_3^-$ could be more adsorbed on those available sorption sites causing the greater percentage of As(III) occupied sites.

It is interesting that the percentage of NO_3^- occupied sites in tetra-solutes is comparable with that in As(III) combined with NO_3^- and HPO_4^{2-} solution. In addition, in this case, the percentage of NO_3^- occupied sites is also greater than those of the other anions. Three possible reasons can be given.

(1) The observed adsorption rate constant of NO_3^- (Table 4-5) was much greater than those of As(III) and SO_4^{2-}. Then, NO_3^- should be faster adsorbed on the sorption sites than those two anions.

(2) NO_3^- has smaller anionic radius and one negative charge. Therefore, it could be adsorbed on the available sorption sites that the neighboring sorption sites were occupied by other anions without anionic radii overlapping and lower the repulsion effect between adsorbate charges.

(3) Due to the one negative charge of NO_3^-, the effect of electrostatic repulsion on NO_3^- adsorption performance should be lower than those of SO_4^{2-} and HPO_4^{2-} which have two negative charges. In addition, when the pH of solution increased, the form of As(III) containing in the solution changed from $H_2AsO_3^-$ into $HAsO_3^{2-}$ as in Reaction (4-4). The electrostatic repulsion should stronger affect As(III) ($HAsO_3^{2-}$) adsorption performance than NO_3^-. Then, NO_3^- could be adsorbed on the sorption sites better than the other anions.

The other interesting point is the percentages of SO_4^{2-} occupied sites are lower than those of the other anions in every observed case as shown in Figure 4-20.

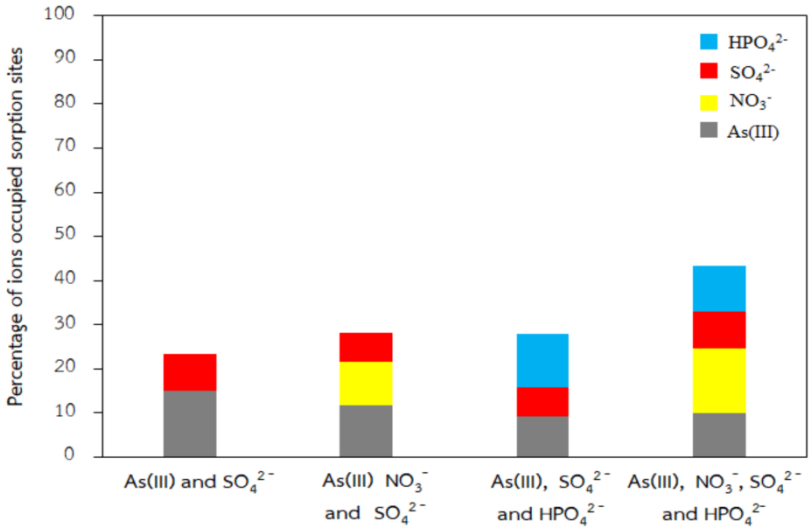

Figure 4-20 The percentages of As(III), NO_3^-, SO_4^{2-} and HPO_4^{2-} occupied sites when As(III) mixed with SO_4^{2-}, As(III) combined with NO_3^- and SO_4^{2-}, As(III) combined with SO_4^{2-} and HPO_4^{2-} and As(III) combined with NO_3^-, SO_4^{2-} and HPO_4^{2-}.

Four reasons can be explained why the percentages of SO_4^{2-} occupied sites are lower than the other anions in every observed case.

(1) As the adsorption results in Figure 4-5, the COS sorption sites had capability to adsorb HPO_4^{2-} and As(III) better than that of SO_4^{2-}. In addition, bi-solutes system also indicated that the binding affinity between the COS sorption sites and SO_4^{2-} was lower than those of HPO_4^{2-} and As(III). These caused less SO_4^{2-} occupied sites.

(2) The observed adsorption rate constants of SO_4^{2-} (Table 4-5) were lower than those of the other anions in every observed case. This implies that SO_4^{2-} should be adsorbed on the sorption sites after the other three anions causing the less available sorption sites for adsorbing SO_4^{2-}.

(3) The anionic radius of SO_4^{2-} is comparable in size with As(III) and HPO_4^{2-}. Thus, SO_4^{2-} could not be adsorbed on the sorption sites that the neighboring sorption sites were occupied by As(III) and HPO_4^{2-}. In addition, SO_4^{2-} was adsorbed on the

sorption sites slower than those two anions. Therefore, the available sorption sites that SO_4^{2-} could be adsorbed were very limited.

(4) SO_4^{2-} has two negative charges. Thus, the effect of electrostatic repulsion on SO_4^{2-} adsorption performances should be stronger than that of As(III) in the form of $H_2AsO_3^-$ and NO_3^- which have one negative charge. Then, SO_4^{2-} should be more difficult to be adsorbed on the sorption sites than the other two anions.

Furthermore, the total percentages of As(III) and anions occupied sites tend to increase with the increasing in the number of anions containing in the solution as illustrated in Figure 4-21. This should be because of the greater number of adsorbates containing in the solution, the more chance of adsorbates to be adsorbed on the sorption sites.

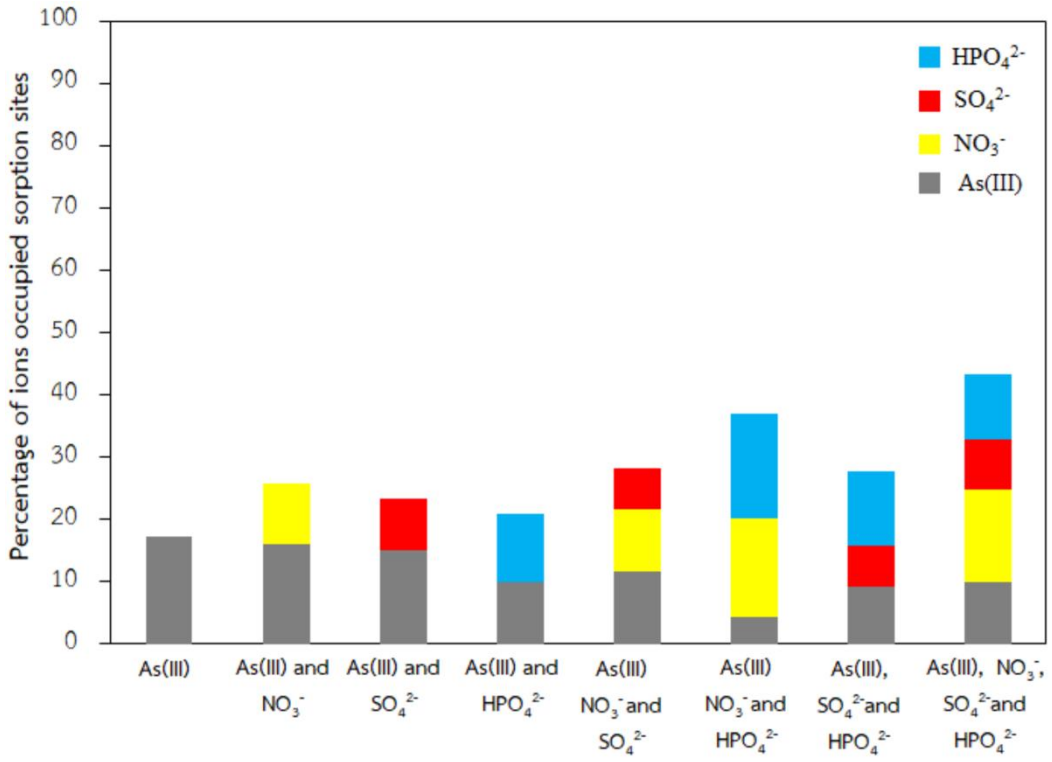

Figure 4-21 The percentages of As(III), NO_3^-, SO_4^{2-} and HPO_4^{2-} occupied sites in single-solutes, bi-, tri- and tetra-solutes.

4.3.5. The morphologies of COS before and after As(III) and anions removal tests

The morphologies of COS after As(III) and anions removals in bi-, tri- and tetra-solutes were observed by SEM (Carl Zeiss EVO®MA10). The SEM images are illustrated in Figure 4-22.

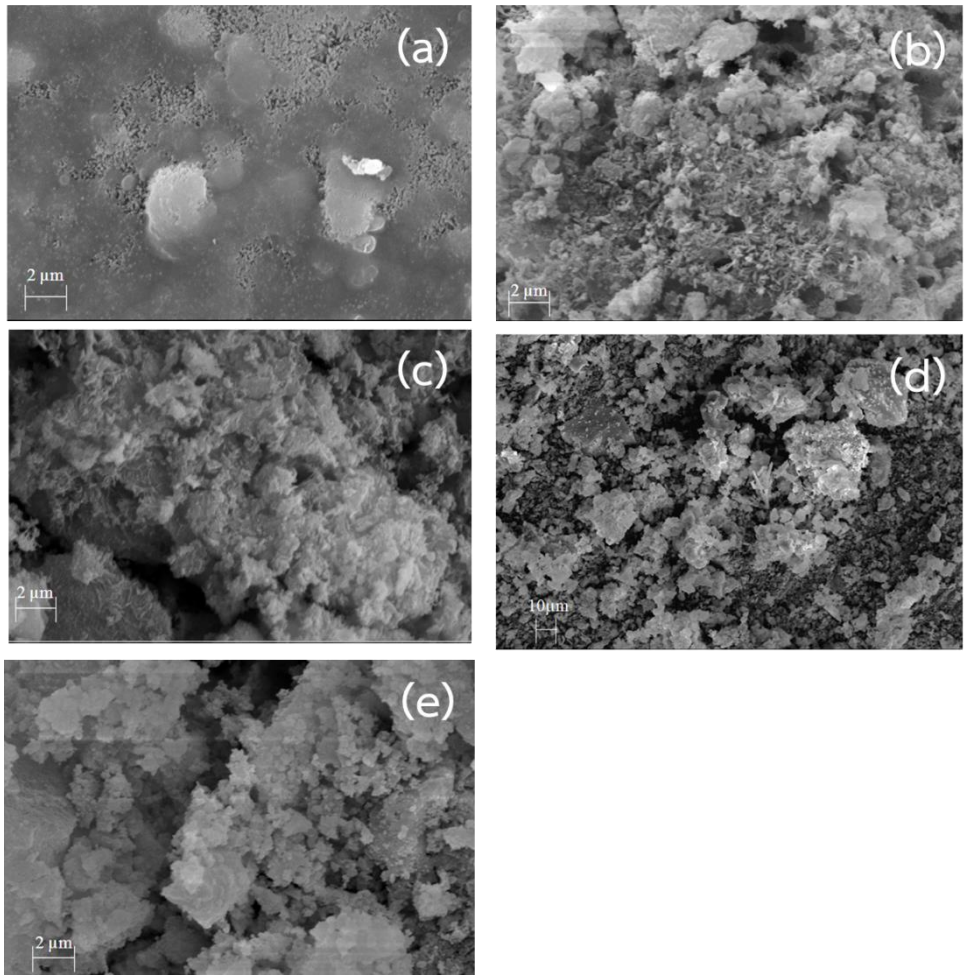

Figure 4-22 SEM images of COS after removal tests of (a) As(III) mixed with NO_3^-, (b) As(III) mixed with SO_4^{2-}, (c) As(III) mixed with HPO_4^{2-}, (d) As(III) combined with NO_3^- and SO_4^{2-} and (e) As(III) combined with NO_3^- and HPO_4^{2-}, As(III) combined with SO_4^{2-} and HPO_4^{2-} and As(III) combined with NO_3^-, SO_4^{2-} and HPO_4^{2-}.

The SEM images in Figure 4-22 show that, after As(III) and anions removal tests, the porous structure of COS in Figure 4-6 (b) changed into the different forms as in Figures 4-22 (a) - (e). It can be seen in Figures 4-22 (a) and (b) that, when As(III) mixed with NO_3^- or SO_4^{2-}, the grass-leaves like morphology of As(III) adsorption on COS surface was still observed even though some areas were covered by flat surface as in Figure 4-22 (a) and mixed by flaky matter as in Figure 4-22 (b). The flat surface and the flaky matter that were observed in Figures 4-22 (a) and (b) should be the results of competing adsorption of NO_3^- and SO_4^{2-}, respectively.

It can also be seen in Figure 4-22 (d) that, when As(III) combined with NO_3^- and SO_4^{2-}, the morphologies of COS after removal test look like the mixed morphologies of COS after As(III) mixed with NO_3^- and As(III) mixed with SO_4^{2-} removal tests.

Considering Figures 4-22 (c) and (e), the surface morphologies of COS after As(III) mixed with HPO_4^{2-} removal test (Figure 4-22 (c)) look similar with the one that were taken from COS after As(III) removal tests in tri-solutes which the solution contained HPO_4^{2-} and tetra-solutes (Figure 4-22 (e)). However, in Figure 4-22 (c), the grass leaves - like morphology can still be observed.

For As(III) combined with NO_3^- and HPO_4^{2-}, As(III) combined with SO_4^{2-} and HPO_4^{2-} and As(III) combined with NO_3^-, SO_4^{2-} and HPO_4^{2-} removal tests, the surface morphologies of COS after removal tests are illustrated in Figure 4-22 (e). It can be seen that the COS surface looks less flaky while grass leaves – like morphology cannot be observed but the adsorption result indicated that As(III) was adsorbed on the COS sorption sites. The un-observed grass leaves – like morphology should be due to the high percentages of HPO_4^{2-} removal. The removal results showed that the total percentages of HPO_4^{2-} removal by adsorption and precipitation were greater than 83.25%. Therefore, most of COS surface area after those removal tests should be covered by the morphologies of HPO_4^{2-}. In addition, due to the great number of

adsorbates adsorbed on the COS surface, the morphologies of COS surface were more complex and difficult to observe.

PART B : As(III) removal by using OS-TRHA adsorbent pellet

4.4 Characterization of RHA and TRHA

4.4.1 XRF and XRD analysis

The chemical compositions of RHA and TRHA were evaluated by an XRF. Table 4-8 presents RHA and TRHA compositions which were expressed as oxides.

Table 4-8 XRF results of OS, COS, RHA and TRHA (wt%).

	% content	
Composition	RHA	TRHA
CaO	0.74	0.82
MgO	0.50	0.57
Na_2O	-	0.20
SO_3	0.18	0.20
SiO_2	79.30	87.00
P_2O_5	1.25	1.32
Cl	0.58	0.14
Fe_2O_3	0.47	0.29
Al_2O_3	0.54	0.56
K_2O	2.51	2.52
MnO	0.13	0.14
Loss on ignition	12.14	1.80

From Table 4-8, XRF results show that RHA and TRHA composed of silicon approximately 79.30 wt% and 87.00 wt%, respectively. Loss on ignitions (LOI) of RHA and TRHA in Table 4-8 were determined by weight loss of those substances after calcining at 700 °C for 8 h. The results in Table 4-8 show that the LOI of RHA is greater than that of TRHA by approximately 85%. This indicates that the percentage of silicon in TRHA should be greater than that of RHA because the moisture,

unburned carbon and other impurities containing in RHA were removed during the RHA calcination process at 600 °C for 13 h.

The crystalline phase of RHA and TRHA was observed by XRD. The XRD peaks of RHA and TRHA are illustrated in Figure 4-23.

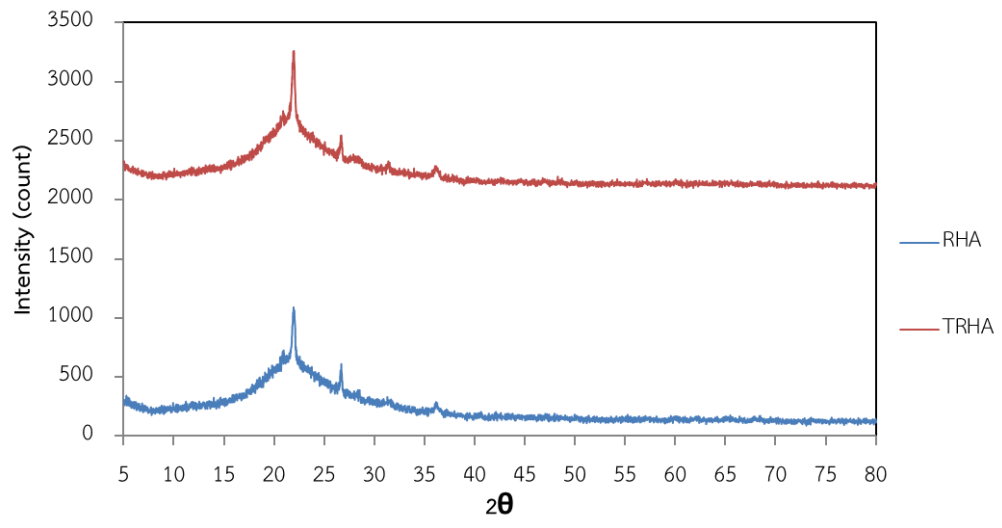

Figure 4-23 XRD patterns of RHA and TRHA.

XRD peaks of RHA and TRHA in Figure 4-23 show the broad smooth hump peak at 2θ approximately 22°. Habeeb and Mahmud [43] and Hassan et al. [40] reported that the broad peak of XRD at the position in the range of 2θ = 22° - 25° referred to amorphous form of SiO_2. Thus, the silicon which contained in RHA and TRHA should exist in the form of amorphous SiO_2. Based on XRF, XRD and LOI results, the removal of moisture, unburned carbon and other impurities containing in RHA during the RHA calcination process at 600 °C for 13 h caused the increase in percentage of SiO_2 in TRHA (Table 4-8). The XRF and XRD results indicate that, after the heat treatment, the percentage of SiO_2 in TRHA increased while SiO_2 was still in the form of amorphous structure.

4.5 OS-TRHA adsorbent pellet characterization

4.5.1. XRD analysis of OS-TRHA adsorbent pellets before and after As(III) adsorption tests

XRD patterns of OS-TRHA adsorbent pellet prepared from OS particle size range of <106 μm with OS:TRHA ratio of 0.7:0.3 before and after As(III) adsorption tests are illustrated in Figure 4-24.

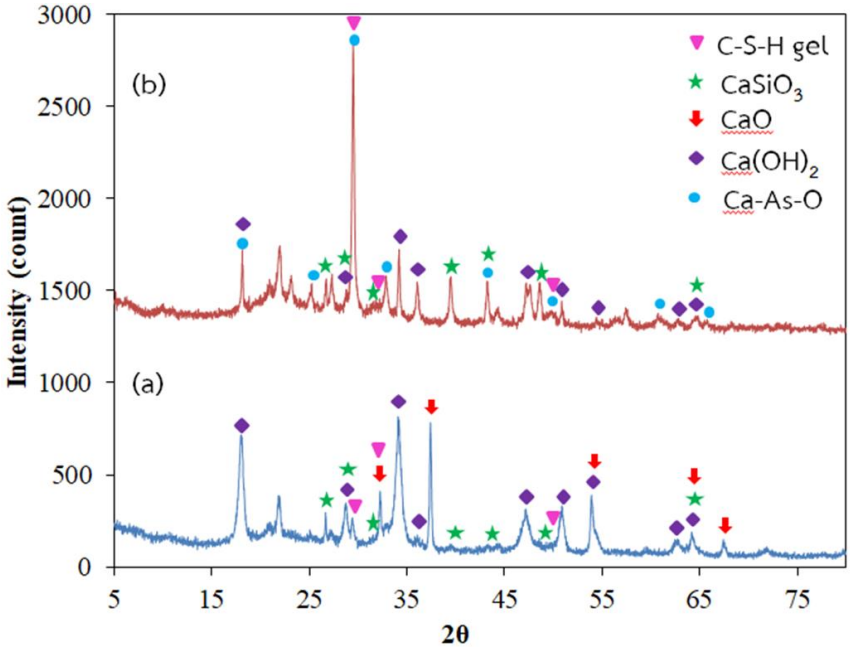

Figure 4-24 XRD patterns of the OS-TRHA adsorbent pellet (a) before and (b) after As(III) removal tests.

The XRD peaks in Figure 4-24 (a) show that, before As(III) adsorption test, the crystalline substances detected in OS-TRHA adsorbent pellet are calcium silicate ($CaSiO_3$), calcium silicate hydrate (C-S-H) compounds, calcium oxide (CaO) and calcium hydroxide ($Ca(OH)_2$). Meanwhile, the peak patterns of $CaCO_3$ and amorphous SiO_2 observed in the XRD results of OS (Figure 4-1) and TRHA (Figure 4-23), respectively were not observed in XRD peaks of OS-TRHA adsorbent pellet. This implies that, during the OS-TRHA adsorbent pellet preparation, some $CaCO_3$ in OS should react with amorphous SiO_2 in TRHA and form $CaSiO_3$ and C-S-H compounds.

The remaining $CaCO_3$ in OS-TRHA adsorbent pellet also changed into CaO as in Reaction (2-62) during the calcination step in OS-TRHA adsorbent pellet preparation.

After As(III) adsorption test, XRD peaks of OS-TRHA adsorbent pellet in Figure 4-24 (b) corresponding to CaO were not detected whereas Ca-As-O peaks could be observed. It can be also seen in Figures 4-24 that, after As(III) adsorption test, the intensity peaks of $Ca(OH)_2$ of OS-TRHA adsorbent pellet significantly decrease while the peaks corresponding to $CaSiO_3$ and C-S-H compounds insignificantly change. This indicates that, when OS-TRHA adsorbent pellet was added into the As(III) solution, CaO in the OS-TRHA adsorbent pellet should react with water and turn into $Ca(OH)_2$. Then, $Ca(OH)_2$ could further react with As(III) to be Ca-As-O.

4.5.2. Solubility tests of COS and OS-TRHA adsorbent pellets

The solubility tests of COS and OS-TRHA adsorbent pellets were performed in Erlenmeyer flasks with rubber corks. In this section, the pH of solution was adjusted to be 7. After that, COS and OS-TRHA adsorbent pellet were individually added into the solution and kept for 24 h. The final pHs of the solutions were measured. The amounts of dissolved COS and OS-TRHA adsorbent pellet reported in terms of dissolved CaO are presented in Figure 4-25. It is noted that COS <106, 106-150 and 150-250 in Figure 4-25 referred to COS prepared from OS particle size ranges of <106 μm, 106-150 μm and 150-250 μm, respectively. Meanwhile, pellets <106, 106-150 and 150-250 referred to OS-TRHA adsorbent pellets prepared from OS:TRHA ratio of 0.7:0.3 with OS particle size ranges of <106 μm, 106-150 μm and 150-250 μm, respectively.

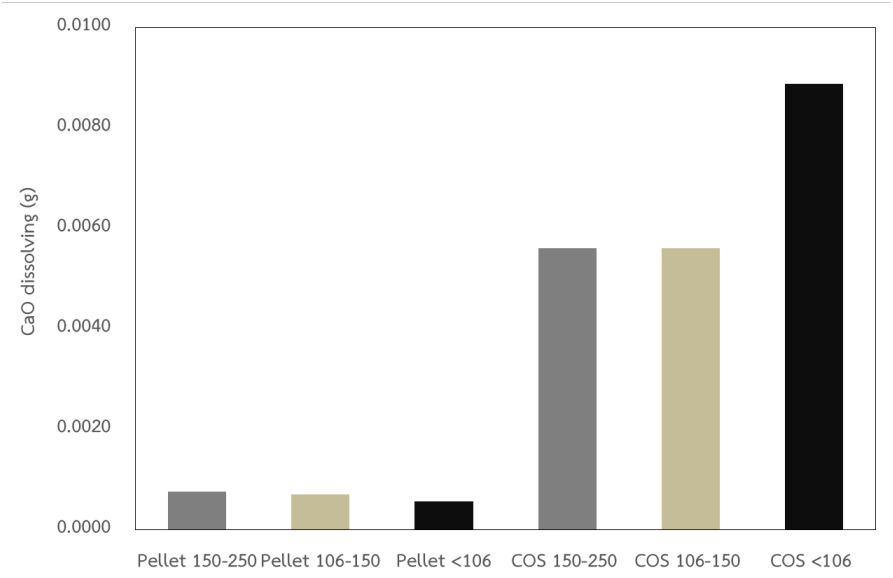

Figure 4-25 The amount of CaO in COS and in OS-TRHA adsorbent pellets dissolved in the solutions.

Figure 4-25 shows that the amounts of dissolved CaO of OS-TRHA adsorbent pellets are much lower than that of COS in all observed OS particle size ranges. Two possible reasons can be given to explain why the OS-TRHA adsorbent pellets are much less dissolved in the solution than COS.

(1) The amount of CaO containing in OS-TRHA adsorbent pellets was lower than that of COS. As mentioned in the previous section, some $CaCO_3$ in the OS-TRHA adsorbent pellet precursor transformed into $CaSiO_3$ and C-S-H which were insoluble compounds. Thus, less CaO was produced after calcination at 700°C for 8 h causing the less CaO dissolving in the solution.

(2) The surface area of OS-TRHA adsorbent pellets was much less than that of COS resulting in less contact of CaO with water in the solution and therefore less dissolution could occur.

It can be also seen in Figure 4-25 that COS prepared from OS particle size range of <106 μm provides the greatest amount of CaO dissolved in the solution due to the largest contact area. Meanwhile, the amount of dissolved CaO of OS-TRHA

adsorbent pellet prepared from OS particle size range of <106 μm is slightly lower than those of OS-TRHA adsorbent pellets prepared from the other two particle size ranges. This should be because the smaller particle size of OS could be well compacted, the solution should less diffuse into the pellet causing the less dissolving of CaO.

4.6. The effects of OS particle sizes and OS:TRHA ratios on stability and As(III) adsorption performance of OS-TRHA adsorbent pellet

In this section, initially, OS and COS were pelletized by using a metal mould and hydraulic press. After OS and COS pellet preparation, the OS and COS pellets were individually added into solution (pH7) and kept for 24. The shapes of the pellets were observed. Figure 4-26 shows OS and COS pellets before and after adding into the solution.

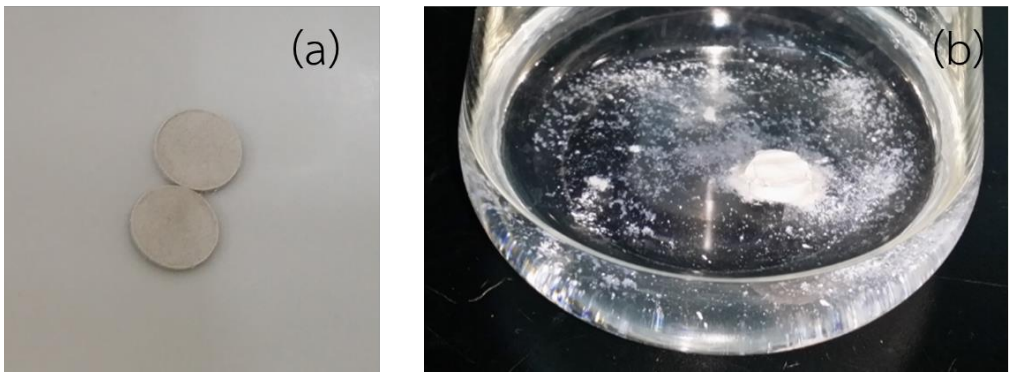

Figure 4-26 The OS and COS-pellets (a) before (b) after adding into the solution.

It can be seen in Figure 4-26 (a) that, after OS and COS pellets preparation, the color of those pellets was almost white and the diameter of the pellets was approximately 10 mm. After OS and COS pellets were individually added into the solution, those pellets cracked within 5 min as shown in Figure 4-26 (b). This should be because of the dissolving CaO containing in OS and COS pellets and the porous structure of those pellets which caused the more diffusion of water into the pellets. This result indicates that the OS and COS could not be pelletized directly.

In order to pelletize the COS powder, the binder precursor is necessary to mix with OS or COS. In this work, RHA was chosen to be a binder as it contained amorphous SiO_2 which could introduce pozzolanic reaction with CaO [150]. The OS-RHA pellets and COS-RHA pellets were then prepared by the metal mould and hydraulic press. The stability of the OS-RHA and COS-RHA pellets was tests following the same procedure of the OS and COS pellets tests. The results showed that, after the OS-RHA and COS-RHA pellets were individually added into the solution, those pellets cracked within 5 - 10 min. The crack of those pellets should be because the high unburned carbon and other impurities containing in RHA could inhibit formation of $CaSiO_3$ and C-S-H compound in the pozzolanic reaction [150]. Thus, the pretreatment process was applied to remove the unburned carbon and other impurities containing in RHA.

In this work, the RHA was calcined at 600 ℃ for 13 h in order to remove the impurities containing in RHA. The treated RHA was called treated rice husk ash (TRHA). Figure 4-27 shows RHA before and after heat treatment.

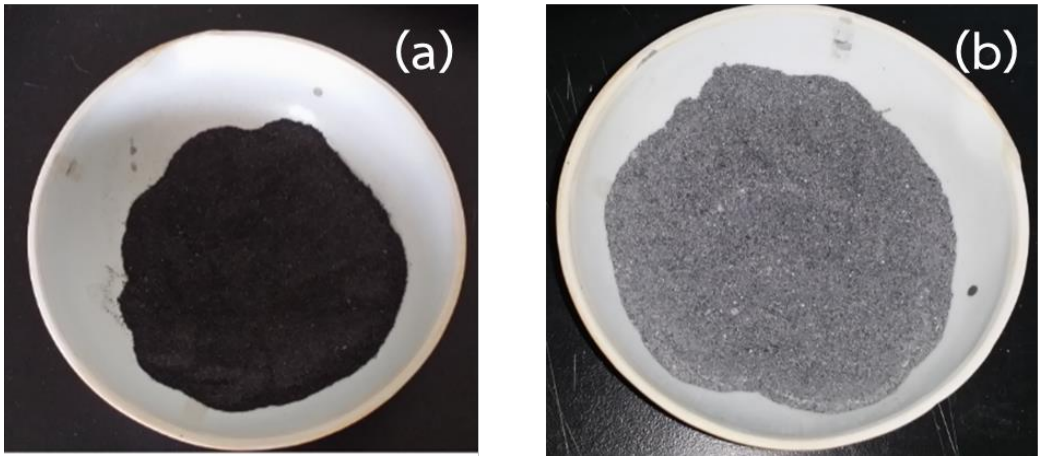

Figure 4-27 (a) RHA and (b) TRHA.

It can be seen in Figure 4-27 that, after heat treatment process, the black color of RHA in Figure 4-27 (a) changed into gray as in Figure 4-27 (b). This is because some unburned carbon and impurities were removed during the calcination process.

Table 4-8 and Figure 4-23 indicated that TRHA contained the percentage of SiO_2 as high as 87 wt% while the structure of SiO_2 in TRHA was still in the amorphous form which could produce the pozzolanic reaction. Then, TRHA was used to be a binder for adsorbent pellets preparation.

In order to find the most appropriate condition for OS-TRHA adsorbent pellet preparation, the OS particle size ranges of <106 μm, 106-150 μm and 150-250 μm were weighed and mixed with TRHA in the different ratios. After OS-TRHA adsorbent pellets preparation process, the stability and As(III) adsorption performances of OS-TRHA adsorbent pellets were tests in Erlenmeyer flasks. Figure 4-28 (a) illustrated the OS-TRHA adsorbent pellets after preparation process while Figures 4-28 (b) and (c) show the OS-TRHA adsorbent pellets after the stability and As(III) adsorption tests.

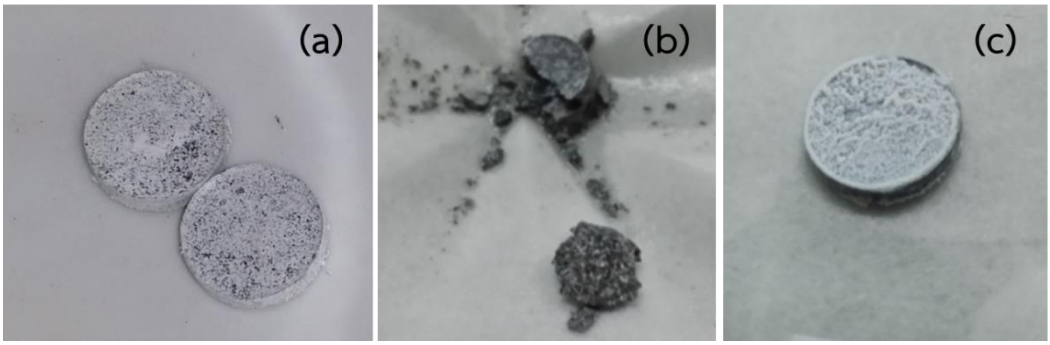

Figure 4-28 The OS-TRHA adsorbent pellets before adsorption test (a), the cracked (b) and the un-cracked (c) OS-TRHA adsorbent pellets after adsorption tests.

The stability and As(III) adsorption capacity of OS-TRHA adsorbent pellets results are presented in Table 4-9. It is noted that the As(III) adsorption tests were performed twice and the As(III) adsorption capacities were reported as the average values.

Table 4-9 The stability and As(III) adsorption capacity of OS-TRHA adsorbent pellets with different conditions.

OS particle size range (μm)	OS:TRHA	Stability	Adsorption capacity (mg/g)
	0:1.0		1.38
<106	1.0:0		241.67
150-250	0.8:0.2	Crack	42.50±0.09
150-250	0.7:0.3	Crack	22.38±2.85
150-250	0.6:0.4	Crack	24.26±24.23
150-250	0.5:0.5	Crack	29.69±2.40
106-150	0.8:0.2	Crack	35.64±7.47
106-150	0.7:0.3	Crack	14.02±0.65
106-150	0.6:0.4	Crack	34.08±10.65
106-150	0.5:0.5	Crack	31.26±1.65
<106	0.8:0.2	Crack	33.10±0.41
<106	0.7:0.3	Not Crack	26.20±2.02
<106	0.6:0.4	Not Crack	19.50±2.83
<106	0.5:0.5	Not Crack	14.01±0.05

In this section, firstly, the stability of OS-TRHA adsorbent pellets was determined. As seen in Table 4-9, the OS-TRHA adsorbent pellets prepared from OS particle size ranges of 106-150 μm and 150-250 μm with every observed ratio cracked (Figure 4-28 (b)) within 30 min after adding into As(III) solution. Meanwhile, the OS-TRHA adsorbent pellets prepared from OS particle size range of < 106 μm with OS:TRHA ratios of 0.7:0.3 to 0.5:0.5 did not crack (Figure 4-28 (c)) even after finishing the adsorption experiment (within 24 h).

Two reasons that can be explained why the OS-TRHA adsorbent pellets prepared from OS particle size range of < 106 μm with ratios of 0.7:0.3 to 0.5:0.5 did not crack are.

(1) The OS particle size range of <106 μm contained the particles with the sizes that small enough to be well compacted and better sintered than the larger ones. Therefore, after the OS-TRHA adsorbent pellets were added into the solution, the solution could less diffuse into the denser adsorbent pellets causing lower CaO to dissolve.

(2) The OS particle size range of <106 μm had larger surface area that allowed the pozzolanic reaction to occur and formed $CaSiO_3$ and C-S-H compounds which were binder substances more than the other two OS size ranges. Then, $CaSiO_3$ and C-S-H compounds could bind the precursor powder to be stable without cracking.

However, the OS-TRHA adsorbent pellet prepared from OS particle size range of <106 μm with ratio of 0.8:0.2 cracked after adding into the solution. This should be because, in this condition, the OS-TRHA adsorbent pellet contained less amount of TRHA that resulted in the insufficient $CaSiO_3$ and C-S-H compounds to bind the precursor particles in the pellet.

After considering the stability tests, As(III) adsorption capacities of un-cracked adsorbent pellets were further compared. Considering Table 4-9, the As(III) adsorption capacity of COS prepared from OS particle size range of <106 is extremely greater than that of TRHA. As mentioned earlier, COS composed of CaO as high as 97%wt. The XRD (Figure 4-7) and As(III) adsorption results (Table 4-9) indicate that $Ca(OH)_2$ which transformed from CaO in COS should be the sorption sites for adsorbing As(III) in the solution. On the contrary, As(III) adsorption capacity of TRHA was very poor. It means that TRHA had few sorption sites which could adsorb As(III) in the solution.

For OS-TRHA adsorbent pellets, Table 4-9 shows that the As(III) adsorption capacities of OS-TRHA adsorbent pellets are greater than that of TRHA. This implies that OS-TRHA adsorbent pellets have sorption sites more than TRHA. Due to the XRD result in Figure 4-24, the sorption sites for adsorbing As(III) in OS-TRHA adsorbent

pellets should be $Ca(OH)_2$ which transformed from $CaCO_3$ in OS. However, the As(III) adsorption capacities of OS-TRHA adsorbent pellets are lower than that of COS because some $CaCO_3$ in OS-TRHA adsorbent pellet changed into $CaSiO_3$ and C-S-H compounds which are inactive compound for adsorbing As(III).

It can also be seen in Table 4-6 that As(III) adsorption capacity of OS-TRHA adsorbent pellet prepared from OS particle size range of < 106 μm with ratio of 0.7:0.3 is greater than those of the pellets prepared from OS same size range with the ratios of 0.6:0.4 and 0.5:0.5, respectively. The As(III) adsorption capacity increased with the increase of OS containing in OS-TRHA adsorbent pellet. This result confirmed the previous statement that $Ca(OH)_2$ should be the sorption sites for adsorbing As(III).

The results of stability test and As(III) adsorption capacity indicate that the adsorbent pellet prepared from OS particle size range of <106 μm with ratio of 0.7:0.3 was the most appropriate condition for preparation OS-TRHA adsorbent pellet to remove As(III) in aqueous solution.

Furthermore, the errors of As(III) adsorption capacity of cracked pellets were in the range of 0.21% - 62.37% while un-cracked pellets had the errors of As(III) adsorption in the range of 0.88% - 15.08%. The greater error of the cracked pellets was because of the uncontrolled cracking patterns of the cracked pellets causing in different area of cracked pieces exposed to the solution.

4.7. Morphologies of OS-TRHA adsorbent pellets before and after As(III) adsorption tests

The surface morphologies of TRHA, COS and OS-TRHA adsorbent pellets prepared from OS particle size ranges of <106 μm, 106-150 μm and 150-250 μm with OS:TRHA ratio of 0.7:0.3 before and after As(III) adsorption tests were observed by

using SEM. Figure 4-29 illustrates the SEM images of TRHA and COS before and after As(III) adsorption tests.

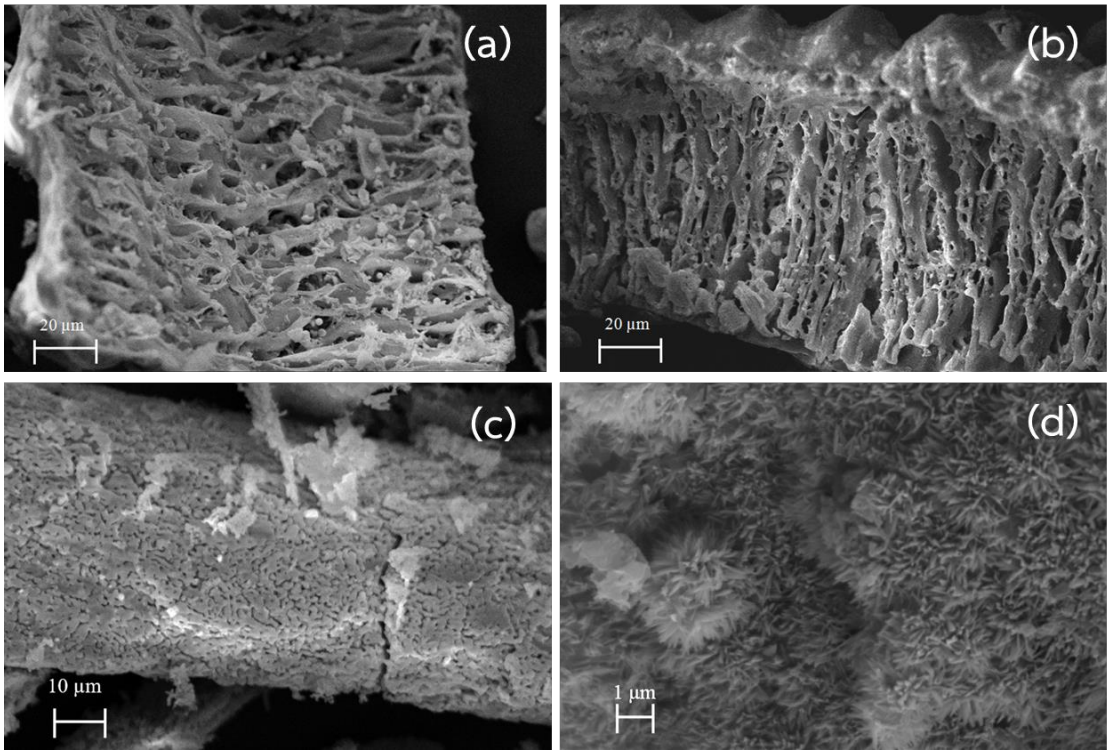

Figure 4-29 SEM images of TRHA (a) before (b) after As(III) adsorption tests and COS (c) before and (d) after As(III) adsorption tests.

The SEM images in Figures 4-29 (a) and (b) show that the morphologies of TRHA before and after As(III) adsorption tests look similar. Since, TRHA was rarely adsorbed As(III). Conversely, the SEM images of COS in Figure 4-29 shows that, after As(III) adsorption test, the porous structure of COS in Figure 4-29 (c) changed into the grass-leaves like morphology (Figure 4-29 (d)). This morphology looks similar to the morphology of arsenic immobilized on lime in Phenrat et al. work which reported that the grass-leaves like morphology was one form of Ca-As compound [158].

The surfaces of OS-TRHA adsorbent pellet before and after As(III) adsorption tests were also observed by SEM. The SEM images are presented in Figure 4-30.

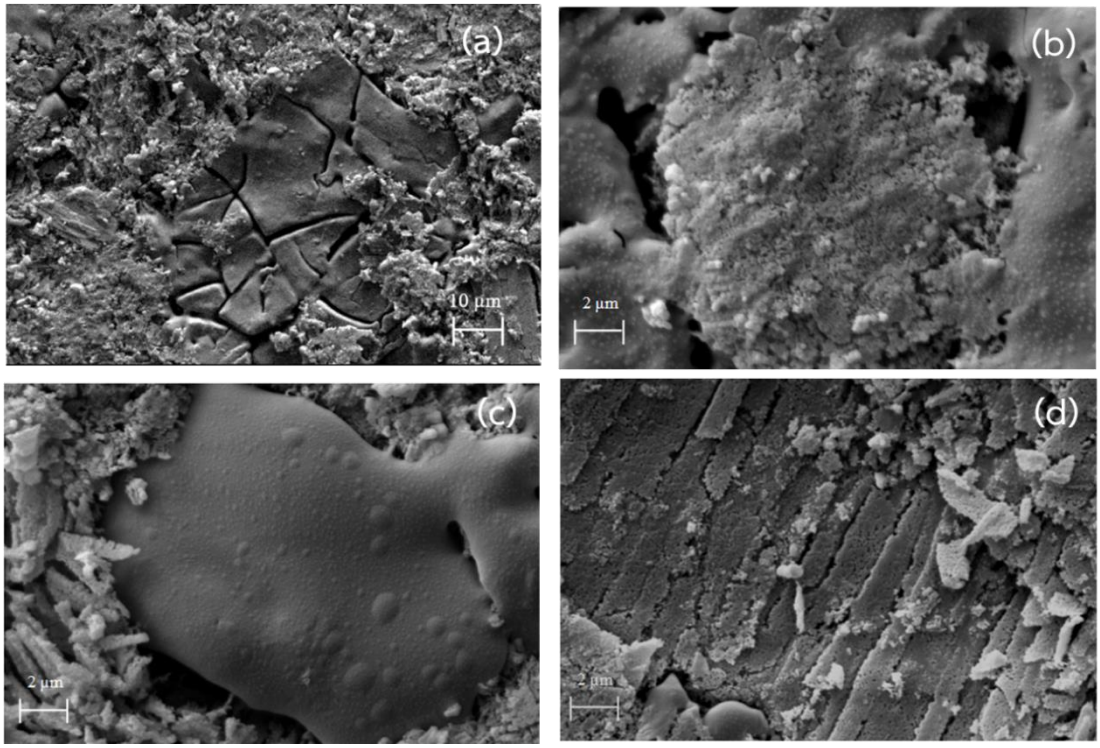

Figure 4-30 The SEM images of surface OS-TRHA adsorbent pellet before adsorbed As(III) prepared from OS size ranges of (a) <106 µm, (b) - (d) 106-150 µm and 150-250 µm.

Figure 4-30 (a) shows that, before As(III) adsorption test, the surface morphologies of OS-TRHA adsorbent pellet prepared from OS particle size range of <106 µm could be classified into two types; the rough one and the smooth one. Meanwhile, the surface morphologies of OS-TRHA adsorbent pellets prepared from the other two particle size ranges of OS could be observed in three forms; the rough surface (Figure 4-30 (b)), the smooth surface (Figure 4-30 (c)) and the layer of porous bars (Figure 4-30 (d)). It can be seen that the rough surface in the Figure 4-30 (b) and the smooth surface in the Figure 4-30 (c) look like the surface morphologies of the OS-TRHA adsorbent pellet prepared from OS particle size range of <106 µm (Figure 4-30 (a)). Meanwhile, the layers of porous bars in the OS-TRHA adsorbent pellets is similar to the porous morphology of COS before As(III) adsorption test in Figure 4-29 (c). This implies that some parts of OS-TRHA adsorbent pellets prepared from OS

particle size ranges of 106-150 μm and 150-250 μm were still in the form of porous bars structure of COS.

The porous bars structure of OS-TRHA adsorbent pellets observed in Figure 4-30 (d) should be the other reason that caused the crack of OS-TRHA adsorbent pellet and the greater dissolving of the OS-TRHA adsorbent pellets prepared from OS particle size ranges of 106-150 μm and 150-250 μm. When the OS-TRHA adsorbent pellets prepared from OS particle size ranges of 106-150 μm and 150-250 μm were added into the solution, the solution could better diffuse into the pores of the porous structure in those pellets and contact with CaO inside the adsorbent pellets. Since CaO is a soluble compound, some of it inside the pellet could dissolve causing the crack of OS-TRHA adsorbent pellet.

After As(III) adsorption tests, the morphologies of OS-TRHA adsorbent pellets were also observed by SEM. SEM images are shown Figure 4-31.

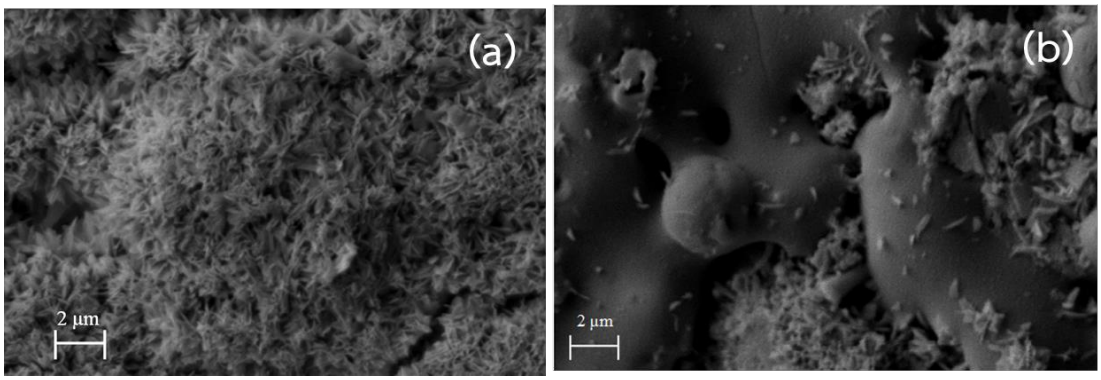

Figure 4-31 SEM images of OS-TRHA adsorbent pellet surface after adsorbed As(III).

It can be seen in Figure 4-31 that, after As(III) adsorption tests, the morphologies of OS-TRHA adsorbent pellets prepared from every observed OS particle size range could be classified into two forms; the grass leaves-like matter (Figure 4-31 (a)) and the smooth surface (Figure 4-31 (b)). The grass leaves-like morphology on the surface of OS-TRHA adsorbent pellets looks like the morphology of COS after As(III) adsorption test in Figure 4-29 (d) which was one form of calcium-

arsenite compound. Meanwhile, the smooth surface in Figure 4-31 (b) looks similar to the smooth surface of OS-TRHA adsorbent pellets before As(III) adsorption test (Figure 4-30 (c)).

Furthermore, EDX technique was used to determine the chemical composition containing in the grass leaves-like matter and the smooth surface. The EDX results are presented in Figure 4-32.

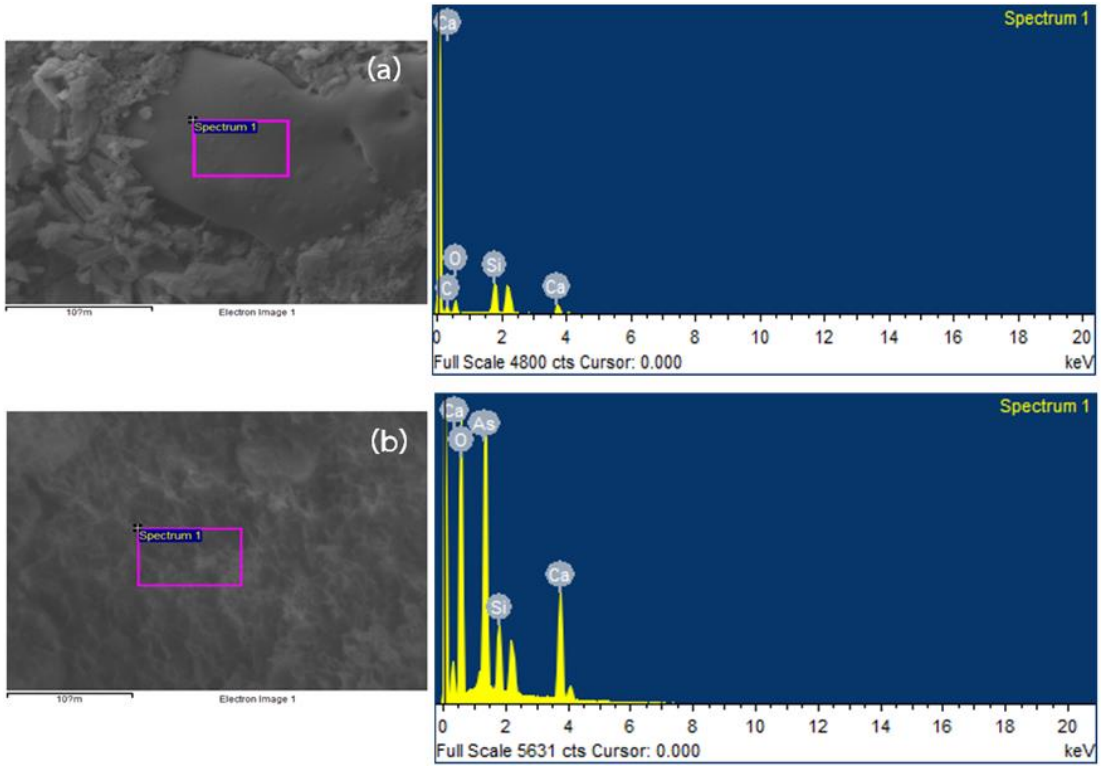

Figure 4-32 The EDX results of (a) the smooth surface (b) grass-leaves like morphology of OS-TRHA adsorbent pellets.

The EDX result of grass leaves-like morphology in Figure 4-32 (b) shows Ca, O and As elements which should refer to Ca-As-O. This result agrees with the XRD result (Figure 4-24) which indicated that As(III) should be adsorbed on CaO adsorption sites on the OS-TRHA adsorbent pellet in the form of Ca-As-O. For the smooth surface, the EDX result (Figure 4-32 (a)) shows Ca, O and Si elements which should refer to $CaSiO_3$ and C-S-H compounds. As seen in Figures 4-30 (c) and 4-31 (b), the smooth surface morphology was observed both before and after As(III) adsorption

tests. This implies that the smooth surface should be the surface of $CaSiO_3$ and C-S-H compounds which was inactive with As(III) adsorption.

The cross-section morphologies of OS-TRHA adsorbent pellets prepared from OS particle size ranges of <106 μm, 106-150 μm and 150-250 μm with OS:TRHA ratio of 0.7:0.3 before and after As(III) adsorption tests were also observed by using SEM as shown in Figure 4-33.

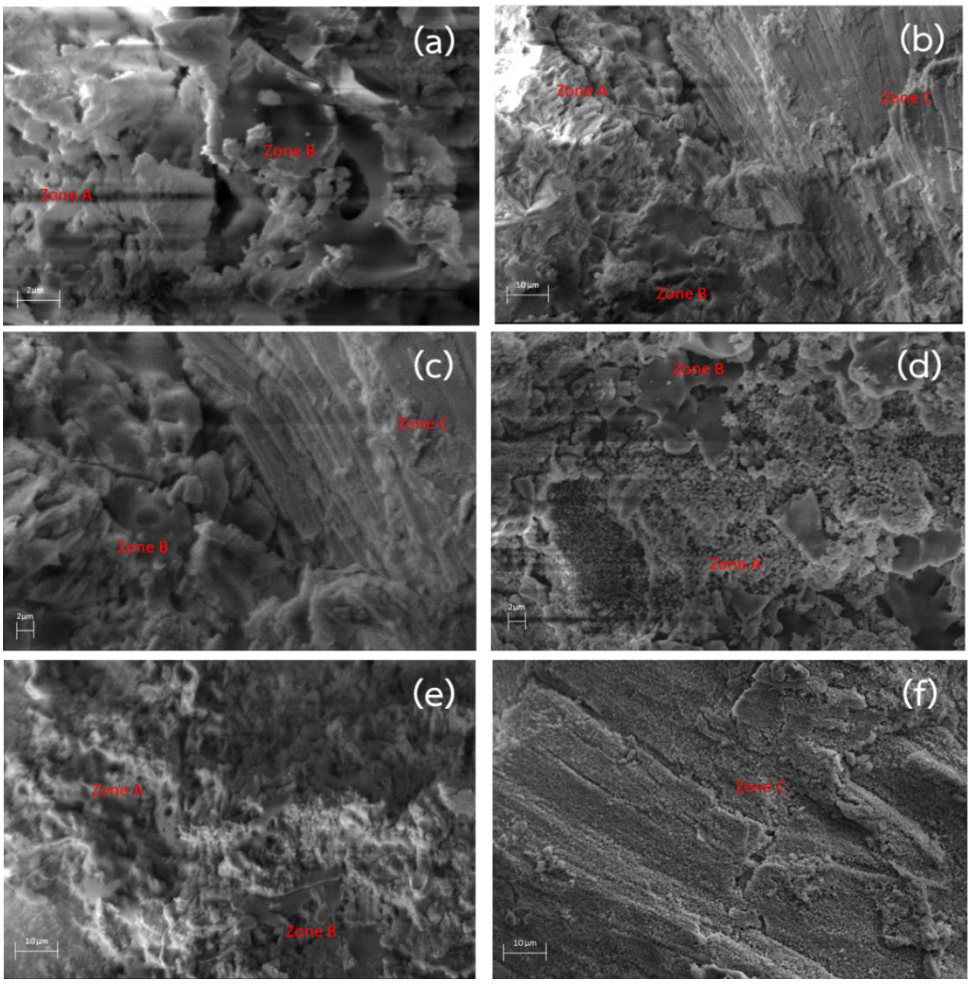

Figure 4-33 SEM images of cross-section OS-TRHA adsorbent pellet before adsorbed As(III) prepared from OS particle size ranges of (a) <106 μm, (b) - (c) 106-150 μm and 150-250 μm and OS-TRHA adsorbent pellet after adsorbed As(III) prepared from OS particle size ranges of (d) <106 μm, (e) - (f) 106-150 μm and 150-250 μm.

As seen in Figure 4-33, before As(III) adsorption test, the cross-section morphologies of OS-TRHA adsorbent pellet prepared from OS particle size range of <106 μm (Figure 4-33 (a)) could be divided into two types; the rough one and the smooth one like the surface morphologies of OS-TRHA adsorbent pellet in Figure 4-30 (a). Meanwhile, the cross-section morphologies of OS-TRHA adsorbent pellet prepared from OS particle size ranges of 106-150 μm and 150-250 μm could be classified into three forms; the rough surface (Figure 4-33 (b)), the smooth surface (Figure 4-33 (b)) and the layers of porous bars (Figure 4-33 (c)) like the surface morphologies of OS-TRHA adsorbent pellets in Figures 4-30 (b) - (d).

After As(III) adsorption tests, the cross-section morphologies of OS-TRHA adsorbent pellets prepared from OS particle size ranges of <106 μm (Figure 4-33 (d)), 106-150 μm and 150-250 μm (Figures 4-33 (e) - (f)) are similar to the cross-section morphologies of OS-TRHA adsorbent pellets before As(III) adsorption tests in Figures 4-33 (a) - (c). The grass-leaves like morphology of Ca-As-O was not observed in the cross-section surface of OS-TRHA adsorbent pellets. This indicates that As(III) should not diffuse and be adsorbed inside the OS-TRHA adsorbent pellets. The As(III) should be adsorbed only on the surface of OS-TRHA adsorbent pellets.

4.8. Adsorption mechanism of As(III) on OS-TRHA adsorbent pellet

In this section, the adsorption mechanism of As(III) on OS-TRHA adsorbent pellet was investigated. Considering XRF in Tables 4-1 and 4-8 and XRD in Figures 4-1 and 4-23, OS and COS mainly composed of $CaCO_3$ and CaO, respectively while almost SiO_2 containing in RHA and TRHA was in the form of amorphous phase. Furthermore, XRD result in Figure 4-24 (a) indicated that, after pellet preparation process, the OS-TRHA adsorbent pellet composed of $CaSiO_3$, C-S-H, CaO and $Ca(OH)_2$. Based on the XRD and XRF results, during the OS-TRHA adsorbent pellet preparation process, the following reactions should take place.

$$SiO_2 + 2H_2O \longrightarrow H_4SiO_4 \qquad (4\text{-}10)$$

$$H_4SiO_4 + CaCO_3 \longrightarrow CaH_2SiO_4 + H_2CO_3 \quad (4\text{-}11)$$

$$H_2CO_3 \xrightarrow{\Delta} H_2O + CO_2 \quad (4\text{-}12)$$

$$CaH_2SiO_4 \xrightarrow{\Delta} CaSiO_3 + H_2O \quad (4\text{-}13)$$

$$CaCO_3 \xrightarrow{\Delta} CaO + CO_2 \quad (2\text{-}62)$$

$$CaO + SiO_2 \xrightarrow{\Delta} CaSiO_3 \quad (4\text{-}14)$$

In the preparation process, when OS and TRHA were weighed and blended with a few drops of water, the amorphous SiO_2 in TRHA contacted with water and changed into H_4SiO_4 as in Reaction (4-10). Then, H_4SiO_4 could further react with some $CaCO_3$ in OS and form CaH_2SiO_4 (C-S-H) and H_2CO_3 as in Reaction (4-11). After the mixture paste was shaped into the pellet by a metal mould, the pellet was calcined at 700°C for 8 h. During the calcination process, H_2CO_3 decomposed and released H_2O and CO_2 as shown in Reaction (4-12). Hager [169] and Rodriguez et al. [170] reported that C-S-H compounds could transform into $CaSiO_3$ at calcining temperature above 600°C. However, in this work, the XRD peaks of OS-TRHA adsorbent pellet after preparation process in Figure 4-24 (a) corresponding to $CaSiO_3$ and C-S-H compounds were detected. It means that some CaH_2SiO_4 (C-S-H compounds) should decompose into $CaSiO_3$ and release H_2O as in Reaction (4-13) while the rest still remained in the OS-TRHA adsorbent pellet. Meanwhile, the remaining $CaCO_3$ in OS released CO_2 and changed into CaO as in Reaction (2-62). In addition, during the calcination process, some CaO could further react with SiO_2 and form $CaSiO_3$ as in Reaction (4-14).

After As(III) adsorption process, the As(III) adsorption results in Table 4-6 showed that the OS-TRHA adsorbent pellet could adsorb As(III) with the maximum adsorption capacity about 26.20 mg/g. pHs of solution before and after As(III) removal tests were measured. The result showed that, after As(III) adsorption test, pH of As(III) solution increased from pH 7 to pH about 11. As described before, after adding OS-THRA adsorbent pellet into the solution, some CaO in the pellet could dissolve into the solution as in Reaction (4-2) causing the increase in pH of solution. The precipitation result (Section 4.2.1) showed that the precipitate of As(III) and Ca^{2+} was

not observed within 48 h. Considering the XRD result in Figure 4-24, after As(III) adsorption test, the XRD peaks corresponding to CaO were not detected while the peaks corresponding to Ca-As-O were observed. In addition, the intensities of the peaks corresponding to $Ca(OH)_2$ decreased. This implies that, after the OS-TRHA adsorbent pellet was put into As(III) solution, CaO in the pellet should change into $Ca(OH)_2$ and further adsorb As(III) containing in the solution. However, after As(III) adsorption test, XRD peaks of $CaSiO_3$ and C-S-H compounds (Figure 4-24 (b)) were still observed and their intensities insignificantly changed. The SEM images and EDX results in Figures 4-30 - 4-32 indicated that the smooth morphology observed on OS-TRHA adsorbent pellets before and after As(III) adsorption tests should be $CaSiO_3$ and C-S-H compounds which should not react with As(III). The solubility tests in Figure 4-25 also showed that the $CaSiO_3$ and C-S-H compounds in OS-TRHA adsorbent pellet caused less CaO dissolving. Moreover, the $CaSiO_3$ and C-S-H compounds in the pellet could bind the precursor powders in the pellet to be stable without cracking.

According to the information obtained from those experiments, the OS-TRHA adsorbent pellet could be divided into two parts. The first part is CaO which could adsorb As(III). The other part is $CaSiO_3$ and C-S-H compounds which could not react with As(III) but it could bind the precursor powders in the pellet to be stable without cracking. Then, the reactions of As(III) adsorption by OS-TRHA adsorbent pellet could be proposed as the following reactions.

$$CaO + 2H_2O \longrightarrow Ca(OH)_2 \quad (4\text{-}1)$$

$$Ca(OH)_2 \longleftrightarrow Ca^{2+} + 2OH^- \quad (4\text{-}2)$$

$$Ca(OH)_2 + H_3AsO_3 \longrightarrow HCaAsO_3 + 2H_2O \quad (4\text{-}15)$$

$$H_3AsO_3 + OH^- \longrightarrow H_2AsO_3^- + H_2O \quad (4\text{-}16)$$

$$Ca(OH)_2 + H_2AsO_3^- \longrightarrow HCaAsO_3 + H_2O + OH^- \quad (4\text{-}3)$$

$$H_2AsO_3^- + OH^- \longrightarrow HAsO_3^{2-} + H_2O \quad (4\text{-}4)$$

$$Ca(OH)_2 + HAsO_3^{2-} \longrightarrow HCaAsO_3 + 2OH^- \quad (4\text{-}5)$$

$$Ca^{2+} + HAsO_3^{2-} \longrightarrow HCaAsO_3 \quad (4\text{-}17)$$

After OS-TRHA adsorbent pellet was added into As(III) solution, CaO in the pellet changed into $Ca(OH)_2$ as in Reaction (4-1) causing the absence of CaO peaks in XRD (Figure 4-24 (b)). Some $Ca(OH)_2$ could dissolve and dissociate into Ca^{2+} and OH^- as in Reaction (4-2) causing the increase in pH of solution. The adsorption tests showed that the pH of solution increased from 7 to 11. As mentioned before, the species of As(III) depended on pH of solution [1, 12, 35, 126]. The fraction of As(III) species versus pH of solution is illustrated in Figure 4-34.

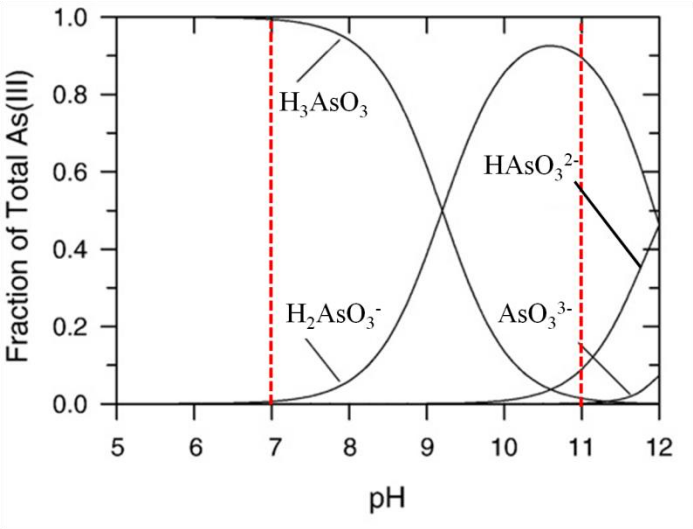

Figure 4-34 The distribution of As(III) species as a function of pH at 25 °C [12].

It can be seen in Figure 4-34 that, at pH 7, almost As(III) exists in the form of H_3AsO_3. When pH of solution increases, H_3AsO_3 is deprotonated by OH^- into $H_2AsO_3^-$ (Reaction (4-16)) and $H_2AsO_3^-$ is further deprotonated into $HAsO_3^{2-}$ (Reaction (4-4)). During adsorption process, H_3AsO_3, $H_2AsO_3^-$ and $HAsO_3^{2-}$ reacted with un-dissolved $Ca(OH)_2$ in OS-TRHA adsorbent pellet by ligand exchange and formed $CaHAsO_3$ as in Reactions (4-15), (4-3) and (4-5), respectively. The formation of $CaHAsO_3$ caused the decrease in the intensity of peaks of $Ca(OH)_2$ and the appearance of Ca-As-O peaks in Figure 4-24 (b).

Furthermore, it is interesting that pH of solution after As(III) adsorption test (pH 11) was lower than that of the OS-TRHA adsorbent pellet after adding into

distilled water in the solubility test (pH 11.3). Two possible reasons can be given to describe why final pH in the As(III) adsorption experiment was lower than pH in the solubility test.

(1) As soon as the OS-TRHA adsorbent pellet was added into the As(III) solution, the dissolution of $Ca(OH)_2$ and the reaction between As(III) and un-dissolved $Ca(OH)_2$ on the OS-TRHA adsorbent pellet surface occurred simultaneously resulting in the coverage of un-dissolved $CaHAsO_3$ on the OS-TRHA adsorbent pellet surface. Then, the dissolution of $Ca(OH)_2$ decreased and causing in the lowering of pH increase.

(2) Along the pH increased, Reactions (4-3) - (4-5), (4-15) and (4-16) should occurred. It can be seen that the Reaction (4-15) did not affect the change in pH of As(III) solution. However, the pH of solution should decrease when As(III) was deprotonated by OH^- as in Reactions (4-4) and (4-16). Meanwhile, the As(III) species reacted with $Ca(OH)_2$ as in Reactions (4-3) and (4-5) caused the increase of pH solution. It can be seen in the diagram in Figure 4-34 that $HAsO_3^{2-}$ appeared at pH above 10. The As(III) exists in form of $HAsO_3^{2-}$ only 0.64% at pH 10 and reaches 68.40% at pH 12.76 [137]. Thus, it can be assumed that the extent of Reaction (4-5) was very low in comparison with Reactions (4-3), (4-4) and (4-16). It means that totally the pH should be in decreasing direction.

Since the $Ca(OH)_2$ contained in the OS-TRHA adsorbent pellet could dissolve and dissociate into Ca^{2+} and OH^- (Reaction (4-2)), As(III) in the form of $HAsO_3^{2-}$ could precipitate with the Ca^{2+} as in Reaction (4-17). However, as previously described, the $CaHAsO_3$ precipitate was not observed within 48 h thus the Reaction (4-17) should not occur in this work. Dutŕe and Vandecasteele [137, 138] reported that Ca^{2+} could precipitate with $HAsO_3^{2-}$ only at pH above 11.91. Moreover, they also introduced Saturation Index (SI) calculated by Equation (4-18) to be the other criterion of precipitation occurrence. They proposed that precipitation could occur when SI value

is greater than zero since the solution was saturated with the ion products i.e. Ca^{2+} and $HAsO_3^{2-}$.

$$\text{Saturation index (SI)} = \log\left(\frac{[Ca^{2+}][HAsO_3^{2-}]}{K_s}\right) \quad (4\text{-}18)$$

where K_s is solubility product of $CaHAsO_3$ that is equivalent to 1.07×10^{-7} [137].

In order to be easy to calculate the SI value, in this work, the concentration of $HAsO_3^{2-}$ was assumed to be equivalent to the As(III) initial concentration. Meanwhile, the concentration of Ca^{2+} was calculated from the OS-TRHA adsorbent pellet solubility in Section 4.5.2. The calculated SI value was equivalent to -0.124. According to the precipitation and calculation results, there are three reasons that can be described why Ca-As(III) precipitate did not observed in this work.

(1) The concentrations of Ca^{2+} solution and $HAsO_3^{2-}$ in this work were lower than the suitable condition for forming the precipitate.

(2) The pH of solution during the experiment was lower than 11.3, hence As(III) should be mainly in the form of $H_2AsO_3^-$ which was not suitable to form $CaHAsO_3$ precipitate.

(3) The period of time to form $CaHAsO_3$ precipitate was too short as the experiment was performed for only 24 h. However, precipitation may occur if the experiment is kept longer as Moon et al. [171] studied the arsenic immobilized by using lime and kaolinite within 4 days - 4 months and found that As(III) was precipitate with lime in form of Ca-As-O ($CaHAsO_3$).

4.9 Adsorption kinetics of As(III) on OS-TRHA adsorbent pellet

4.9.1 The comparison of As(III) adsorption on the OS-TRHA adsorbent pellet and on the ground OS-TRHA adsorbent pellet

The As(III) adsorption of ground and un-ground OS-TRHA adsorbent pellets prepared from OS particle size range of <106 μm with OS:TRHA ratio of 0.7:0.3 were performed via batch tests. Figure 4-35 illustrates As(III) concentration remaining in the solution over time.

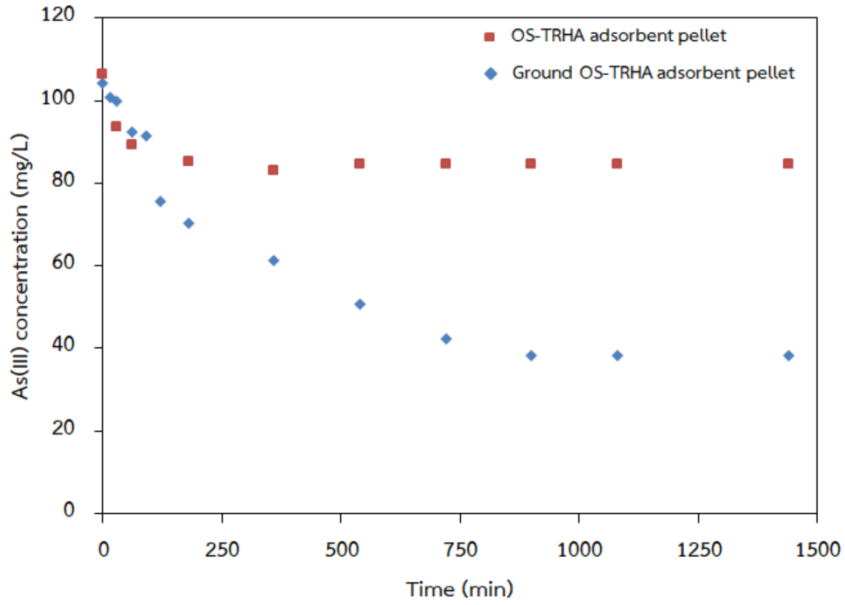

Figure 4-35 The As(III) concentration remaining in the solution with time.

As seen in Figure 4-35, when OS-TRHA adsorbent pellet was put into As(III) solution, As(III) concentration rapidly decreased within 60 min because, at initial period, the OS-TRHA adsorbent pellet had plenty of unoccupied sorption sites and As(III) concentration gradient between the bulk solution and the OS-TRHA adsorbent pellet surface was still high. After that, As(III) concentration slowly decreased with time because of the decrease in the available sorption sites on OS-TRHA adsorbent pellet and As(III) concentration gradient. The adsorption reached equilibrium at approximately 360 min. For the ground OS-TRHA adsorbent pellet, the decreasing

trend of As(III) concentration remaining in the solution was similar to that of the un-ground one. However, the adsorption process of the ground OS-TRHA adsorbent pellet reached equilibrium slower than that of the other one. The final As(III) concentration remaining in the solution of the ground pellet was also lower than that of the un-ground pellet. These should be because the ground OS-TRHA adsorbent pellet had contact surface area greater than the un-ground one. As stated before, the OS-TRHA adsorbent pellet could adsorb As(III) only on the surface of the pellet, when the OS-TRHA adsorbent pellet were ground into the powder, the active sites inside the adsorbent pellet could contact with As(III) solution and adsorb As(III) causing the longer time to reach equilibrium and less As(III) remaining in the solution.

4.9.2 The adsorption kinetics of As(III) on the OS-TRHA adsorbent pellet

To study the adsorption kinetics of As(III), the experiments were performed via batch tests. The As(III) initial concentrations were in the range of 100 mg/L - 200 mg/L with initial pH 7. The pseudo-first order presented by Lagergren in 1898 [76-79] and pseudo-second order proposed by Ho [80, 81] models were investigated to describe the As(III) adsorption on the OS-TRHA adsorbent pellet. The equations of those models are presented as the following.

Pseudo-first order: $$\frac{dq_t}{dt} = k_{a,1}(q_e - q_t) \quad (2\text{-}13)$$

Pseudo-second order: $$\frac{dq_t}{dt} = k_{a,2}(q_e - q_t)^2 \quad (2\text{-}15)$$

where q_t and q_e are the amount of As(III) adsorbed at time t and at equilibrium (mg/g), respectively. The $k_{a,1}$ and $k_{a,2}$ are adsorption rate constants of pseudo-first order (1/min) and pseudo-second order (g/mg min), respectively.

The accuracy of those models was based on the values of the correlation coefficient (R^2) and agreement between $q_{e,exp}$ values obtained from experimental data and $q_{e,cal}$ values calculated from those models. The more R^2 values approaching

to one, the better correlation between the experiment data and the model is. The calculated constant parameters are presented in Table 4-10.

Table 4-10 Kinetic parameters of As(III) adsorption on OS-TRHA adsorbent pellet.

Initial concentration (mg/L)	$q_{e,exp}$	Pseudo first order			Pseudo second order		
		$k_{a,1}$ (min^{-1})	$q_{e,cal}$	R^2	$k_{a,2}$ (g/mg min)	$q_{e,cal}$	R^2
100	10.55	0.01850	8.59	0.99	0.00750	10.72	0.98
120	11.44	0.00290	10.34	0.92	0.00191	8.89	0.93
140	12.40	0.00340	12.49	0.97	0.00078	12.50	0.96
160	13.71	0.00160	9.94	0.73	0.00331	9.24	0.96
180	14.12	0.00250	14.22	0.77	0.00365	13.04	0.99
200	14.64	0.00400	11.91	0.85	0.00332	14.31	0.99

As seen in Table 4-10, the $q_{e,cal}$ values obtained from pseudo-second order model are closer to the $q_{e,exp}$ values than those of pseudo-first order model. Furthermore, the R^2 values of pseudo-second order model are approach to one than those of pseudo-first order model. This indicates that the pseudo-second order model is better fit with the experimental data than the other model. It means that the As(III) adsorption should carry on via chemical adsorption [132, 172] and the rate of As(III) adsorption on the OS-TRHA adsorbent pellet was proportional to the number of available sorption sites and the amount of As(III) containing in the solution. The average observed adsorption rate constant calculated from pseudo-second order model is approximately 0.0034 g/mg min. Moreover, the result shows that the $q_{e,exp}$ values increases from 10.55 to 14.64 mg/g as As(III) initial concentration increases from 100 mg/L - 200 mg/L. Two reasons can be given to explain this result.

(1) The concentration difference of As(III) between the bulk solution and OS-TRHA adsorbent surface increased with the increase of As(III) initial concentration causing the increase in the mass transfer driving force.

(2) The more increase of As(III) initial concentration, the more amount of As(III) in the solution causing the increase in the chance of As(III) to be adsorbed on the sorption sites of OS-TRHA adsorbent pellet.

4.10. Adsorption isotherms of OS-TRHA adsorbent pellet

To study the behavior of As(III) adsorption on OS-TRHA adsorbent pellet, the linear forms of Langmuir (Equation (2-32)) and Freundlich (Equation (2-34)) adsorption isotherms were applied to fit the experimental data. The adsorption parameters are presented in Table 4-11.

$$\frac{1}{q_e} = \frac{1}{q_m} + \frac{1}{K_L q_m C_e} \quad (2\text{-}32)$$

$$\log q_e = \log K_F + \frac{1}{n} C_e \quad (2\text{-}34)$$

where K_L is Langmuir equilibrium adsorption constant while K_F is Freundlich adsorption constant and 1/n relates to the adsorption capacity and intensity of adsorption.

Table 4-11 Adsorption parameters corresponding to Langmuir and Freundlich isotherms.

Langmuir isotherm			Freundlich isotherm		
K_L (L/mg)	q_{max} (mg/g)	R^2	K_F (L/g)	1/n	R^2
0.0099	23.26	0.98	0.1784	0.4425	0.96

Table 4-11 shows that R^2 corresponding to Langmuir isotherm is closer to one than that corresponding to Freundlich isotherm. This implies that the behavior of As(III) adsorption on OS-TRHA adsorbent pellet should be better described by Langmuir isotherm which means that As(III) should be monolayer adsorbed on the OS-TRHA adsorbent pellet at specific sorption sites on the adsorbent surface with no significant interaction among adsorbate species [83].

4.11. Determination of $CaSiO_3$ and C-S-H compounds in the OS-TRHA adsorbent pellet

As described before, the OS-TRHA adsorbent pellet could be classified into two parts. The first part is CaO which is the sorption sites for adsorbing As(III) in the form of Ca-As-O. The other one is $CaSiO_3$ and C-S-H compounds which are the binder compound in the OS-TRHA adsorbent pellet. The $CaSiO_3$ and C-S-H compounds are inactive compound for adsorbing As(III). In order to determine the amount of inactive $CaSiO_3$ and C-S-H compounds obtained from Reactions (4-11), (4-13) and (4-14), initially, all $CaCO_3$ which contained in OS was assumed to be converted into CaO in the OS-TRHA adsorbent pellet as in Reaction (2-62). According to the As(III) adsorption mechanism discussed in Section 4.8, CaO could be divided into three fractions as in Equation (4-19).

$$\mathbf{CaO_{overall}} = \mathbf{CaO_{dissolve}} + \mathbf{CaO_{ads}} + \mathbf{CaO_{rxn}} \qquad (4\text{-}19)$$

while $CaO_{dissolve}$ = CaO dissolving in the solution

CaO_{ads} = CaO that can convert into As(III) reactive sites

CaO_{rxn} = CaO reacting with SiO_2 in TRHA during the preparation process

In this section, the OS-TRHA adsorbent pellet prepared from OS particle size range of <106 μm with OS:TRHA ratio of 0.7:0.3 was determined. The initial weight of OS ($CaCO_3$) containing in the OS-TRHA was approximately 0.21 g. After the calcination process, $CaCO_3$ transformed into CaO as in Reaction (2-62). The weight of CaO in the OS-TRHA adsorbent pellet could be calculated from Equation (4-20). Thus, 0.21 g of $CaCO_3$ should convert into approximately 0.1177 g of CaO.

$$\mathrm{W.of\ CaO\,(g)} = \mathrm{W.of\ CaCO_3(g)} \times \frac{56.08\ \mathrm{g/mol}}{100.09\ \mathrm{g/mol}} \qquad (4\text{-}20)$$

The dissolved CaO was determined by dissolving the ground OS-TRHA adsorbent pellet in distilled water with initial pH 7. The pHs of solution before and

after dissolving (24 h) were measured. As described before, when CaO in the OS-TRHA adsorbent pellet contacted with water, it changed into $Ca(OH)_2$ as in Reaction (4-1) and some of it could further dissolve in water and dissociate into Ca^{2+} and OH^- as in Reaction (4-2). In this section, assuming that all dissolved $Ca(OH)_2$ dissociated into Ca^{2+} and OH^-, based on the change of pH in the solubility test of ground OS-TRHA adsorbent pellet from 7 to 11.4, the $CaO_{dissolve}$ can be calculated as approximately 0.0007 g.

For CaO_{ads}, it was also assumed to have the same properties as COS. Based on As(III) adsorption capacity of COS (241.67 mg/g), the ground OS-TRHA adsorbent pellet could remove As(III) approximately 70.50 mg/L which was equivalent to the ability to remove As(III) by 0.0513 g of COS or CaO_{ads}. Thus, CaO_{rxn} in Equation (4-19) could be calculated as approximately 0.0657 g. Therefore, the inactive CaO ($CaSiO_3$ and C-S-H compounds) in OS-TRHA adsorbent pellet could be calculated as about 55.8 wt%. It means that 75 wt% of the OS-TRHA adsorbent pellet is $CaSiO_3$ and C-S-H compounds. In addition, the ratio of $CaO:SiO_2$ in the pozzolanic reaction was also calculated. $CaO:SiO_2$ ratio is equivalent to 0.8:1 which is in the range of the C-S-H compounds that was reported by Yu et al.[173] and Dia et al.[174].

4.12. The larger scale of As(III) removal by OS-TRHA adsorbent pellets

To observe the As(III) adsorption performance of OS-TRHA adsorbent pellet in the larger scale, 3-4 g of OS-TRHA adsorbent pellets was added into 2 L of synthetic As(III) contaminated water. The initial As(III) concentration was equivalent to 34 mg/L which was comparable with arsenic concentration in water resources in Thailand. The experiment was set as in Figure 4-36. The OS-TRHA adsorbent pellets were changed every 2 days, 3 times. The concentrations of As(III) remaining in the solution were measured by an inductively coupled plasma (ICP, In-house method based on Standard Methods for Examination of Water and Wastewater 20th Edition [155]).

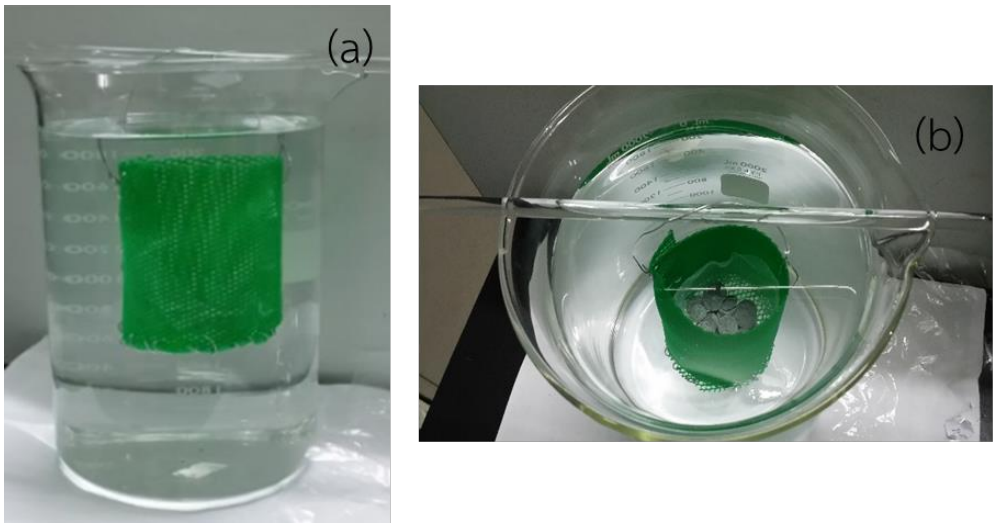

Figure 4-36 The images of (a) side view and (b) top view of the larger scale of As(III) removal experiment.

The result showed that OS-TRHA adsorbent pellets could remove As(III) from the synthetic As(III) contaminated water for approximately 98.95%. The final concentration of As(III) remaining in the solution was as low as 0.36 mg/L. The pHs of solution before and after As(III) adsorption tests were measured. The result showed that the pH of solution increased from 7 to 12.4 which should be because of the dissolving of OS-TRHA adsorbent pellets. However, pHs of water resources are usually lower than 7 as Pattanapipitpaisal and Suraruk [17] collected the data of groundwater quality in Thailand and reported that pH of ground water was in the range of 5.70 - 6.90. Waste water, particularly dirty acid waste water obtained from many processes such as hydrometallurgy industry, textile industry, mining industry, etc., usually contained highly concentration of arsenic (5,240 mg/L - 14,740 mg/L) which mainly exists in As(III) form with very low pH (0.5 - 3.25) [175, 176]. Many processes have been used to treat the waste water. The main processes consisted of neutralisation by lime, followed by arsenic adsorption [175-177]. Therefore, the OS-TRHA adsorbent pellet should be a good dual-function material to be used as As(III) removal material and pH neutralizer compound in the single step.

4.13. The comparison of COS and OS-TRHA adsorbents with other materials

The maximum As(III) adsorption capacities of COS and OS-TRHA adsorbent pellet in this work compared to other materials is presented in Table 4-12.

Table 4-12 Comparison of As(III) removal capacity of COS and OS-TRHA adsorbent pellets with other materials.

Name of material	As(III) removal capacity (mg/g)	Reference
COS 150-250 μm (Initial pH 11)	345.09	Present work
COS<106 μm (Initial pH 7)	241.67	Present work
OS-TRHA adsorbent pellet with OS:TRHA ratio of 0.7:0.3 (Initial pH 7)	26.20	Present work
$FePO_4$ (Amorphous)	21.00	[71]
$FePO_4$ (Crystalline)	16.00	[71]
Iron oxide coated cement (IOCC)	0.69	[26]
Iron-oxide-coated natural rock (IOCNR)	1.647	[178]
Iron oxide coated sand (IOCS)	0.05	[131]
Raw red mud (RRM)	8.86	[27]
Activated red mud (ARM)	11.80	[27]
Bentonite	0.317	[179]
Shale	0.181	[179]

Table 4-12 Comparison of As(III) removal capacity of COS and OS-TRHA adsorbent pellets with other materials (continue).

Name of material	As(III) removal capacity (mg/g)	Reference
Amorphous Iron hydroxide (HFO)	28.00	[29]
Goethite	22.0, 7.50	[28, 29]
Oxisol	2.60	[28]
Char carbon (CC)	5.04	[25]
Carbon produced by arcing of graphite rods (AC)	4.56	[25]
Activated carbon	29	[25]
Innovative coal-based mesoporous activated carbon (NCPAC)	1.491	[180]
Commercial available carbon (CPAC, 200 meshes)	0.713	[180]
Coconut (Cocos nucifera L.) fiber	0.118	[181]
Coconut husk carbon	146.30	[132]
Zinc peroxide functionalized synthetic graphite (FSG)	18.8	[182]
Silica gel supported Fe-Ag-PVA nanocomposite (G.Y-9)	0.024	[183]
Silica gel supported Mn-Ag-PVA nanocomposite (G.Y-10)	0.022	[183]
Chitosan-iron oxyhydroxide (CFOH) bead	7.2	[37]
Copper (II) oxide nanoparticles	1.10	[30]

As seen in Table 4-12, in As(III) adsorption tests with initial concentration of 1000 mg/L (pH 11), the maximum As(III) adsorption capacity of COS prepared from OS particle size range of 150-250 μm was about 345.09 mg/L. Meanwhile, in As(III) adsorption test with initial concentration 100 mg/L (pH 7), the maximum As(III) adsorption capacity of COS prepared from OS particle size range of <106 μm was approximately 241.67 mg/L. When comparing the maximum As(III) adsorption capacities of COS prepared from OS particle size ranges of <106 μm and 150-250 μm with other materials in Table 4-12, the maximum As(III) adsorption capacities of those COS are greater than those of the other materials.

It can be also seen in Table 4-12 that the As(III) adsorption capacity of the OS-TRHA adsorbent pellet prepared from OS particle size range of <106 μm with OS:TRHA ratio of 0.7:0.3 is about 9 times lower than that of COS prepared from OS particle size range of <106 μm. However, the As(III) adsorption capacity of the OS-TRHA adsorbent pellet is still high when comparing with the maximum As(III) adsorption capacities of the other kind materials in literature. Therefore, COS and OS-TRHA adsorbent pellet are the promising adsorbent used to remove As(III) as it provides high adsorption capacities with very low cost of raw materials.

Chapter 5

Conclusions and suggestions

5.1 Conclusions

This research studied As(III) removal from contaminated water by using COS and OS-TRHA adsorbent pellets. These adsorbents were prepared from waste materials i.e. OS and RHA that caused the environmental problems. The experiments were divided into two parts. In part A, the effect of anions on As(III) adsorption performances by using COS prepared from OS particle size range of 150 - 250 μm was investigated. Meanwhile, the As(III) removal by using OS-TRHA adsorbent pellet was studied in part B. The results could be concluded as the following.

PART A : The effect of anion contamination on As(III) adsorption performance by using COS as an adsorbent

1. After calcination of OS at 700°C for 8 h, $CaCO_3$ in OS transformed into CaO in COS. The smooth layer surface of OS also changed into the porous structure on the COS surface.

2. After adding COS into the solution, some CaO in COS dissolved and dissociated into Ca^{2+} and OH^-. pH_{zpc} of COS was about 12.1.

3. As(III) NO_3^-, SO_4^{2-} were removed from contaminated water via adsorption process in the forms of Ca-As-O, $Ca(NO_3)_2 \cdot 2H_2O$ and $CaSO_4$, respectively. Meanwhile, HPO_4^{2-} was removed via adsorption and precipitation processes in the form of $CaHPO_4$. HPO_4^{2-} could precipitate with Ca^{2+} approximately 46.62% while the precipitates of As(III), NO_3^-, SO_4^{2-} with Ca^{2+} were not observed.

4. In individual adsorption tests, COS had capability to adsorb HPO_4^{2-} greater than those of As(III), NO_3^- and SO_4^{2-}, respectively.

5. In bi-solutes system, binding affinity between COS sorption sites and HPO_4^{2-} was stronger than those of As(III) and SO_4^{2-} and NO_3^-, respectively.

6. The adsorption rate constants of HPO_4^{2-} were greater than those of the other anions in every observed case. Conversely, the adsorption rate constants of SO_4^{2-} were lower than those of the others. Furthermore, when the solution contained HPO_4^{2-}, the observed adsorption rate constants of NO_3^- were greater than those of As(III).

7. The amounts of As(III) and anions occupied on the sorption sites depended on (1) the binding affinity between sorption sites and adsorbates, (2) the interaction between the adsorbates (adsorbates charge repulsion) and (3) the effect of electrostatic attraction/repulsion between the adsorbent surface charge and adsorbates charge.

8. After As(III) adsorption process, the porous surface of COS looked like it was covered by grass leaf - like matter. Meanwhile, the COS surface seemed to be covered by small grains after SO_4^{2-} adsorption test. The flaky matter was observed after COS was used to remove NO_3^- and HPO_4^{2-}.

9. In bi-, tri-, and tetra-solutes systems, the morphologies of COS after removal process were more complex. The different morphologies of used COS depended on type of adsorbates and number of adsorbates containing in the solution.

PART B : As(III) removal by using OS-TRHA adsorbent pellet

10. After calcination process of RHA at 600°C for 13 h, the unburned carbon and other impurities containing in RHA were removed while SiO_2 in TRHA was still in the amorphous structure.

11. After preparation process, OS-TRHA adsorbent pellet composed of CaO, $CaSiO_3$ and C-S-H compounds.

12. The dissolving of CaO in OS-TRHA adsorbent pellets prepared from every observed OS particle size range was about 86.40% - 93.70% less than that in COS prepared from the same OS particle size rages.

13. The OS-TRHA adsorbent pellet prepared from OS particle size range of <106 μm with OS:THRA ratio of 0.7:0.3 was the best condition for preparation OS-TRHA adsorbent pellet. It could provide the maximum As(III) adsorption capacity of about 26.20 mg/g.

14. After adsorption process, CaO in OS-TRHA adsorbent pellet could adsorb As(III) and form Ca-As-O whereas $CaSiO_3$ and C-S-H compounds did not react with As(III) but it could bind the precursor powders to be stable without cracking.

15. Before adsorption process, the smooth surface and the rough surface were observed on OS-TRHA adsorbent pellets prepared from every observed OS particle size ranges while the porous bars structure was detected only on the OS-TRHA adsorbent pellets prepared from OS particle size ranges of 106-150 and 150-250 μm. After adsorption process, the rough surface and porous bars seem to be covered by the grass-leaves like morphology whereas the smooth surface was still observed on the OS-TRHA adsorbent pellets prepared from OS every observed particle size range.

16. The As(III) adsorption data of OS-TRHA adsorbent pellet prepared from OS particle size rage of <106 μm with OS:TRHA ratio of 0.7:0.3 fitted with pseudo-second order adsorption rate model. The calculated average observed adsorption rate was approximately 0.0034 g/mg min. Meanwhile, the equilibrium data of As(III) adsorption on OS-TRHA adsorbent pellet prepared from OS particle size rage of <106 μm with OS:TRHA ratio of 0.7:0.3 followed the Langmuir isotherm.

17. The calculated amount of $CaSiO_3$ and C-S-H compounds containing in the OS-TRHA adsorbent pellet prepared from OS particle size range of <106 μm with OS:TRHA ratio of 0.7:0.3 was approximately 75 wt%.

5.2 Suggestions

The future work concerns the effects of other ions containing in the water resources and the applications of adsorbent pellet for removing As(III) in the water resources. There are some ideas that should be useful for the future work.

1. The effect of anions and cations on As(III) adsorption performance by COS should be more studied. As the result of As(III) adsorption by COS under the presence of NO_3^-, SO_4^{2-} and HPO_4^{2-} showed that, when the solution contained other anions, the As(III) adsorption performances decreased. In water resources, there are many kinds of ion containing in the water that should also affect As(III) adsorption performance. Thus, it should be run more tests and more study about those effects.

2. The effects of anions and cations on As(III) adsorption by using OS-TRHA adsorbent pellet should be more studied. As mentioned above, when the solution contained other anions in the solution, the As(III) adsorption performances decreased depending on type and number of anions containing in the solution. In addition, the contaminated water in the water resources contained many kinds of anion and cation. Thus, it is also necessary to study the effects of anions and cations containing in the water resources on As(III) removal performance by OS-TRHA adsorbent pellet.

3. The effect of acidic pH solution (pH<7) on As(III) adsorption performance by using OS-TRHA adsorbent pellets should be also studied. As mentioned before, in many processes, almost waste water, pH solution is in the range of acidic pH (pH 0.5 - 3.25) [175, 176]. According to XRD and As(III) adsorption results, the OS-TRHA adsorbent pellet composed of CaO which is the sorption sites for adsorbing As(III). CaO could react with acid in the solution and causing the increase of pH solution. Thus, the OS-TRHA adsorbent pellets could be used as a dual function adsorbent. But, in the case of pH solution is very low, the CaO in OS-TRHA adsorbent pellet should be more dissolved into the solution and causing the lower As(III) adsorption performance. Thus, it is important to run more experiments and study about this effect.

4. The pilot scale of As(III) removal by OS-TRHA adsorbent pellet is also needed to study in order to test the adsorption performance of OS-TRHA adsorbent pellets in the water treatment process before applying the OS-TRHA adsorbent pellet into the water resources.

5. The application of OS-TRHA adsorbent pellet after being used in water treatment is also necessary to study. The adsorption and desorption results indicated that As(III) should form the chemical bonding with CaO in the OS-TRHA adsorbent pellet. Thus, it is difficult to desorb from the adsorbent pellet. Then, the OS-TRHA adsorbent pellet should not be regenerated to use as the recycle adsorbent for As(III) removal. As mentioned before, OS and RHA were used in the construction materials i.e. the replacement cement in the concrete, brick production, ceramic production, etc. Thus, the used OS-TRHA adsorbent pellet should be able to apply in the construction materials like OS and RHA. However, As(III) is a hazardous material therefore it needs to carefully run more tests such as synthetic precipitation leaching procedure (SPLP, US EPA Method 1312) (US EPA, 1994), toxicity characteristic leaching procedure (TCLP, US EPA Method 1311) (US EPA, 1997) [184], etc. to assure that As(III) will not leak from those materials and cause the harm to human health and environment problem.

References

[1] Mohan D. and Pittman Jr. C.U. "Arsenic removal from water/wastewater using adsorbents:A critical review" **Journal of Hazardous Materials**. vol.142, no.1-2, 2007. pp.1-53.

[2] Ng J.C., Wang J. and Shraim, A. "A global health problem caused by arsenic from natural sources" **Chemosphere.** vol.52, 2003. pp.1353-1359.

[3] Mazumder G.N. "Chronic arsenic toxicity: clinical features, epidemiology, and treatment: experience in West Bengal" **Journal of Environmental Science and Health, Part A Toxic/Hazardous Substances and Environmental Engineering.** vol.38, 2003. pp.141-163.

[4] Choong T.S.Y. et al. "Arsenic toxicity, health hazards and removal techniques from water: an overview" **Desalination**. vol.217, no. 1-3, 2007. pp.139-166.

[5] Chen C.J. et al. "Atherogenicity and carcinogenicity of high-arsenic artesian well water" **Arteriosclerosis**. vol.8, 1988. pp.452-460.

[6] Nicolli H.B., Suriano J.M., and Gomez P. "Groundwater contamination with arsenic and other trace elements in an area of the Pampa, Province of Cordoba, Argentina" **Environmental Geology and Water Sciences.** vol.14, 1989. pp.3-16.

[7] Smedley, P.L. and Kinniburgh. D.G. "**Chapter 1. Source and behaviour of arsenic in natural waters in United Nations Synthesis Report on Arsenic in Drinking Water.**" [Online]. Available: http://www.who.int/water_sanitation_health/dwq/arsenic3/en/. 2001.

[8] Dhar R.K. et al. "Groundwater arsenic calamity in Bangladesh" **Current science**. vol. 73, 1997. pp.48-59.

[9] Mandal B.K. et al. "Arsenic in groundwater in seven districts of West Bengal, India—the biggest arsenic calamity in the world" **Current science.** vol. 70, 1996. pp. 976-986.

[10] Yinlong J. "Progress on arsenic in China" **Proc. the First International workshop on arsenic pollution of Drinking Water in South Asia and China, national Institute of Environmental Studies, R-166-201, Tokyo, Japan**, 2001 pp.35-39.

[11] Berg M. et al. "Arsenic contamination of groundwater and drinking water in Vietnam: a human health threat" **Environmental Science & Technology**. vol. 35, 2001. pp.2621-2622.

[12] Sharma V.K. and Sohn M. "Aquatic arsenic: Toxicity, speciation, transformations, and remediation" **Environment International**. vol. 35, no. 4, 2009. pp.743-759.

[13] Williams M. et al. "Arsenic contamination in surface drainage and groundwater in part of the southeast Asian tin belt, Nakhon Si Thammarat Province, southern Thailand" **Environmental Geology and Water Sciences**. vol.27, 1996. pp.16-33.

[14] Pansamut, S. and Wattayakorn G. "Arsenic contamination in water from suphanburi province, Thailand" **Journal of Environmental Research And Development**. vol. 4, no. 3, 2010. pp.678-686.

[15] Siripitayakunkit, U., Thaicharoen S., and Thonghong A. "Chronic Arsenic Poisoning in Ronpiboon, Nakhon Si Thammarat,2000" **Journal of Health Science**. vol. 12, no.1, 2003. pp.89-93.

[16] Kohnhorst A. et al. "Groundwater arsenic in central Thailand" **Proc. 28th WEDC Conference SUSTAINABLE ENVIRONMENTAL SANITATION AND WATER SERVICES. Kolkata (Calcutta), India**, 2002.

[17] Pattanapipitpaisal P. and Suraruk P. "Groundwater Quality and Arsenic Contamination in Amphoe Khemmarat, Ubon Ratchathani, Thailand" **Journal of Environmental Science and Engineering A**. vol. 1, 2012 pp.133-141.

[18] Hossain M.M. et al. "Prediction of Groundwater Arsenic Contamination using Geographic Information System and Artificial Neural Network" **Environment Asia.** vol. 6, no.1, 2013. pp.38-44.

[19] Maji S.K., Kao Y.H. and Liu C.W. "Arsenic removal from real arsenic-bearing groundwater by adsorption on iron-oxide-coated natural rock (IOCNR)" **Desalination**. vol. 280, no.1-3, 2011. pp.72-79.

[20] Maji S.K., Pal A., and Pal T. "Arsenic removal from real-life groundwater by adsorption on laterite soil" **Journal of Hazardous Materials**. vol. 151, no.2-3, 2008. pp.811-820.

[21] Maiti A. et al. "Adsorption of arsenite using natural laterite as adsorbent" **Separation and Purification Technology.** vol. 55, no 3. 2007. pp. 350-359.

[22] Zhang G. et al. "Preparation and evaluation of a novel Fe-Mn binary oxide adsorbent for effective arsenite removal" **Water Research**. vol. 41, no.9, 2007. pp.1921-1928.

[23] Xia S. et al. "Arsenic removal from groundwater by acclimated sludge under autohydrogenotrophic conditions" **Journal of Environmental Sciences.** vol. 26, 2014. pp.248-255.

[24] Dermatas D. et al. "An evaluation of arsenic release from monolithic solids using a modified semi-dynamic leaching test" **Journal of Hazardous Materials**. vol. 116, no. 1-2, 2004. pp.25-38.

[25] Pattanayak J. et al. “A parametric evaluation of the removal of As(V) and As(III) by carbon-based adsorbents” **Carbon**. vol. 38, no. 4, 2000. pp.589-596.

[26] Kundu S. and Gupta A.K. “Adsorptive removal of As(III) from aqueous solution using iron oxide coated cement (IOCC): Evaluation of kinetic, equilibrium and thermodynamic models” **Separation and Purification Technology**. vol. 51, 2006. pp.165-172.

[27] Altundoğan H.S. et al. “Arsenic adsorption from aqueous solutions by activated red mud” **Waste Management**. vol. 22, no.3, 2002. pp.357-363.

[28] Ladeira A.C.Q. and Ciminelli V.n.S.T.C. “Adsorption and desorption of arsenic on an oxisol and its constituents” **Water Research**. vol. 38, no.8, 2004. pp. 2087-2094.

[29] Lenoble V. et al. “Arsenic Adsorption onto Pillared Clays and Iron Oxides” **Journal of Colloid and Interface Science.** vol. 255, no.1, 2002. pp.52-58.

[30] Goswami A., Raul P.K., and Purkait M.K. “Arsenic adsorption using copper (II) oxide nanoparticles” **Chemical Engineering Research and Design**. vol. 90, no. 9, 2012 pp.1387-1396.

[31] Alidoust D. et al. “Mechanism of cadmium biosorption from aqueous solutions using calcined oyster shells” **Journal of Environmental Management**. vol. 150, 2015. pp.103-110.

[32] Kwon H.B. et al. “Recycling waste oyster shells for eutrophication control” **Resources, Conservation and Recycling**. vol. 41, no.1, 2004. pp.75-82.

[33] Lee Y.H. et al. “Composted Oyster Shell as Lime Fertilizer Is More Effective Than Fresh Oyster Shell” **Bioscience, Biotechnology, and Biochemistry**. vol. 74, no.8, 2010. pp.1517-1521.

[34] Li G. et al. “Properties of cement-based bricks with oyster-shells ash” **Journal of Cleaner Production**. vol. 91, 2015. pp.279-287.

[35] Khownpurk P., Wongpromrat W. and Chandra-ambhorn W. “Arsenic Adsorption Using the Adsorbent Synthesised from Oyster Shell” **Key Engineering Materials** vol. 728, 2017. pp.327-334.

[36] Sigdel A. et al. “Arsenic removal from aqueous solutions by adsorption onto hydrous iron oxide-impregnated alginate beads” **Journal of Industrial and Engineering Chemistry**. vol. 35, 2016. pp.277-286.

[37] Hasan S. et al. “Dispersion of FeOOH on Chitosan Matrix for Simultaneous Removal of As(III) and As(V) from Drinking Water” **Separation Science and Technology**. vol. 49, 2014. pp. 2863-2877.

[38] Amano Y., Matsushita Y. and Machida, M. “Arsenic Adsorption by Activated Carbon with Different Amounts of Basic Sites under Different Solution pH and Coexistent Ions” **Separation Science and Technology**. vol. 49, 2014. pp. 345-353.

[39] Mangwandi C. et al. “Design, production and characterisation of granular adsorbent material for arsenic removal from contaminated wastewater” **Chemical Engineering Research and Design**. vol. 110, 2016. pp.70-81.

[40] Hassan J.U., Noha M.Z. and Ahmad Z.A. “Chemical and Mineralogical Properties of Rice Husk Ash (RHA)” **Jurnal Teknologi (Sciences & Engineering).** vol. 70, no.5, 2014. pp.1-3.

[41] Srinivasreddy A.B., McCarthy T.J. and Lume E. “Effect of rice husk ash on workability and strength of concrete” **Proc. 6th Biennial Concrete Institute of Australia's National Conference (Concrete 2013), Australia, 2013**. pp.1-10.

[42] Prasara A. J. and Gheewala S.H. "Sustainable utilization of rice husk ash from power plants: A review" **Journal of Cleaner Production**. vol. 167, 2016. pp. 1020-1028.

[43] Habeeb G.A. and Mahmud H.B. "Study on properties of rice husk ash and its use as cement replacement material" **Materials Research**. vol. 13, no.2, 2010. pp.185-190.

[44] Saad S.A. et al. "Pozzolanic Reaction Mechanism of Rice Husk Ash in Concrete – A Review" **Applied Mechanics and Materials**. vol. 773-774, 2015. pp.1143-1147.

[45] Ramezanianpour A.A., Mahdi khani M. and Ahmadibeni G. "The Effect of Rice Husk Ash on Mechanical Properties and Durability of Sustainable Concretes" **International Journal of Civil Engineering**. vol. 7, no. 2, 2009. pp.83-91.

[46] Feng Q. et al. "Study on the pozzolanic properties of rice husk ash by hydrochloric acid pretreatment" **Cement and Concrete Research**. vol. 34, no.3, 2004. pp.521-526.

[47] Villar-Cociña E. et al. "Pozzolanic behavior of bamboo leaf ash: Characterization and determination of the kinetic parameters" **Cement and Concrete Composites**. vol. 33, no.1, 2011. pp.68-73.

[48] Azizian S., Haerifar M. and Basiri-Parsa J. "Extended geometric methad: A simple approach to derive adsorption rate constants of Langmuir-Frundlich kinetic" **Chemosphere**. vol. 68, 2007. pp.2040-2046.

[49] Azizian S. "Kinetic models of sorption: a theoretical analysis" **Journal of Colloid and Interface Science**. vol. 276, no.1, 2004. pp.47-52.

[50] Roberts G.W. **Chemical reactions and chemical reactors**. United States of America: John Wiley and Sons,Inc. 2009.

[51] Chapra S.C. and Canale R.P. **Numerical methods for engineers, sixth ed.** New York: McGraw-Hill. 2010.

[52] Juillot F. et al. "Remobilization of arsenic from buried wastes at an industrial site: mineralogical and geochemical control" **Applied Geochemistry** vol. 14, no.8, 1999. pp.1031-1048.

[53] Moon D.H., Dermatas D. and Menounou N. "Arsenic immobilization by calcium-arsenic precipitates in lime treated soils" **Science of The Total Environment**. vol. 330, no.1-3, 2004. pp.171-185.

[54] Liu S. et al. "Micro/nanostructured porous Fe-Ni binary oxide and its enhanced arsenic adsorption performances" **Journal of Colloid and Interface Science**. vol 458, 2015. pp.94-102.

[55] Aranda P.R. et al. "Removal of arsenic(V) ions from aqueous media by adsorption on multiwall carbon nanotubes thin film using XRF technique" vol. 5, 2016. pp.21-26.

[56] Ferguson J.F. and Gavis J. "A review of the arsenic cycle in natural waters" **Water Research**. vol. 6, no.11, 1972. pp.1259-1274.

[57] Moon D.H. et al. "Assessment of cement kiln dust (CKD) for stabilization/solidification (S/S) of arsenic contaminated soils" **Journal of Hazardous Materials**. vol. 159, no.2-3, 2008. pp.512-518.

[58] Burguera M. and Burguera J. "Analytical methodology for speciation of arsenic in environmental and biological samples" **Talanta.** vol. 44, no. 9, 1997. pp. 1581-1604.

[59] Walker M., Seiler R. and Meinert M. "Effectiveness of household reverse-osmosis systems in a Western US region with high arsenic in groundwater" **Science of The Total Environment**. vol. 389, no. 2-3, 2008. pp.245-252.

[60] Borah D. et al. "Sorption of As(V) from aqueous solution using acid modified carbon black" **Journal of Hazardous Materials**. vol 162, 2009. pp. 1269-1277.

[61] Oh C. et al. "Removal characteristics of As(III) and As(V) from acidic aqueous solution by steel making slag" **Journal of Hazardous Materials**. vol. 213-214, 2012. pp.147-155.

[62] Salameh Y. et al. "Arsenic(III,V) adsorption onto charred dolomite: Charring optimization and batch studies" **Chemical Engineering Journal**. vol. 259, 2015. pp.663-671.

[63] Marie E.M. "An Uptake on Arsenic Clinics in Laboratory Medicine" vol. 10, 1990. pp. 459-472.

[64] Aposhian H.V. and Aposhian M.M. "Arsenic toxicology: five questions" **Chemical Research in Toxicology.** vol. 19, 2006. pp.1-15.

[65] Schuliga M., Chouchane S. and Snow E.T. "Upregulation of glutathione-related genes and enzyme activities in cultured human cells by sublethal concentration of inorganic arsenic" **Toxicological Sciences.** vol. 70, 2002. pp.183-192.

[66] Wang T.S. et al. "Glutathione peroxidase and catalase modulate the genotoxicity of arsenite" **Toxicology**. vol. 121, no.3, 1997. pp.229-237.

[67] Chang K.N. et al. "Identification of galectin I and thioredoxin peroxidase II as two arsenic-binding proteins in Chinese hamster ovary cells" **Biochemical Journal**, vol. 371, 2003. pp.495-503.

[68] Králik M. "Adsorption, chemisorption, and catalysis" **Chemical Papers**, vol. 68, no. 12, 2014. pp.1625-1638.

[69] Bajpai A.K. and Rajpoot M. “Adsorption Techniques-A Review” **Journal of Scientific and Industrial Research.** vol. 58, 1999. pp.844-860.

[70] Gabelman A. “Adsorption Basics: Part 1” **Back to Basics , American Institute of Chemical Enginees (AlChE)** 2017. pp. 48-53.

[71] Lenoble V. et al. “Arsenic removal by adsorption on iron(III) phosphate” **Journal of Hazardous Materials**. vol. 123, no.1-3, 2005. pp.262-268.

[72] Bang S. et al. “Removal of arsenic from groundwater by granular titanium dioxide adsorbent” **Chemosphere**. vol. 60, no.3, 2005. pp.389-397.

[73] Bang S. et al. “Effects of silicates, phosphate, and bicarbonate on arsenic removal and treatment of arsenic in Bangladesh groundwater with ferric salts” **Proc. the World Congress of Korean Scientists and Engineers-2002. The Korean Federation of Science and Technology Societies**, 2002. pp.839-844.

[74] ศิลปรัตน์ ชีวรัตน์, รุ่งโรจน์กิจไพศาล ปริญญา และ จรัสโชติพินิต ปวีณา “การดูดซับตะกั่วโดยการพัฒนาตัวกลางดูดซับที่ได้จากเปลือกหอยแครง (Adsorption of lead by developed from cockle shell)” วิทยานิพนธ์วิทยาศาตรบัณฑิต, สถาบันเทคโนโลยีพระจอมเกล้าเจ้าคุณทหารลาดพระบัง. 2544.

[75] Maiti A. et al. “Comparison of treated laterite as arsenic adsorbent from different locations and performance of best filter under field conditions” **Journal of Hazardous Materials**. vol. 262, 2013. pp.1176-1186.

[76] Qui H. et al. “Critical review in adsorption kinetic models” **Journal of Zhejiang University SCIENCE A**. vol. 10, no.5, 2009. pp.716-724.

[77] Ho Y.S. and McKay G. “The sorption of lead(II) ions on peat” **Water Research**. vol. 33, no.2, 1999. pp.578-584.

[78] Lagergren S. “About the theory of so-called adsorption os soluble substances” **Hanlingar**. vol. 24, 1891. pp. 1-39.

[79] Malana M.A., Qureshi R.B. and Ashiq M.N. “Adsorption studies of arsenic on nano aluminium doped manganese copper ferrite polymer (MA, VA, AA) composite: Kinetics and mechanism” **Chemical Engineering Journal**. vol. 172, no.2-3, 2011. pp.721-727.

[80] Ho Y.S. “Review of second-order model for adsorption system” J**ournal of Hazardous Materials**. vol. 136, 2006. pp.681-689.

[81] Ho Y.S. and MCKAY G. “Pseudo-second order model for sorption processes” **Process Biochemistry**. vol. 34, 1999. pp.451-465.

[82] Tan I.A.W., Ahmad A.L. and Hameed B.H. “Adsorption of basic dye on high-surface-area activated carbon prepared from coconut husk: Equilibrium, kinetic and thermodynamic studies” **Journal of Hazardous Materials**. vol. 154, no.1-3, 2008. pp.337-346.

[83] Sener, S. “Use of solid wastes of the soda ash plant as an adsorbent for the removal of anionic dyes: Equilibrium and kinetic studies” **Chemical Engineering Journal**. vol. 138, no.1-3, 2008. pp.207-214.

[84] Foo K.Y. and Hameed B.H. “Insights into the modeling of adsorption isotherm systems” **Chemical Engineering Journal**. vol. 156, no.1, 2010. pp.2-10.

[85] Chung H.K. et al. “Application of Langmuir and Freundlich isotherms to predict adsorbate removal efficiency or required amount of adsorbent” **Journal of Industrial and Engineering Chemistry**. vol. 28, 2015. pp.241-246.

[86] Hernández-Flores H. et al. “Concrete/maghemite nanocomposites as novel adsorbents for arsenic removal” **Journal of Molecular Structure**. vol. 1171, 2018. pp.9-16.

[87] Chemistry learning free online education resource. "**Langmuir Adsorption Isotherm.**" [Online]. Available : http://www.chemistrylearning.com/langmuir-adsorption-isotherm/. 2017.

[88] Tian Y. et al. "Synthesis of magnetic wheat straw for arsenic adsorption" **Journal of Hazardous Materials.** vol.193, 2011. pp.10-16.

[89] Feng N., Guo X. and Liang S. "Adsorption study of copper (II) by chemically modified orange peel" **Journal of Hazardous Materials**. vol. 164, no.2-3, 2009. pp.1286-1292.

[90] Chemistry learning free online education resource. "**Freundlich Adsorption Isotherm.**" [Online]. Available : http://www.chemistrylearning.com/adsorption-isotherm/. 2017.

[91] Luo H. et al. "Waste oyster shell as a kind of active filler to treat the combined wastewater at an estuary" **Journal of Environmental Sciences**. vol. 25, no.10, 2013. pp.2047-2055.

[92] Yoon H. et al. "Oyster shell as substitute for aggregate in mortar" **waste management and research**. vol. 22, no.3, 2004. pp.158-170.

[93] Yang E.I., Yi S.T. and Leem Y.M. "Effect of oyster shell substituted for fine aggregate on concrete characteristics: Part I. Fundamental properties" **Cement and Concrete Research.** vol. 35, no.11, 2005. pp.2175-2182.

[94] Erni S., Gagoek H. and Purwanto K. "Green concrete made of oyster shell waste to support green building material" **Jurnal Teknologi (Sciences & Engineering)**. vol. 78, no.5, 2016. pp.203-207.

[95] Yoon G.L. et al. "Chemical-mechanical characteristics of crushed oyster-shell" **Waste Management**. vol. 23, no.9, 2003. pp.825-834.

[96] Shin W.S., Kang K. and Kim Y.K. “Adsorption Characteristics of Multi-Metal Ions by Red Mud, Zeolite, Limestone, and Oyster Shell” **Environmental Engineering Research**. vol. 19, no.2, 2014. pp.15-22.

[97] วงศ์พร้อมรัตน์ วิจิตรา และ สุวรรณประภา ชัชพล. “**การดูดซับอิออนของโลหะหนักในน้ำเสียโดยตัวดูดซับจากเปลือกหอยนางรม**” วิทยานิพนธ์วิศวกรรมศาสตรบัณฑิต สาขาวิชาวิศวกรรมเคมี, สถาบันเทคโนโลยีพระจอมเกล้าเจ้าคุณทหารลาดกระบัง. 2552.

[98] Tsai H.C., Lo S.L. and Kuo J. “Using pretreated waste oyster and clam shells and microwave hydrothermal treatment to recover boron from concentrated wastewater” **Bioresource Technology**. vol. 102, no.17, 2011. pp.7802-7806.

[99] Hsu T.C. “Experimental assessment of adsorption of Cu^{2+} and Ni^{2+} from aqueous solution by oyster shell powder” **Journal of Hazardous Materials**. vol. 171, no.1-3, 2009. pp.995-1000.

[100] สุธากุลวิรัฐ ชัชนันท์, วัฒนาศรีสกุล ชุติศรณ์ และ สบายใจ นภาดาว. “**การศึกษาจลนพลศาสตร์ของการดูดซับโลหะแคดเมียมในน้ำเสียโดยใช้ตัวดูดซับที่สังเคราะห์จากเปลือกหอยนางรม**” วิทยานิพนธ์วิศวกรรมศาสตรบัณฑิต สาขาวิชาวิศวกรรมเคมี, สถาบันเทคโนโลยีพระจอมเกล้าเจ้าคุณทหารลาดกระบัง. 2554.

[101] เพิ่มพงศาเจริญ นนทชัย, พลนวน ปวีณา และ คุณานิธ วิทวัส. “**การศึกษาการดูดซับโลหะหนักโดยใช้ตัวดูดซับที่สังเคราะห์จากเปลือกหอยนางรม**” วิทยานิพนธ์วิศวกรรมศาสตรบัณฑิต สาขาวิชาวิศวกรรมเคมี, สถาบันเทคโนโลยีพระจอมเกล้าเจ้าคุณทหารลาดกระบัง. 2553.

[102] Woo S.M. and Lee T.H. “The engineering properties of rice-hull-ash as a soil stabilizer” **Journal of the Chinese Institute of Engineers**. vol. 1, 1978. pp.87-95.

[103] Hwang C.L., Huynh T.P. and Risdianto Y. “An application of blended fly ash and residual rice husk ash for producing green building bricks” **Journal of the Chinese Institute of Engineers**. vol. 39, 2016 pp. 850-858.

[104] Della V.P., Kuhn I. and Hotza D. “Rice husk ash as an alternate source for active silica production” **Materials Letters**. vol. 57, 2002. pp.818-821.

[105] Onojah A.D., Agbendeh N.A. and Mbakaan C. “Rice husk ash refractory: the temperature dependent crystalline phase aspects” **International Journal of Recent Research and Applied Studies.** vol. 15, no.2, 2013 pp.246-248.

[106] Balapour M., Ramezanianpour A. and Hajibandeh E. “An investigation on mechanical and durability properties of mortars containing nano and micro RHA” **Construction and Building Materials**. vol. 132, 2017. pp.470-477.

[107] Ugheoke I.B. and Mamat O. “A critical assessment and new research directions of rice husk silica processing methods and properties” **Maejo International Journal of Science and Technology.** vol. 6, no.3, 2012. pp.430-448.

[108] Haslinawati M.M. et al. “Effect of Temperature on Ceramic from Rice Husk Ash” **International Journal of Basic & Applied Sciences.** vol. 9, no.9, 2009. pp. 22-25.

[109] Jamil M. et al. “Pozzolanic contribution of rice husk ash in cementitious system” **Construction and Building Materials.** vol. 47, 2013. pp.588-593.

[110] El-Dakroury A. and Gasser M.S. “Rice husk ash (RHA) as cement admixture for immobilization of liquid radioactive waste at different temperatures” **Journal of Nuclear Materials.** vol. 381, no.3, 2008. pp.271-277.

[111] Park K.B., Kwon S.J. and Wang X.Y. “Analysis of the effects of rice husk ash on the hydration of cementitious materials” **Construction and Building Materials**. vol. 105, 2016. pp.196-205.

[112] Muley S., Nandgude T. andPoddar S. “Extrusion–spheronization a promising pelletization technique: In-depth review” **Asian Journal of Pharmaceutical Sciences**. vol. 11, no.6, 2016. pp.684-699.

[113] Ahir A.A. et al. “Pelletization Technology: Methods and Applications -A Review” **Research Journal of Pharmacy and Technology**. vol. 8, no.2, 2015. pp.131-138.

[114.] Hirjau M. et al. “Pelletization techniques used in pharmaceutical fields” **Practica Farmaceutică.** vol. 4, no.3, 2011. pp.206-211.

[115] โฆษวิทิตกุล นงภัส. “**คู่มือข้อมูลเครื่องมือวิเคราะห์ชั้นสูง ศูนย์เครื่องมือวิทยาศาสตร์และเทคโนโลยีมหาวิทยาลัยเทคโนโลยีสุรนารี**” [Online] Available : http://www.google.co.th/url?sa=t&rct=j&q=&esrc=s&source=web&cd=9&cad=rja&uact=8&ved=0CFwQFjAI&url=http%3A%2F%2Fcste.sut.ac.th%2F2014%2F%3Fdl_id%3D55&ei=xVpuU6LyPMarkAWD0oHoAQ&usg=AFQjCNHHClMns-kwWMlKCLUajTKuqq_nrA. 2555.

[116] เห็นประเสริฐแท้ ศุภฤกษ์. “ทำไมต้องมีเทคนิคการเลี้ยวเบนของรังสีเอ็กซ์” **MTEC**. 2555. pp.12-18.

[117] Bunaciu A.A., Udristioiu E.G. and Aboul-Enein H.Y. “X-Ray Diffraction: Instrumentation and Applications” **Critical Reviews in Analytical Chemistry.** vol. 45, 2015. pp.289-299.

[118] Cambridge Univerity. “Powder diffraction” [Online] Available : https://www.doitpoms.ac.uk/tlplib/xray-diffraction/powder.php. 2018.

[119] Liao Y. “Bragg Condition/Law/Bragg Scattering/Bragg angle” [Online] Available : http://www.globalsino.com/EM/page3882.html. 2018.

[120] Baghaw H. “**Scanning Electron Microscopy.**” [Slide]. Ireland : Centre for microscopy and analysis (CMA). 2012.

[121] JEOL Service advanced technology. "SEM - Scanning Electron Microscope A to Z- basic knowledge for using the SEM." [Slide]. Japan : JEOL Service advanced technology.

[122] Preocanin T. and Kallay N. "Application of >>Mass Titration <<to Determination of Surface Charge of Metal Oxides" **CROATICA CHEMICA ACTA**. vol. 71, no.4, 1998. pp.1117-1125.

[123] Cardenas-Pena A.M., Ibanez J.G. and Vasquez-Medrano R. "Determination of the Point of Zero Charge for Electrocoagulation Principites from an Iron Anode" **International Journal of Electrochemical Science**. vol. 7, 2012. pp.6142-6153.

[124] Foo K.Y. and Hameed B.H. "Textural porosity, surface chemistry and adsorptive properties of durian shell derived activated carbon prepared by microwave assisted NaOH activation" **Chemical Engineering Journal.** vol. 187, 2012. pp.53-62.

[125] Hassan A.F., Abdel-Mohsen A.M. andElhadidy H. "Adsorption of arsenic by activated carbon, calcium alginate and their composite beads" **International Journal of Biological Macromolecules**. vol. 68, 2014. pp.125-130.

[126] Kwok K.C.M. et al. "Mechanism of arsenic removal using chitosan and nanochitosan" **Journal of Colloid and Interface Science**. vol. 416, 2014. pp.1-10.

[127] Sherren A.T. "**The 2001 Edition of Laboratory Directions for Analytical Chemistry I**." [Online] Available : http://atsherren.faculty.noctrl.edu/chm 210 /preface.htm. 2018.

[128] Husain A. "Pharmaceutical Analysis: Oxidation Reduction Titrations" [e-book] Pharmacy e-Book. 2017.

[129] ทรงศิริกุล อานนท์. “**ผลกระทบจากน้ำท่วมต่อการตกค้างของสารหนูในบ่อน้ำผิวดิน ที่อำเภอร่อนพิบูลย์ จังหวัดนครศรีธรรมราช ภาคใต้ของประเทศไทย**” วิทยานิพนธ์วิทยาศาสตรมหาบัณฑิต สาขาเทคโนโลยีบริหารสิ่งแวดล้อม บัณฑิตวิทยาลัย มหาวิทยาลัยมหิดล. 2537.

[130] ภักดีพิน พีรดา “**การหาอัตราส่วนรูปลักษณ์ของสารหนู As(III) ต่อ As(V) ในน้ำ**” วิทยานิพนธ์วิทยาศาสตรมหาบัณฑิต สาขาวิชาเคมี มหาวิทยาลัยวลัยลักษณ์. 2548.

[131] Yang J.S., Kwon M.J., Park Y.T. and Choi J. “Adsorption of Arsenic from Aqueous Solutions by Iron Oxide Coated Sand Fabricated with Acid Mine Drainage” **Separation Science and Technology.** vol. 50, 2015 pp. 267-275.

[132] Manju G.N., Raji C. and Anirudhan T.S. “Evaluation of coconut husk carbon for the removal of arsenic from water” **Water Research**. vol. 32, 1998 pp. 3062-3070.

[133] Rajapaksha A.U. et al. “Natural Red Earth as a low cost material for arsenic removal: Kinetics and the effect of competing ions” **Applied Geochemistry**. vol. 26, no.4, 2011. pp.648-654.

[134] Xing R. et al. “Comparison of antifungal activities of scallop shell, oyster shell and their pyrolyzed products” **Egyptian Journal of Aquatic Research**. vol. 39, 2013. pp. 83-90.

[135] Islam M. and Patel R.K. “Evaluation of removal efficiency of fluoride from aqueous solution using quick lime” **Journal of Hazardous Materials**. vol. 143, no.1-2, 2007. pp.303-310.

[136] Moon D.H., Dermatas D. and Menounou N. “Arsenic immobilization by calcium-arsenic precipitates in lime treated soils” **Science of The Total Environment** vol. 330, no.1-3, 2004. pp.171-185.

[137] Dutre´ V. and Vandecasteele C. "Solidification/stabilization of arsenic-contaminated waste: leach tests and behaviour of arsenic in the leachate" **Waste Management.** vol. 15, no.4, 1995. pp. 55-62.

[138] Dutre´ V. and Vandecasteele C. "Immobilization Mechanism of Arsenic in Waste Solidified Using Cement and Lime" **Environmental Science Technology**. vol. 32, 1998. pp.2782-2787.

[139] Phenrat T., Marhaba T.F. and Rachakornkij M. "A SEM and X-ray study for investigation of solidified/stabilized arsenic- iron hydroxide sludge" **Journal of Hazardous Materials**. vol. 118, no.1-3, 2005. pp.185-195.

[140] Yu X. et al. "Synthesis and characterization of multi-amino-functionalized cellulose for arsenic adsorption" **Carbohydrate Polymers**. vol. 92, no.1, 2013. pp.380-387.

[141] Yang G., Liu Y. and Song S. "Competitive adsorption of As(V) with co-existing ions on porous hematite in aqueous solutions" **Journal of Environment Chemical Engineering**. vol. 3, 2015. pp.1497-1503.

[142] Guan X. et al. "Removal of arsenic from water: Effects of competing anions on As(III) removal in KMnO4-Fe(II) process" Water Research. vol. 43, no.15, 2009. pp.3891-3899.

[143] Meng X., Bang S. and Korfiatis G.P. "Effects of silicate, sulfate, and carbonate on arsenic removal by ferric chloride" **Water Research**. vol. 34, no.4, 2000. pp.1255-1261. [138] Park C.M. et al. "Influence of solution pH, ionic strength, and humic acid on cadmium adsorption onto activated biochar: Experiment and modeling" **Journal of Industrial and Engineering Chemistry**. vol. 48, 2017. pp.186-193.

[144] Park C.M. et al. "Influence of solution pH, ionic strength, and humic acid on cadmium adsorption onto activated biochar: Experiment and modeling" **Journal of Industrial and Engineering Chemistry**. vol. 48, 2017. pp.186-193.

[145] Das D.P., Das J. and Parida K. "Physicochemical characterization and adsorption behavior of calcined Zn/Al hydrotalcite-like compound (HTlc) towards removal of fluoride from aqueous solution" **Journal of Colloid and Interface Science**. vol. 216, no.2, 2003. pp.213-220.

[146] Wan D. et al. "Adsorption of nitrate and nitrite from aqueous solution onto calcined (Mg-Al) hydrotalcite of different Mg/Al ratio" **Chemical Engineering Journal**. vol. 195-196, 2012. pp.241-247.

[147] Ferreira O.P. et al. "Evaluation of boron removal from water by hydrotalcite-like compounds" **Chemosphere**. vol. 62, no.1, 2006. pp.80-88.

[148] Yu Y., Wu R. and Clark M. "Phosphate removal by hydrothermally modified fumed silica and pulverized oyster shell" **Journal of Colloid and Interface Science**. vol. 350, no.2, 2010. pp. 538-543.

[149] Tobermorite. Available : https://en.wikipedia.org/wiki/Tobermorite. 2017

[150] Alavéz-Ramírez R. et al. "The use of sugarcane bagasse ash and lime to improve the durability and mechanical properties of compacted soil blocks" **Construction and Building Materials**. vol. 34, 2012. pp.296-305.

[151] United states environment protection agency (EPA). "**Method 352.1: Nitrogen, Nitrate (Colorimetric, Brucine) by Spectrophotometer.**" [Online]. Available : https://www.epa.gov/. 2018.

[152] United states environment protection agency (EPA). "**Method 9038: Sulfate (Turbidimetric)**" [Online]. Available : https://www.epa.gov/. 2018.

[153] United states environment protection agency (EPA). "**Method 365.3: Phosphorous, All Forms (Colorimetric, Ascorbic Acid, Two Reagent)**" [Online]. Available : https://www.epa.gov/. 2018.

[154] Doolittle P. "Ascorbic acid method for phosphorus determination" [Online]. Available: http://community.asdlib.org/activelearningmaterials/files/2014/06/Lake_Study_Ascorbic_Acid_Method_for_Determining_Phosphorous.pdf. 2014. 2018

[155] American Public Health Asscociation (APHA), American Water Works Association (AWWA), Water Environment Federation (WEF). **Standard Methods for the Examination of Water and Wastewater 20th ed.** American Public Health Asscociation. 1998.

[156] Atesok G., Somasundaran P. and Morgan L.J. "Adsorption properties of Ca^{2+} on Na-kaolinite and its effect on flocculation using polyacrylamides" **Colloids and Surfaces**. vol. 32, 1988. pp.127-138.

[157] Zhang F.S. and Itoh H. "Iron oxide-loaded slag for arsenic removal from aqueous system" **Chemosphere.** vol. 60, no.3, 2005. pp.319-325.

[158] Phenrat T., Marhaba T.F. and Rachakornkij M. "A SEM and X-ray study for investigation of solidified/stabilized arsenic-iron hydroxide sludge" **Journal of Hazardous Materials**. vol. 118, no.1-3, 2005. pp.185-195.

[159] Wikipedia, "**Sodium hydroxide**." [Online] Available : https://en.wikipedia.org/wiki/Sodium_hydroxide. 2018.

[160] Centers for Disease Control and Prevention. "**Sodium hydroxide**" [Slide] USA : The National Institute for Occupation Safety and Health (NIOSH). 2016.

[161] Meng X. et al. "Combined effects of anions on arsenic removal by iron hydroxides" **Toxicology Letters**. vol. 133, no.1, 2002. pp.103-111.

[162] Caporale A.G. et al. “Effect of particle size of drinking-water treatment residuals on the sorption of arsenic in the presence of competing ions” **Journal of Hazardous Materials**. vol. 260, 2013. pp.644-651.

[163] Roobottom H.K. et al. “Thermochemical Radii of Complex Ions” **Journal of Chemical Education**. vol. 76, no.11, 1999. pp.1570-1573.

[164] Wikipedia. “Arsenous acid.” [Online] Available : https://en.wikipedia.org/wiki/Arsenous_acid. 2018.

[165] Wikipedia. “Arsenic acid.” [Online] Available : https://en.wikipedia.org/wiki/Arsenic_acid. 2018

[166] Huang J.H. “Impact of competitive adsorption on microbial arsenate reduction at the water-goethite interface” **Applied Geochemistry**. vol. 88, 2018. pp.59-67.

[167] Jian M. et al. “Adsorptive removal of arsenic from aqueous solution by zeolitic imidazolate framework-8 (ZIF-8) nanoparticles” **Colloids and Surfaces A: Physicochemical and Engineering Aspects**. vol. 465, 2015. pp.67-76.

[168] Igoscience. “Printable Periodic Table of Elements – Atomic Radius” [Online] Available : http://igoscience.com/printable-periodic-table-of-elements-atomic-radius/. 2015.

[169] Hager I. “Behaviour of cement concrete at high temperature” **BULLETIN OF THE POLISH ACADEMY OF SCIENCES TECHNICAL SCIENCES**. vol. 61, no.1, 2013. pp.1454-154.

[170] Rodriguez E.T. et al. “Thermal stability of C-S-H phases and applicability of Richardson and Groves' and Richardson C-(A)-S-H(I) models to synthetic C-S-H” **Cement and Concrete Research.** vol. 93, 2017. pp.45-56.

[171] Moon D.H., Dermatas D. and Menounou N. "Arsenic immobilization by calcium–arsenic precipitates in lime treated soils" **Science of the Total Environment**. vol. 330, 2004. pp.171-185.

[172] Ho Y.S. and McKay G. "Pseudo-second order model for sorption processes" **Process Biochemistry**. vol. 34, 1999. pp.451-465.

[173] Yu P. et al. "Structure of Calcium Silicate Hydrate (C-S-H): Near-, Mid-, and Far-Infrared Spectroscopy" **Journal of the American Ceramic Society**. vol. 82, no.3, 1999. pp.742-748.

[174] Dai W., Shui Z.H. and Duan P. "Study on the Structural Model of Calcium Silicate Hydrate based on Computer Simulation" **International Conference on Computer Technology and Science (ICCTS2012).** vol. 47, 2012. pp.1-5

[175] Cui J. et al. "A new process of continuous three-stage co-precipitation of arsenic with ferrous iron and lime" **Hydrometallurgy**. vol. 146, 2014. pp.169-174.

[176] Du Y. et al. "A novel strategy for arsenic removal from dirty acid wastewater via $CaCO_3$-$Ca(OH)_2$-Fe(III) processing" **Journal of Water Process Engineering**. vol. 12, 2016. pp.41-46.

[177] De Klerk R.J. et al. "Continuous circuit coprecipitation of arsenic(V) with ferric iron by lime neutralization: Process parameter effects on arsenic removal and precipitate quality" **Hydrometallurgy.** vol. 111-112, 2012. pp.65-72.

[178] Maji S.K. et al. "Implementation of the adsorbent iron-oxide-coated natural rock (IOCNR) on synthetic As(III) and on real arsenic-bearing sample with filter" **Applied Surface Science**. vol. 284, 2013. pp.40-48.

[179] Mar K.K. et al. “Comparison of Arsenic Adsorption on Lignite, Bentonite, Shale, and Iron Sand from Indonesia” **Procedia Earth and Planetary Science**. vol. 6, 2013. pp.242-250.

[180] Li W.G. et al. “Adsorption characteristics of arsenic from micro-polluted water by an innovative coal-based mesoporous activated carbon” **Bioresource Technology**. vol. 165, 2014. pp.166-173.

[181] Nashine A.L. and Tembhurkar A.R. “Equilibrium, kinetic and thermodynamic studies for adsorption of As(III) on coconut (Cocos nucifera L.) fiber” **Journal of Environmental Chemical Engineering**. vol. 4, 2016. pp.3267–3273.

[182] Uppal H. et al. “Zinc peroxide functionalized synthetic graphite: An economical and efficient adsorbent for adsorption of arsenic (III) and (V)” **Journal of Environmental Chemical Engineering.** vol. 4, 2016. pp.2964-2975.

[183] Ahmad H.B. et al. “Synthesis of some novel adsorbents for antimicrobial activity and removal of arsenic from drinking water” **Korean Journal of Chemical Engineering.** vol. 32, no.4, 2015. pp.661-666.

[184] Choi W.H., Lee S.R. and Park J.Y. “Cement based solidification/stabilization of arsenic-contaminated mine tailings” **Waste Management**. vol. 29, no.5, 2009. pp.1766-1771.

Appendix

Appendix A

Calibration curves of As(III) and anions

Calibration curves

In this work, the concentrations of As(III), NO_3^- , SO_4^{2-} and HPO_4^{2-} remaining in solution were analyzed by redox titration with $KMnO_4$, Brucine method, Turbidimetric method and Colorimetric & Ascorbic acid method, respectively. The concentration of $KMnO_4$, NO_3^- , SO_4^{2-} and HPO_4^{2-} were determined by using UV-spectrophotometer with wavelength of 520 nm, 420 nm, 420 nm and 880 nm, respectively. The calibration curves of $KMnO_4$, NO_3^- , SO_4^{2-} and HPO_4^{2-} are presented in Figures A-1 to A-4.

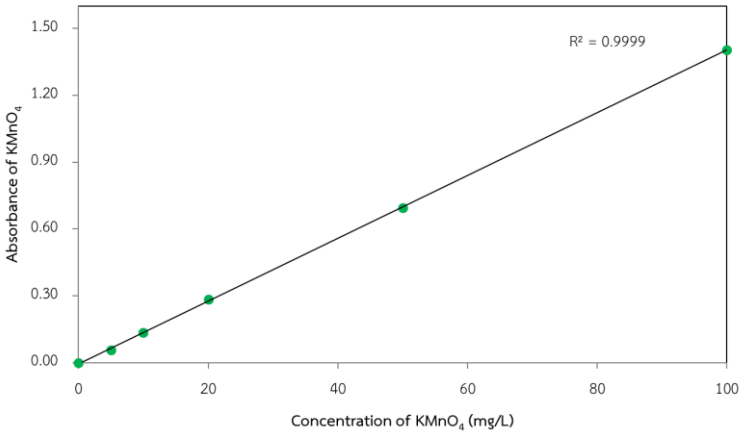

Figure A-1 Calibration curve of $KMnO_4$.

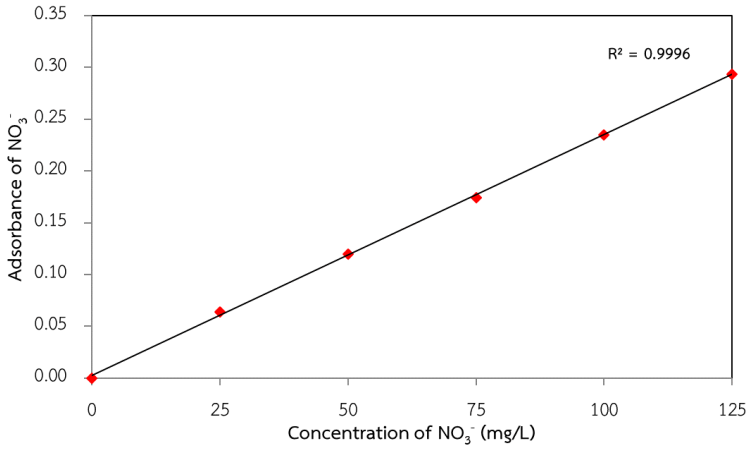

Figure A-2 Calibration curve of NO_3^-.

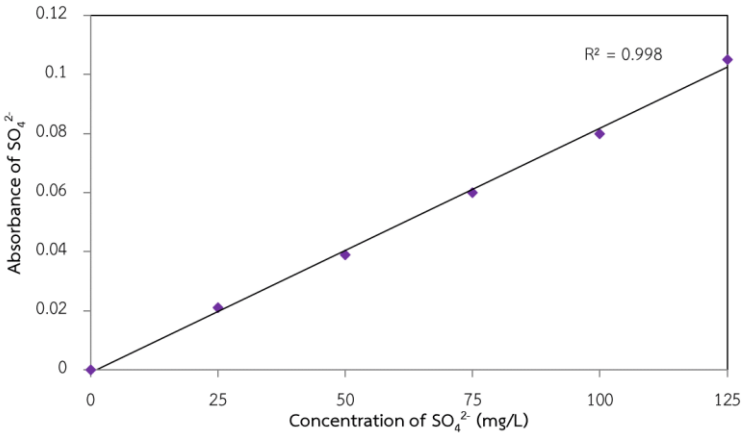

Figure A-3 Calibration curve of SO_4^{2-}.

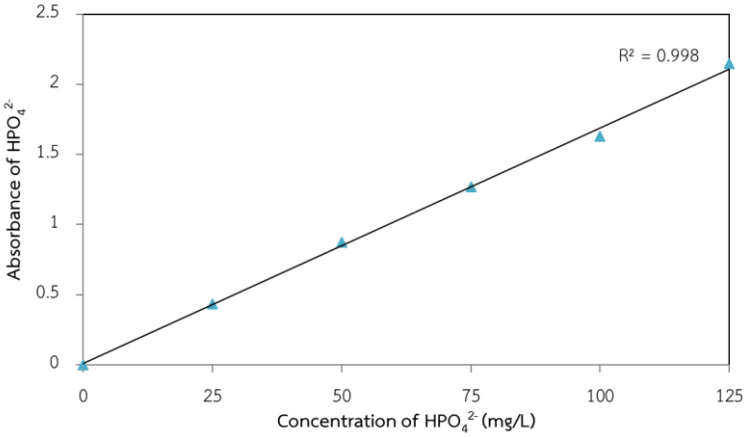

Figure A-4 Calibration curve of HPO_4^{2-}.

Appendix B

Experimental data of As(III) and anions individual adsorption on COS

Experimental data of As(III) and anions individually adsorption on COS

The experimental data of As(III) and anions individually removal by using OS is presented in Table B-1. It is noted that the amount of COS used in each case is approximately 1 g.

Table B-1 Experimental data of As(III) and anions individually removal by COS.

Anions	Initial concentration (mg/L)	Final concentration (mg/L)	Precipitation (mg/L)	Adsorption (mg/L)	Adsorption capacity (mg/g)
As(III)	1016.00	13.00	0.00	1003.00	345.09
NO_3^-	1195.58	871.60	0.00	323.98	111.71
SO_4^{2-}	1076.92	817.31	0.00	259.62	89.24
HPO_4^{2-}	1775.56	208.14	579.41	988.01	378.40

Appendix C

Experimental data of As(III) and anions desorption

Experimental data of As(III) and anions desorption

The experimental data of As(III) and anions in desorption test is shown in Table C-1. It is note that, the adsorption process of As(II) and anions was in the period of initial time - 1440 min while the desorption process of those anions was in the period of 1440 min - 1860 min.

Table C-1 Concentrations of As(III) and anions.

	Concentration of anion			
time	As(III) (mg/L)	NO_3^- (mg/L)	SO_4^{2-} (mg/L)	HPO_4^{2-} (mg/L)
0	111.54	102.04	113.46	95.86
1440	72.79	32.63	98.91	9.21
1860	73.55	25.72	86.96	10.49

Appendix D

Publications

Separation Science and Technology

ISSN: 0149-6395 (Print) 1520-5754 (Online) Journal homepage: https://www.tandfonline.com/loi/lsst20

As(III) removal under the presence of competitive anions using the calcined ground oyster shell as the adsorbent

P. Khownpurk & W. Chandra-Ambhorn

To cite this article: P. Khownpurk & W. Chandra-Ambhorn (2019): As(III) removal under the presence of competitive anions using the calcined ground oyster shell as the adsorbent, Separation Science and Technology, DOI: 10.1080/01496395.2019.1577269

To link to this article: https://doi.org/10.1080/01496395.2019.1577269

SEPARATION SCIENCE AND TECHNOLOGY
https://doi.org/10.1080/01496395.2019.1577269

Taylor & Francis
Taylor & Francis Group

As(III) removal under the presence of competitive anions using the calcined ground oyster shell as the adsorbent

P. Khownpurk and W. Chandra-Ambhorn

Department of Chemical Engineering, Faculty of Engineering, King Mongkut's Institute of Technology Ladkrabang, Ladkrabang, Thailand

ABSTRACT

The calcined ground oyster shell was used as the adsorbent to remove As(III) from contaminated water under the presence of anions. The solubility and precipitation tests indicated that As(III), NO_3^-, and SO_4^{2-} were removed by adsorption process whereas HPO_4^{2-} was removed by precipitation and adsorption processes. The adsorption results showed that, in bi-solutes, HPO_4^{2-} strongly interfered with As(III) removal. In the case of tri- and tetra-solutes, the adsorption performances of As(III) and anions depended on (1) the binding affinity between the sorption sites and adsorbates, (2) observed adsorption rate constant of adsorbates, (3) electrostatic interaction, and (4) adsorbates interaction.

ARTICLE HISTORY
Received 9 May 2018
Accepted 2 January 2019

KEYWORDS
Arsenic removal; adsorption; adsorption kinetics; competitive anion; calcined ground oyster shell

Introduction

Arsenic contamination in ground water is an environmental problem affecting people health in many areas around the world as it can cause many types of cancers, pigmentation change, neurological disorders, muscular weakness, etc. for long-term intake.[1,2] The WHO has set the guideline of the maximum drinking standard as 10 μg/L. There are many countries, for example, Bangladesh, India, China, Western US, Vietnam, Thailand, etc., reported the contamination of arsenic above the WHO standard limit.[2–7] Arsenic usually contaminates in the natural water in trivalent form (As(III)) and pentavalent form (As(V)). The toxicity and mobility of As(III) are more than that of As(V).[7,8] Many industries such as copper extraction and refinery and agriculture pesticide used As_2O_3 in their processes.[9,10] Therefore, As(III) should be the major form of arsenic in contaminated water. As(III) is more difficult to remove than As(V). In some processes, As(III) was pretreated by oxidizing into As(V) before removal by coprecipitation or adsorption.[11,12] Due to the high toxicity and the removal difficulty, As(III) contaminated in water is the critical issue that needs to be focused.

Adsorption is the promising technique that has the advantages of high efficiency, low cost, simplicity, and usability for both As(III) and As(V) removals.[6,8,13–15] Many kinds of adsorbent from synthetic materials like iron oxide-coated sand,[16] iron (III) hydroxide-loaded coral limestone,[17] activated carbons,[1,18] carbon black,[5] zeolitic imidazolate framework-8 (ZIF-8),[19] ZIF-8 nanoparticles,[20] or from low cost materials, such as orange juice residue,[21] soils,[14] clays,[1] and minerals[7,8] have been applied to remove arsenic.

Plenty of tons per year of waste oyster shells are produced around the world. Some researchers have investigated the capability to use the waste oyster shells both in the forms of raw oyster shell powder and calcined oyster shell powder as adsorbents to remove heavy metals, such as boron, cadmium, copper, and nickel.[22–24] In the previous work, As(III) adsorbent was prepared by calcination of oyster shells powder at 700°C in air for 8 h and called calcined ground oyster shell(COS). The COS could remove As(III) from aqueous solution with maximum capacity of 195.5 mg/g (pH 11).[25] However, in water resources, the soluble ions contained in water, such as sulfate (SO_4^{2-}), bicarbonate (HCO_3^-), carbonate ($CaCO_3$), chloride (Cl_2), nitrate (NO_3^-), phosphate (PO_4^{3-}), etc. may affect As(III) removal performance.[26–28] The interference of competitive ions on arsenic removal performance depends on (1) the nature of the adsorbent and adsorbate. If sorption sites of adsorbent have capability to adsorb competitive ions greater than arsenic, those competitive ions can strongly interfere arsenic removal performance as the results of Bang *et al.*[29] and Bang *et al.*[30] works. Their results showed that silicate and PO_4^{3-} strongly interfered with arsenic removal by iron

CONTACT W. Chandra-ambhorn walairat.ch@kmitl.ac.th Department of Chemical Engineering, Faculty of Engineering, King Mongkut's Institute of Technology Ladkrabang, Ladkrabang, Bangkok 10520, Thailand

Color versions of one or more of the figures in the article can be found online at www.tandfonline.com/lsst.

hydroxide but it was insignificantly interfered with arsenic removal by TiO_2 at neutral pH. (2) pH of solution during the adsorption process. The change of pH of solution could affect species of adsorbates and surface charge of adsorbents. For oxide and hydroxide materials, the surface of the adsorbent could be ionized by protonation or deprotonation.[31–35] Park *et al.*[36] who studied Cd(II) removal from aqueous solution by activated biochar (torrefied loblolly pine) reported that Cd(II) adsorption performance increased with increasing pH (from pH 3 to 8) because of the electrostatic attraction between Cd^{2+} which was the main form of Cd(II) at this pH range and the negative surface charge of activated biochar. Furthermore, the tendency of multicharge anions could adsorb on the positive adsorbent surface greater than the monovalent anion.[37–39] Das *et al.*[37] studied the adsorption of fluoride by calcined Zn/Al hydrotalcite-like compound, a super abundant positive surface charge. They found that the decrease in percentage of fluoride adsorption under the presence of PO_4^{3-} was greater than that of SO_4^{2-} because charge density of PO_4^{3-} was greater. Furthermore, Lui *et al.*[19] studied the adsorption of arsenic and antimony (Sb(V)) by ZIF-8 in single-solute and bi-solutes and reported that at pH lower than 9.5, the adsorption capacity of As(III) decreased when As(III) combined with Sb(V) because the charge density of Sb(V) in the form of $Sb(OH)_6^-$ was greater than that of As(III) in the form of H_3AsO_3. However, the effect of Sb(V) on As(III) adsorption performance declined with the elevated pH because the positive charge of the adsorbent decreased with the increase of pH.

In this work, oyster shells were used as a starting material for CaO-rich adsorbent preparation. The abilities to adsorb As(III) and some competitive anions, such as NO_3^-, SO_4^{2-}, and hydrogen phosphate (HPO_4^{2-}) using this adsorbent were investigated individually. The removals of As(III) under the presence of anion(s) were also studied in order to observe the effect of competitive anions on the removal efficiency of As(III). The observed adsorption rate constants were estimated and the adsorption mechanism was proposed.

Materials and methods

Chemicals and materials

All chemicals were analytical grade and all solutions were prepared with distilled water. The 1000 mg/L stock solutions of As(III), NO_3^-, SO_4^{2-}, and HPO_4^{2-} were prepared from As_2O_3 (Ajax Finechem), $NaNO_3$ (CARLO ERBA), Na_2SO_4 (CARLO ERBA), and Na_2HPO_4 (CARLO ERBA), respectively. Furthermore, the pH adjusters were prepared from NaOH (Ajax Finechem) and HCl (Qrec).

The preparation and characterization of COS

COS was prepared from oyster shells collected from some restaurants in Chanthaburi province, Thailand. The oyster shells were washed and scrubbed until the dirtiness was removed and then ground and sieved. The 150–250 μm oyster shell powder was calcined at 700°C in air for 8 h before being kept in a desiccator.

The chemical composition of COS was evaluated using XRF (Philips model PW2400, Philip, Japan). The XRD technique (XRD 6100, SHIMADZU, Japan) was also used to characterize oyster shell powder, COS, and soaked COS. The surface area of the oyster shell powder and COS were measured using Brunauer–Emmett–Teller (BET) nitrogen gas sorption method (Belsorp max model, BEL, Japan). The morphology of COS was observed by using a scanning electron microscope (SEM, Carl Zeiss EVO®MA10, Germany).

COS solubility and precipitation tests

The solubility test of COS was performed by adding 1000 mL of distilled water into an Erlenmeyer flask covered with a rubber cork. The initial pH of distilled water was adjusted to be 11 using 0.1 M of NaOH or/and HCl. After that, 0.3 g of the COS was further added into the flask and stirred for 7 h. Finally, the mixture was filtrated through Whatman filter paper no. 1 in order to remove COS and pH of the filtrate was measured.

The precipitation test was carried out by adding As(III) stock solution into the filtrate with the volume ratio of 1:9 in order to obtain the 1000 mL of 100 mg/L As(III). After continuously stirred the solution for 7 h, the solution was filtered and then the pH of the filtrate and As(III) concentration were measured. The same procedure was performed with other anions: NO_3^-, SO_4^{2-}, and HPO_4^{2-}.

Adsorption experiments

Adsorption of As(III), NO_3^-, SO_4^{2-}, and HPO_4^{2-} ions was observed individually by batch tests. The As(III), NO_3^-, SO_4^{2-}, and HPO_4^{2-} stock solutions were separately added into Erlenmeyer flasks. Then, pH of the solution in each flask was adjusted to be 11 by using 0.1 M of NaOH and/or HCl. After that, COS was added and the solution was stirred for 24 h. The COSs were filtered out by Whatman filter paper no. 1 and the concentrations of As(III), NO_3^-, SO_4^{2-}, and HPO_4^{2-} were determined. The final pHs of solution were measured by a pH meter (Hanna instrument, HI 98107).

The effect of competitive anions on As(III) adsorption performance was also studied. The As(III) and anions stocks solutions were mixed and diluted with distilled water in order to obtain the initial concentration

of each ion in the solutions as 100 mg/L. Then, pH of the initial solution was adjusted to 11 using 0.1 M of NaOH and/or HCl. After that, 0.3 g of COS was added into the solution. During agitation, samples were taken at appropriate time intervals. The concentrations of As(III), the other competitive anions in the samples were analyzed. The final pHs of solution were measured by a pH meter (Hanna instrument, HI 98107). The adsorption capacity of As(III) and anions were calculated as in Equation (1):

$$\mathrm{As(III)oranionremovalcapacity}(q_t) = \frac{(C_0 - C_e)V}{W} \quad (1)$$

where C_0 and C_e are the concentrations of As(III) or anion at initial and at equilibrium (mg/L), respectively while V is the volume of solution (L) and W is the mass of the material used in the As(III) or anion removal test (g).

Moreover, the adsorption kinetics of As(III) and anions were also studied. To determine the observed adsorption rate constants of As(III) and anions, the following assumptions were set: (1) As(III) and anions adsorbed on the sorption sites as monolayer; (2) the sorption sites of the adsorbent were uniform; (3) there were no interactions between adsorbates; (4) the molecules of As(III) or anions in the bulk solution did not displace the molecules that occupied on the sorption sites; (5) the number of active sites on COS was assumed to be equivalent to the maximum adsorption capacity of COS in As(III) combined with NO_3^-, SO_4^{2-}, and HPO_4^{2-} adsorption test (838.21 mg/g); (6) desorption rates of As(III) and anions were negligible comparing with adsorption rate. Adsorption rate equations were derived as in Equations (2)–(4):

$$\frac{dC_A}{dt} = k_{ad,A}C_A(1 - \theta_A - \theta_B) \quad (2)$$

$$\frac{dC_A}{dt} = k_{ad,A}C_A(1 - \theta_A - \theta_B - \theta_c) \quad (3)$$

$$\frac{dC_A}{dt} = k_{ad,A}C_A(1 - \theta_A - \theta_B - \theta_C - \theta_D) \quad (4)$$

where $k_{ad,A}$ is observed adsorption rate constant of substance A (min^{-1}) and θ_A, θ_B, θ_C and θ_D are the fractions of sorption sites covered by substances A, B, C, and D, respectively.

Since the concentration of substance A in the bulk solution decreased by adsorption of substance A on the sorption sites of the adsorbent, therefore

$$C_A = C_{0,A} - \beta_A\theta_A \quad (5)$$

where $C_{0,A}$ is the initial concentration of substance A (mg/L) and β_A is a constant defined as in Equation (6):

$$\beta_A = \frac{M_c q_m}{MW_A V} \quad (6)$$

where M_c is mass of adsorbent (g), q_m is the maximum capacity of the adsorbent (mg/g), MW_A is molecular weight of substance A (g/mol), and V is volume of solution (L).

The observed adsorption rate constants were initially estimated by using the extended geometric method purposed by Azizian *et al.*[40,41] After that the values of As(III) and anion occupied sites (θ_A, θ_B, θ_C, and θ_D) in Equations (2)–(4) were solved by Runge–Kutta method[42,43] and compared with the experimental results. The observed adsorption rate constants were gradually adjusted until the values of As(III) and anion occupied sites were well fitted with the experimental data.

Analytical methods

The concentration of As(III) was analyzed by the titration with $KMnO_4$ while the concentrations of NO_3^-, SO_4^{2-}, and HPO_4^{2-} that remained in the samples were analyzed by Brucine method, Turbidimetric method, and Colorimetric and Ascorbic acid method, respectively. Furthermore, after the batch tests, some COSs were also analyzed by SEM (Carl Zeiss EVO®MA10)/EDX (Oxford Instrument X-Max20).

Results and discussion

COS characterization

According to XRF results, the calcination of ground oyster shell in air at 700°C for 8 h made the change of main composition of the ground oyster shell from $CaCO_3$ to be CaO with the percentage as much as 97%. The BET results are shown in Table 1.

It can be seen that the specific surface area of ground oyster shell increased by almost eight times after calcined which should be the consequence of the absence of CO_2 molecules. The BET analysis was also performed with the commercial grade CaO and the result shows that its specific surface area is comparable with COS. The specific surface area of COS is also compared with the specific surface areas of CaO-rich materials reported by Salameh and the coworkers[7] and Islam and Patel.[44] The results show that the specific surface area of COS is around two times greater than that of the dolomite charred at the same condition and also

Table 1. Physical properties of COS in comparison with the raw material and similar materials from other sources.

	Properties			
Material	Specific volume (cm^3(STP)/g)	Specific surface area (m^2/g)	Total pore volume (cm^3/g)	Mean pore diameter (nm)
Ground oyster shell	0.47	2.05	0.003	5.63
COS	3.63	15.80	0.018	4.67
Commercial grade calcium oxide	3.73	16.22	0.021	5.16
Charred dolomite[7]	–	7.31	–	–
Thermally treated quicklime[38]	–	11.75	–	–

greater than that of the quicklime thermally treated at 450°C for 4 h for almost 75%.

The SEM images of ground oyster shell, COS, and moist COS were also taken as illustrated in Fig. 1.

As observed from Fig. 1, COS and moist COS are more porous than the ground oyster shell caused by the absence of CO_2 from the structure during calcination. When comparing with moist COS, it can be observed that COS morphology looks similar but the surface of moist looks slightly rougher. This might be because when CaO contacts with water, it transforms into $Ca(OH)_2$.

COS solubility and precipitation tests

Since around 97% of COS is CaO, when it is in water, the chemical reaction occurs as in Reaction (7):

$$CaO + H_2O \rightarrow Ca(OH)_2 \quad (7)$$

Some of $Ca(OH)_2$ can dissolve in water. Therefore, the amount of dissolved $Ca(OH)_2$ was estimated based on the change of pH. According to the solubility test, pH of the solution changed from 11.0 to 11.6. This means that about 0.0835 g or 27.8% of COS became dissolve $Ca(OH)_2$.

To observe the occurrence of precipitation of the anions with dissolved $Ca(OH)_2$, precipitation tests were performed with each observed anion. The results showed that, for As(III), NO_3^-, and SO_4^{2-}, no precipitate was observed in the solution and there were no significant changes in pH and concentrations of these anions. This implies that precipitation between COS and As(III), NO_3^- and SO_4^{2-} should not occur and, therefore, these anion removals by COS via adsorption can reasonably be assumed. On the other hand, in the case of HPO_4^{2-}, the result showed that after adding HPO_4^{2-} solution into the filtrate, white precipitate was clearly observed and the concentration of HPO_4^{2-} decreased by 46.6%. This means that HPO_4^{2-} can be removed by COS via both precipitation and adsorption.

As(III) and competitive anions adsorption characteristics

In this section, the batch tests were performed to observe the anion removal abilities of COS. The initial pH 11 was chosen to be the condition of the experiments as it provided the highest removal percentage of As(III) and at this pH, As(III) absorbed was in the form of $H_2AsO_3^-$.[1,13,25] Figure 2 shows the adsorption capacities of COS with respect to $H_2AsO_3^-$, NO_3^-, SO_4^{2-}, and HPO_4^{2-} obtained from the batch tests. It is noted that the effect of precipitation was eliminated by using the precipitation data in the previous section.

The values in Fig. 2 represent the capability of non-dissolved COS to adsorb each anion. It can be seen that COS has the capability to adsorb HPO_4^{2-} more than $H_2AsO_3^-$ for about 10% while NO_3^- and SO_4^{2-} can be adsorbed by COS for less than three times of the amounts of $H_2AsO_3^-$ and HPO_4^{2-} adsorbed.

The morphologies of COS after the adsorption tests were also investigated via SEM images as shown in Fig. 3. It can be observed that the surfaces of COS after adsorbing these four anions were different. However, all four images illustrate the COS surfaces covered by each anion as the surfaces do not look as porous as the surface of fresh COS shown in Fig. 1(c). Comparing the morphologies of COS surfaces after adsorption

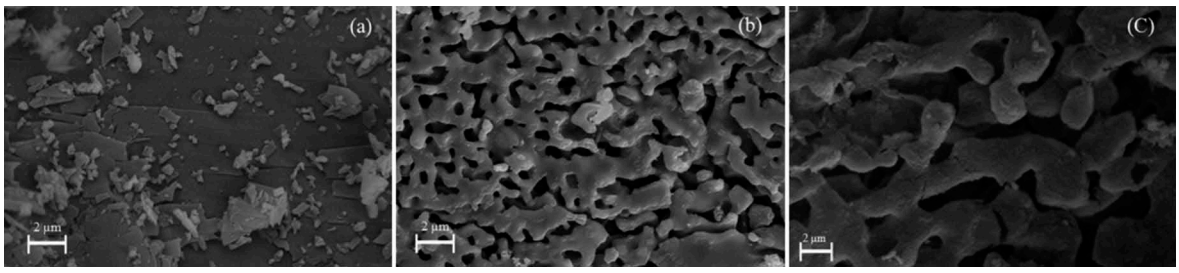

Figure 1. The SEM images of (a) ground oyster shell [25], (b) COS, and (c) moist COS.

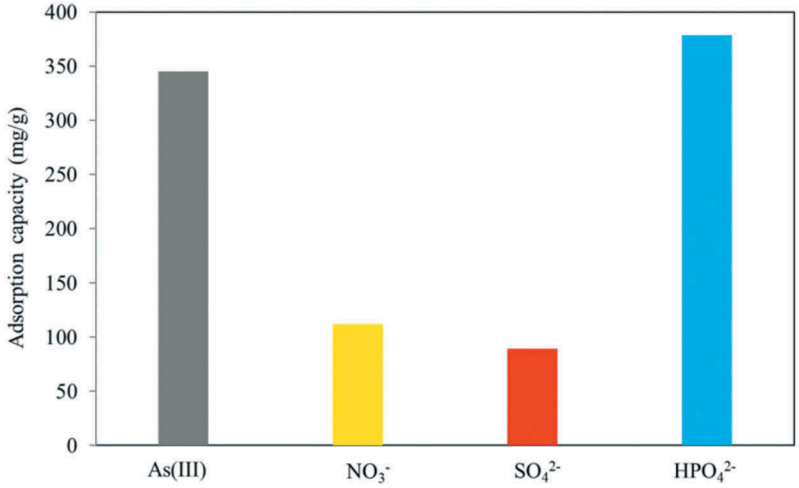

Figure 2. Adsorption capacity of COS corresponding to individual ions.

tests with the four observed anions, in Fig. 3a, it looks like the surfaces were covered by grass leaf – like matter when $H_2AsO_3^-$ adsorbed on the COS surface. This morphology looked similar to the morphology of arsenic immobilized on lime in the work of Phenrat *et al.*[45] who studied the iron–arsenic sludge immobilized by using cement and lime. Figure 3b, d corresponding to NO_3^- and HPO_4^{2-} adsorption tests shows the COS surfaces that look flaky while the COS surface after SO_4^{2-} adsorption appears to be covered by small grains.

As(III) and anions adsorption on the COS could be explained by Reactions (7)–(14).

$$Ca(OH)_2 \rightarrow Ca^{2+} + 2OH^- \quad (8)$$

$$Ca(OH)_2 + H_2AsO_3^- \rightarrow HCaAsO_3 + H_2O + OH^- \quad (9)$$

$$H_2AsO_3^- + OH^- \rightarrow HAsO_3^{2-} + H_2O \quad (10)$$

$$Ca(OH)_2 + HAsO_3^{2-} \rightarrow HCaAsO_3 + 2OH^- \quad (11)$$

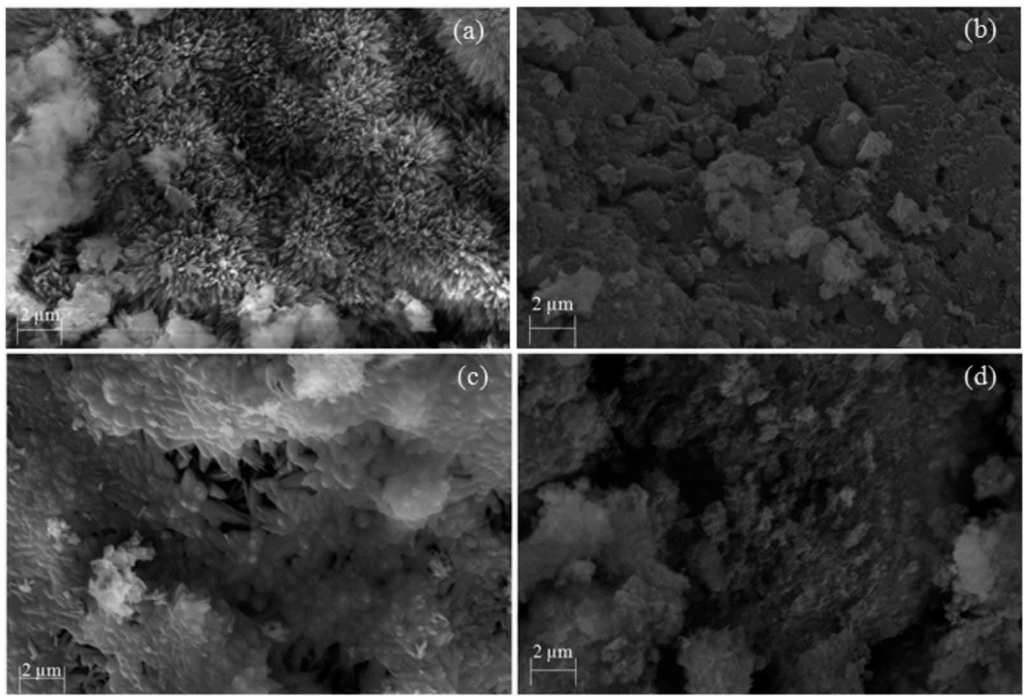

Figure 3. SEM images of COS after being used to adsorb (a) As(III), (b) NO_3^-, (c) SO_4^{2-}, and (d) HPO_4^{2-}.

$$Ca(OH)_2 + 2NO_3^- \rightarrow Ca(NO_3)_2 + 2OH^- \quad (12)$$

$$Ca(OH)_2 + SO_4^{2-} \rightarrow CaSO_4 + 2OH^- \quad (13)$$

$$Ca(OH)_2 + HPO_4^{2-} \rightarrow CaHPO_4 + 2OH^- \quad (14)$$

After COS was added into the solution, CaO in COS changed into $Ca(OH)_2$ as Reaction (7). Some of $Ca(OH)_2$ could dissolve in the solution and dissociate into Ca^{2+} and OH^- which caused the increase in pH of the solution as Reaction (8). Initially, pH of the solution was approximately 11, As(III) and the other anions should be in the form of $H_2AsO_3^-$,[46] NO_3^-, SO_4^{2-}, and HPO_4^{2-}.[47,48] These anions should adsorb on the undissolved COS by ligand exchange as in Reactions (9), (12)–(14). While pH of the solution increased from pH 11 to pH 12.3–12.6, $H_2AsO_3^-$ was further deprotonated by OH^- into $HAsO_3^{2-}$ as in Reaction (10). Then, $HAsO_3^{2-}$ adsorbed on the undissolving COS as Reaction (11). As seen in Reactions (9), (11), (13), and (14), $H_2AsO_3^-$, $HAsO_3^{2-}$, SO_4^{2-}, and HPO_4^{2-} form mononuclear bidentate complexes with Ca-OH while NO_3^- forms mononuclear monodentate complex with Ca-OH as in Reaction (12).

As described before, the removal of the observed anions by COS could occur in different ways as it provided different adsorption capacities and morphologies. Therefore, the $H_2AsO_3^-$ adsorption performance would probably be interfered by these competitive anions in water. The effect of the observed competitive anions on the adsorption of $H_2AsO_3^-$ was then investigated and the percentages of the anions remaining in the solution after adsorption experiment are shown in Table 2. It is noted that the removal percentages of HPO_4^{2-} in this table were the values which the effect of precipitation was eliminated by using the data in the precipitation tests.

Considering the cases which As(III) were paired with NO_3^-, SO_4^{2-}, and HPO_4^{2-}, it can be seen that the presence of HPO_4^{2-} as a competitive anion caused the adsorption of $H_2AsO_3^-$ to decrease the most, *i.e.* decreased by 45.62%. Meanwhile, SO_4^{2-} and NO_3^- less affected the decrease of $H_2AsO_3^-$ adsorption performance, *i.e.* by 15.9% and 8.6%, respectively. These results correlate with the adsorption capacity trend observed from the individual anion adsorption experiments presented in Fig. 2. Rajapaksha *et al.*[14] studied the feasibility to use natural red earth (NRE) which consisted of Fe_2O_3 and Al_2O_3 as the adsorbent to adsorb arsenic in water. They investigated the effect of NO_3^-, SO_4^{2-}, and HPO_4^{2-} on the adsorption of arsenic on NRE and the results were in the similar trend with the results in this paper.

Considering the effect of HPO_4^{2-} on the As(III) adsorption, the reasons why HPO_4^{2-} could considerably interfere the adsorption of $H_2AsO_3^-$ should be because their anionic radii have comparable size and by the nature of COS, it provided comparable adsorption capacities for $H_2AsO_3^-$ and HPO_4^{2-} as illustrated in Fig. 2. This competitive As(III) and phosphate adsorption result is also in good agreement with the results of Huang[49], Jian *et al.*[20], and Meng *et al.*[50] who studied the competitive adsorption between As(III) and phosphate on goethite, ZIF-8 nanoparticles, and iron hydroxide, respectively. All of them found that the amount of As(III) adsorbed on their materials decreased when phosphate was present.

It is interesting that although the presence of NO_3^- caused the decrease of $H_2AsO_3^-$ adsorption by only 8.6%, the adsorption percentage of NO_3^- was as high as almost 37%. Three possible explanations can be given. (1) The binding affinity between sorption sites and NO_3^- was lower than that of As(III) causing in less reduction of As(III) adsorption. (2) Since the radius of NO_3^- is smaller than As(III), NO_3^- should be able to adsorb on the sorption sites which neighboring sorption sites were occupied by As(III) without the overlap between the radii of NO_3^- and As(III) and better reach the sorption sites inside the pores of COS causing in high adsorption capacity of NO_3^-. (3) Since NO_3^- adsorbed on the adsorbent in the form of monomolecular monodentate complex with Ca-OH, two ions of NO_3^- could adsorb on one sorption site while As(III) forms monomolecular bidentate complex with Ca-OH, only one ion of As(III) could adsorb on one sorption site. For the rest experiments which $H_2AsO_3^-$ was mixed with the other two or three anions, the ability of COS to remove NO_3^- increased particularly when HPO_4^{2-} was present. The removal performance of $H_2AsO_3^-$ dropped down the most when it was mixed with HPO_4^{2-} and NO_3^-. However, SO_4^{2-} seems not to be affected by the other anions as its removal percentages were comparable in every experiment.

Table 2. Effect of competitive anions on As(III) adsorption performance.

	Removal percentage of each anion			
Anions in the system	As(III)	NO_3^-	SO_4^{2-}	HPO_4^{2-}
As(III)	74.90	–	–	–
As(III) + NO_3^-	68.46	37.62	–	–
As(III) + SO_4^{2-}	63.02	–	25.60	–
As(III) + HPO_4^{2-}	40.73	–	–	42.00
As(III) + NO_3^- + SO_4^{2-}	53.06	43.73	23.15	–
As(III) + NO_3^- + HPO_4^{2-}	20.83	67.30	–	53.95
As(III) + SO_4^{2-} + HPO_4^{2-}	40.00	–	21.19	43.44
As(III) + NO_3^- + SO_4^{2-} + HPO_4^{2-}	42.53	65.73	27.97	37.57

The adsorption kinetics of As(III) and anions were also investigated. As described before, the observed adsorption rate constants were obtained by fitting the calculated results with the experimental data. Figure 4 shows the data fitting of the fractions of adsorbed sites versus time corresponding to the case of As(III) mixed with NO_3^-, SO_4^{2-}, and HPO_4^{2-}. It can be seen that the calculated results of NO_3^- and SO_4^{2-} occupied sites are well fit with the experimental data while the calculated results of As(III) and HPO_4^{2-} considerably deviate from the experimental ones. Since it was assumed that there was no interaction between the adsorbates but in fact there should be the interaction between each anion either more or less depending on charge repulsion and radius overlapping. Radii of As(III) and HPO_4^{2-} are comparable and charge of As(III) was negative (ranging from −1 to −2 depending on pH of the solution during adsorption process) which should cause negative charge repulsion with HPO_4^{2-}. Therefore, the interaction between As(III) and HPO_4^{2-} should be significant and should be the cause of calculated result deviation from the experimental data.

The observed adsorption rate constants of As(III) and anions obtained from the fitting with the experimental data are presented in Table 3.

As seen in Table 3, in the case of bi-solutes, the observed adsorption rate constant of HPO_4^{2-} was greater than that of As(III) while the observed adsorption rate constants of NO_3^- and SO_4^{2-} were lower than that of As(III). This implies that HPO_4^{2-} should adsorb on the sorption sites faster than other anions. When As(III) combined with anions in tri- and tetra-solutes, the observed adsorption rate constants of HPO_4^{2-} were still greater than that of other anions thus it should also adsorb on the sorption sites faster than the others. It can be seen in Table 3 that when the solution contained HPO_4^{2-}, the observed adsorption rate constants of NO_3^- were greater than those of As(III) in every case. In the case of SO_4^{2-}, its observed adsorption rate constants were the lowest in every condition of interest thus it should be the slowest adsorb on the sorption sites.

To investigate more about the interaction between As(III) adsorption and other anion(s) presented in the system, the theoretical amount of the adsorption sorption sites of COS was estimated by assuming that one molecule of undissolved CaO represented one adsorption active site. According to the adsorption mechanism mentioned above, it could be assumed that As(III), SO_4^{2-}, and HPO_4^{2-} form mononuclear bidentate complexes with Ca-OH while NO_3^- forms mononuclear monodentate complex with Ca-OH. The percentages of each anion adsorbed on the sorption sites were then calculated and plotted as in Fig. 5.

In Fig. 5, when As(III) was combined with other anion(s) in bi-, tri-, and tetra-solutes, the percentages of As(III) occupied sorption sites decreased from 17.17% (without anions) to different values depending on types and number of anions contained in solutions. In the case of bi-solutes, the percentages of As(III) occupied sites slightly decreased when As(III) paired with NO_3^- or SO_4^{2-} but it dramatically decreased when As(III) paired with HPO_4^{2-}. This implies that

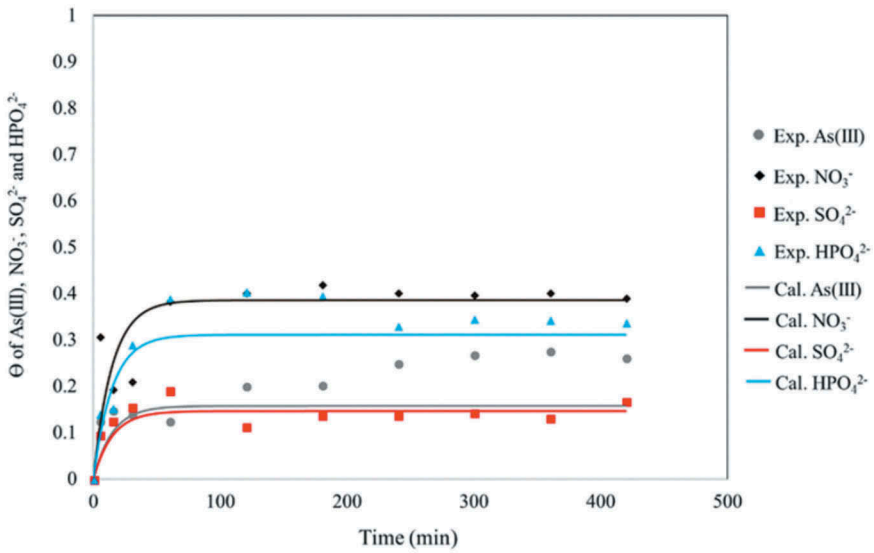

Figure 4. The variation of $\theta$of As(III), NO_3^-, SO_4^{2-}, and HPO_4^{2-} with time. The symbols are the experimental data and solid lines are predicted values.

Table 3. The observed adsorption rate constants of As(III) and anions.

Anions in the system	Observed adsorption rate constant (k_{ad} ×10^5, min^{-1})			
	As(III)	NO_3^-	SO_4^{2-}	HPO_4^{2-}
As(III)	2.3			
As(III) + NO_3^-	3.5	2.0		
As(III) + SO_4^{2-}	1.8		0.6	
As(III) + HPO_4^{2-}	2.0			4.0
As(III) + NO_3^- + SO_4^{2-}	1.6	1.5	0.6	
As(III) + NO_3^- + HPO_4^{2-}	1.2	3.4		4.0
As(III) + SO_4^{2-} + HPO_4^{2-}	1.3		0.8	2.6
As(III) + NO_3^- + SO_4^{2-} + HPO_4^{2-}	8.9	19.5	7.8	20.0

the binding affinity of HPO_4^{2-} on the sorption sites should be greater than that of As(III), SO_4^{2-}, and NO_3^-, respectively.

Furthermore, Fig. 5 shows that the decrease in percentages of As(III) occupied sites in tri- and tetra-solutes was greater than that of As(III) paired with anions because in tri- and tetra-solutes, the solutions contained a large number of anions which could compete to adsorb on the sorption sites. Moreover, the interaction between anions contained in the solution might interfere As(III) adsorption on the sorption sites such as the case of As(III) combined with NO_3^- and HPO_4^{2-}. As illustrated in Fig. 5, the percentage of As(III) occupied sites dramatically decreased. The percentage of HPO_4^{2-} occupied sites was greater than that of NO_3^- and As(III), respectively. From the results in Table 3 and bi-solutes adsorption tests in Table 2, HPO_4^{2-} should adsorb on the sorption sites faster and greater than the other anions. As mentioned before, the net surface charge of COS within the initial period was positive and better adsorbed HPO_4^{2-} which has charge density greater than As(III) and NO_3^-. After that As(III) and NO_3^- should gradually adsorb on the remaining sorption sites. In bi-, tri-, and tetra-solutes, there are various molecular sizes of adsorbates. When the adsorbates adsorbed on the nearby sorption sites, the adsorbates interaction, *i.e.* the overlapping of anionic radii, the repulsion between the negative charge of anions should occur. Therefore, only the adsorbate that has low interaction with anions occupied on the sorption sites should be preferred to adsorb on the available neighboring sorption site. As mentioned above, the radius of NO_3^- was smaller than that of As(III) and HPO_4^{2-}; thus, the interaction due to overlapping of anionic radii should be less resulting in the greater percentage of NO_3^- occupied site. Meanwhile, during adsorption process, the COS dissolution and adsorption mechanism in Reactions (8), (9), and (12)–(14) caused the increase of pH solution. Therefore, the form of As(III) changed from $H_2AsO_3^-$ into $HAsO_3^{2-}$ as in Reaction (10) during adsorption process. Soon after $H_2AsO_3^-$ changed into $HAsO_3^{2-}$, the charge density of NO_3^- was lower than that of $HAsO_3^{2-}$ thus repulsion between neighboring adsorbates and NO_3^- should become lower, thus NO_3^- should adsorb on the sorption sites better than As(III).

Moreover, it is interesting that when SO_4^{2-} was added in the system of As(III) with NO_3^- and HPO_4^{2-}, the percentage of HPO_4^{2-} occupied sites decreased from 16.66% to 10.35% as illustrated in Fig. 5. There are two reasons that could explain why SO_4^{2-} affected HPO_4^{2-} adsorption. (1) The radius of SO_4^{2-} is comparable with As(III) and HPO_4^{2-}. Therefore, it has more chance that SO_4^{2-} would obstruct or block HPO_4^{2-} and As(III) from reaching the sorption sites where the

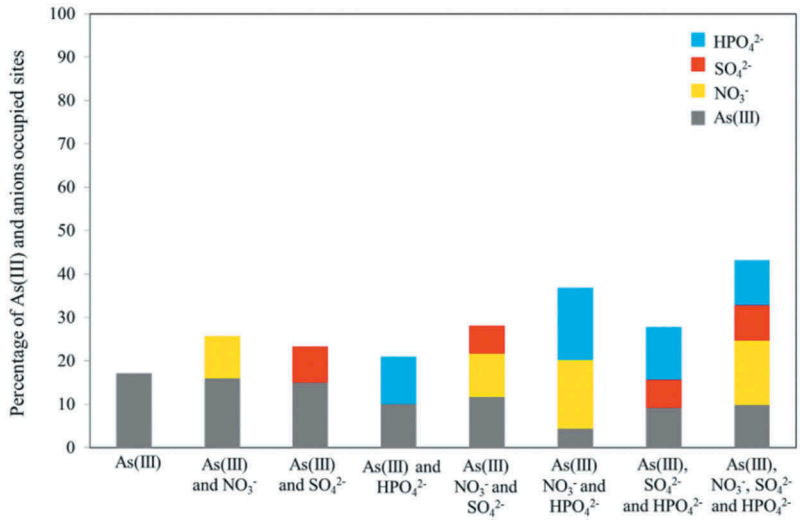

Figure 5. The percentages of As(III) and anions occupied sites.

neighboring sorption sites were occupied by SO_4^{2-}. However, SO_4^{2-} had two negative charges while HPO_4^{2-} also had two negative charges but As(III) was mostly in the form of $H_2AsO_3^-$, the repulsion between two negative – anions should be stronger, hence SO_4^{2-} should affect the adsorption of HPO_4^{2-} more than As(III). (2) The two negative charges of SO_4^{2-} should rapidly balance the positive adsorbent surface charge causing the rapid increase in electrostatic repulsion between adsorbent surface charge and negative charge of anions. HPO_4^{2-} which has two negative charges should be affected by electrostatic interaction causing the decrease in the percentage of HPO_4^{2-} occupied sites.

The morphologies of COS after adsorption tests were observed by SEM and the result is illustrated as in Fig. 6. It can be seen that grass leaf-like morphology representing As(III) adsorption can still be obviously observed in Fig. 6a, b even though some areas were coated by flat surface in Fig. 6a and mixed by flaky matter in Fig. 6b which should be the results of competing adsorptions of NO_3^- and SO_4^{2-}, respectively. In Fig. 6c, the surface of COS looks similar with the one taken from COS after HPO_4^{2-} adsorption test in Fig. 6d. However, grass leaf-like morphology can still slightly be observed. In Fig. 6d which is the morphology of COS after the adsorption experiment which all observed anions were mixed in the solution, the surface looks less flaky while grass leaf-like morphology cannot be observed.

Conclusions

COS was used as the adsorbent to remove As(III) in contaminated water under the presence of NO_3^-, SO_4^{2-}, and HPO_4^{2-}. The precipitation tests indicated that As(III), NO_3^-, and SO_4^{2-} should be removed by COS via adsorption process whereas HPO_4^{2-} should be removed by COS via precipitation and adsorption processes. As(III), SO_4^{2-}, and HPO_4^{2-} should form mononuclear bidentate complexes with Ca-OH while NO_3^- should form mononuclear monodentate complex with Ca-OH. In individual ion adsorption tests, the adsorption capacity of HPO_4^{2-} was greater than those of As(III), NO_3^-, and SO_4^{2-}, respectively. In bi-, tri-, and tetra- solutes systems, HPO_4^{2-} could interfere with As(III) adsorption more than NO_3^- and SO_4^{2-} . The percentages of As(III) occupied sites could decrease from 17.17% into about 5% under the presence of competitive anion(s) which probably depended on (1) adsorbent properties, *e.g.* chemical composition, surface charge, etc., (2) binding affinity between adsorbent and adsorbates, (3) the physical and chemical properties of adsorbates, *i.e.* anionic radius, charge density, (4) adsorption rate constant, (5) the electrostatic attraction or repulsion between adsorbent and adsorbates, and (6) the adsorbates interaction during the adsorption process.

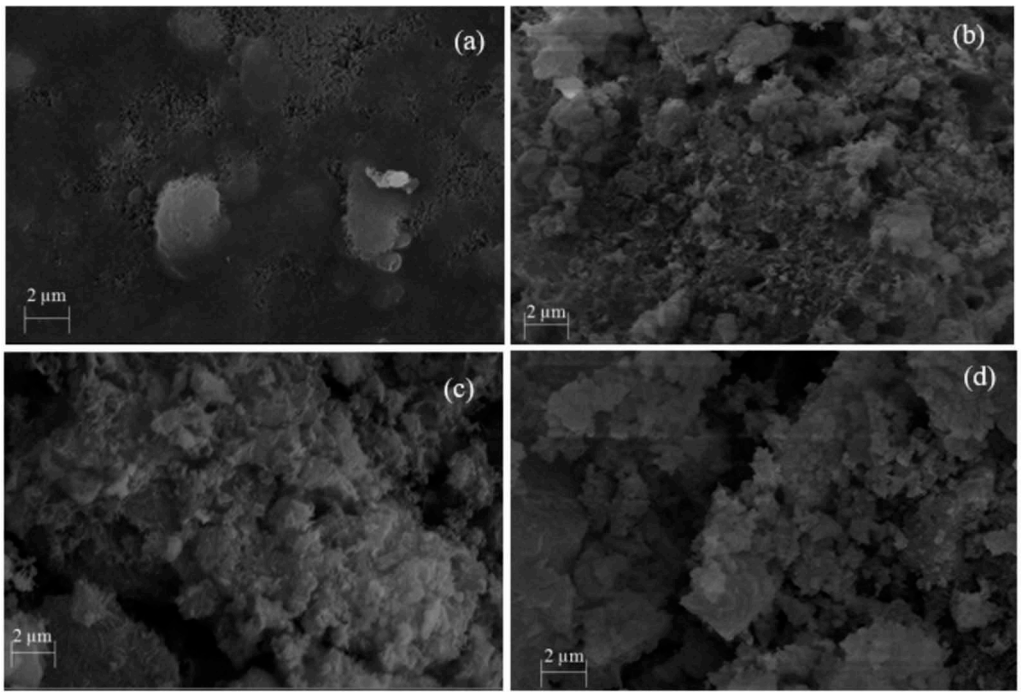

Figure 6. SEM images of COS after competitive anion adsorption tests of (a) As(III) paired with NO_3^-, (b) As(III) paired with SO_4^{2-}, (c) As(III) paired with HPO_4^{2-}, and (d) As(III) combined with NO_3^-, SO_4^{2-}, and HPO_4^{2-}.

Funding

This work was supported by the King Mongkut's Institute of Technology Ladkrabang [KREF015905].

References

[1] Mohan, D.; Pittman, C.U. (2007) Arsenic removal from water/wastewater using adsorbents- a critical review. *Journal of Hazardous Materials*, 142: 1–53. doi:10.1016/j.jhazmat.2007.01.006

[2] Ng, J.C.; Wang, J.; Shraim, A. (2003) A global health problem caused by arsenic from natural sources. *Chemosphere*, 52: 1353–1359. doi:10.1016/S0045-6535(03)00470-3

[3] Berg, M.; Tran, H.C.; Nguyen, T.C.; Pham, H.V.; Schertenleib, R.; Giger, W. (2001) Arsenic contamination of groundwater and drinking water in Vietnam: a human health threat. *Environmental Science and Technology*, 35: 2621–2626.

[4] Walker, M.; Seiler, R.; Meinert, M. (2008) Effectiveness of household reverse-osmosis systems in a Western US region with high arsenic in groundwater. *Science of the Total Environment*, 389: 245–252. doi:10.1016/j.scitotenv.2007.08.061

[5] Borah, D.; Satagawa, S.; Kato, S.; Kojima, T. (2009) Sorption of As(V) from aqueous solution using acid modified carbon black. *Journal of Hazardous Materials*, 162: 1269–1277. doi:10.1016/j.jhazmat.2008.06.015

[6] Oh, C.; Rhee, S.; Oh, M.; Park, J. (2012) Removal characteristics of As(III) and As(V) from acidic aqueous solution by steel making slag. *Journal of Hazardous Materials*, 213–214: 147–155. doi:10.1016/j.jhazmat.2012.01.074

[7] Salameh, Y.; Albadarin, A.B.; Allen, S.; Walker, G.; Ahmad, M.N.M. (2015) Arsenic(III,V) adsorption onto charred dolomite: charring optimization and batch studies. *Chemical Engineering Journal*, 259: 663–671. doi:10.1016/j.cej.2014.08.038

[8] Maiti, A.; Das Gupta, S.; Basu, J.K.; De, S. (2007) Adsorption of arsenite using natural laterite as adsorbent. *Separation and Purification Technology*, 55: 350–359. doi:10.1016/j.seppur.2007.01.003

[9] Dermatas, D.; Moon, D.H.; Menounou, N.; Meng, X.; Haires, R. (2004) An evaluation of arsenic release from monolithic solids using a modified semi-dynamic leaching test. *Journal of Hazardous Materials*, 116: 25–38. doi:10.1016/j.jhazmat.2004.04.023

[10] Dutre´, V.; Vandecasteele, C. (1998) Immobilization mechanism of arsenic in waste solidified using cement and lime. *Environmental Science Technology*, 32: 2782–2787. doi:10.1021/es971090j

[11] Shao, B.; Guan, Y.; Tian, Z.; Guan, X.; Wu, D. (2016) Advantages of aeration in arsenic removal and arsenite oxidation by structural Fe(II) hydroxides in aqueous solution. *Colloids and Surfaces A*, 506: 703–710. doi:10.1016/j.colsurfa.2016.07.049

[12] Samad, A.; Furukawa, M.; Katsumata, H.; Suzuki, T.; Kaneco, S. (2016) Photocatalytic oxidation and simultaneous removal of arsenite with CuO/ZnO photocatalyst. *Journal of Photochemistry and Photobiology A: Chemistry*, 325: 97–103. doi:10.1016/j.jphotochem.2016.03.035

[13] Zhang, F.S.; Itoh, H., (2005) Iron oxide-loaded slag for arsenic removal from aqueous system. *Chemosphere*, 60 (3): 319–325. doi:10.1016/j.chemosphere.2004.12.019

[14] Rajapaksha, A.U.; Vithanage, M.; Jayarathna, L.; Kumara, C.K. (2011) Natural red earth as a low cost material for arsenic removal: kinetics and the effect of competing ions. *Applied Geochemistry*, 26: 648–654. doi:10.1016/j.apgeochem.2011.01.021

[15] Pourbeyram, S.; Alizadeh, S.; Gholizadeh, S. (2016) Simultaneous removal of arsenate and arsenite from aqueous solutions by graphene oxide-zirconium (GO-Zr) nanocomposite. *Journal of Environmental Chemical Engineering*, 4: 4366–4373. doi:10.1016/j.jece.2016.10.003

[16] Yang, J.S.; Kwon, M.J.; Park, Y.T.; Choi, J., (2015) Adsorption of arsenic from aqueous solutions by iron oxide coated sand fabricated with acid mine drainage. *Separation Science and Technology*, 50 (2): 267–275. doi:10.1080/01496395.2014.956224

[17] Maeda, S.; Ohki, A.; Saikoji, S.; Naka, K., (1992) Iron(III) hydroxide-loaded coral limestone as an adsorbent for Arsenic(III) and Arsenic(V). *Separation Science and Technology*, 27 (5): 681–689. doi:10.1080/01496399208018911

[18] Amano, Y.; Matsushita, Y.; Machida, M., (2014) Arsenic adsorption by activated carbon with different amounts of basic sites under different solution pH and coexistent ions. *Separation Science and Technology*, 49 (3): 345–353. doi:10.1080/01496395.2013.838789

[19] Liu, B.; Jian, M.; Wang, H.; Zhang, G.; Liu, R.; Zhang, X.; Qu, J. (2018) Comparing adsorption of arsenic and antimony from single-solute and bi-solute aqueous systems onto ZIF-8. *Colloids and Surfaces A*, 538: 164–172. doi:10.1016/j.colsurfa.2017.10.068

[20] Jian, M.; Liu, B.; Zhang, G.; Liu, R.; Zhang, X. (2015) Adsorptive removal of arsenic from aqueous solution by zeoliticimidazolate framework-8 (ZIF-8) nanoparticles. *Colloids and Surfaces A*, 465: 67–76. doi:10.1016/j.colsurfa.2014.10.023

[21] Ghimire, K.N.; Inoue, K.; Makino, K.; Miyajima, T., (2002) Adsorption removal of arsenic using orange juice residue. *Separation Science and Technology*, 37 (12): 2785–2799. doi:10.1081/SS-120005466

[22] Tsai, H.C.; Lo, S.L.; Kuo, J. (2011) Using pretreated waste oyster and clam shells and microwave hydrothermal treatment to recover boron from concentrated wastewater. *Bioresource Technology*, 102: 7802–7806. doi:10.1016/j.biortech.2011.06.036

[23] Alidoust, D.; Kawahigashi, M.; Yoshizawa, S.; Sumida, H.; Watanabe, M. (2015) Mechanism of cadmium biosorption from aqueous solutions using calcined oyster shells. *Journal of Environmental Economics and Management*, 150: 103–110. doi:10.1016/j.jenvman.2014.10.032

[24] Hsu, T.C.;. (2009) Experimental assessment of adsorption of Cu^{2+} and Ni^{2+} from aqueous solution by oyster shell powder. *Journal of Hazardous Materials*, 171: 995–1000. doi:10.1016/j.jhazmat.2009.06.105

[25] Khownpurk, P.; Wongpromrat, W.; Chandra-Ambhorn, W. (2017) Arsenic adsorption using the adsorbent synthesised from oyster shell. *Key Engineering Materials*, 728: 327–334. doi:10.4028/www.scientific.net/KEM.728

[26] Sigdel, A.; Park, J.; Kwak, H.; Park, P.K. (2016) Arsenic removal from aqueous solutions by adsorption onto hydrous iron oxide-impregnated alginate beads. *Journal of Industrial and Engineering Chemistry*, 35: 277–286. doi:10.1016/j.jiec.2016.01.005

[27] Maji, S.K.; Kao, Y.H.; Liu, C.W. (2011) Arsenic removal from real arsenic-bearing groundwater by adsorption on iron-oxide-coated natural rock (IOCNR). *Desalination*, 280: 72–79. doi:10.1016/j.desal.2011.06.048

[28] Hasan, S.; Ghosh, A.; Race, K.; Schreiber, R.; Prelas, M., (2014) Dispersion of FeOOH on chitosan matrix for simultaneous removal of As(III) and As(V) from drinking water. *Separation Science and Technology*, 49 (18): 2863–2877. doi:10.1080/01496395.2014.949774

[29] Bang, S.; Patel, M.; Lippincott, L.; Meng, X. (2005) Removal of arsenic from groundwater by granular titanium dioxide adsorbent. *Chemosphere*, 60: 389–397. doi:10.1016/j.chemosphere.2004.12.008

[30] Bang, S.; Meng, X.; Korfiatis, G.P.; Bang, K. (2002) Effects of silicates, phosphate, and bicarbonate on arsenic removal and treatment of arsenic in Bangladesh groundwater with ferric salts. Proceeding of the world congress of Korean scientists and engineers-2002. *The Korean Federation of Science and Technology Societies*, 839–844.

[31] Preocanin, T.; Kallay, N. (1998) Application of mass titration to determination of surface charge of metal oxides. *Croatica Chemica Acta*, 71: 1117–1125.

[32] Cardenas-Pena, A.M.; Ibanez, J.G.; Vasquez-Medrano, R. (2012) Determination of the point of zero charge for electrocoagulation precipitates from an iron anode. *International Journal of Electrochemical Science*, 7: 6142–6153.

[33] Foo, K.Y.; Hameed, B.H. (2012) Textural porosity, surface chemistry and adsorptive properties of durian shell derived activated carbon prepared by microwave assisted NaOH activation. *Chemical Engineering Journal*, 187: 53–62. doi:10.1016/j.cej.2012.01.079

[34] Hassan, A.F.; Abdel-Mohsen, A.M.; Elhadidy, H. (2014) Adsorption of arsenic by activated carbon, calcium alginate and their composite beads. *International Journal of Biological Macromolecules*, 68: 125–130. doi:10.1016/j.ijbiomac.2014.04.006

[35] Kwok, K.C.M.; Koong, L.F.; Chen, G.; Mackay, G. (2014) Mechanism of arsenic removal using chitosan and nanochitosan. *Journal of Colloid and Interface Science*, 416: 1–10. doi:10.1016/j.jcis.2013.10.031

[36] Park, C.M.; Han, J.; Chu, K.H.; Al-Hamadani, Y.A. J.; Her, N.; Heo, J.; Yoon, Y. (2017) Influence of solution pH, ionic strength, and humic acid on cadmium adsorption onto activated biochar: experiment and modeling. *Journal of Industrial and Engineering Chemistry*, 48: 186–193. doi:10.1016/j.jiec.2016.12.038

[37] Das, D.P.; Das, J.; Parida, K. (2003) Physicochemical characterization and adsorption behavior of calcined Zn/Al hydrotalcite-like compound (HTlc) towards removal of fluoride from aqueous solution. *Journal of Colloid and Interface Science*, 261: 213–220. doi:10.1016/S0021-9797(03)00082-1

[38] Wan, D.; Liu, H.; Liu, R.; Qu, J.; Li, S.; Zhang, J. (2012) Adsorption of nitrate and nitrite from aqueous solution onto calcined (Mg–al) hydrotalcite of different Mg/Al ratio. *Chemical Engineering Journal*, 195–196: 241–247. doi:10.1016/j.cej.2012.04.088

[39] Ferreira, O.P.; Moraes, S.G.; Duran, N.; Cornejo, L.; Alves, O.L. (2006) Evaluation of boron removal from water by hydrotalcite-like compounds. *Chemosphere*, 62: 80–88. doi:10.1016/j.chemosphere.2005.04.009

[40] Azizian, S.; Haerifar, M.; Basiri-Parsa, J. (2007) Extended geometric method: a simple approach to derive adsorption rate constants of Langmuir-Frundlich kinetic. *Chemosphere*, 68: 2040–2046. doi:10.1016/j.chemosphere.2007.02.042

[41] Azizian, S.;. (2004) Kinetic models of sorption: a theoretical analysis. *Journal of Colloid and Interface Science*, 276: 47–52. doi:10.1016/j.jcis.2004.03.048

[42] Roberts, G.W.;. (2009) *Chemical Reactions and Chemical Reactors*, John Wiley and Sons. Inc.: United States of America.

[43] Chapra, S.C.; Canale, R.P. (2010) *Numerical Method for Engineers*, 6th ed.; McGraw-Hill: New York.

[44] Islam, M.; Patel, R.K., (2007) Evaluation of removal efficiency of fluoride from aqueous solution using quick lime. *Journal of Hazardous Materials*, 143 (1–2): 303–310. doi:10.1016/j.jhazmat.2006.09.030

[45] Phenrat, T.; Marhaba, T.F.; Rachakornkij, M., (2005) A SEM and X-ray study for investigation of solidified/stabilized arsenic-iron hydroxide sludge. *Journal of Hazardous Materials*, 118 (1–3): 185–195. doi:10.1016/j.jhazmat.2004.10.019

[46] Sharma, V.K.; Sohn, M., (2009) Aquatic arsenic: toxicity, speciation, transformations, and remediation. *Environment International*, 35 (4): 743–759. doi:10.1016/j.envint.2009.01.005

[47] Currie, S.J.; VanZomeren, C.M.; Berkowitz, J.F. (2017) Utilizing wetlands for phosphorus reduction in great lakes watersheds: a review of available literature examining soil properties and phosphorus removal efficiency. *The U.S. Army Engineer Research and Development Center (ERDC), Environmental Laboratory, 3903 Halls Ferry Road, Vicksburg, MS 39180-6199, United States*. 1–131.

[48] Markou, G.; Georgakakis, D., (2011) Cultivation of filamentous cyanobacteria (blue-green algae) in agro-industrial wastes and wastewaters: a review. *Applied Energy*, 88 (10): 3389–3401. doi:10.1016/j.apenergy.2010.12.042

[49] Huang, J.H.;. (2018) Impact of competitive adsorption on microbial arsenate reduction at the water-goethite interface. *Applied Geochemistry*, 88: 59–67. doi:10.1016/j.apgeochem.2017.03.012

[50] Meng, X.; Korfiatis, G.P.; Bang, S.; Bang, K.W. (2002) Combined effects of anions on arsenic removal by iron hydroxides. *Toxicology Letters*, 133: 103–111. doi:10.1016/S0378-4274(02)00080-2

Journal of the Chinese Institute of Engineers

ISSN: 0253-3839 (Print) 2158-7299 (Online) Journal homepage: https://www.tandfonline.com/loi/tcie20

Removal of As(III) from aqueous solution by the oyster shell powder–treated rice husk ash composite (OS-TRHA) pellet

Pichnipa Khownpurk & Walairat Chandra-Ambhorn

To cite this article: Pichnipa Khownpurk & Walairat Chandra-Ambhorn (2019): Removal of As(III) from aqueous solution by the oyster shell powder–treated rice husk ash composite (OS-TRHA) pellet, Journal of the Chinese Institute of Engineers, DOI: 10.1080/02533839.2019.1598284

To link to this article: https://doi.org/10.1080/02533839.2019.1598284

Published online: 15 Apr 2019.

JOURNAL OF THE CHINESE INSTITUTE OF ENGINEERS
https://doi.org/10.1080/02533839.2019.1598284

Removal of As(III) from aqueous solution by the oyster shell powder–treated rice husk ash composite (OS-TRHA) pellet

Pichnipa Khownpurk and Walairat Chandra-Ambhorn

Department of Chemical Engineering, Faculty of Engineering, King Mongkut's Institute of Technology Ladkrabang, Bangkok, Thailand

ABSTRACT

OS-TRHA pellets prepared from oyster shell (OS) powder and treated rice husk ash (TRHA) were used as the adsorbent for arsenite (As(III)) removal from contaminated water. The effect of the OS:TRHA ratio on As(III) removal performance was investigated via batch tests. The most appropriate ratio of OS and TRHA for OS-TRHA pellet preparation was 0.7:0.3 since it provided the acceptable As(III) adsorption capacity of about 26.2 mg g^{-1} without cracking. The OS-TRHA pellets before and after As(III) adsorption tests were characterized by X-ray diffraction (XRD) and scanning electron microscope (SEM). The mechanism of As(III) adsorption by OS-TRHA pellets was proposed. The experimental data correlated with the pseudo-second-order adsorption rate, and the adsorption behavior was better described by the Langmuir adsorption isotherm. The results of XRD, SEM, As(III) adsorption tests and calculation based on the Ca balance indicated that 25 wt% of OS-TRHA pellets was CaO that could react with As(III) and formed Ca-As-O ($CaHAsO_3$) on the surface of the OS-TRHA pellets, while the other 75 wt% of OS-TRHA pellets was composed of $CaSiO_3$ and C-S-H compounds which bound the precursor powders into stable pellets without cracking.

ARTICLE HISTORY
Received 30 January 2018
Accepted 26 February 2019

KEYWORDS
Arsenic; pelletizing; oyster shell; rice husk ash

1. Introduction

Arsenic contamination in water is a worldwide problem as it causes diseases such as cancers, nerve tissue injuries and Blackfoot disease that have affected more than 100 million people around the world (Mohan and Pittman 2007; Mazumder 2003; Choong et al. 2007). In Thailand, arsenic contamination in groundwater has been found in many areas of 25 provinces, particularly in Suphanburi Province, Ubon Ratchathani and Nakorn Si Thammarat (Pansamut and Wattayakorn 2010; Kohnhorst et al. 2002; Pattanapipitpaisal and Suraruk 2012; Hossain et al. 2013).

Arsenic is a metalloid that exists in various oxidation states such as −3, 0, +3 and +5. In water, most arsenic exists in the forms of arsenite (As(III)) and arsenate (As(V)). It has been reported that As(III) is more toxic, more mobile and more difficult to remove from contaminated water than As(V) (Maji, Kao, and Liu 2011; Maji, Pal, and Pal 2008; Maiti et al. 2007; Sharma and Sohn 2009; Zhang et al. 2007). Furthermore, As_2O_3 is used in many industries such as agricultural pesticides, the glass industry and the copper refining industry (Dermatas et al. 2004). In order to remove arsenic from contaminated water, several methods have been used. Adsorption is the one most widely applied to remove arsenic due to its simplicity and low operating cost. There are many types of materials applied as adsorbents to remove arsenic from contaminated water, such as char-carbon (Pattanayak et al. 2000), iron oxide-coated cement (IOCC) (Kundu and Gupta 2006), activated red mud (ARM) (Altundoğan et al. 2002), etc.

It was reported in 2005 that 4 million tons of waste oyster shell (OS) were produced and needed to be utilized or removed (Alidoust et al. 2015). $CaCO_3$ is the main constituent of OS (Yoon et al. 2003) and can be used as a raw material to produce CaO, the adsorbent for heavy metals adsorption (Alidoust et al. 2015; Tsai, Lo, and Kuo 2011). In addition, Tseng (1988) investigated whether adding CaO to Portland cement, used to remove hazardous sludges by solidification/stabilization, could enhance the strength of Portland cement and reduce the leachability of heavy metals from the Portland cement. The previous work reported that calcined OS (COS) powder could be used to remove As(III) from contaminated water with a maximum As(III) adsorption capacity as high as approximately 195.5 mg g^{-1} (pH 11) (Khownpurk, Wongpromrat, and Chandra-Ambhorn 2017). However, fine COS powder was difficult to separate from treated water. There are many methods used to solve this problem, such as increasing the particle size of the adsorbent or transforming the adsorbent powder into granules (Mangwandi et al. 2016). In this work, pelletization, the method normally used to prepare electrolyte pellets in solid oxide fuel cells (Su et al. 2011; Zhang et al. 2004), was applied; this improves the functionality of the As(III) removal material by blending it with other compounds and forming pellets. This method can control the size and shape of the pellets in order for them to be easier to separate from treated water.

Rice husk ash (RHA) is an SiO_2 source used in many processes such as concrete and brick production, ceramic production, soil stabilization, etc. (Prasara and Gheewala 2016; Woo and Lee 1978; Hwang, Huynh, and Risdianto 2016). It has been reported that the potential global RHA production is approximately 70–78 million tons per year (Hassan, Noha, and Ahmad 2014; Srinivasreddy, McCarthy, and Lume 2013). Therefore, there is plenty of waste RHA, particularly in Thailand, where rice is an industrial crop. Villar-Cociña et al. (2011) and other researchers reported that amorphous SiO_2 could react with

CONTACT Walairat Chandra-ambhorn walairat.ch@kmitl.ac.th Department of Chemical Engineering, Faculty of Engineering, King Mongkut's Institute of Technology Ladkrabang, 1 Soi Chalongkrung 1, Bangkok 10520, Thailand

$Ca(OH)_2$, a pozzolanic reaction, and form calcium silicate hydrate (C-S-H), which helped improve the strengths of concrete, mortar, compacted soil block, etc. (Habeeb and Mahmud 2010; Prasara and Gheewala 2016; Srinivasreddy, McCarthy, and Lume 2013).

In order to develop the As(III) removal material to be environmental-friendly and easily further removed through use as a construction material, the waste OS and RHA were used as raw materials for adsorbent preparation. In this research, OS powder was mixed with treated RHA (TRHA) and pelletized. The sample pellets are called OS powder-TRHA composite pellets (OS-TRHA pellets). The most appropriate ratio of OS and TRHA was determined. The adsorption behavior and kinetics of As(III) adsorption on OS-TRHA pellets were also studied. The mechanism of As(III) adsorption on the OS-TRHA pellets was proposed.

2. Materials and methods

2.1. Preparation of the OS-TRHA pellets

The OS and RHA used in this work were collected from restaurants in Chanthaburi province and a power plant in Thailand, respectively. The TRHA was obtained by calcination of the RHA at 600°C in air for 13 h. OS-TRHA pellets were prepared from OS sized <106 μm and TRHA. The OS and TRHA were weighed and combined in various ratios. Distilled water was added into the mixture to provide plasticity. Adapting from the method to pelletize electrolyte pellet (Su et al. 2011; Zhang et al. 2004), 0.3 g of paste was filled in a pellet mold and hydraulically pressed (Winner, model 30 tons) at a pressure of 30 kg-f cm^{-2} for 5 min. Finally, the OS-TRHA pellets obtained were calcined at 700°C in air for 8 h. The chemical compositions of the RHA, TRHA and OS were evaluated by X-ray fluorescence spectrometry (XRF, Bruker model S8 Tiger). The OS-TRHA pellets were also characterized by an X-ray diffractometer (XRD 6100, SHIMADZU, Japan) with Cu-Kα radiation, at 40 kV and 2θ range from 5° to 80° with the scan speed of 2.0° min^{-1}. The morphologies of the OS-TRHA pellets were observed by using a scanning electron microscope (SEM, Carl Zeiss EVO®MA10).

2.2. Solubility and precipitation tests

First, 0.2 g of COS, OS-TRHA pellets and ground OS-TRHA pellets prepared from OS with a ratio of 0.7:0.3 were added into 100 ml distilled water (pH 7) filled in Erlenmeyer flasks and kept for 24 h. Finally, the solutions were filtered through Whatman filter paper no. 1 and the pHs of the solutions were determined by using a pH meter (Hanna instrument, HI 98,107). The amounts of dissolved COS, OS-TRHA pellets and ground OS-TRHA pellets were calculated.

Since some CaO in the OS-TRHA pellets could dissolve in water, precipitation of Ca^{2+} and As(III) was tested by adding 0.00081 mol L^{-1} (100 mg L^{-1}) of As(III) solution into the aqueous solution which contained about 0.00149 mol L^{-1} of dissolved CaO and was kept for 48 h. After that the solution was filtered through Whatman filter paper no. 1 and the As(III) concentration was determined by titration with $KMnO_4$.

2.3. The As(III) adsorption by OS-TRHA pellets

The performance of As(III) adsorption by using the OS-TRHA pellets and ground OS-TRHA pellets was investigated in Erlenmeyer flasks covered with rubber corks. First, the stock solution of As(III) was diluted to 100 mg L^{-1} with distilled water. The solution pH was adjusted to pH 7 by using 0.1 M of NaOH and/or HCl. After that, the OS-TRHA pellets and ground OS-TRHA pellets were individually added into Erlenmeyer flasks which contained 100 ml of As(III) solution and were kept for 24 h. Finally, the concentration of As(III) remaining in the solution was determined by using titration with $KMnO_4$. The As(III) adsorption capacity of the OS-TRHA pellets was calculated using Equation (1).

$$\text{As(III)adsorption capacity } (q_t) = \frac{(C_0 - C_e)V}{W}, \quad (1)$$

where C_0 and C_e are the concentrations of As(III) at the initial stage and at equilibrium (mg L^{-1}), respectively, while V is the volume of the solution (L) and W is the mass of the material used in the As(III) adsorption test (g).

To study the adsorption kinetics of the OS-TRHA pellets, the OS-TRHA pellets prepared with the OS:TRHA ratio of 0.7:0.3 were added into 100 mg L^{-1} of As(III) solution (pH 7). The samples were taken immediately after the pellets were added and at 30, 60, 180, 360, 540, 720, 900, 1080 and 1440 min after addition. The linear forms of pseudo-first-order (Equation (2)) (Lagergren 1891; Malana, Qureshi, and Ashiq 2011) and pseudo-second-order models (Equation (3)) (Ho 2006; Ho and McKay 1999) were applied to fit the experimental data. Furthermore, the equilibrium data were determined by fitting with linear forms of Langmuir and Freundlich adsorption isotherms as in Equations (4) and (5), respectively.

$$ln(q_e - q_t) = ln\, q_e - k_{a,1}t, \quad (2)$$

$$\frac{t}{q_t} = \frac{1}{k_{a,2}q_e^2} + \frac{1}{q_e}t, \quad (3)$$

$$\frac{1}{q_e} = \frac{1}{q_m} + \frac{1}{K_L q_e C_e}, \quad (4)$$

$$\log q_e = \log K_F + \frac{1}{n}C_e, \quad (5)$$

where q_t and q_e are the amounts of As(III) adsorbed at time t and at equilibrium (mg g^{-1}), respectively, $k_{a,1}$ and $k_{a,2}$ are adsorption rate constants of pseudo-first-order (min^{-1}) and pseudo-second-order (g mg^{-1} min^{-1}), respectively. K_L is the Langmuir equilibrium adsorption constant, while K_F is the Freundlich adsorption constant and $1/n$ relates to the adsorption capacity and intensity of adsorption.

3. Results and discussion

3.1. Material characterization

3.1.1. XRF analysis

The compositions of the OS, COS, RHA and TRHA were determined by X-ray Fluorescence (XRF). The main elements

Table 1. Compositions of OS, COS, RHA and TRHA (wt%).

	% content			
Composition	OS	COS	RHA	TRHA
CaO	95.99	97.00	0.74	0.82
MgO	0.65	0.90	0.50	0.57
Na_2O	0.98	0.50	-	0.20
SO_3	0.73	0.50	0.18	0.20
SiO_2	0.70	0.40	79.30	87.00
P_2O_5	0.20	0.20	1.25	1.32
Cl	-	0.10	0.58	0.14
Fe_2O_3	-	0.10	0.47	0.29
Al_2O_3	0.42	0.10	0.54	0.56
SrO	0.33	0.10	-	-
K_2O	-	0.10	2.51	2.52
MnO	-	-	0.13	0.14
Loss on ignition			12.14	1.80

(expressed as oxides) presented in OS, COS, RHA and TRHA are shown in Table 1.

The XRF results show that the major composition of OS was $CaCO_3$, while the COS consisted of 97 wt% of CaO, which was caused by the transformation of $CaCO_3$ (Khownpurk, Wongpromrat, and Chandra-Ambhorn 2017). Furthermore, Table 1 shows that silica (SiO_2) is the main constituent of RHA (79.30%) and TRHA (87.00%), followed by K_2O, P_2O_5, CaO, Cl and Al_2O_3, respectively. Loss on ignition (LOI) was determined by the weight loss of RHA and TRHA after calcining at 700°C for 8 h. It was found that the LOI of RHA was more than that of TRHA by approximately 85%. The XRF and LOI results indicated that the percentage of SiO_2 in TRHA increased due to the removal of moisture, unburned carbon and other impurities from the RHA after calcination at 600°C for 13 h.

3.1.2. XRD analysis

The XRD patterns of the OS-TRHA pellets before and after As(III) adsorption tests are presented in Figure 1.

It can be seen from the XRD pattern of the OS-TRHA pellets before the As(III) adsorption test (Figure 1(a)) that the crystalline substances detected are calcium silicate ($CaSiO_3$), calcium silicate hydrate (C-S-H), calcium oxide (CaO) and calcium hydroxide ($Ca(OH)_2$). However, after As(III) adsorption (Figure 1(b)), the peaks corresponding to CaO can no longer be observed while the other peaks corresponding to Ca-As-O can be observed. This means that the CaO reacted with water and turned into $Ca(OH)_2$ and further reacted with As(III) to become Ca-As-O.

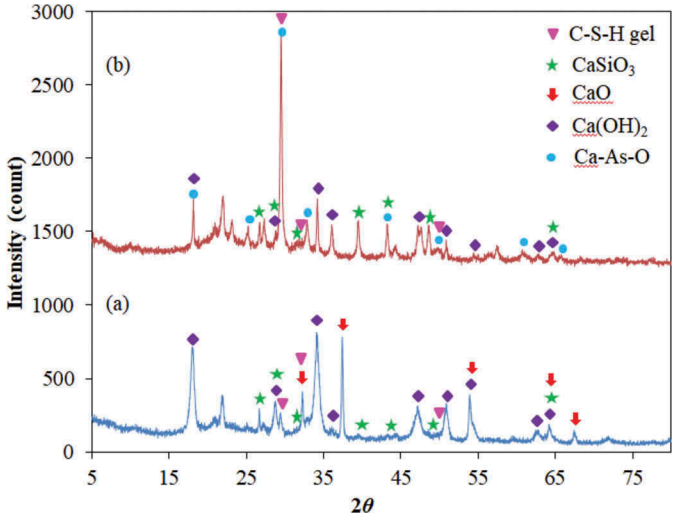

Figure 1. XRD patterns of the OS-TRHA pellets (a) before and (b) after As(III) adsorption tests.

3.1.3. The solubility and precipitation tests

The solubility test showed that the pH of the solution increased from 7 (pH of water before adding COS, ground OS-TRHA pellets and OS-TRHA pellets) to 12.5, 11.4 and 11.3 after adding COS, ground OS-TRHA pellets and OS-TRHA pellets, respectively, for 24 h. This means that some CaO, after reacting with water, could dissolve in the water and dissociate into Ca^+ and OH^-, resulting in the increase of the solution pH. Based on the increasing pH, the amounts of CaO in COS, ground OS-TRHA pellets and OS-TRHA pellets dissolved in the water were equivalent to 4.39, 0.34 and 0.29 wt%, respectively. The reason why the solubility of OS-TRHA pellets is much less than that of COS is because OS-TRHA pellets contained less CaO and some of this CaO reacted with the TRHA (insoluble) and formed $CaSiO_3$ and C-S-H compounds, which are insoluble substances (Seidell 1919). In the case of the OS-TRHA pellets, the ground OS-TRHA pellets could dissolve in the distilled water more than the un-ground OS-TRHA pellets because the contact surface area of the ground OS-TRHA pellets was greater.

The result of the precipitation test showed that, after 48 h, the precipitate was not observed and the As(III) concentration changed insignificantly. The pH of the Ca^{2+} solution before and after adding As(III) into the solution was approximately equal (pH 11.6). This implies that the precipitation of Ca-As(III) did not occur. The precipitation result in this work agrees with the work of Dutŕe and Vandecasteele (1995, 1998), who studied the immobilization of arsenic-containing waste by using cement and lime and reported that Ca^{2+} in solution precipitated with $HAsO_3^{2-}$ in the form of $CaHAsO_3$ only at a pH above 11.91.

3.2. As(III) adsorption result

The As(III) adsorption capacities of the OS-TRHA pellets with different OS:TRHA ratios are illustrated in Figure 2.

It can be seen that the As(III) adsorption capacity of TRHA is extremely low in comparison with the As(III) adsorption capacity of COS, which is as high as 241.67 mg g^{-1} of CaO. This implies that the CaO provides sorption sites in the OS-TRHA pellets. The As(III) adsorption capacities of OS-TRHA pellets with different OS:TRHA ratios also confirmed the previous statement, as the As(III) adsorption capacity increased with the increasing fraction of OS. Furthermore, this also implies that the products of the reaction of OS and TRHA, such as $CaSiO_3$ and C-S-H compounds, do not contain sorption sites for the As(III) adsorption process.

The adsorption kinetics of OS-TRHA was also investigated. The result showed that As(III) adsorption on OS-TRHA pellets approached equilibrium within 24 h. The kinetic parameters are shown in Table 2.

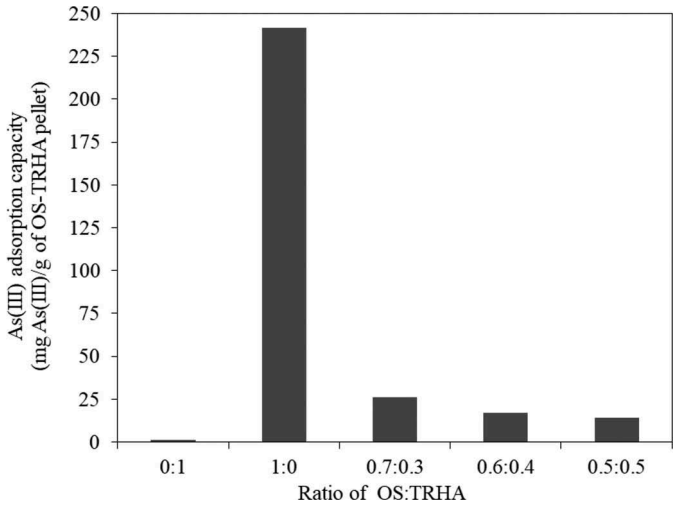

Figure 2. As(III) adsorption capacities of As(III) on the TRHA, COS and the OS-TRHA pellets.

Table 2. Kinetic parameters of As(III) adsorption on OS-TRHA pellets.

	Pseudo-first-order			Pseudo-second-order		
$q_{e,exp}$ (mg g^{-1})	$q_{e,cal}$ (mg g^{-1})	$k_{a,1}$ (min^{-1})	R^2	$q_{e,cal}$ (mg g^{-1})	$k_{a,2}$ (g mg^{-1} min^{-1})	R^2
10.55	8.59	0.019	0.99	10.72	0.0075	0.98

It can be seen that although the values of R^2 corresponding to both fits are comparable, $q_{e,cal}$ calculated from the pseudo-second-order model is much closer than that of the pseudo-first-order model. Therefore, As(III) adsorption on the OS-TRHA pellets can be better described by the pseudo-second-order model, which means that As(III) adsorption can carry on via chemical adsorption, and the rate of As(III) adsorption on the pellets is proportional to the square of the number of available active sites (Ho and McKay 1999; Manju, Raji, and Anirudhan 1998).

Moreover, the adsorption isotherm was determined using the equilibrium data of As(III) adsorption on OS-TRHA pellets. The adsorption isotherm parameters are presented in Table 3.

As seen in Table 3, R^2 corresponding to the Langmuir isotherm is closer to 1 than that corresponding to the Freundlich isotherm. This implies that the behavior of As(III) adsorption on OS-TRHA pellets can be better described by the Langmuir isotherm, which means that As(III) adsorption on the OS-TRHA pellets is monolayer (Sener 2008). The As(III) adsorption capacity of OS-TRHA pellets in this work compared with other materials is presented in Table 4.

It can be seen from Table 4 that, although the As(III) adsorption capacity of the OS-TRHA pellets decreased by nine times compared with COS powder, its As(III) adsorption capacity is still high when compared with the As(III) adsorption capacities of other kinds of materials.

Table 3. Adsorption parameters corresponding to Langmuir and Freundlich isotherms.

Langmuir isotherm			Freundlich isotherm		
K_L (L mg^{-1})	q_{max} (mg g^{-1})	R^2	K_F (L g^{-1})	$1/n$	R^2
0.0017	82.6446	0.8588	5.3015	0.8964	0.8386

Table 4. Comparison of As(III) adsorption capacity of OS-TRHA pellets made from OS and TRHA with other materials.

Material	As(III) adsorption capacity (mg g^{-1})	Reference
COS<106 μm	241.67	Present work
OS-TRHA pellets (OS: TRHA = 0.7:0.3)	26.20	Present work
Iron oxide coated cement (IOCC)	0.69	(Kundu and Gupta 2006)
Iron-oxide-coated natural rock (IOCNR)	1.647	(Maji et al. 2013)
Raw red mud (RRM)	8.86	(Altundoğan et al. 2002)
Activated red mud (ARM)	11.80	(Altundoğan et al. 2002)
Bentonite	0.317	(Mar et al. 2013)
Shale	0.181	(Mar et al. 2013)
Char carbon (CC)	5.04	(Pattanayak et al. 2000)
Zinc peroxide functionalized synthetic graphite (FSG)	18.8	(Uppal, Hemlata, and Singh 2016)

3.3. Morphology

The SEM images of TRHA and OS before and after the As(III) adsorption tests are illustrated in Figure 3.

It can be seen that the TRHA morphologies before and after the As(III) adsorption tests in Figure 3(a) and 3(b) look similar. From the result of the As(III) adsorption test shown in Figure 2, the As(III) adsorption capacity of TRHA was very low. This could be the reason for the insignificant change in the morphology of TRHA after the As(III) adsorption test. In the case of COS, a grass leaf-like morphology appears on the COS surface after the As(III) adsorption test, as in Figure 3(d). The As(III) adsorption test and XRD results revealed that COS reacted with As(III) and formed Ca-As-O (Khownpurk, Wongpromrat, and Chandra-Ambhorn 2017), which appeared as the grass-leaf-like structure. Phenrat, Marhaba, and Rachakornkij (2005) studied iron–arsenic sludge immobilized by using cement and lime and also found that the morphology of arsenic immobilized on lime by forming calcium-arsenic compound was in the form of the grass-leaf-like structure.

The surface morphologies of the OS-TRHA pellets with the OS:TRHA ratio of 0.7:0.3 before and after the As(III) adsorption tests are presented in Figure 4.

It can be seen that the morphologies of the OS-TRHA pellets were classified into two forms: the rough surface and the smooth surface, as in Figure 4(a,b), respectively. The energy dispersive X-ray spectroscopy (EDX) results (not shown in this paper) showed that the smooth surface consisted of calcium, silica and oxygen which indicated $CaSiO_3$ and/or C-S-H compounds. After the As(III) adsorption test, the morphologies of the OS-TRHA pellets can be seen in two forms. The first one is the grass-leaf-like morphology (Figure 4(c)) which looks similar to the morphology of COS after the As(III) adsorption test. The other one (Figure 4(d)) looks similar to the second form of OS-TRHA pellet morphology before the As(III) adsorption test in Figure 4(b). This indicates that As(III) reacts with CaO on the rough area of the OS-TRHA pellets and forms Ca-As-O, while the smooth area which consisted of $CaSiO_3$ and/or C-S-H compounds was not able to react with the As(III). In addition, the cross-sectional areas of the OS-TRHA pellets before and after the As(III) adsorption tests were also analyzed by SEM and EDX and the As(III) compound could not be detected.

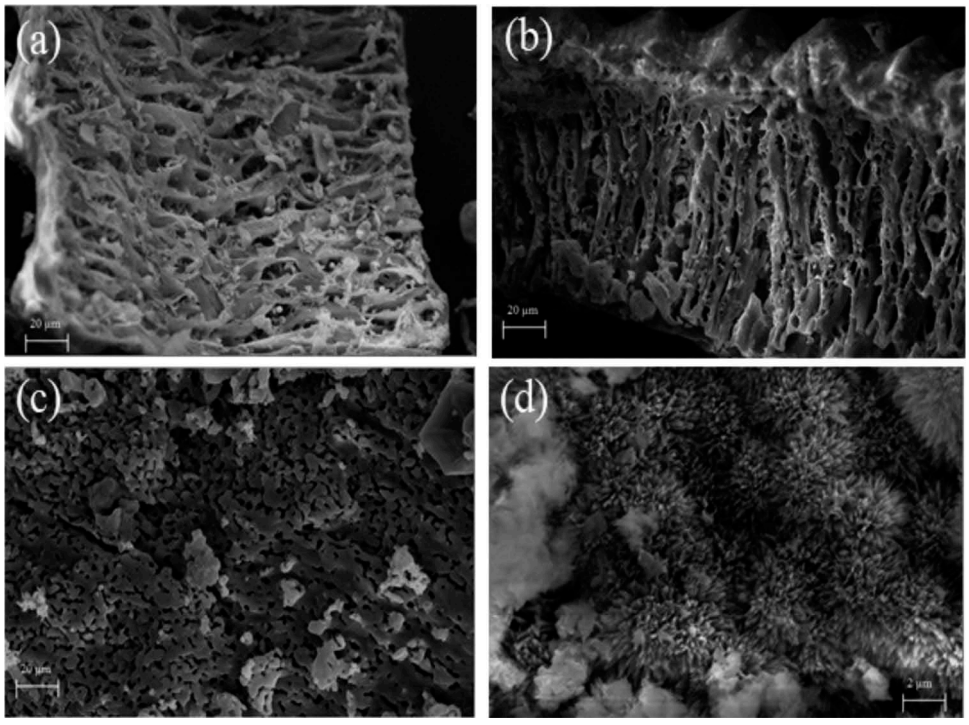

Figure 3. The SEM images of TRHA (a) before, (b) after As(III) adsorption tests and COS (c) before, (d) after As(III) adsorption tests.

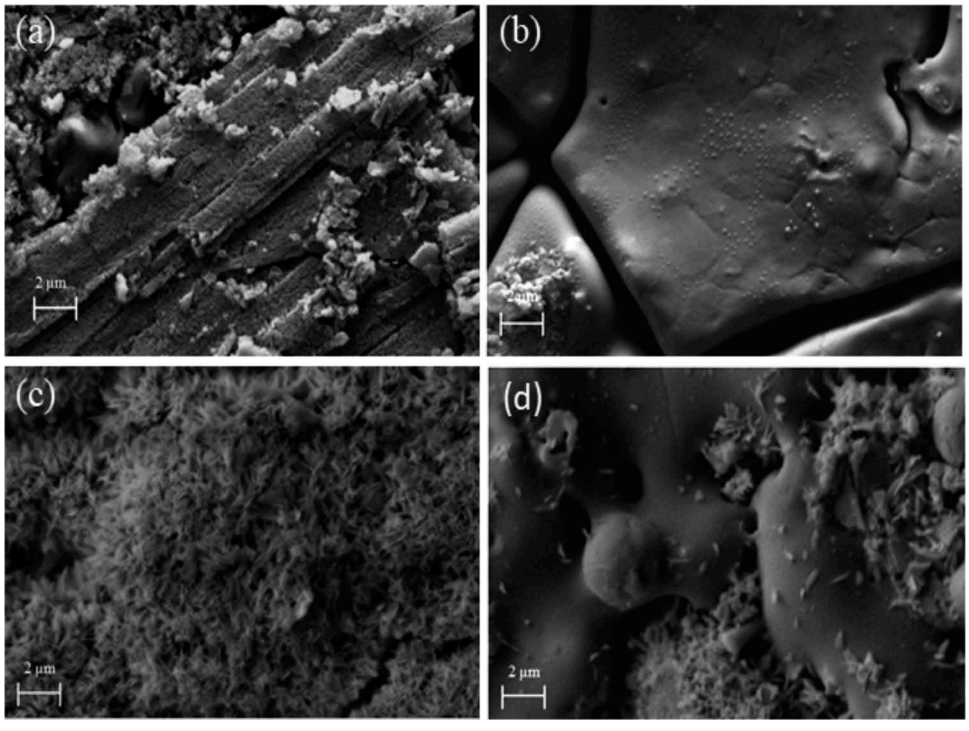

Figure 4. The SEM images of (a) and (b) the OS-TRHA pellet surface before As(III) adsorption test, (c) and (d) the OS-TRHA pellet surface after As(III) adsorption test.

3.4. As(III) adsorption mechanism

The XRF result showed that COS consisted of 97% CaO, while RHA and TRHA consisted of SiO_2 79.3 and 87 wt%, respectively. Furthermore, the XRD results of RHA and TRHA showed a broad smooth humped peak at about 22° (not shown in this paper). Habeeb and Mahmud (2010) and Hassan, Noha, and Ahmad (2014) reported that the broad XRD peak at the position of 2θ = 22–25° referred to an amorphous form of SiO_2. This indicates that calcination at 600°C for 13 h did not change the amorphous form of SiO_2 in the RHA, but removed moisture, unburned carbon and other impurities. The OS and COS could not be pelletized directly. Therefore, TRHA was chosen to be a binder as it contained SiO_2 which could introduce

a pozzolanic reaction with CaO (Alavéz-Ramírez et al. 2012). The appropriate ratio of precursors for the pelletization was determined. It was found that mixing OS (instead of COS) with TRHA with the fraction range of 0.5–0.7 could form OS-TRHA pellets without cracking. As mentioned before, the XRD result of the OS-TRHA pellets after calcination at 700°C for 8 h (Figure 1(a)) showed the peaks of $CaSiO_3$, C-S-H, CaO and $Ca(OH)_2$. During the pelletizing process, the following reactions are assumed to take place.

$$SiO_2 + 2H_2O \rightarrow H_4SiO_4, \quad (6)$$

$$H_4SiO_4 + CaCO_3 \rightarrow CaH_2SiO_4 + H_2CO_3, \quad (7)$$

$$CaH_2SiO_4 \xrightarrow{\Delta} CaSiO_3 + H_2O, \quad (8)$$

$$CaCO_3 \xrightarrow{\Delta} CaO + CO_2, \quad (9)$$

$$CaO + SiO_2 \xrightarrow{\Delta} CaSiO_3. \quad (10)$$

Reactions (6) and (7) occur during mixing OS with TRHA and water. First, SiO_2 in the TRHA reacts with water during pelletizing and forms H_4SiO_4 as in Reaction (6). Then, H_4SiO_4 further reacts with $CaCO_3$ and forms CaH_2SiO_4 (C-S-H) and H_2CO_3 as in Reaction (7). During the calcination process at 700°C for 8 h, H_2CO_3 decomposes and is released as H_2O and CO_2. Hager (2013) and Rodriguez et al. (2017) reported that the C-S-H compounds transformed to $CaSiO_3$ at above 600°C. Therefore, some of the CaH_2SiO_4 could decompose into $CaSiO_3$ and release H_2O as in Reaction (8) resulting in the appearance of both $CaSiO_3$ and C-S-H peaks in the XRD pattern in Figure 1(a). Meanwhile, $CaCO_3$ releases CO_2 and transforms into CaO as in Reaction (9). Then, CaO reacts with SiO_2 and also forms $CaSiO_3$ as in Reaction (10).

The As(III) adsorption test showed that the OS-TRHA pellets prepared from OS and TRHA could remove As(III) with an adsorption capacity of about 26.2 mg g^{-1}. The solution pHs before and after the As(III) adsorption tests were measured. The result showed that the pH of As(III) solution increased from 7 to 11. As mentioned before, the solubility test showed that the pH of the solution increased from 7 to 11.3 after putting the OS-TRHA pellets into distilled water due to the dissolution of $Ca(OH)_2$. According to the XRD results in Figure 1, the intensities of the $Ca(OH)_2$ peaks decreased after As(III) adsorption, while the intensities of the $CaSiO_3$ and C-S-H peaks changed insignificantly. According to the information obtained from the experiments, the mechanism of As(III) adsorption by using the OS-TRHA pellets can be proposed as the following reactions.

$$CaO + 2H_2O \rightarrow Ca(OH)_2, \quad (11)$$

$$Ca(OH)_2 \leftrightarrow Ca^{2+} + 2OH^-, \quad (12)$$

$$Ca(OH)_2 + H_3AsO_3 \rightarrow HCaAsO_3 + 2H_2O, \quad (13)$$

$$H_3AsO_3 + OH^- \rightarrow H_2AsO_3^- + H_2O, \quad (14)$$

$$Ca(OH)_2 + H_2AsO_3^- \rightarrow HCaAsO_3 + H_2O + OH^-, \quad (15)$$

$$H_2AsO_3^- + OH^- \rightarrow HAsO_3^{2-} + H_2O, \quad (16)$$

$$Ca(OH)_2 + HAsO_3^{2-} \rightarrow HCaAsO_3 + 2OH^-, \quad (17)$$

$$Ca^{2+} + HAsO_3^{2-} \rightarrow HCaAsO_3. \quad (18)$$

After putting the OS-TRHA pellets into the As(III) solution, CaO converted into $Ca(OH)_2$ as in Reaction (11), causing the absence of a CaO peak in the XRD result after the As(III) adsorption test (Figure 1(b)). After that, some of the $Ca(OH)_2$ dissolved and dissociated into Ca^{2+} and OH^- as in Reaction (12), causing the pH in the solution to increase. The As(III) could be in different species depending on the pH of the solution (Khownpurk, Wongpromrat, and Chandra-Ambhorn 2017; Sharma and Sohn 2009; Mohan and Pittman 2007; Kwok et al. 2014). Most of the As(III) was in the form of H_3AsO_3 at pH 7. As the pH increased, the H_3AsO_3 was deprotonated by OH^- into $H_2AsO_3^-$ as in Reaction (14), until at pH 10 the $H_2AsO_3^-$ was further deprotonated into $HAsO_3^{2-}$ as in Reaction (16). During the As(III) adsorption process, H_3AsO_3, $H_2AsO_3^-$ and $HAsO_3^{2-}$ reacted with the undissolved $Ca(OH)_2$ on the surface of the OS-TRHA pellets by ligand exchange and formed $CaHAsO_3$ as in Reactions (13), (15) and (17), respectively. This causes the appearance of Ca-As-O peaks in the XRD pattern and the decrease in the intensity of $Ca(OH)_2$ after As(III) adsorption. As mentioned before, the final pH of the As(III) solution after As(III) adsorption (pH 11) was lower than the final pH of the OS-TRHA pellets after being put into distilled water (pH 11.3). There are two reasons that could explain why the final pH in the As(III) adsorption experiment did not reach the level of pH in the solubility or blank test. One is that, soon after the OS-TRHA pellets were put into the As(III) solution, the dissolution of $Ca(OH)_2$ and the reaction between As(III) and undissolved $Ca(OH)_2$ on the OS-TRHA pellet surfaces occurred simultaneously, resulting in the coverage of undissolved $CaHAsO_3$ on the OS-TRHA pellets, and therefore reducing the dissolution of $Ca(OH)_2$ that caused the pH to increase. The other possible reason is that, along with the pH increase, Reactions (13)–(17) occurred. Reaction (13) did not affect the change in pH. However, the deprotonations of As(III) species in Reactions (14) and (16) caused the pH to decrease, while the reactions of As(III) species and $Ca(OH)_2$ in Reactions (15) and (17) caused the pH to increase. As previously mentioned, $HAsO_3^{2-}$ appeared at pH above 10. Dutŕe and Vandecasteele (1995) reported that, at pH 10, As(III) existed in the form of $HAsO_3^{2-}$ only for 0.64% and reached 68.40% at pH 12.76. Therefore, it can be assumed that the extent of Reaction (17) was very small in comparison with Reactions (14)–(16). This means that, by neglecting Reaction (17), the effect of Reactions (14) and (16) on the change of pH should be stronger than that of Reaction (15) and, therefore, the total pH of the solution should be in the decreasing direction. Moreover, As(III) in the form of $HAsO_3^{2-}$ could precipitate with Ca^{2+} from Reaction (12) as in Reaction (18). However, in this work, the precipitation test indicated that no $CaHAsO_3$ precipitate was observed within 48 h. Therefore, Reaction (18) should not

occur in our case. As mentioned before, Dutŕe and Vandecasteele (1995, 1998) reported that Ca^{2+} could precipitate with $HAsO_3^{2-}$ only at pH above 11.91. In this work, the solution pH was lower than 11.3, hence the As(III) would be mainly in the form of $H_2AsO_3^-$, which was not suitable to form $CaHAsO_3$ precipitate.

3.5. Determination of $CaSiO_3$ and C-S-H compounds in the OS-TRHA pellets

As mentioned before, the OS-TRHA pellets are composed of two parts: CaO which can convert into As(III) reactive sites and unreactive compounds ($CaSiO_3$ and C-S-H compounds). In order to determine the amount of unreactive $CaSiO_3$ and C-S-H compounds obtained from Reactions (7), (8) and (10), all of the $CaCO_3$ in OS was assumed to be transformed into CaO in the OS-TRHA pellets (Reaction (9)). Then, the CaO in the OS-TRHA pellets was divided into three fractions as in Equation (19).

$$CaO_{overall} = CaO_{dissolve} + CaO_{ads} + CaO_{rxn}, \quad (19)$$

where $CaO_{dissolve}$ = CaO dissolving in the solution

CaO_{ads} = CaO that can convert into As(III) reactive sites

CaO_{rxn} = CaO reacting with SiO_2 in TRHA during the preparation process

Starting from 0.21 g of OS ($CaCO_3$) in ground OS-TRHA pellets prepared from OS:TRHA in a ratio of 0.7:0.3, assuming that all the dissolved $Ca(OH)_2$ dissociated into Ca^{2+} and OH^-, based on the change of pH in the solubility test of the ground OS-TRHA pellets from 7 to 11.4, the $CaO_{dissolve}$ can be calculated as approximately 0.0007 g. Then, CaO_{ads} was assumed to have the same property as COS. Based on the As(III) adsorption capacity of COS (241.67 mg g^{-1}), the ground OS-TRHA pellets could reduce As(III) by approximately 70.50 mg L^{-1}, which was equivalent to the ability to reduce As(III) by 0.0513 g of COS or CaO_{ads}. Finally, CaO_{rxn} could be determined as approximately 0.0657 g. Therefore, the unreactive CaO in the OS-TRHA pellets was about 55.8 wt%, which was equivalent to 75 wt% of $CaSiO_3$ and C-S-H compounds.

3.6. Application of OS-TRHA pellets for As(III) adsorption

In order to observe the As(III) adsorption by using OS-TRHA pellets on a larger scale, OS-TRHA pellets (3–4 g of total weight) were put into 2 L of synthetic As(III) contaminated water with the concentration equivalent to the arsenic concentration in water resources in Thailand, i.e., 34 mg L^{-1}. The used OS-TRHA pellets were replaced by fresh ones every 2 days, 3 times. The concentration of As(III) in the solution was measured by inductively coupled plasma (ICP, In-house method based on Standard Methods for Examination of Water and Wastewater 20th Edition (APHA, AWWA, and WEF 1998)). The result showed that the OS-TRHA pellets could remove as much as 98.95% of the As(III) from the synthetic As(III) contaminated water. The final concentration of As(III) obtained was as low as 0.36 mg L^{-1}. Although As(III) adsorption by OS-TRHA pellets causes the pH to increase, the pHs of water resources are usually lower than 7; Pattanapipitpaisal and Suraruk (2012) collected the data of groundwater quality in Thailand and reported that the pH of ground water was in the range of 5.70–6.90. Moreover, waste water, particularly dirty acid waste water obtained from many processes such as the hydrometallurgy industry, textile industry, mining industry, etc., usually contains highly concentrated arsenic (5,240–14,740 mg L^{-1}), which mainly exists in As(III) with very low pH (0.5–3.25) (Cui et al. 2014; Du et al. 2016). Many processes have been used to treat the waste water. The main processes consisted of neutralization by lime, followed by arsenic adsorption (De Klerk et al. 2012; Du et al. 2016; Cui et al. 2014). Therefore, OS-TRHA pellets need to be a good dual-function material to be used to remove As(III) and neutralize waste water in one step.

4. Conclusions

OS and TRHA were used as raw materials to produce the OS-TRHA pellets for removing As(III) in contaminated water. The most appropriate ratio of OS:TRHA, providing stable OS-TRHA pellets, was 0.7:0.3. The adsorption kinetics data were fitted with the pseudo-second-order model while the equilibrium data were fitted with the Langmuir isotherm. During the calcination process, some CaO reacted with SiO_2 and formed $CaSiO_3$ and C-S-H compounds which could bind the precursor powder into stable OS-TRHA pellets without cracking. The amount of unreactive $CaSiO_3$ and C-S-H compounds was calculated as about 75% by weight of OS-TRHA pellets. Meanwhile, the unreacted CaO could still convert into $Ca(OH)_2$ and be able to adsorb As(III) in water. The maximum As(III) adsorption capacity was about 26.2 mg g^{-1} of OS-TRHA pellets.

Disclosure statement

No potential conflict of interest was reported by the authors.

Funding

This work was supported by King Mongkut's Institute of Technology Ladkrabang [Grant number KREF015905].

References

Alavéz-Ramírez, R., P. Montes-García, J. Martínez-Reyes, D. C. Altamirano-Ju árez, and Y. Gochi-Ponce. 2012. "The Use of Sugarcane Bagasse Ash and Lime to Improve the Durability and Mechanical Properties of Compacted Soil Blocks." *Construction and Building Materials* 34: 296–305. doi:10.1016/j.conbuildmat.2012.02.072.

Alidoust, D., M. Kawahigashi, S. Yoshizawa, H. Sumida, and M. Watanabe. 2015. "Mechanism of Cadmium Biosorption from Aqueous Solutions Using Calcined Oyster Shells." *Journal of Environmental Management* 150: 103–110. doi:10.1016/j.jenvman.2014.10.032.

Altundoğan, H. S., S. Altundoğan, F. Tümen, and M. Bildik. 2002. "Arsenic Adsorption from Aqueous Solutions by Activated Red Mud." *Waste Management* 22 (3): 357–363. doi:10.1016/S0956-053X(01)00041-1.

APHA (American Public Health Association), AWWA (American Water Works Association) and WEF (Water Environment Federation). 1998. *Standard Methods for the Examination of Water and Wastewater*. 20th ed. Meryland USA: United Book Press.

Choong, T. S. Y., T. G. Chuah, Y. Y. Robiah, F. L. Gregory Koay, and I. Azni. 2007. "Arsenic Toxicity, Health Hazards and Removal Techniques from

Water: An Overview." *Desalination* 217 (1–3): 139–166. doi:10.1016/j.desal.2007.01.015.

Cui, J., Y. Du, H. Xiao, Q. Yi, and D. Du. 2014. "A New Process of Continuous Three-Stage Co-Precipitation of Arsenic with Ferrous Iron and Lime." *Hydrometallurgy* 146: 169–174. doi:10.1016/j.hydromet.2014.03.012.

De Klerk, R. J., Y. Jia, R. Daenzer, M. Gomez, and G. P. Demopoulos. 2012. "Continuous Circuit Coprecipitation of Arsenic(V) with Ferric Iron by Lime Neutralization: Process Parameter Effects on Arsenic Removal and Precipitate Quality." *Hydrometallurgy* 111–112: 65–72. doi:10.1016/j.hydromet.2011.10.004.

Dermatas, D., D. H. Moon, N. Menounou, X. Meng, and R. Haires. 2004. "An Evaluation of Arsenic Release from Monolithic Solids Using a Modified Semi-Dynamic Leaching Test." *Journal of Hazardous Materials* 116 (1–2): 25–38. doi:10.1016/j.jhazmat.2004.04.023.

Du, Y., Q. Lu, H. Chen, Y. Du, and D. Du. 2016. "A Novel Strategy for Arsenic Removal from Dirty Acid Wastewater via $CaCO_3$-$Ca(OH)_2$-Fe(III) Processing." *Journal of Water Process Engineering* 12: 41–46. doi:10.1016/j.jwpe.2016.06.003.

Dutŕe, V., and C. Vandecasteele. 1995. "Solidification/Stabilization of Arsenic-Contaminated Waste: Leach Tests and Behaviour of Arsenic in the Leachate." *Waste Management* 15 (1): 55–62. doi:10.1016/0956-053X(95)00002-H.

Dutŕe, V., and C. Vandecasteele. 1998. "Immobilization Mechanism of Arsenic in Waste Solidified Using Cement and Lime." *Environmental Science Technology* 32 (18): 2782–2787. doi:10.1021/es971090j.

Habeeb, G. A., and H. B. Mahmud. 2010. "Study on Properties of Rice Husk Ash and Its Use as Cement Replacement Material." *Materials Research* 13 (2): 185–190. doi:10.1590/S1516-14392010000020001.

Hager, I. 2013. "Behaviour of Cement Concrete at High Temperature." *Bulletin of the Polish Academy of Sciences Technical Sciences* 61 (1): 145–154. doi:10.2478/bpasts-2013-0013.

Hassan, J. U., M. Z. Noha, and Z. A. Ahmad. 2014. "Chemical and Mineralogical Properties of Rice Husk Ash (RHA)." *Jurnal Teknologi (Sciences & Engineering)* 70 (5): 1–3. doi:10.11113/jt.v70.3508.

Ho, Y. S. 2006. "Review of Second-Order Model for Adsorption System." *Journal of Hazardous Materials* 136 (3): 125–130. doi:10.1016/j.jhazmat.2005.12.043.

Ho, Y. S., and G. McKay. 1999. "The Sorption of Lead(II) Ions on Peat." *Water Research* 33 (2): 578–584. doi:10.1016/S0043-1354(98)00207-3.

Hossain, M. M., K. Neaupane, N. K. Tripathi, and M. Piantanakulcha. 2013. "Prediction of Groundwater Arsenic Contamination Using Geographic Information System and Artificial Neural Network." *Environment Asia* 6 (1): 38–44. doi:10.14456/ea.2013.6.

Hwang, C. L., T. P. Huynh, and Y. Risdianto. 2016. "An Application of Blended Fly Ash and Residual Rice Husk Ash for Producing Green Building Bricks." *Journal of the Chinese Institute of Engineers* 39 (7): 850–858. doi:10.1080/02533839.2016.1191376.

Khownpurk, P., W. Wongpromrat, and W. Chandra-Ambhorn. 2017. "Arsenic Adsorption Using the Adsorbent Synthesised from Oyster Shell." *Key Engineering Materials* 728: 327–334. doi:10.4028/www.scientific.net/KEM.728.327.

Kohnhorst, A., L. Allan, P. Pokethitiyoke, and S. Anyapo. 2002. "Groundwater Arsenic in Central Thailand." In *Proceedings of 28th WEDC Conference Sustainable Environmental Sanitation and Water Services*, Kolkata (Calcutta), India, 18-22 November 2002: 1–3. Loughborough UK: WEDC.

Kundu, S., and A. K. Gupta. 2006. "Adsorptive Removal of As(III) from Aqueous Solution Using Iron Oxide Coated Cement (IOCC): Evaluation of Kinetic, Equilibrium and Thermodynamic Models." *Separation and Purification Technology* 51 (2): 165–172. doi:10.1016/j.seppur.2006.01.007.

Kwok, K. C. M., L. F. Koong, G. Chen, and G. Mackay. 2014. "Mechanism of Arsenic Removal Using Chitosan and Nanochitosan." *Journal of Colloid and Interface Science* 416: 1–10. doi:10.1016/j.jcis.2013.10.031.

Lagergren, S. 1891. "About the Theory of So-Called Adsorption of Soluble Substances." *Kungliga Svenska Vetenskapsakadimiens Hanlingar* 24 (4): 1–39.

Maiti, A., S. Das Gupta, J. K. Basu, and S. De. 2007. "Adsorption of Arsenite Using Natural Laterite as Adsorbent." *Separation and Purification Technology* 55 (3): 350–359. doi:10.1016/j.seppur.2007.01.003.

Maji, S. K., Y. H. Kao, P. Y. Liao, Y. J. Lin, and C. W. Liu. 2013. "Implementation of the Adsorbent Iron-Oxide-Coated Natural Rock (IOCNR) on Synthetic As(III) and on Real Arsenic-Bearing Sample with Filter." *Applied Surface Science* 284: 40–48. doi:10.1016/j.apsusc.2013.06.154.

Maji, S. K., Y. H. Kao, and C. W. Liu. 2011. "Arsenic Removal from Real Arsenic-Bearing Groundwater by Adsorption on Iron-Oxide-Coated Natural Rock (IOCNR)." *Desalination* 280 (1–3): 72–79. doi:10.1016/j.desal.2011.06.048.

Maji, S. K., A. Pal, and T. Pal. 2008. "Arsenic Removal from Real-Life Groundwater by Adsorption on Laterite Soil." *Journal of Hazardous Materials* 151 (2–3): 811–820. doi:10.1016/j.jhazmat.2007.06.060.

Malana, M. A., R. B. Qureshi, and M. N. Ashiq. 2011. "Adsorption Studies of Arsenic on Nano Aluminium Doped Manganese Copper Ferrite Polymer (MA, VA, AA) Composite: Kinetics and Mechanism." *Chemical Engineering Journal* 172 (2–3): 721–727. doi:10.1016/j.cej.2011.06.041.

Mangwandi, C., S. N. A. Suhaimi, J. T. Liu, R. M. Dhenge, and A. B. Albadarin. 2016. "Design, Production and Characterisation of Granular Adsorbent Material for Arsenic Removal from Contaminated Wastewater." *Chemical Engineering Research and Design* 110: 70–81. doi:10.1016/j.cherd.2016.04.004.

Manju, G. N., C. Raji, and T. S. Anirudhan. 1998. "Evaluation of Coconut Husk Carbon for the Removal of Arsenic from Water." *Water Research* 32 (10): 3062–3070. doi:10.1016/S0043-1354(98)00068-2.

Mar, K. K., D. Karnawati, D. P. E. Sarto, T. I. Putra, and C. B. Tabelin. 2013. "Comparison of Arsenic Adsorption on Lignite, Bentonite, Shale, and Iron Sand from Indonesia." *Procedia Earth and Planetary Science* 6: 242–250. doi:10.1016/j.proeps.2013.01.033.

Mazumder, G. N. 2003. "Chronic Arsenic Toxicity: Clinical Features, Epidemiology, and Treatment: Experience in West Bengal." *Journal of Environmental Science and Health, Part A Toxic/Hazardous Substances and Environmental Engineering* 38 (1): 141–163. doi:10.1081/ESE-120016886.

Mohan, D., and C. U. Pittman Jr. 2007. "Arsenic Removal from Water/Wastewater Using Adsorbents: A Critical Review." *Journal of Hazardous Materials* 142 (1–2): 1–53. doi:10.1016/j.jhazmat.2007.01.006.

Pansamut, S., and G. Wattayakorn. 2010. "Arsenic Contamination in Water from Suphanburi Province, Thailand." *Journal of Environmental Research and Development* 4 (3): 678–686.

Pattanapipitpaisal, P., and P. Suraruk. 2012. "Groundwater Quality and Arsenic Contamination in Amphoe Khemmarat, Ubon Ratchathani, Thailand." *Journal of Environmental Science and Engineering* 1 (2A): 133–141.

Pattanayak, J., K. Mondal, S. Mathew, and S. B. Lalvani. 2000. "A Parametric Evaluation of the Removal of As(V) and As(III) by Carbon-Based Adsorbents." *Carbon* 38 (4): 589–596. doi:10.1016/S0008-6223(99)00144-X.

Phenrat, T., F. Marhaba, and M. Rachakornkij. 2005. "SEM and X-Ray Study for Investigation of Solidified/Stabilized Arsenic-Iron Hydroxide Sludge." *Journal of Hazardous Materials* 118 (1–3): 185–195. doi:10.1016/j.jhazmat.2004.10.019.

Prasara, A. J., and S. H. Gheewala. 2016. "Sustainable Utilization of Rice Husk Ash from Power Plants: A Review." *Journal of Cleaner Production* 167: 1020–1028. doi:10.1016/j.jclepro.2016.11.042.

Rodriguez, E. T., K. Garbev, D. Merz, L. Black, and I. G. Richardson. 2017. "Thermal Stability of C-S-H Phases and Applicability of Richardson and Groves' and Richardson C-(A)-S-H(I) Models to Synthetic C-S-H." *Cement and Concrete Research* 93: 45–56. doi:10.1016/j.cemconres.2016.12.005.

Seidell, A. 1919. *Solubility of Inorganic Compounds. A Compilation of Quantitative Solubility Data from the Periodical Literature*. New York: D. Van Nostrand.

Sener, S. 2008. "Use of Solid Wastes of the Soda Ash Plant as an Adsorbent for the Removal of Anionic Dyes: Equilibrium and Kinetic Studies." *Chemical Engineering Journal* 138 (1–3): 207–214. doi:10.1016/j.cej.2007.06.035.

Sharma, V. K., and M. Sohn. 2009. "Aquatic Arsenic: Toxicity, Speciation, Transformations, and Remediation." *Environment International* 35 (4): 743–759. doi:10.1016/j.envint.2009.01.005.

Srinivasreddy, A. B., T. J. McCarthy, and E. Lume. 2013. "Effect of Rice Husk Ash on Workability and Strength of Concrete." In *Proceedings of 6th*

Biennial Concrete Institute of Australia's National Conference (Concrete 2013), Queensland, Australia, 16–18 October 2013: 1–10. Australia: University of Wollongong.

Su, Y. M., F. C. Kung, T. L. Su, P. C. Tsai, C. Lai, and Y. L. Kuo. 2011. "Material Characteristics and Electric Properties of SiOx-doped GDC Electrolytes." *Journal of the Chinese Institute of Engineers* 34 (1): 31–38. doi:10.1080/02533839.2011.555465.

Tsai, H. C., S. L. Lo, and J. Kuo. 2011. "Using Pretreated Waste Oyster and Clam Shells and Microwave Hydrothermal Treatment to Recover Boron from Concentrated Wastewater." *Bioresource Technology* 102 (17): 7802–7806. doi:10.1016/j.biortech.2011.06.036.

Tseng, D. H. 1988. "Solidification/Stabilization of Hazardous Sludges with Portland Cement." *Journal of the Chinese Institute of Engineers* 11 (3): 219–225. doi:10.1080/02533839.1988.9677061.

Uppal, H., J. T. Hemlata, and N. Singh. 2016. "Zinc Peroxide Functionalized Synthetic Graphite: An Economical and Efficient Adsorbent for Adsorption of Arsenic (III) and (V)." *Journal of Environmental Chemical Engineering* 4 (3): 2964–2975. doi:10.1016/j.jece.2016.05.038.

Villar-Cociña, E., E. V. Morales, S. F. Santos, H. Savastano Jr, and M. Frías. 2011. "Pozzolanic Behavior of Bamboo Leaf Ash: Characterization and Determination of the Kinetic Parameters." *Cement and Concrete Composites* 33 (1): 68–73. doi:10.1016/j.cemconcomp.2010.09.003.

Woo, S. M., and T. H. Lee. 1978. "The Engineering Properties of Rice Hull Ash as a Soil Stabilizer." *Journal of the Chinese Institute of Engineers* 1 (1): 87–95. doi:10.1080/02533839.1978.9676603.

Yoon, G. L., B. T. Kim, B. O. Kim, and S. H. Han. 2003. "Chemical-Mechanical Characteristics of Crushed Oyster-Shell." *Waste Management* 23 (9): 825–834. doi:10.1016/S0956-053X(02)00159-9.

Zhang, G., J. Qu, H. Liu, R. Liu, and R. Wu. 2007. "Preparation and Evaluation of a Novel Fe-Mn Binary Oxide Adsorbent for Effective Arsenite Removal." *Water Research* 41 (9): 1921–1928. doi:10.1016/j.watres.2007.02.009.

Zhang, T. S., J. Ma, L. B. Kong, S. H. Chan, P. Hing, and J. A. Kilner. 2004. "Iron Oxide as an Effective Sintering Aid and a Grain Boundary Scavenger for Ceria-Based Electrolytes." *Solid State Ionics* 167 (1): 203–207. doi:10.1016/j.ssi.2004.01.006.

Author biography

Name	Pichnipa		Khownpurk
Date of birth	11	August	1987
Address	74 Soi Ladprao Wang Hin 70 Ladprao, Ladprao, Bangkok 10230		
Education	2010, Bachelor degree of science, petrochemical technology (International Program), King Mongkut's Institute of Technology Ladkrabang, Thailand 2013, Master degree of Engineering, department of chemical engineering, King Mongkut's Institute of Technology Ladkrabang, Thailand		
Publications	1. Pichnipa Khownpurk and Walairat Chandra-ambhorn. (2018) Preparation and characterization of oyster shell powder-treated rice husk ash adsorbent pellet for As(III) removal. *MATEC Web of Conferences*, 192, 1-4. 2. Pichnipa Khownpurk, Wichitra Wongpromrat and Walairat Chandra-Ambhorn. (2017). Arsenic Adsorption Using the Adsorbent Synthesised from Oyster Shell. *Key Engineering Materials*, 724, 327-334. 3. P. Khownpurk and W. Chandra-ambhon. (2014). Arsenite Adsorption on the Adsorbent Synthesized from Oyster Shells. The 4th TIChE International Conference 2014 (pp.475-477). Chiang Mai, Thailand		

4. พิชญ์นิภา ขวัญเผือก และวลัยรัตน์ จันทรอัมพร. (2556). “การดูดซับสารหนูในน้ำปนเปื้อนด้วยตัวดูดซับสังเคราะห์จากเปลือกหอยนางรม (Adsorption of Arsenic in Contaminated Water by Using Adsorbent Synthesized from Oyster Shell)” การประชุมทางวิชาการ ครั้งที่ 51 มหาวิทยาลัยเกษตรศาสตร์ วันที่ 5-7 กุมภาพันธ์ พ.ศ. 2556. กรุงเทพฯ:มหาวิทยาลัยเกษตรศาสตร์.